UNIVERSITÉ PARIS-EST

Université Paris-Est
École doctorale MSTIC

THÈSE

pour l'obtention du grade de Docteur de l'Université Paris-Est
en spécialité Informatique
présentée et soutenue publiquement par

NICOLAS BOUTRY

le 14 Décembre 2016

UNE ÉTUDE DU BIEN-COMPOSÉ EN n-D

A STUDY OF WELL-COMPOSEDNESS IN n-D

Jury :

Président :	Michel Couprie, Pr., ESIEE-Paris
Rapporteurs :	Rocio González-Díaz, Pr., Universidad de Sevilla Nicolas Passat, Pr., Université de Reims Champagne-Ardenne Jacques-Olivier Lachaud, Pr., Université Savoie Mont Blanc
Examinateurs :	Longin Jan Latecki, Pr., Temple University Loïc Mazo, MCF., Université de Strasbourg
Directeurs de thése :	Laurent Najman, Pr., ESIEE-Paris Thierry Géraud, Pr., EPITA

Digitization of the real world using real sensors has many drawbacks; in particular, we loose "well-composedness" in the sense that two digitized objects can be connected or not depending on the connectivity we choose in the digital image, leading then to ambiguities. Furthermore, digitized images are arrays of numerical values, and then do not own any topology by nature, contrary to our usual modeling of the real world in mathematics and in physics. Loosing all these properties makes difficult the development of algorithms which are "topologically correct" in image processing: e.g., the computation of the tree of shapes needs the representation of a given image to be continuous and well-composed; in the contrary case, we can obtain abnormalities in the final result. Some well-composed continuous representations already exist, but they are not in the same time n-dimensional and self-dual. In fact, n-dimensionality is crucial since usual signals are more and more 3-dimensional (like 2D videos) or 4-dimensional (like 4D Computerized Tomography-scans), and self-duality is necessary when a same image can contain different objects with different contrasts. We developed then a new way to make images well-composed by interpolation in a self-dual way and in n-D; followed with a span-based immersion, this interpolation becomes a self-dual continuous well-composed representation of the initial n-D signal. This representation benefits from many strong topological properties: it verifies the intermediate value theorem, the boundaries of any threshold set of the representation are disjoint union of discrete surfaces, and so on.

Keywords: well-composed, discrete surfaces, digital topology, tree of shapes, mathematical morphology

À Carmen

REMERCIEMENTS

Je voudrais tout d'abord remercier profondement mes deux directeurs de thèse, Thierry Géraud et Laurent Najman, qui, en plus de m'avair coaché pendant ces trois années, m'ont appris une nouvelle manière de penser, plus riche, plus rigoureuse, et plus en profondeur, et qui, je n'en doute pas, me sera profitable toute ma vie.

Je remercie aussi sincèrement tous les membres du Jury pour l'intérêt qu'ils ont porté à mes travaux et pour tout le temps qu'ils ont pu passer a lire mon manuscrit afin de l'améliorer, en matière de clarté, de rigueur, et de lisibilité. Je voudrais aussi remercier en particulier Loïc Mazo, avec qui j'ai eu quelques discussions très intéressantes sur les ordres partiels ces dernières années, mais aussi Michel Couprie, pour m'avoir mis en garde par rapport au danger que représentent les dimensions supérieures à 3 dans le cadre des démonstrations en topologie.

Je voudrais aussi remercier ma femme, Carmen, mes parents, Anne et Pascal, mes beaux-parents, Olga et Daniel, ainsi que ma belle-tante Nẽnẽta, qui auront toujours été là pour moi dans les moments ou j'avais besoin de leur écoute et de leur soutien, et sans qui cette thèse n'aurait pas été la même expérience. Je remercie aussi mes amis: Sylvain, Hugo, Julien, Natadu et Saëltirias, Yves, Robert, Fred, Olivier, Romain, et Ravi, que je remercie pour leur patience, car j'aurai été très peu disponible ces derniers temps.

Bien sûr, je remercie aussi tous mes collègues du LRDE à l'EPITA, qui m'auront toujours permis de travailler dans de très bonnes conditions tout au long de ces trois années, ainsi que mes collègues du LIGM, qui ont toujours été très accueillants lors de mes passages à l'ESIEE. Je remercie aussi tout particulièrement Sylvie Cach qui a toujours su faire preuve d'un professionnalisme exemplaire et d'une disponibilité sans limite.

CONTENTS

1. Introduction . . . 23
2. State-of-the-Art . . . 27
   2.1. Mathematical basics . . . 27
   2.2. Well-composed sets and images . . . 30
   2.3. Topological reparations and well-composed interpolations . . . 42
   2.4. Topics related to well-composedness . . . 46
3. Generalization of well-composedness to dimension n . . . 59
   3.1. The different flavours of n-D WCnesses in brief . . . 59
   3.2. Mathematical basics . . . 60
   3.3. n-D EWCness and n-D DWCness . . . 60
   3.4. Relations between AWCness, DWCness, and CWCness on cubical grids . . . 74
4. Digitally well-composed interpolations in n-D . . . 77
   4.1. Self-dual local interpolations . . . 78
   4.2. A new self-dual n-D DWC interpolation . . . 90
5. Some consequences and applications . . . 109
   5.1. Pure self-duality . . . 109
   5.2. A new representation of digital images . . . 113
   5.3. n-D Marching-Cubes-like algorithms . . . 117
   5.4. Tree of shapes of the sign of the DWC morphological Laplacian . . . 120
6. Perspectives . . . 123
   6.1. About the equivalence between AWCness and CWCness on cubical grids . . . 123
   6.2. Preservation of digital well-composedness . . . 124
   6.3. Graph-based characterizations of AWCness and DWCness . . . 130
   6.4. n-D segmentation and parameterization . . . 137
7. Conclusion . . . 139

Appendices . . . 141
A. Proof that $\mathcal{I}_{\min}(u)$ and $\mathcal{I}_{\max}(u)$ are digitally well-composed . . . 143
B. Topological reparation in n-D . . . 147
C. Axiomatic digital topology . . . 153
D. About the equivalence between AWCness and DWCness . . . 177
E. Well-composed interpolations on polyhedral complexes . . . 187

LIST OF FIGURES

1. Neighborhoods of a point $p \in \mathbb{Z}^2$ . . . 27
2. Square grid using 4-adjacency . . . 28
3. Square grid using 8-adjacency . . . 28
4. The connectivity paradox using 4-adjacency . . . 29
5. The connectivity paradox using 8-adjacency . . . 29
6. Different square grids based on 6-adjacency . . . 29
7. A 6-curve does not always separates the digital plane even if we use 6-adjacency . . . 30
8. $(4,8)$-adjacency on the left and $(8,4)$-adjacency on the right . . . 30
9. A set which is weakly well-composed but not well-composed [102] . . . 31
10. The (black) sets are well-composed in (a) and (c), but the (black) set in (b) is neither well-composed nor weakly well-composed [102]. . . . 31
11. Forbidden patterns into well-composed sets [102] . . . 32
12. The first critical pattern forbidden in 3D well-composed sets . . . 33
13. The second critical pattern forbidden in 3D well-composed sets . . . 33
14. The six possible configurations at a corner point in a 3D well-composed set . . . 34
15. The equivalence of connectivities of a set and its complement does not imply it is well-composed in 3D (p. 171 [97]). . . . 35
16. The two forbidden critical configurations in the continous analog of 2D well-composed sets . . . 37
17. The flat extension of the dilation operator (p. 869 [25]) . . . 38
18. Definition of 2D well-composedness on 2D arbitrary grids . . . 39
19. A set which is face-connected and whose complement is not face-connected . . . 40
20. A truncated octahedra (p. 13 [118]) . . . 40
21. A cell complex which would not be well-composed according to Stelldinger [163] . . . 41
22. The equivalent in 2D of the repairing method of Gonzalez-Diaz *et al.* . . . 43
23. Repairing of a complex containing a critical edge [67] . . . 43
24. Repairing of a complex containing a critical vertex [67] . . . 43
25. Repairing of more complex forbidden configurations [67] . . . 44
26. Differents configurations using Majority Interpolation [165] . . . 44
27. A reconstruction based on cubical grids in 3D leads to critical configurations [166] . . . 46
28. Even the digitization of a smooth bordered 3-manifold can contain a 2D critical configuration [166]. . . . 47
29. A r-regular object and its reconstructions . . . 48
30. An image and its rigid transformation [135] . . . 48
31. Forbidden pattern in regular images [135] . . . 48
32. Patterns that are completely destructured by the rigid transformation [134] . . . 49
33. Modified patterns whose topology is preserved under the rigid transformation [134] 49
34. From seeds to well-composed regions . . . 50
35. Glamorous glue applied to regions results in a well-composed region . . . 50
36. The irreducible thick configuration [8] . . . 51
37. An irreducible gray-level well-composed image and its crest network [116] . . . 51
38. The initial image, the reduced gradient, and the resulting watershed [116]. . . . 52
39. Simplicial set of a $(4,8)$ digital picture whose Euler characteristic is equal to 1 . . . 53
40. Simplicial set of a $(8,4)$ digital picture whose Euler characteristic is equal to 0 . . . 53
41. A simple closed curve in $\mathbb{R}^2$ is a Jordan curve . . . 54

42. 8-curves and 4-curves are not always Jordan curves in $\mathbb{Z}^2$ . . . 54
43. A well-composed curve is always a Jordan curve in $\mathbb{Z}^2$ . . . 55
44. A simple closed curve in $\mathbb{H}^2$ is a Jordan curve . . . 55
45. Different kinds of simple closed curves according to Wang and Battacharya . . . 55
46. The continuous analog of a set which is not well-composed . . . 56
47. The continuous analog of a well-composed set . . . 56
48. Non-Jordan surfaces . . . 57
49. Jordan surfaces . . . 57
1. 2D, 3D and 4D blocks . . . 61
2. In the raster scan order: the white points are 1-antagonists, 2-antagonists, 3-antagonists, and 4-antagonists . . . 62
3. The white points on the left draw a 2D primary critical configuration, and the white points on the right draw a secondary 2D critical configuration. . . . 62
4. The white points on the left draw a 3D primary critical configuration, and the white points on the right draw a secondary 3D critical configuration. . . . 63
5. The white points on the left draw a 4D primary critical configuration, and the white points on the right draw a secondary 4D critical configuration. . . . 63
6. Step-by-step construction of the $2n$-path joining the two (red) antagonists into $X \cap S$ into $\mathbb{Z}^n$ . . . 64
7. DWCness implies EWCness . . . 66
8. EWCness does not imply DWCness in n-D ($n \geq 3$) . . . 67
9. From single-valued functions to set-valued/interval-valued functions (continuous and discrete cases) . . . 71
10. A family of large upper threshold sets of an interval-valued image . . . 72
11. A family of strict upper threshold sets of an interval-valued image . . . 73
12. Possible set configurations in 2D . . . 74
13. Possible set configurations in 3D . . . 75
1. Subdividing the domain $\mathcal{D}$ into $\mathcal{D}'$ to interpolate . . . 77
2. Illustration of the cubical subdivision process on a block S . . . 79
3. $\mathrm{Subd}(S) \subseteq \left(\frac{\mathbb{Z}}{2}\right)^n$ as a poset . . . 80
4. Parenthood relationship in the graph of a subdivided block . . . 81
5. Ancesters of the point z at the center of the subdivided block . . . 82
6. Groups of the point z at the center of the subdivided block . . . 82
7. Ordered computing of the values of the interpolation . . . 83
8. Other kinds of subdivisions/interpolations . . . 85
9. The 3 possible configurations in 2D (modulo reflections and rotations) . . . 86
10. $u'\big|_{\mathcal{G}(z)}$ for $z \in \mathbb{E}_2$ for any self-dual local interpolation after the application of f_1 (with m any value $\in \mathbb{R}$). . . . 87
11. The Hasse diagrams for the α- and the U-configurations (left) and for the Z-configuration (right) . . . 87
12. An image, and its interpolations using the *median*, the *mean/median*, the *min* and the *max* operators respectively (see Definition 37 for more details). . . . 88
13. A counter-example proving that no self-dual local interpolations makes images DWC in 3D . . . 89
14. The initial image u . . . 90
15. The "continuous" interpolation U . . . 91
16. Flattening process . . . 91
17. The interpolation of u . . . 91
18. Computation of the tree of shapes . . . 92
19. The front propagation algorithm applied on a digitally well-composed interval-valued image U . . . 94
20. A situation impossible to obtain with $p, q \in \mathcal{D}$ being $2n$-neighbors in $(\mathbb{Z}/s)^n$ . . . 96
21. The 4 possible scenarii when only two $2n$-neighbors p and q in $\mathcal{D}'$ are considered . . . 97
22. Assuming U is digitally well-composed and $u^\flat$ is not digitally well-composed, we obtain incompatible properties . . . 100

23. Two possible configurations when dilating the domain $\mathcal{D}_{k-1}$ into $\mathcal{D}_k$ with our structuring elements. . . . 102
24. The complete process in detail . . . 105
25. From U_+ to $u^\flat$ . . . 106
26. A self-dual digitally well-composed interpolation of image of Figure 13 . . . 107
1. A gray-level image (in the middle), its min-tree and its max-tree (on the left), and its tree of shapes [61] (on the right). . . . 109
2. Incoherences using 4-connectivity for both upper and lower threshold sets . . . 109
3. Incoherences using 8-connectivity for both upper and lower threshold sets . . . 110
4. An image u, its min/max interpolations, and u_{DWC} which is self-dual . . . 110
5. The tree of shapes of the min, max, and self-dual interpolations . . . 111
6. The initial image u containing a ball and a full torus and its self-dual interpolation . . . 111
7. On the left, u seen from the top, and on the right, u_{DWC} seen from the top . . . 111
8. The tree of shapes of u . . . 112
9. Grain filtering on an image u: our self-dual representation leads to "pure" self-duality 112
10. From u to its underlying graph structure using the dual pair (c_8, c_4) . . . 113
11. All the possible cubical connectivity grids are equivalent on a digitally well-composed image . . . 113
12. From span-based immersion to continuous representations . . . 114
13. $\Delta[U \trianglerighteq 2]$, depicted in red, contains a pinch (in yellow) . . . 115
14. Our method to obtain an AWC plain map . . . 116
15. Lorensen's Marching Cubes Lookup Table [113] . . . 117
16. The "hole problem" using Marching Cubes ([157]) . . . 118
17. Lookup tables of Daragon [44, 43] in the 3D case . . . 119
18. n-D approach of Lachaud [96], based on the convex hull . . . 119
19. Summary of the method used by Huyhn *et al.* [80] . . . 120
20. An inclusion tree and its corresponding image [80] . . . 121
1. Morphological dilation does not preserve digital well-composedness using a structuring element based on 4-connectivity . . . 124
2. Morphological dilation does not preserve digital well-composedness using a structuring element based on 8-connectivity . . . 124
3. Morphological erosion does not preserve digital well-composedness using a structuring element based on 4-connectivity . . . 124
4. Morphological erosion does not preserve digital well-composedness using a structuring element based on 8-connectivity . . . 124
5. The original Barbara image . . . 127
6. The 44417 critical configurations in the original Barbara image . . . 127
7. Our self-dual interpolation of the Barbara image . . . 128
8. A grain filter of the DWC interpolation of the Barbara image with a threshold $\lambda = 10$ 128
9. A grain filter of the DWC interpolation of the Barbara image with a threshold $\lambda = 320$ 129
10. A grain filter of the DWC interpolation of the Barbara image with a threshold $\lambda = 1280$ 129
11. A 3D digitally well-composed binary image, the mask, and a marker of the same size 130
12. The geodesic dilation of the marker in the binary image is also digitally well-composed . . . 130
13. A discretized sphere with values on the 2-faces . . . 131
14. How to characterize AWCness in 2D . . . 132
15. Boundaries of the different threshold sets around z^2 . . . 132
16. A 3D image which is not AWC . . . 133
17. Some examples of graphs $\mathcal{G}(u, z)$ . . . 134
18. The boundary of the well-composed object is a manifold . . . 138
1. Links betweens the different flavors of well-composedness on cubical grids . . . 140
2. A (subdivided) torus and its incidence graph [42] (p. 50) . . . 140
1. Hierarchical representation of an image . . . 148
2. Number of critical configurations as a function of the size of the image given in number of pixels . . . 150

3. Number of corrections as a function of the number of initial critical configurations . 151
4. Original image u . . . 151
5. Zero-crossings of the original Laplacian . . . 151
6. Zero-crossings of the Laplacian modified by the increasing process . . . 152
7. Text segmentation results . . . 152
1. Different representations of the same cubical complex . . . 158
2. The closures $\alpha(x)$, $\alpha(y)$, $\alpha(z)$ in $\mathbb{H}^2$ [42] (p. 34). . . . 159
3. The openings $\beta(x)$, $\beta(y)$, $\beta(z)$ in $\mathbb{H}^2$ [42] (p. 34). . . . 159
4. The neighborhoods $\theta(x)$, $\theta(y)$, $\theta(z)$ in $\mathbb{H}^2$ [42] (p. 34). . . . 160
5. A binary image u_{bin} in $\mathbb{Z}^2$ [42] (p. 31). . . . 160
6. u_{bin} [42] (p. 31) supplied with the $(4,8)$-topology on the left and with the $(8,4)$-topology on the right (the foreground is in black and the background in white). . . . 160
7. Different immersions of u_{bin} into $\mathbb{H}^2$ [42] (p. 31) . . . 161
8. A path in $\mathbb{H}^2$ [42] (p. 34) . . . 161
9. A simple closed curve in $\mathbb{H}^2$ [42] (p. 34). . . . 162
10. Three examples of orders $|X|, |Y|, |Z|$ ([42], p. 37) . . . 163
11. The join operator $*$ is not commutative ([42], p. 37) . . . 163
12. Some order joins representing a *simplicial complex* on the left and a sphere on the right [42] (p. 37) . . . 164
13. A 2-surface: the sphere $\mathcal{S}_2$ [42] (p. 50) . . . 164
14. Different kinds of *adherences* of a 2-element in $\mathbb{H}^3$ [42] (p. 54) . . . 165
15. Examples of simplicial complexes ([42], p. 40) . . . 167
16. From a subcomplex to its simplicial neighborhood ([42], p. 46) . . . 171
17. From an order to its chain complex ([42], p. 46) . . . 172
18. From a simplicial complex to a frontier order ([42], p. 86) . . . 173
19. A cubical complex and the frontier order of the central square into this order . . . 173
20. From a full subcomplex to its derived neighborhood ([42], p. 98) . . . 174
1. A 4D digitally well-composed set (depicted in blue) and its complement (in red) . . . 178
2. Bijection between $\mathbb{H}^1$ and $(\mathbb{Z}/2)$ . . . 178
3. The subspace $|\beta^{\square}(z)|$ we are working in to study AWCness (2D/3D cases) . . . 179
4. Examples of 0-surfaces (in black) . . . 180
5. Examples of 1-surfaces . . . 180
6. From a 2D critical configuration in $\mathbb{Z}^2$ to a critical point z^* in $\mathbb{H}^2_0$ . . . 181
7. From the 3D critical configuration to the critical point . . . 182
8. Assuming that X is DWC, $|\beta^{\square}_{\mathfrak{N}}(z)|$ is a 0-surface when $\dim(z) = n-2$ . . . 183
9. Examples of opposites in $\mathbb{H}^2$ . . . 184
10. Structure of $\beta^{\square}_{\mathfrak{N}}(z)$ when we have $(n - \dim(z)) = 3$ assuming that $|\beta^{\square}_{\mathfrak{N}}(z)|$ is not connected . . . 184
1. A polyhedral complex on the left and its border on the right . . . 188
2. Among these orders, the only bordered 2-surface is the one on the right . . . 189
3. A triangulated Möbius ruban is a bordered 2-manifold . . . 189
4. Topological structure being (or not) bordered 2-surfaces . . . 189
5. $[u \leq 0]$ and $[u \leq 1]$ are AWC, but $[u \geq 1]$ is not AWC . . . 190
6. Dual cells . . . 190
7. From a partition of a simplicial complex to its corresponding cell complex (one color by 2-cell) . . . 191
8. Families of n-cells: AWC on the left and not AWC on the right . . . 192
9. Functions on cell complexes: AWC on the left and not AWC on the right . . . 192
10. An image defined u on the n-dimensional convex polyhedral domains of a polyhedral complex . . . 193
11. Chain complex of the initial image . . . 194
12. Using derived neighborhoods directly on the initial domain does not lead to a satisfactory result . . . 194
13. Using derived neighborhoods on the chain complex of the domain of u does not lead to a satisfactory result neither. . . . 195

14. Using frontier orders on the chain complex of the closure of the domain of the image disconnects the pixels . . . 195
15. Using directly frontier orders on a simplicial complex is not self-dual . . . 196
16. From u defined on the n-cells of a polyhedral complex to U defined on all the faces of the complex . . . 196
17. U' defined on all the 0-faces of the subdivided complex . . . 197
18. The same image U' with an additional border . . . 197
19. $u^\flat_+$ (with the temporary border) . . . 197
20. $u^\flat$ (without the temporary border) . . . 197
21. $\mathcal{F}([u^\flat \leq 1], \mathcal{C}^{\mathfrak{Pc}^n})$ . . . 198
22. $\Delta N^1(\mathcal{F}([u^\flat \leq 0], \mathcal{C}^{\mathfrak{Pc}^n}), \mathcal{C}^{\mathfrak{Pc}^n})$ . . . 198
23. $\Delta N^1(\mathcal{F}([u^\flat \leq 1], \mathcal{C}^{\mathfrak{Pc}^n}), \mathcal{C}^{\mathfrak{Pc}^n})$ . . . 199
24. $\Delta N^1(\mathcal{F}([u^\flat \leq 2], \mathcal{C}^{\mathfrak{Pc}^n}), \mathcal{C}^{\mathfrak{Pc}^n})$ . . . 199
25. The new valued cell complex representing an AWC function . . . 200
26. Cubical subdivision vs double derived subdivision . . . 200
27. From a cell complex to its hierarchical subdivision . . . 201
28. From the hierarchical subdivision of a polyhedral complex to its chain complex . . . 201
29. The cell complex resulting of the chain complex of the hierarchical subdivision: the geometry of the initial cells is preserved. . . . 202
30. From u to U . . . 202
31. The propagation computation . . . 203
32. A self-dual interpolation of u . . . 203
33. The dual cell resulting from the chain complex of the hierarchical subdivision . . . 205
34. Our self-dual representation on cell complexes . . . 206

LIST OF ACRONYMS

- AWC: Well-Composed in the sense of Alexandrov
- CC: Critical Configuration
- CWC: Continuous Well-Composedness
- DWC: Digital Well-Composedness
- EWC: Well-Composed based on the Equivalence of connectivities
- FPA: Front-Propagation Algorithm
- IVM: Interval-Valued Map
- MC: Marching Cubes
- MM: Mathematical Morphology
- PL: Piecewise Linear
- ToS: Tree of Shapes
- WC: Well-Composed

LIST OF SYMBOLS

- Basics:
  - n is the dimension of the space,
  - $s \geq 1$ is the (domain) subdivision factor,
  - $\mathbb{B} = \{e^1, \ldots, e^n\}$ is the canonical basis of $\mathbb{Z}^n$,
  - x_i is the i^{th} coordinate, $i \in [\![1, n]\!]$, of $x \in \mathbb{R}^n$,
  - # denotes the cardinal operator,
- Single-valued images:
  - $\mathbb{Z}^n$, $\left(\frac{\mathbb{Z}}{2}\right)^n$, $(\mathbb{Z}/s)^n$ are the sets/images spaces,
  - $\mathcal{D} \subseteq (\mathbb{Z}/s)^n$ is the domain of a given image,
  - $\mathbb{V}$ is the value space of a given image,
  - u_{bin} represents a binary image,
  - $\mathbb{I}\text{m}(A, \mathcal{D}, \mathbb{V})$ is the space of all possible images whose space is A, whose domain is $\mathcal{D}$ and whose value space is $\mathbb{V}$,
- Interval-valued images:
  - $\lceil U \rceil$ is the upper bound of the interval-valued image U,
  - $\lfloor U \rfloor$ is the lower bound of the interval-valued map U,
- Threshold sets:
  - $\lambda \in \mathbb{R}$ is a threshold value belonging to $\mathbb{R}$,
  - $\forall\, u : \mathcal{D} \to \mathbb{R}$, $[u \geq \lambda]$ is the large upper threshold set of u for a threshold $\lambda \in \mathbb{R}$,
  - $\forall\, u : \mathcal{D} \to \mathbb{R}$, $[u \leq \lambda]$ is the large lower threshold set of u for a threshold $\lambda \in \mathbb{R}$,
  - $\forall\, u : \mathcal{D} \to \mathbb{R}$, $[u > \lambda]$ is the strict upper threshold set of u for a threshold $\lambda \in \mathbb{R}$,
  - $\forall\, u : \mathcal{D} \to \mathbb{R}$, $[u < \lambda]$ is the strict lower threshold set of u for a threshold $\lambda \in \mathbb{R}$,
  - $\forall\, U : \mathcal{D} \rightsquigarrow \mathbb{R}$, $[U \trianglerighteq \lambda]$ is the large upper threshold set of U for a threshold $\lambda \in \mathbb{R}$,
  - $\forall\, U : \mathcal{D} \rightsquigarrow \mathbb{R}$, $[U \trianglelefteq \lambda]$ is the large lower threshold set of U for a threshold $\lambda \in \mathbb{R}$,
  - $\forall\, U : \mathcal{D} \rightsquigarrow \mathbb{R}$, $[U \triangleright \lambda]$ is the strict upper threshold set of U for a threshold $\lambda \in \mathbb{R}$,
  - $\forall\, U : \mathcal{D} \rightsquigarrow \mathbb{R}$, $[U \triangleleft \lambda]$ is the strict lower threshold set of U for a threshold $\lambda \in \mathbb{R}$,
- Neighborhoods and connectivity:
  - $\mathcal{N}_{2n}(p, A)$ is the $2n$-neighborhood of p in A,
  - $\mathcal{N}^*_{2n}(p, A)$ is the $2n$-neighborhood of p minus p in A,
  - $\mathcal{N}_{3^n-1}(p, A)$ is the $(3^n - 1)$-neighborhood of p in A,
  - $\mathcal{N}^*_{3^n-1}(p, A)$ is the $(3^n - 1)$-neighborhood of p minus p in A,
  - $\mathcal{CC}_{X,A}$ is the set of connected components of $X \subset A$ in A,
- Blocks and antagonism:
  - $\mathcal{B}(A)$ is the set of blocks in the space A,

- $\mathcal{F} = (f^1, \ldots, f^k) \subseteq \mathbb{B}$ is the family of vectors associated to a block,
- $S(z, \mathcal{F})$ is the block associated to z and to the family $\mathcal{F}$ into $\mathbb{Z}^n$,
- $S_s(z, \mathcal{F})$ is the block associated to z and to the family $\mathcal{F}$ into $(\mathbb{Z}/s)^n$,
- $S \in \mathcal{B}(A)$ is a block in A,
- $\mathrm{antag}_S(p)$ is the antagonist in the block S to $p \in S$,

- Interval values:
  - $\mathrm{intvl}(a, b)$ is the interval value $[\min(a, b), \max(a, b)]$ of the values $a, b \in \mathbb{R}$,
  - $\mathrm{Span}(V)$ is the span of the (finite) set of values $V \subset \mathbb{R}$,
  - $[\![a, b]\!]$ is the discrete interval $[a, b] \cap \mathbb{Z}$ with $a, b \in \mathbb{Z}$ such that $a \leq b$,
  - $\mathrm{ConvHull}(A)$ is the convex hull of the set $A \subseteq \mathbb{R}^n$,

- Interpolations:
  - $\mathcal{I}$ denotes an interpolation method,
  - $\mathcal{I}_{\mathrm{op}}$ denotes an interpolation method based on an operator op,
  - $\mathcal{I}_{\min}$ is the min-based n-D interpolation,
  - $\mathcal{I}_{\max}$ is the max-based n-D interpolation,
  - $\mathcal{I}_{\mathrm{med}}$ is the median-based n-D interpolation,
  - $\mathcal{I}_{\mathrm{Span}}$ is the span-based interval-valued n-D interpolation,

- Continuous analogs and boundaries in $\mathbb{R}^n$:
  - $\mathrm{CA}(z)$ is the continuous analog of $z \in \mathbb{Z}^n$ (a cube or radius $\frac{1}{2}$ centered at z),
  - $\mathrm{CA}(X)$ is the union of the continuous analogs of the points of $X \subset \mathbb{Z}^n$,
  - $\mathrm{bdCA}(X)$ is the topological boundary of the continuous analog of $X \subset \mathbb{Z}^n$,
  - $\mathrm{Int}(A)$ is the topological interior of $A \subset \mathbb{R}^n$,
  - $\partial(A)$ is the topological boundary of $A \subset \mathbb{R}^n$,

- Mathematical morphology:
  - se is a structuring element,
  - ε is the morphological erosion operator,
  - δ is the morphological dilation operator,
  - $\mathcal{L}$ is the morphological Laplacian operator,
  - δ_{Geod} is the (morphological) geodesic dilation,

- Front-propagation algorithm:
  - u is a single-valued image,
  - U is a set-valued/interval-valued image,
  - U_+ is the interval-valued interpolation with an added border at ℓ_∞,
  - $u^\flat$ is the output image of our n-D self-dual interpolation method before we remove the border,
  - u_{DWC} is the output image of our n-D self-dual interpolation method,
  - $\mathfrak{FP}$ denotes the output of the front-propagation algorithm,
  - ℓ_∞ is the median value of the inner border of the input image in the $\mathfrak{FP}$ algorithm,
  - p_∞ is the point corresponding to the exterior in the $\mathfrak{FP}$ algorithm,
  - Q is a (hierarchical or not) queue,
  - $Q[\ell]$ is the queue at level ℓ in the $\mathfrak{FP}$ algorithm,
  - ℓ is the current level in the $\mathfrak{FP}$ algorithm,

- $\ell(z)$ is the value of ℓ when we enqueue z into the hierarchical queue Q,
- $t(z)$ is the enqueuing time of the point z in the $\mathfrak{FP}$ algorithm,

- Remarkable sets of Section 4.1
  - $(\mathcal{P})$ is a set of properties that "usual" well-composed interpolations have to verify,
  - $I_0(u', z)$ corresponds to the set of values that $u'(z)$ can take ensuring in-betweeness of u' in $\mathcal{G}(z)$ using an usual interpolation method,
  - $I_{WC}(u', z)$ corresponds to the set of values that $u'(z)$ can take ensuring well-composedness of u' in $\mathcal{G}(z)$ using an usual interpolation method,
  - $I_{sol}(u', z) = I_0(u', z) \cap I_{WC}(u', z)$ using an usual interpolation method,
- $\left(\frac{\mathbb{Z}}{2}\right)^n$ as a poset:
  - $\mathrm{Subd}(A)$ is the cubical subdivision of a bounded hyperrectangle $A \subseteq \mathbb{Z}^n$,
  - $\frac{1}{2}(z)$ is the set of indices of the coordinates of z that are not integers,
  - $\mathbb{E}_i$ is the set of points in $\left(\frac{\mathbb{Z}}{2}\right)^n$ of order $i \in [\![0, n]\!]$,
  - $\mathfrak{o}(z)$ is the order of $z \in \left(\frac{\mathbb{Z}}{2}\right)^n$,
  - $\mathbb{P}(z)$ are the parents of $z \in \left(\frac{\mathbb{Z}}{2}\right)^n$,
  - $\mathcal{G}(z)$ is the group of $z \in \left(\frac{\mathbb{Z}}{2}\right)^n$,
  - $\mathbb{A}(z)$ are the ancesters of $z \in \left(\frac{\mathbb{Z}}{2}\right)^n$,
  - $\mathrm{opp}(z)$ is the set of couples of opposites relatively to $z \in \left(\frac{\mathbb{Z}}{2}\right)^n$,
  - $\mathbb{1}(x)$ is the set of *integral coordinates* of $x \in (\mathbb{Z}/2)^n$,
  - $\frac{1}{2}(x)$ is the set of *half coordinates* of $x \in (\mathbb{Z}/2)^n$,
- Ordered sets:
  - R is a binary relation,
  - $\mathcal{O}$ represents a set of arbitrary elements,
  - $\alpha \subseteq \mathcal{O} \times \mathcal{O}$ is an order relation on $\mathcal{O}$,
  - $|\mathcal{O}| = (\mathcal{O}, \alpha)$ is the set $\mathcal{O}$ supplied with its order relation α,
  - $\alpha^{\square}(x) = \alpha(x) \setminus \{x\}, \forall x \in \mathcal{O}$,
  - $\alpha_X = \alpha \cap X \times X$,
  - $\forall x \in X, \alpha_X(x) = \{y \in X \,;\, (x, y) \in \alpha\}$,
  - $\alpha(X) = \bigcup_{x \in X} \alpha(x)$,
  - β is the inverse of α,
  - $\beta^{\square}(x) = \beta(x) \setminus \{x\}, \forall x \in \mathcal{O}$,
  - $\beta_X = \beta \cap X \times X$,
  - $\forall x \in X, \beta_X(x) = \{y \in X \,;\, (y, x) \in \alpha\}$,
  - $\beta(X) = \bigcup_{x \in X} \beta(x)$,
  - $\theta = \alpha \cup \beta$,
  - $\theta^{\square}(x) = \theta(x) \setminus \{x\}, \forall x \in \mathcal{O}$,
  - $\theta_X = \theta \cap X \times X$,
  - $\forall x \in X, \theta_X(x) = \alpha_X(x) \cup \beta_X(x)$,
  - $\theta(X) = \bigcup_{x \in X} \theta(x)$,

- From $(\mathbb{Z}/2)^n$ to Khalimsky grids:
  - $\mathbb{H}^n$ denotes the Khalimsky grid of dimension n,
  - $\mathbb{H}^n_k$, $k \in [\![0, n]\!]$, denotes the elements of $\mathbb{H}^n$ of dimension k,
  - $\mathcal{Z} : \mathbb{H}^1 \to (\mathbb{Z}/2)$ is the homeomorphism between $\mathbb{H}^1$ and $(\mathbb{Z}/2)$,
  - $\mathcal{Z}_n : \mathbb{H}^n \to (\mathbb{Z}/2)^n$ is the homeomorphism between $\mathbb{H}^n$ and $(\mathbb{Z}/2)^n$,
  - $\mathcal{H}$ is the inverse of the topological isomorphism $\mathcal{Z}$,
  - $\mathcal{H}_n$ is the inverse of the topological isomorphism $\mathcal{Z}_n$,
  - $\mathcal{U}_{\mathbb{H}^1}$ is the topology of $\mathbb{H}^1$,
  - $\mathcal{U}_{(\mathbb{Z}/2)}$ is the topology associated to $(\mathbb{Z}/2)$ as an isomorph of $\mathbb{H}^1$,
  - $\mathcal{U}_{\mathbb{H}^n}$ is the topology of $\mathbb{H}^n$,
  - $\mathcal{U}_{(\mathbb{Z}/2)^n}$ is the topology associated to $(\mathbb{Z}/2)^n$ as an isomorph of $\mathbb{H}^n$
- Khalimsky grids:
  - $a \wedge b = \sup(\alpha(a) \cap \alpha(b))$,
  - $a \vee b = \inf(\beta(a) \cap \beta(b))$,
  - $\dim(f)$ is the dimension of the face $f \in \mathbb{H}^n$,
- Chapter D:
  - $X \subseteq \mathbb{Z}^n$ is a subset of $\mathbb{Z}^n$
  - $Y = \mathbb{Z}^n \setminus X$ is a subset of $\mathbb{Z}^n$
  - $\mathcal{X} = \mathcal{H}_n(X) \subseteq \mathbb{H}^n_n$ is the isomorph of X into the Khalimsky grids,
  - $\mathcal{Y} = \mathcal{H}_n(Y) \subseteq \mathbb{H}^n_n$ is the isomorph of Y into the Khalimsky grids,
  - $\mathcal{IMM}(X) = \mathrm{Int}(\alpha(\mathcal{H}_n(X)))$ is the immersion of X into $\mathbb{H}^n$
  - $\mathfrak{N}$ is the topological boundary of $\mathcal{IMM}(X)$ into $\mathbb{H}^n$
  - $\mathcal{CC}(\mathfrak{N})$ are the connected components of $\mathfrak{N}$,
  - $z^* = \mathcal{H}_n(p) \wedge \mathcal{H}_n(p')$ is a *critical point* when $X \cap S(p, p')$ is a primary/secondary critical configuration,
  - $(\mathcal{P}_k) \equiv \left\{ \forall z \in N \cap \mathbb{H}^n_{n-k},\ |\beta^{\square}_{\mathfrak{N}}(z)| \text{ is a } (n-2-\dim(z))\text{-surface} \right\}.$,
  - $(\mathcal{P}'_k) \equiv \left\{ \forall z \in \mathfrak{N} \cap \mathbb{H}^n_{n-k},\ |\beta^{\square}_{\mathfrak{N}}(z)| \text{ is connected} \right\}.$,
  - $\mathcal{I}$ is the family of indices such that $\{F_i\}_{i\in\mathcal{I}} = \mathcal{CC}(|\beta^{\square}_{\mathfrak{N}}(z)|)$,
  - $\{F_i\}_{i\in\mathcal{I}}$ are the connected components of $|\beta^{\square}_{\mathfrak{N}}(z)|$,
  - $S(z) \equiv \mathcal{Z}_n(\beta(z) \cap \mathbb{H}^n_n)$ is the block centered at $z \in \mathbb{H}^n$,
  - $\mathcal{T}(u)$ is the set of $(\dim(z)+1)$-faces included into $\alpha(u) \cap \beta^{\square}(z)$,
  - $\mathcal{T}(F_i)$ is the set of $(\dim(z)+1)$-faces of F_i,
  - $\mathfrak{a} = \bigvee_{t\in\mathcal{T}(F_1)} t$ and $\mathfrak{b} = \bigvee_{t\in\mathcal{T}(F_2)} t$ are the characteristical points of F_1 and F_2 respectively,
- Combinatorial and piecewise linear topologies:
  - C is a simplicial complex,
  - Λ_C is the support of the simplicial (sub)complex C,
  - $\mathcal{C}^X$ is the chain complex of the order $|X|$,
  - $|C_{K/K'}|$ is the frontier order of K into Λ_C relatively to C
  - $N(K, C)$ is the simplicial neighborhood of K into C,
  - $\Delta(K, C)$ is the border of the derived neighborhood of K into C,
  - K^1 or $[K]^1$ is the chain complex of K,

- $N^1(K, C)$ is the derived neighborhood of the subcomplex K into C,
- K^n or $[K]^n$ is the n^{th} derived subdivision of K,
- $\mathrm{Char}(|X|)$ the set of characteristical faces of the order $|X|$,
- ∂X is the border of the order $|X|$,
- $\mathrm{Int}(|X|)$ is the interior of $|X|$,
- $\mathfrak{CC}^n$ is a cell complex,
- $\{S^i\}_{i\in\mathcal{I}}$ is a family of cells of $\mathfrak{CC}^n$
- $\{P^i\}_{i\in\mathcal{I}}$ is a partition of the set of n-cells of $\mathfrak{CC}^n$,
- $\mathfrak{CC}^n_n$ is the set of n-faces of $\mathfrak{CC}^n$.

1

INTRODUCTION

As told by Rosenfeld in 1979 in [144], "digital pictures are rectangular arrays of non-negative numbers". Effectively, these pictures, which are yet today very common, are simply sets of pixels, that is structures with a position and a value. However, no notion of neighborhood or of continuity are defined on these sets by nature at the contrary to the world we are living in, and which they are assumed to be able to capture.

To give back as much as possible the topology of the plane to these arrays, Rosenfeld considered that two points are neighbors depending on their relative positions in these arrays [143]: roughly speaking, they should be neighbors iff they are "close enough". However, on arrays, there are more than one possible manner to define that two pixels are neighbors: they can be 4-neighbors if their L^1 distance is lower than or equal to one, and they are 8-neighbors if their L^∞ distance is lower than or equal to one (and they are not the only possible connectivities on $\mathbb{Z}^2$).

As we can see, two main drawbacks appear when using this notion: (1) the distance between two different pixels cannot be as small as we want, contrary to the continuous world like Euclidian spaces where the distance between two points can tend toward zero, (2) ambiguities are possible since two pixels can be 8-neighbors but not 4-neighbors.

In Euclidian spaces, a set is said *connected* iff it is not the disjoint union of two open non-empty sets. However, $\mathbb{Z}^2$ is not supplied with a topology by nature, and then connectedness is not possible in that sense. Rosenfeld had then to extend *connectivity-by-path* from continuous spaces to digital spaces instead: two points are *pathwise connected* into a set iff there exists a *path* joining them into this set, and a set is *connected by path* iff any two points of this set are pathwise connected in this set. However, this notion of connectivity is not topological in $\mathbb{Z}^2$.

Furthermore, the Jordan curve theorem does not usually hold on these "digital spaces" (see the connectivity paradox), that is, a simple closed digital curve does not always separate the plane into two components. To obviate this problem, we can use *well-composed digital curves*, in the sense that they contain no couple of points which are 8-neighbors but not 4-neighbors, and then they satisfy the Jordan curve theorem. However, they can be difficult to obtain in practice.

For all these reasons, we were looking for a new **representation** for digital images. In fact, we think that *continuity* is crucial for an image, for both its *domain* and its *value domain*: we need to be able to define usual concepts as *open sets*, *neighborhoods*, *closed sets* on the *domain* of the image, and we need to be able to define a distance between two values (or two subsets of) $\mathbb{R}^n$ in the value domain. More precisely, we believe that *set-valued maps* defined on an *Alexandrov space*, where connectivity by path and connectivity are equivalent, and whose domain value is either $\mathbb{R}$, or $\mathbb{Z}$, or even $\mathbb{H}^1$ (the *Khalimsky line*), can be very useful in practice.

Such functions, in particular the *plain maps*, verify many classical theorems, like the *intermediate value theorem*, and have many nice topological properties: the "inverse image" of a set preserves the topology of the set, the direct image of a connected set is a connected set, and under some conditions on the domain, the set of *shapes* of this image is a *tree* (the *tree of shapes* is then well-defined), and so on.

Another point was fundamental to us: we need to be n-dimensional. Effectively, common signals are 2D images, but also 2D videos (which are in fact 3D signals), 3D images like

Magnetic Resonance images, or even 3D videos like Computed Tomography scans (which are 4D signals).

Also, we wanted our representation to be *well-composed* in the sense that the boundaries of its threshold sets are discrete surfaces; in this case, these boundaries will verify some *separation properties*; in particular, their triangulations using the chain complexes will be (at least) *combinatorial (pseudo)manifolds*, which separate the space into two components, an exterior which is unbounded and an interior which is bounded (which is a digital version of the Jordan-Brouwer separation theorem).

Finally, we wanted our interpolation to be *self-dual*, that is, it must treat in a same way dark components over a bright background or bright components over a dark background; since we do not always know in advance the contrast of the objects we have to treat, or since we can have several objects of different contrasts to treat at the same time in a same signal, it is salutary to have such a representation.

Our goal was then to find a self-dual digital continuous well-composed representation of n-D signals. So, our plan is the following. In the next chapter, we proceed to a state-of-the-art in matter of well-composedness on cubical grids, on Khalimsky grids, and on arbitrary grids, and then in matter of topological reparations and of well-composed interpolations.

After a renaming of the 4 different kinds of well-composednesses on cubical grids, we will present our first main contribution: the generalization of *well-composedness based on the equivalence of connectivities* and *digital well-composedness* to dimension $n \geq 2$, their characterizations, and the proof that digital well-composedness implies well-composedness based on the equivalence of connectivities in n-D. We will also recall briefly how these 4 definitions are known to be related in 2D and 3D in the community of digital topology, and we will summarize their relations in n-D on cubical grids.

Then, we will present our second main contribution: the proof that no self-dual local interpolation makes images DWC in n-D under usual contraints. In the continuity of this statement, we will propose our third main contribution: a new non-local self-dual interpolation which makes images DWC on cubical grids in n-D. This theoretical result comes from the fact that applying our front-propagation algorithm on any DWC interval-valued map results in a DWC single-valued map. The proof is provided in this thesis.

The next chapter presents some consequences of our works in this thesis: (1) a span-based immersion in the Khalimsky grids applied to our self-dual DWC interpolation results in an AWC self-dual representation of n-D signals (at least in 2D and 3D), (2) our self-dual interpolation leads to "pure" self-duality for self-dual operators and to underlying graph structure which do not depend on the values of the new (DWC) representation, (3) a conjecture relating the Marching-Cubes-like algorithms in n-D and DWCness, (4) promising segmentations based on the tree of shapes of the sign of the self-dual DWC interpolation of the morphological Laplacian.

Some embryonic promising researches are also detailed in the perspectives: first we expose that we think that CWCness and AWCness are equivalent on cubical grids, second we show that well-composedness has been observed to be preserved using monotone plannings, geodesic dilation/erosion, and grain filters, and third we expose a new way to characterize AWCness of images defined on polyhedral complexes.

In the appendices, we provide a proof of the well-known DWCness of the n-D *min* and *max interpolations*. After that, we propose the first n-D method able to topologically repair gray-level images defined on cubical grids. Also, after a recall of the mathematical background necessary for the sequel, we propose a sketch of the proof of the equivalence between AWCness and DWCness on cubical grids in n-D. Then, we propose two new interpolation methods starting from a gray-level image defined on the n-faces of a polyhedral complex and resulting in an image, defined on a *cell complex*, that we conjecture to be AWC. The first method is based on derived neigborhoods but does not preserve the geometry of the initial cells, and the second uses a new subdivision method that we introduce in this thesis (called *hierarchical subdivision*

because it induces an hierarchy in the computed cells), which minimizes the deformation of the geometry of the cells. A definition of bordered discrete surface is also introduced and seems very promising.

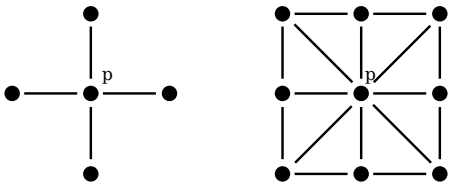

Figure 1.: Neighborhoods of a point $p \in \mathbb{Z}^2$

2 STATE-OF-THE-ART

In this chapter, we will begin with some recalls about *digital topology* [144, 89]: we will show how the existence of the *connectivity paradoxes* in the digital plane led to use a *dual pair* of connectivities to restore the properties of the (topological) plane in the continuous world (like the Jordan Separation Theorem), how Latecki got rid of this paradox by introducing "well-composed" sets in 2D in [102], and how he extended this concept to 3D in [97]. We will continue with some complements about 2D/3D well-composedness that Latecki brought in [100] when generalizing well-composedness to n-D, $n \geq 2$. The first definition of well-composed 2D gray-level images will also be described. Then we will show how Wang and Battacharya [178] extended 2D well-composedness to arbitrary grids, how Stelldinger [163] extended well-composedness to n-D cellular complexes, and how Najman and Géraud [127] extended n-D well-composedness to Alexandrov spaces.

2.1 MATHEMATICAL BASICS

In this section, we recall the well-known concepts of digital topology, followed with the connectivity paradoxes and the presentation of the dual pairs of adjacencies usually used to get rid of these paradoxes.

2.1.1 *Digital topology in $\mathbb{Z}^2$*

Here are the basic definitions of *digital topology* [144, 89] when we work in the *digital plane* $\mathbb{Z}^2$.

Let S be a subset of the digital plane, the points in S will be termed *foreground* points, while those of its complement in the digital plane, $S^c \equiv \mathbb{Z}^2 \setminus S$, will be termed the *background* points. Note that the background points (respectively the foreground points) will be depicted using white points or black depending on the context.

The *4-neighbors* of a point $(x, y) \in \mathbb{Z}^2$ are the points $(x+1, y)$, $(x-1, y)$, $(x, y+1)$ and $(x, y-1)$. The *8-neighbors* of a point $(x, y) \in \mathbb{Z}^2$ are its four 4-neighbors together with its four *diagonal neighbors* $(x+1, y+1)$, $(x+1, y-1)$, $(x-1, y+1)$ and $(x-1, y-1)$.

For $n \in \{4, 8\}$, the *n-neighborhood* of a point $P = (x, y) \in \mathbb{Z}^2$ is the set $\mathcal{N}_n(P)$ consisting of P and its n-neighbors. $\mathcal{N}_n^*(P)$ is the set of all n-neighbors of P without P itself: $\mathcal{N}_n^*(P) = \mathcal{N}_n(P) \setminus \{P\}$. Figure 1 depicts on the left the 4-neighborhood and on the right the 8-neighborhood of a point $p \in \mathbb{Z}^2$.

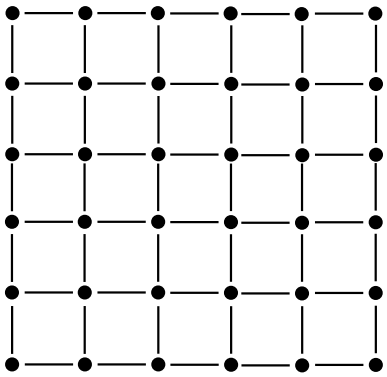

Figure 2.: Square grid using 4-adjacency

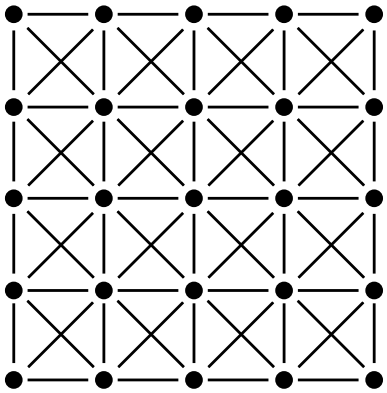

Figure 3.: Square grid using 8-adjacency

Let P, Q be two points of $\mathbb{Z}^2$. We say that a sequence of points $(P = P_1, \ldots, P_n = Q)$ of $\mathbb{Z}^2$ is a *n-path*, $n \in \{4, 8\}$, from P to Q iff $P_i \in \mathcal{N}_n^*(P_{i-1})$ for $i \in [\![2, n]\!]$, and it is a *path* if it is a n-path for some $n \in \{4, 8\}$.

A set $X \subseteq \mathbb{Z}^2$ is said *n-connected* iff for every pair of points $P, Q \in X$, there exists a n-path in X from P to Q, and *connected* if it is connected for some $n \in \{4, 8\}$.

A *n-component* of a set $S \subseteq \mathbb{Z}^2$ is a greatest n-connected subset of S. Depending on whether 4- or 8-connectedness is used, we mean 4- or 8-components.

A set $C \subset \mathbb{Z}^2$ is called a *simple closed curve* or *Jordan curve* if it is connected and each of its points has exactly two neighbors in C. Depending on wheter we use 4- or 8-neighborhoods, we call C a *4-curve* or a *8-curve*.

Note that to avoid pathological situations [144], we require that a 4-curve contains at least 8 points and that a 8-curve contains at least 4 points.

2.1.2 *The connectivity paradox*

Let V be equal to the set $\mathbb{Z}^2$, and $E \subset V \times V$ be the irreflexive symmetrical binary relation such that any two points $p, q \in V$ verify $(p, q) \in E$ iff p and q are n-adjacent. We call the points of V the *vertices* and the elements of E the *edges*. We obtain this way a *graph structure* $\mathcal{G} = (V, E)$ based on the n-adjacency. These structures representing the *digital plane* supplied with the n-adjacency can be observed on Figure 2 for $n = 4$ and Figure 3 for $n = 8$.

Now, assuming that we have a set of foreground points $S \subset \mathbb{Z}^2$ that is given and which depicts a 4- or a 8-curve in $\mathbb{Z}^2$, we could hope that the Jordan Separation Theorem (seen in the introduction) holds as in the continuous world. However, when we draw a 4-curve in the digital plane supplied with the 4-adjacency as shown on Figure 4, this curve separates the digital plane into 3 components, two of them are bounded and the third is unbounded. In

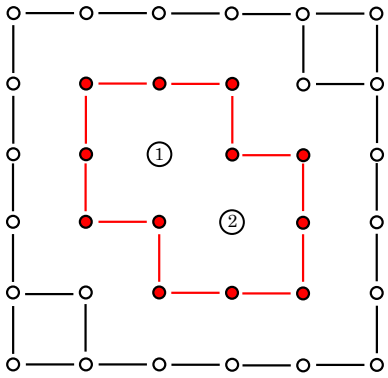

Figure 4.: The connectivity paradox using 4-adjacency

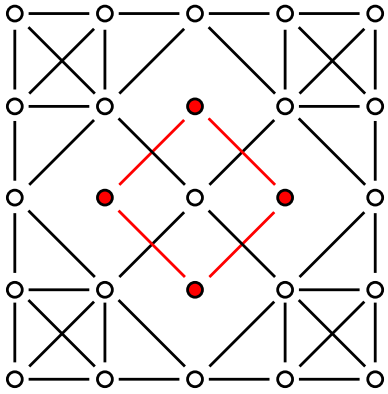

Figure 5.: The connectivity paradox using 8-adjacency

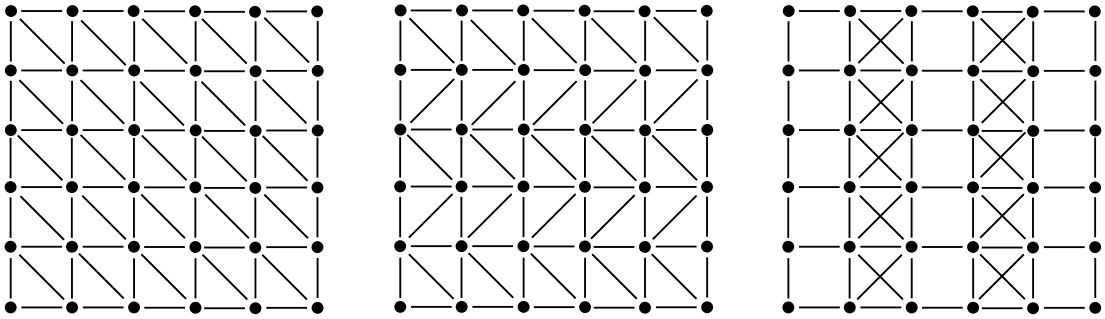

Figure 6.: Different square grids based on 6-adjacency

a certain manner, we have two "interiors". The Jordan Separation Theorem does not hold in discrete spaces using 4-adjacency.

We can also draw an 8-curve in the digital plane, as shown on Figure 5, and we obtain that the complement of the 8-curve is an only connected component. The "interior" and the "exterior" are the same component. Then the Jordan Separation Theorem fails with the 8-adjacency too.

Rosenfeld called these phenomena the *connectivity paradoxes* [150, 89, 102] and explained that this failure follows from the fact that we use the same adjacency for the foreground and the background.

Effectively, we can remark that when we use 6-adjacency, such as depicted on Figure 6, a 6-curve does not always satisfy the Jordan Separation Theorem (see Figure 7): it works using the first or second grids but not the other. Furthermore, even if these grids are regular, they are not invariant by translation or rotation. For these reasons, we will not use 6-adjacency in this thesis.

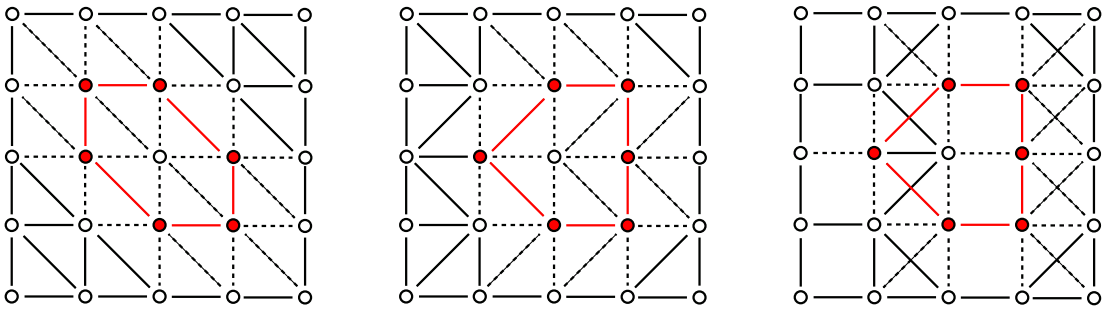

Figure 7.: A 6-curve does not always separates the digital plane even if we use 6-adjacency

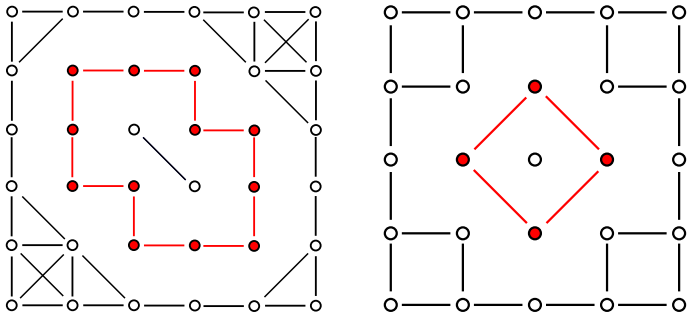

Figure 8.: $(4,8)$-adjacency on the left and $(8,4)$-adjacency on the right

2.1.3 *Dual pair of adjacencies*

Using a *dual pair of adjacencies*, as recommended in [47] for the first time, can be salutary. The $(8,4)$-adjacency, meaning that we use 8-adjacency for the foreground and 4-adjacency for the background, or the $(4,8)$-ajacency, meaning that we use 4-adjacency for the foreground and 8-adjacency for the background, make the Jordan Separation Theorem (JST) true. This is depicted on Figure 8: on the left, the 4-curve separates the plane into two 8-components, and on the right, the 8-curve separates the plane into two 4-components.

However, using a dual pair of connectivities is efficient but has a main drawback: the result depends on the chosen couple of adjacencies. In other words, we have to choose, depending on the application, one couple of adjacencies or its dual, and we are not always able to know *a priori* which couple is the most adapted to our needs and will give the expected results. Effectively, a set of connected components of a given set clearly depends on the chosen couple of adjacencies, and then the consequences can be dramatical in some applications as in *object counting* [89].

Another consequence of dual adjacencies is that we cannot attribute adjacencies to more than two colors: even if this method can be effective using binary images, we could be stuck using *multilabel images*. It seems then natural to look for another manner to make true the JST.

2.2 WELL-COMPOSED SETS AND IMAGES

Let us now recall the seminal definitions of well-composednesses.

2.2.1 *Well-composedness on $\mathbb{Z}^2$*

In 1995, Latecki *et al.* introduced in [102] a class of subsets of $\mathbb{Z}^2$ which are free from topological paradoxes like the connectivity paradoxes developed above, and which allow to obtain the same results whatever the chosen connectivities for the foregound and for the background.

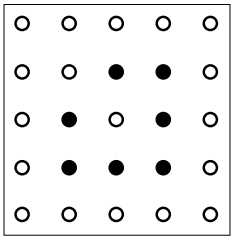

Figure 9.: A set which is weakly well-composed but not well-composed [102]

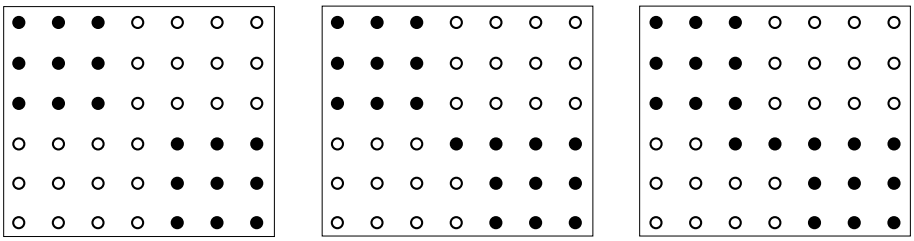

Figure 10.: The (black) sets are well-composed in (a) and (c), but the (black) set in (b) is neither well-composed nor weakly well-composed [102].

Furthermore, these sets have many nice topological properties [102]: the Jordan Separation Theorem holds for them, their Euler characteristic are locally computable (by a counting process of local patterns), the problems of irreducible thick disappear, and so on.

So, let us begin with the seminal definitions of *well-composed sets* in the digital plane $\mathbb{Z}^2$.

Definition 1 (Weakly well-composed sets [102]). *Let S be a subset of $\mathbb{Z}^2$. S is said* weakly well-composed *iff any 8-component is a 4-component.*

For example, as shown on Figure 9 [102], this set is weakly well-composed, since it is made of one 8-component (in black) which is also a 4-component. Since this definition is not *self-dual*, that is, S weakly well-composed does not imply that its complementary is well-composed, Latecki strenghtened this definition in the following manner [102]:

Definition 2 (Well-composed sets [102]). *Let S be a subset of $\mathbb{Z}^2$. S is said* well-composed *iff S and its complement S^c in $\mathbb{Z}^2$ are both weakly well-composed.*

As shown on Figure 10, the (black) set S on Subfigure (a) is made of two 8-components which are also 4-components. The set on Subfigure (c) is made of one only 8-component which is also a 4-component. At the contrary, the set on Subfigure (b) is made of one only 8-component which is made of two 4-components, and then is neither weakly well-composed nor well-composed.

Then Latecki reformulated the notion of well-composedness using *local 4-connectivity*.

Definition 3 (Local 4-connectivity [102]). *A set $S \subseteq \mathbb{Z}^2$ is said* locally 4-connected *iff the points of S in the 8-neighborhood of any point of S are 4-connected, i.e., $S \cap \mathcal{N}_8(P)$ is 4-connected for every point P in S.*

Notice that this notion is self-dual, even if the definition relies on S and not on both S and S^c.

Proposition 1 (Self-duality of local 4-connectivity [102]). *Let S be a subset of $\mathbb{Z}^2$. If S is locally 4-connected, then S^c is locally 4-connected.*

Then we come to the theorem linking local 4-connectivity to well-composedness.

Theorem 1 (Local 4-connectivity [102]). *A set $S \subseteq \mathbb{Z}^2$ is well-composed iff it is locally 4-connected.*

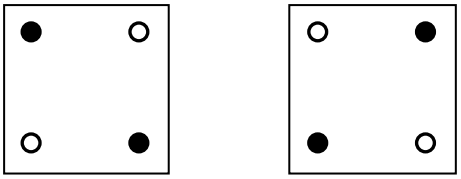

Figure 11.: Forbidden patterns into well-composed sets [102]

Using Theorem 1, it is clear that the patterns, called "critical configurations", depicted on Figure 11 and representing two points which are 8-adjacent but not 4-adjacent, cannot occur in a well-composed set.

Now, we can come to an essential proposition stating that, in well-composed sets, "the connectivities are equivalent".

Proposition 2 (Equivalence of connectivities [102]). *Let S be a well-composed subset of $\mathbb{Z}^2$. Then S is 4-connected iff it is 8-connected.*

Since a set is not always connected, Latecki generalized this proposition to any well-composed set in the digital plane.

Proposition 3 (Equivalence of connectivities [102]). *Let S be a well-composed subset of $\mathbb{Z}^2$. Then every 4-component of S is a 8-component of S and vice versa.*

Obviously, considering a digital set $X \subset \mathbb{Z}^2$ or a *binary digital image* $(\mathbb{Z}^2, X)$, such that it is the characteristic function of X, is equivalent, which means that all the theory relative to well-composed sets holds for binary images.

2.2.2 *Well-composedness on $\mathbb{Z}^3$*

As we have seen just before, a 2D well-composed set is a set such that its 8-components and its 4-components are the same. Therefore we could imagine that it is also the case for 3D sets: a subset of $\mathbb{Z}^3$ whould be well-composed iff its components are the same whatever the chosen connectivity. However it is not the case: the equivalence of connectivities in 3D is not strong enough to obtain the same nice topological properties as in the 2D case.

Let us recall what is *well-composedness* for 3D sets according to Latecki [97].

A *three-dimensional digital set* is a finite subset of $\mathbb{Z}^3$. Then, the *continuous analog* $\mathrm{CA}(p)$ of a point $p \in \mathbb{Z}^3$ is the closed unit cube centered at this point with faces parallel to the coordinate planes:

$$\mathrm{CA}(p) = \{q \in \mathbb{R}^3 \; ; \; \|p - q\|_\infty \leq 1/2\}$$

where for any $(x, y, z) \in \mathbb{R}^3$, $\|(x, y, z)\|_\infty \equiv \max\{|x|, |y|, |z|\}$.

This operator is fundamental since it allows to go from the discrete space $\mathbb{Z}^3$ to the continuous (Euclidian) space $\mathbb{R}^3$.

The *continuous analog $CA(X)$ of a digital set $X \subset \mathbb{Z}^3$* is the union of the continuous analogs of the points belonging to the set X:

$$\mathrm{CA}(X) = \bigcup_{p \in X} \mathrm{CA}(p).$$

Note that the function $\mathrm{CA} : \mathcal{P}(\mathbb{Z}^3) \to \mathcal{P}(\mathbb{R}^3)$ admits an inverse which is the (subset) digitization operator $\mathrm{Dig}_\in : \mathcal{P}(\mathbb{R}^3) \to \mathcal{P}(\mathbb{Z}^3)$ defined such that for any set $Y \subset \mathbb{R}^3$, $\mathrm{Dig}_\in(Y) = \{p \in \mathbb{Z}^3 \; ; \; p \in Y\}$. Effectively, for any $X \subset \mathbb{Z}^3$,

$$\mathrm{Dig}_\in(CA(X)) = X.$$

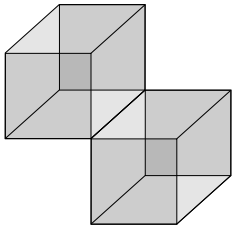

Figure 12.: The first critical pattern forbidden in 3D well-composed sets

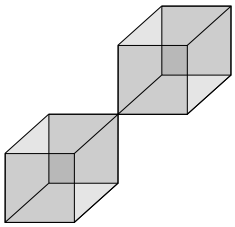

Figure 13.: The second critical pattern forbidden in 3D well-composed sets

However the inverse is not always true: $\mathrm{CA}(\mathrm{Dig}_{\in}(Y)) = Y$ iff Y is an union of unit cubes centered at points of $\mathbb{Z}^3$.

Then, we will denote $\mathrm{bdCA}(X)$ the topological boundary of $\mathrm{CA}(X)$:

$$\mathrm{bdCA}(X) = \mathrm{CA}(X) \setminus \mathrm{Int}(\mathrm{CA}(X)),$$

where $\mathrm{Int}(.)$ is the *interior operator*.

Latecki noticed in [97] that the topological boundary is equal to the *face boundary* defined as the union of the set of closed faces, that is, the unit closed squares in $\mathbb{R}^3$ which are parallel to one of the coordinate planes, each of which is the common face of a cube in $\mathrm{CA}(X)$ and a cube not in $\mathrm{CA}(X)$. For the interested reader, some additional equivalent definitions can be found in [97].

Summarily, as developed in [97, 9, 78, 149]; a point of a 3D digital set can be interpreted as a unit cube in $\mathbb{R}^3$; a digital object can be interpreted as a connected set of cubes in $\mathbb{R}^3$; and the surface of an object in $\mathbb{R}^3$ is the set of faces of the cubes that separate the object from its complement.

Definition 4 (3D well-composed sets [97])**.** *Let X be a subset of $\mathbb{Z}^3$. We say that X is a* 3D well-composed set *iff the boundary of its continuous analog* $\mathrm{bdCA}(X)$ *is a 2-manifold, that is, if for any point $p \in X$, the (open) neighborhood of p in* $\mathrm{bdCA}(X)$ *is homeomorphic to* $\mathbb{R}^2$.

Note that this definition is self-dual: for any $X \subset \mathbb{Z}^3$, $\mathrm{bdCA}(X) = \mathrm{bdCA}(X^c)$ and then X is well-composed iff X^c is well-composed.

Like for the 2D case, well-composedness can be characterized using local patterns based on adjacencies. Two points $p, q \in \mathbb{Z}^3$ are said to be *face-adjacent* iff their continuous analogs $\mathrm{CA}(p)$ and $\mathrm{CA}(q)$ share a face, that is, a unit closed square which is parallel to one of the coordinate planes, which is equivalent to say that p and q have all their coordinates equal but one which differs from one. Two points $p, q \in \mathbb{Z}^3$ are said to be *edge-adjacent* iff their continuous analogs $\mathrm{CA}(p)$ and $\mathrm{CA}(q)$ share an edge, that is, a line segment parallel to one of the coordinate axes, but not a face, which is equivalent to say that one their coordinate is equal and the other two differ from one. Two points $p, q \in \mathbb{Z}^3$ are said to be *corner-adjacent* iff their continuous analogs $\mathrm{CA}(p)$ and $\mathrm{CA}(q)$ share a point (but not an edge), which is equivalent to say that their three coordinates differ from one.

This way, Latecki [97] defined the local pattern corresponding to a set of two points that are edge-adjacent as the *first type of critical configuration* $\begin{pmatrix} 1 & 0 \\ 0 & 1 \end{pmatrix}$ (see Figure 12) and the local

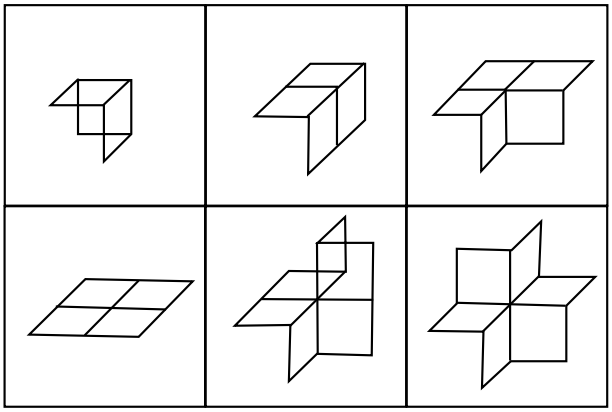

Figure 14.: The six possible configurations at a corner point in a 3D well-composed set

pattern corresponding to a set of two points that are corner-adjacent as the *second type of critical configuration* $\left(\begin{array}{cc|cc} 1 & 0 & 0 & 0 \\ 0 & 0 & 0 & 1 \end{array}\right)$ (see Figure 13). This leads to the (local) characterization of 3D well-composedness.

Proposition 4 (Characterization of 3D WC sets [97])**.** *Let S be a digital set in $\mathbb{Z}^3$. S is well-composed iff there is no occurence neither of the first nor of the second critical configurations in S or its complement in $\mathbb{Z}^3$ (modulo 90 degrees rotations and translations).*

The complete proof is in [97] (pp. 166–167). Summarily, it relies on the fact that any set containing one of these critical configurations contains a "pinch" such that at these critical locations, no point of the boundary owns an open neighborhood homeomorphic to an open disk, and then to $\mathbb{R}^2$. Conversely, if the set S does not contain any critical configuration of any type, then at each point belonging to the interior of a face, any neighborhood which is small enough will be homeomorphic to an open disk, at any point belonging to the interior of the union of two adjacent faces of the boundary sharing an edge; the neighborhood of this point is homeomorphic to an open disk (whatever if the two faces are parallel or perpendicular), and at the corners of the faces included in the boundary, only 6 configurations are possible (see Figure 14). In the six cases the corner admits a neighborhood homeomorphic to an open disk, which concludes the proof of Latecki.

However we can denote that this study has been processed case-by-case and then seems difficult to extend in higher dimensions.

Reformulated using closed surfaces, it can be said that a digital set $X \subset \mathbb{Z}^3$ is well-composed iff each connected component of the boundary of its continuous analog is a *simple closed surface*, which means that each connected component of the boundary of the continuous analog of a 3D well-composed set satisfies the *Jordan-Brouwer Separation Theorem*, stating that a simple closed surface in $\mathbb{R}^3$ separates the 3D space into two components: the interior which is bounded and the exterior which is unbounded.

Another direct consequence is that the continuous analog of any (finite) 3D well-composed set is a *bordered 3-manifold*, that is, a set $M \subseteq \mathbb{R}^3$ such that the open neighborhood $N_M(x)$ (based on the Euclidian distance) of each element $x \in M$ into M is homeomorphic to a relatively open subset of a closed half-space in $\mathbb{R}^3$.

Latecki also introduced a characterization of 3D well-composed sets using m-adjacencies. Two points are said *6-adjacent (6-neighbors)* iff their continuous analog share a face, *18-adjacent (18-neighbors)* iff their continuous analogs share a face or an edge, and *26-adjacent (26-neighbors)* iff their continuous analogs share a face, an edge, or a corner (of a unit cube centered at a point of $\mathbb{Z}^3$). For any $p \in \mathbb{Z}^3$, $\mathcal{N}_{18}(p)$ and $\mathcal{N}_{26}(p)$ correspond obviously to the set of the 18-neighbors or p and to the set of the 26-neighbors of p respectively.

Using these definitions, the following proposition holds.

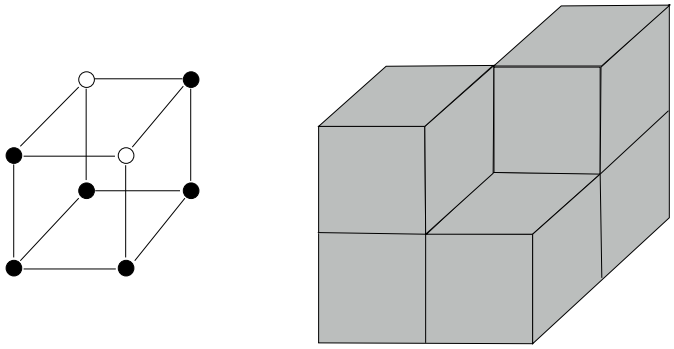

Figure 15.: The equivalence of connectivities of a set and its complement does not imply it is well-composed in 3D (p. 171 [97]).

Proposition 5 (3D WCness and adjacencies [97]). *Let X be a digital subset of $\mathbb{Z}^3$. Assume now that $X_1 = X$ and $X_0 = X^c$. Then, X is well-composed iff the two following conditions hold for $\kappa \in \{0, 1\}$:*

- *for every two 18-adjacent points x and y in X_κ, there exists a 6-path joining x to y into $\mathcal{N}_{18}(x) \cap \mathcal{N}_{18}(y) \cap X_\kappa$,*
- *for every two 26-adjacent points x and y in X_κ, there exists a 6-path joining x to y into $\mathcal{N}_{26}(x) \cap \mathcal{N}_{26}(y) \cap X_\kappa$.*

Using this proposition, we clearly understand that local 18/26-connectivities in well-composed sets imply 6-connectivity. Let us recall that for $m \in \{6, 18, 26\}$, a m-component of a set X is a greater connected subset of X based on the m-connectivity (by path).

Proposition 6 (3D WCness and 6-connectivity [97]). *Let X be a digital subset of $\mathbb{Z}^3$ and assume we use the notation of the proposition presented before. Then each 26-component of X_κ is a 6-component of X_κ, and each 18-component of X_κ is a 6-component of X_κ.*

In other words, 3D well-composed sets (and their complement in $\mathbb{Z}^3$) have their connectivities equivalent. However, it is important to notice that the converse is not always true: there exist non-well-composed 3D sets such that the set of their 26-components is the same as the set of their 6-components and such that the set of the 26-components of their complementary is the same as the set of the 6-components of the complementary. For that, see the set $\left(\begin{array}{cc|cc} 0 & 1 & 1 & 1 \\ 1 & 0 & 1 & 1 \end{array}\right)$ depicted on Figure 15.

2.2.3 *Well-composedness on $\mathbb{Z}^n$*

In [100], Latecki generalized the notion of well-composedness to digital sets in discrete spaces $\mathbb{Z}^n$ of dimension n, with n a integer greater than or equal to 2.

The *continuous analog* of a point $p = (p_1, \ldots, p_n) \in \mathbb{Z}^n$ is the Cartesian product:

$$\mathrm{CA}((p_1, \ldots, p_n)) = [p_1 - 1/2, p_1 + 1/2] \times \cdots \times [p_n - 1/2, p_n + 1/2],$$

which can also be reformulated in this equivalent manner:

$$\mathrm{CA}(p) = \{q \in \mathbb{R}^3 \; ; \; \|p - q\|_\infty \leq 1/2\}.$$

Then it follows that as before the *continuous analog* $\mathrm{CA}(X)$ *of a set* $X \subset \mathbb{Z}^n$ is the union of the continuous analogs of the points of the set X, and the topological boundary of this set in $\mathbb{R}^n$ is called for short $\mathrm{bdCA}(X)$.

Now let us recall some basics about topology in Euclidian spaces: we call *n-dimensional bordered manifold* a subset of $\mathbb{R}^n$ such that each point in it admits a neighborhood which is

homeomorphic to a relatively open subset of a closed half-space in $\mathbb{R}^n$, and such that this set is not a n-manifold without boundary. Each connected component of a n-dimensional bordered manifold is called a *n-dimensional surface*.

Then Latecki defined in [100] (p. 99) *well-composedness* for sets in n-D spaces using the notion of bordererd manifolds as well:

Definition 5 (n-D WCness [100]). *Let $X \subset \mathbb{Z}^n$ be a digital set. X is said to be* well-composed *iff* $\mathrm{CA}(X)$ *is a n-dimensional bordered manifold.*

For this reason, well-composed sets are sometimes called *digital bordered manifolds* [100].

This can be reformulated with an equivalent definition using only the boundary of the continuous analog:

Definition 6 (n-D WCness [100]). *Let $X \subset \mathbb{Z}^n$ be a digital set. X is said to be well-composed iff* $\mathrm{bdCA}(X)$ *is a $(n-1)$-dimensional manifold (without boundary).*

The equivalence of these two definitions follows from the fact that a set which is an union of n-dimensional cubes is an n-dimensional bordered manifold iff its boundary is a $(n-1)$-manifold.

Let us notice that a manifold has not to be connected, contrary to surfaces, and then a well-composed set has not to be connected.

Even if Latecki defined well-composedness for n-D, its main works about well-composedness [102, 97, 100, 49, 73, 99, 98, 101, 157, 158, 165, 166] focus on 2D and 3D sets (on regular cubical grids).

2.2.4 *Well-composed segmented digital images*

We can mention the existence of *segmented digital images* [100] which are $(k+2)$-uples:

$$(\mathbb{Z}^n, X_0, X_1, \ldots, X_k),$$

such that $X_i \cap X_j = \emptyset$ for $0 \leq i < j \leq k$ and each $X_i \subseteq \mathbb{Z}^n$ is finite or its complement X_i^c is finite for $i \in [\![0, k]\!]$. Then a segmented digital image is said *well-composed* iff each set X_i for $i \in [\![0, k]\!]$ is well-composed.

For example, an usual binary image $(\mathbb{Z}^n, X)$ is a particular case of segmented digital image, where $\mathbb{Z}^n$ is partitioned into only two components, the foreground and the background.

Let us recall that the union of two different sets extracted from a well-composed segmented digital image is generally not well-composed, because the well-composedness is not preserved by the union operator.

2.2.5 *Complementing the framework in 2D and in 3D*

In [102], Latecki asserted that a 2D digital set which is well-composed cannot contain neither the pattern $\begin{pmatrix} 1 & 0 \\ 0 & 1 \end{pmatrix}$ nor its 90 degrees rotation because a well-composed set is locally 4-connected. But it was not clear that a set which does not contain any of these patterns was well-composed. In 2000, he finally confirmed this intuition using Theorem 1 (p. 101 of [100]).

Proposition 7. *Let $S \subseteq \mathbb{Z}^2$ be a digital set. X is well-composed (in the sense of Definition 6) iff its continuous analog* $\mathrm{CA}(X)$ *does not contain the* critical configurations *depicted on Figure 16.*

In other words, this set is well-composed iff the (local) patterns $\begin{pmatrix} 0 & 1 \\ 1 & 0 \end{pmatrix}$ and $\begin{pmatrix} 1 & 0 \\ 0 & 1 \end{pmatrix}$ do not occur in S.

Thanks to the self-duality of these local patterns, this definition is self-dual.

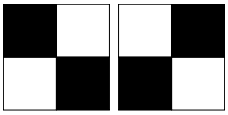

Figure 16.: The two forbidden critical configurations in the continous analog of 2D well-composed sets

Then Latecki asserted that, in 2D, Definition 6 and Definition 2 of well-composed sets are equivalent:

Proposition 8 (Equivalence of connectivities of 2D WC sets [100])**.** *A set $X \subset \mathbb{Z}^2$ is well-composed (in the sense of Definition 6) iff every 8-component of X is a 4-component of X and every 8-component of X^c is a 4-component of X^c.*

All these definitions of 2D well-composedness are then equivalent.

In the 3D case, as stated by the Proposition 5 in [100] (p. 105), a digital set $X \subseteq \mathbb{Z}^3$ is well-composed in the sense of Definition 6 iff the critical configurations of type one or two do not occur in neither $\mathrm{CA}(X)$ not $\mathrm{CA}(X^c)$.

Some propositions in [100] have to be noticed since they rely on the equivalence of connectivities at a local level.

Proposition 9. *A digital set $X \subset \mathbb{Z}^2$ is well-composed iff for every two points $x, y \in X$ such that they are 8-adjacent, there exists $z \in X$ such that z is 4-adjacent to both x and y.*

Thanks to the topology of the plane, it is equivalent to say that for every two points $x, y \in X^c$ such that they are 8-adjacent, there exists $z \in X^c$ such that z is 4-adjacent to both x and y, which simplifies Proposition 9. However, in 3D, Latecki observed that:

Proposition 10. *A digital set $X \subset \mathbb{Z}^3$ is well-composed iff the following conditions hold for $\kappa \in \{0, 1\}$ (we recall that $X_0 = X^c$ and that $X_1 = X$):*

- *for every two 18-adjacent points but not 6-adjacent $x, y \in X_\kappa$, there exists a point z in X_κ that is 6-adjacent to x and y,*
- *for every two 26-adjacent points but not 18-adjacent $x, y \in X_\kappa$, there exists a 6-path in X_κ joining x and y into $\mathcal{N}_{26}(x) \cap \mathcal{N}_{26}(y) \cap X_\kappa$.*

In this case, the property has to be true in both cases, that is, for X and X^c.

2.2.6 *Well-composed gray-level images in 2D*

As we have seen before, a 2D digital (binary) image [100] (p. 102) is a 4-uple $(\mathbb{Z}^2, X, k, l)$ where X is a subset of $\mathbb{Z}^2$ such that either X or X^c is finite. X corresponds to the *foreground* and is associated to the k-adjacency, and $X^c \equiv \mathbb{Z}^2 \setminus X$ corresponds to the *background* of the image and is associated to the l-adjacency. To avoid the connectivity paradox, the couple (k, l) is generally a dual pair of adjacencies. Equivalenty, this image can be interpreted as the characteristic function of the set X in $\mathbb{Z}^2$, that is, a mapping I from $\mathbb{Z}^2$ to $\{0, 1\}$ such that $I(p) = 1$ if $p \in X$ and $I(p) = 0$ if $p \in X^c$.

A 2D gray-level image is then a couple $I = (\mathbb{Z}^2, u)$ where $u : \mathbb{Z}^2 \to [\![0, 255]\!]$ (or more generally from $\mathbb{Z}^2$ to any finite set supplied with a total order relation) is a mapping from $\mathbb{Z}^2$ to $[\![0, 255]\!]$. This image I is generally identified with its mapping u since these two concepts are equivalent.

Then we can apply a very straightforward operation called *binarization* of a gray-level image relatively to a given threshold. Given a gray-level image $u : \mathbb{Z}^2 \to [\![0, 255]\!]$ and a threshold $\lambda \in \mathbb{Z}$, the resulting *binarization* of u relatively to λ is equal to the binary image $u_{\mathrm{bin}} : \mathbb{Z}^2 \to \{0, 1\}$ defined for any $p \in \mathbb{Z}^2$ such that $u_{\mathrm{bin}}(p) = 1$ if $u(p) \geq \lambda$ and $u_{\mathrm{bin}}(p) = 0$ if $u(p) < \lambda$.

Now that we have defined what is a binarization of a gray-level image, we can recall the seminal definition of *well-composed 2D gray-level images* of Latecki [100]:

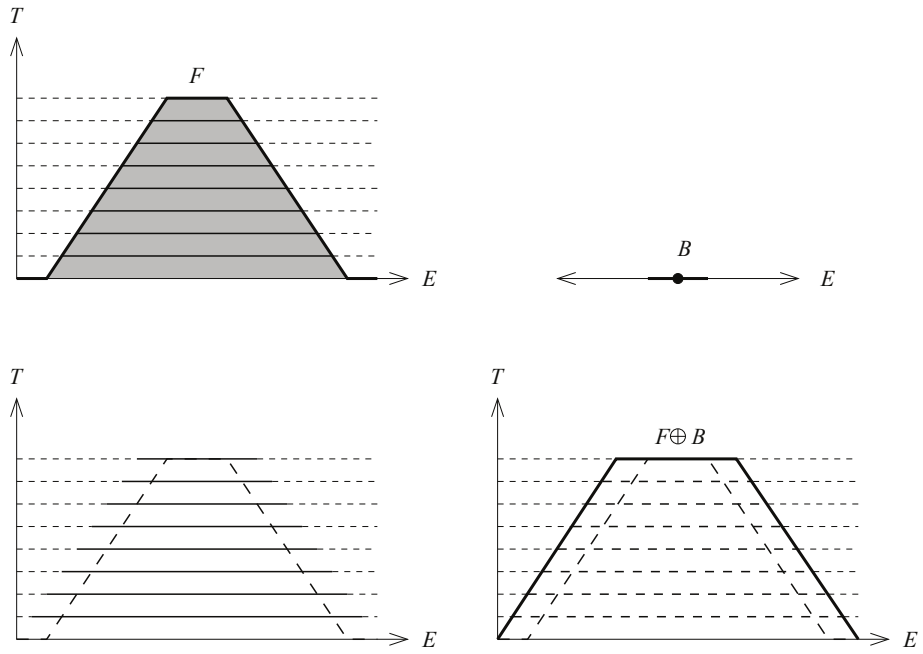

Figure 17.: The flat extension of the dilation operator (p. 869 [25])

Definition 7. *A gray-level image is said* well-composed *iff for every threshold, its binarization results in a binary well-composed image.*

Latecki introduced also a characterization of 2D well-composed gray-level images, which shows how much the different binarizations are intercorrelated.

Proposition 11 ([100])**.** *A gray-level image $I = (\mathbb{Z}^2, u)$ is well-composed iff for any restriction of u to a 2×2 square, denoted by $\begin{pmatrix} a & b \\ c & d \end{pmatrix}$, the diagonal intervals have a non-empty intersection:*

$$[\min(a,d), \max(a,d)] \cap [\min(b,c), \max(b,c)] \neq \emptyset.$$

We will see later how much this characterization is powerful, useful, and how it can be extended to n-D gray-level images.

Note that this notion of binarization by a given threshold comes from *cross-section topology* [121, 21, 18, 17] and is also much used in mathematical morphology [25, 152, 77, 76, 140], because this interpretation of an image gives access to many powerful operators on gray-level images that can be obtained using a very simple procedure as depicted on Figure 17: starting from a set operator ϕ, we decompose the image by computing its binarizations, we apply on each binarization the operator ϕ, and then we use a *stacking* procedure to obtain the resulting image $\phi^T(u)$. This way, an operator on gray-level images has been computed/defined.

2.2.7 *Well-composedness on arbitrary grids in 2D*

According to Wang and Battacharya [178], we can extend the definition of well-composedness coming from the rectangular grids to arbitrary grids in 2D in the following manner. We assume that we have a (locally finite) arbitrary grid system of (closed) pixels paving the topological space $\mathbb{R}^2$ such that the boundary of each pixel is a Jordan curve, as depicted on Figure 18.

A set X of pixel in then said *well-composed* iff for any point p belonging to the boundary of X, the set of pixels of X containing p is *edge-connected* [178], which means that for any two pixels in this set, there exists a sequence of pixels of this set going from the first to the second such that two consecutive elements share an edge. Figure 18 depicts a well-composed set in dark gray: at each boundary point p of X, the set made of the pixels containing p in X is edge-connected (the edge shared by the two pixels is in blue).

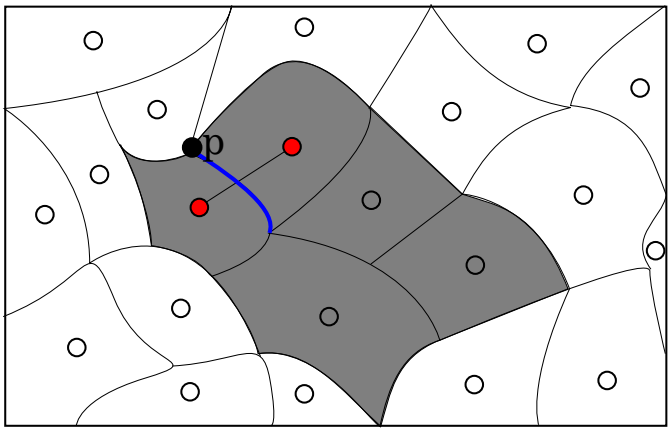

Figure 18.: Definition of 2D well-composedness on 2D arbitrary grids

Effectively, in the case of rectangular pixels, we obtain that a set X is well-composed in the sense of Latecki [102] iff 8-connectivity (vertex-connectedness) implies 4-connectivity (edge-connectedness).

A particular grid system is the hexagonal grid where every set of pixels is well-composed [178], which is obviously not the case of the rectangular grid.

Serra and Kiran [155] worked on this last topic: $\mathbb{R}^n$ is partitioned into a set of regular open sets, called a *tessellation*, and the complement in $\mathbb{R}^n$ of its union, called the *net*. In this framework [155], they recall an observation of Fedorov [56] which states that the only possible tessellations (inherited from a Voronoï grid system) such that its elements are identical (up to a translation) are in 2D the square and the hexagonal grid systems, and in 3D the cube, the hexagonal prism, the truncated octahedron[1], and the two elongated and rhombic dodecahedra.

Among them, only the hexagonal grid system and the truncated octahedron verify that any two elements of the tessellation, such that their adherence intersect, share a face of dimension $(n-1)$, *i.e.* an edge in 2D and a (2D) face in 3D. In other words, any (finite) set of elements of these tessellations is *strongly adjacent*: there exists a small open disk/ball in 2D/3D such that any intersection of adherences of two adjacent elements of X contains this disk/ball.

Then the link between the works of Wang and Battacharya [178] and Serra and Kiran [155] is straightforward: the strong adjacency is similar to well-composedness on arbitrary grids but the difference relies on the fact that strong adjacency is based on open sets and that well-composedness on arbitrary grids is based on closed sets.

Furthermore, if we consider a tessellation and an arbitrary grid system which are *isomorphic* in the sense that they have the same topological structure up to a closure/opening, every subset of this tessellation which is strongly adjacent has its isomorph in the arbitrary grid system which is well-composed, and conversely. For this reason, these definitions seem "equivalent".

We could easily extend the definition of well-composedness of Wang and Battacharya on a (locally finite) arbitrary grid in n-D such that boundaries of the *voxels* covering $\mathbb{R}^n$ are *connected* $(n-1)$*-manifolds* (see [72, 112, 92, 3] for complements about the Jordan-Brouwer theorem in n-D). Then, we could say that any set X of voxels is *well-composed on an arbitrary grid in* $\mathbb{R}^n$ iff for any face f of dimension $k \in [\![0, n-1]\!]$ belonging to the boundary of X, the set Y of voxels of X containing f (respectively the set Y' of voxels not in X and containing f) are *face-connected*, which means that for any two voxels in this set Y (respectively Y'), there exists a sequence of voxels of this same set going from the first to the second such that two consecutive elements share a face of dimension $(n-1)$.

Note that self-duality in the n-dimensional case is ensured because of the double condition, the first relative to X and the second relative to the complement of X (see Figure 19).

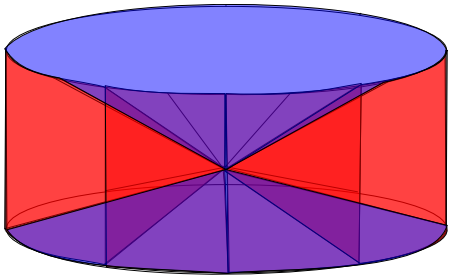

Figure 19.: A set X where the set of voxels in X (in red) containing the boundary point p (at the center of the cylinder) is face-connected and such that the set of voxels in the complement of X (in blue) is not face-connected.

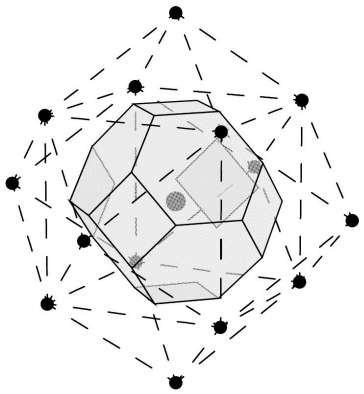

Figure 20.: A truncated octahedra (p. 13 [118])

This way, we obtain that, in the grid system made of truncated octahedra (see Figure 20) covering $\mathbb{R}^3$, every set of voxels is well-composed. Effectively, as stated by L. Mazo in his thesis [118], two voxels in such a grid system share either a face of dimension 2 or nothing. This means that two voxels which belong to a set X and which are connected in this set X are face-connected in this same set X, and that the converse is true for X^c. This way, every set in such a space is well-composed.

This adjacency is known as $2(2^n - 1)$ adjacency in n-D (6-adjacency in 2D, 14-adjacency in 3D, and so on), but shows a strong anisotropy on the graph of the covered domain [118].

2.2.8 *Well-composedness on cell complexes in* $\mathbb{R}^n$

As defined in Stelldinger's book [163], a *cell complex in* $\mathbb{R}^n$ is a set of *convex polyhedra* in $\mathbb{R}^n$, called *cells*, such that every face of each cell belongs to this complex, and such that for any two faces of the complex, their intersection is a common face of both these two faces.

The *dimension* of a cell is the maximum number of contained independent vectors after translating the cell so that it covers the origin, and a cell of dimension $m \geq 0$ is called a *m-cell*. The *dimension* of a cell complex is the maximal dimension of its cells.

Two cells of a complex are said *m-ajdacent* if their intersection is a m'-cell with $m' \geq m$. Two cells are *adjacent* iff they are adjacent for some m. They are *incident* iff they are adjacent and of different dimensions (then one cell is subset of the other). A *complete cell complex of dimension* m is a cell complex where each cell of dimension $m' < m$ is incident to at least one cell with dimension m.

1 The Voronoï polyhedron of a body-centered cubic grid, also called *BCC grid* [167] is well-known for its guarantees in matter of topology preservation.

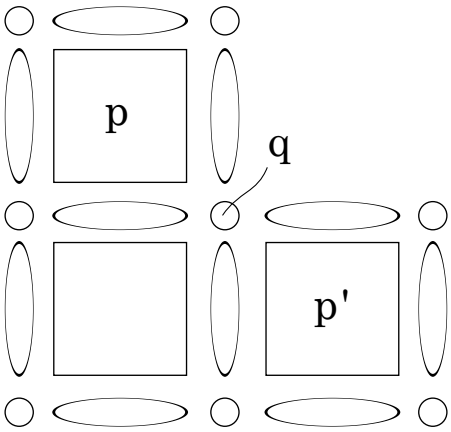

Figure 21.: A cell complex which would not be well-composed according to Stelldinger [163]

A cell complex is called *well-composed* if it is complete, of dimension n, and if any two adjacent n-cells are $(n-1)$-adjacent. A set in $\mathbb{R}^n$ is said *well-composed* iff there exists a well-composed cell complex such that the union of its cells is equal to this set.

According to Stelldinger [163], this definition extends the ones of Latecki [97, 100] and Wang and Bhattacharya [178] for arbitrary cell complexes in any dimension.

However, it seems that the cell complex such as depicted on Figure 21 made of three edge-connected unit squares depicting a "L", plus their faces, depicts a cell complex which would be well-composed according to Latecki, since the boundary of the complex is a simple closed curve. However it would not be well-composed according to Stelldinger, since this set contains two squares p and p' which share a vertex q, and then are adjacent, but which do not share any edge. The definition of Latecki and Stelldinger seems then not to be equivalent.

2.2.9 *Well-composedness in Alexandrov spaces in n-D*

Well-composedness exists also in *Alexandrov spaces*, that is, topological spaces that verify the $T0$ separation axiom and that are *discrete spaces* (these notions are detailed is Chapter C).

Effectively, let $\mathcal{X}$ be a finite subset of an Alexandrov space $\mathcal{A}$, then this set is said to be *well-composed* iff its topological boundary $\mathfrak{N} = \alpha(\mathcal{X}) \cap \alpha(\mathcal{A} \setminus \mathcal{X})$, where α is the *closure operator*, is a disjoint union of *discrete surfaces* [91, 53].

Based on cross-section-topology, Najman and Géraud [127] extended this notion from sets to *plain maps* (see Section C.19 for further details) using *threshold sets*. Let $U : \mathcal{A} \rightsquigarrow \mathbb{R}$ be a plain map, then for any $\lambda \in \mathbb{R}$, the following sets:

$$
\begin{aligned}
[U \trianglerighteq \lambda] &= \{ z \in \mathcal{A} \mid \exists v \in U(z), v \geq \lambda \}, \\
[U \triangleright \lambda] &= \{ z \in \mathcal{A} \mid \forall v \in U(z), v > \lambda \}, \\
.[U \triangleleft \lambda] &= \{ z \in \mathcal{A} \mid \forall v \in U(z), v < \lambda \}, \\
[U \trianglelefteq \lambda] &= \{ z \in \mathcal{A} \mid \exists v \in U(z), v \leq \lambda \}.
\end{aligned}
$$

are called *threshold sets* of U. Then, a plain map is said *well-composed* iff its threshold sets are well-composed.

As we will see later, we renamed this definition into "well-composedness in the sense of Alexandrov" or "AWCness", to differentiate it from well-composedness on $\mathbb{Z}^n$.

Two main approaches exist to make a set or an image well-composed on a cubical grid: *topological reparations* and *well-composed interpolations*.

The first one is called *topological reparation*, because we consider that we give back to the objects in the image the topological properties they had before the digitization process; mainly, digitized objects should have a boundary which is a $(n-1)$-manifold.

The second approach correspond to *interpolations*, since their restriction to the initial domain is then assumed to be exactly the initial image. However, without constraints, there is no guarantee that the interpolation has the same topology as the initial image. For example, the 1D image • • represents two connected pixels, valued at 1. One non-constrained interpolation can then be • ◦ •, where ◦ denotes a pixel valued at 0. The two black points are then disconnected. For this reason, we will consider only what we call *in-between interpolations*, that is, interpolations such that the secondary pixels have values that are between the values of the primary pixels. They have the property not to create new extrema in the image when the interpolation is done. This way, in-between interpolations preserve the topology of the initial image.

2.3.1 *Topological repairing on cubical grids*

Digital images resulting from a convenient digitization of a manifold should be well-composed, assuming that the digitization procedure preserves the topology of the initial object. Effectively, real objects, or most of them, have a boundary which is a (topological) manifold.

However, it is well-known that it is not always the case in image processing: the choice of digitization is not always adapted, the resolution of the digitization can be too large, and so on. Moreover, it has been shown [166] that even using digitization by intersection, which results in well-composed images in 2D for a sufficient resolution [73], does not provide bordered 3-manifolds by reconstruction using cubical voxels, whatever the chosen resolution.

It seems then useful to know how to make digital images well-composed in n-D if we want to give back to the objects the property such that their boundary is a manifold. Latecki [98, 100] called this procedure "topological repairing", and introduced the first method in 2D able to do it. As usual, the ones correspond to the object/foreground and the zeros to the background. His method proceeds then by changing the zeros where critical configurations occur into the binary initial image into ones. Also, depending on the neighborhood surrounding the critical configuration and the possible propagation of the critical configuration, a different method is chosen to eliminate the critical configurations in this neighborhood. This method is translation-invariant and 90 degrees rotation invariant, and guarantees that the number of modifications is minimal.

Then, Siqueira *et al.* [157, 158] proposed a 3D randomized method which makes any 3D binary image well-composed in the sense that the boundary of the continuous analog of the resulting object (made with cubical voxels) will be a 2-manifold. Since no assumption is made on the topology of the initial object, no topological equivalence is ensured, but a theoretical bound ensures that the maximal number of new critical configurations which will appear during the elimination of the m initial configurations is lower than or equal to $m/2$.

Siqueira *et al.* [157, 158] also developed an algorithm able to make 3D multilabel images well-composed following this same principle of "topological repairing".

TOPOLOGICAL REPAIRING OF CUBICAL COMPLEXES Gonzalez-Diaz *et al.* [67] introduced in 2011 a method able to topologically repair a cubical complex associated to a 3D binary digital image into a polyhedral complex which is homotopy equivalent and well-composed, that is, whose boundary is a 2-manifold. The polyhedron of the geometric realization of the boundary of this interpolation is then made of simple closed surfaces in $\mathbb{R}^3$, on which cohomological information [70, 69, 64, 65, 68] is computable. The proposed (local) method

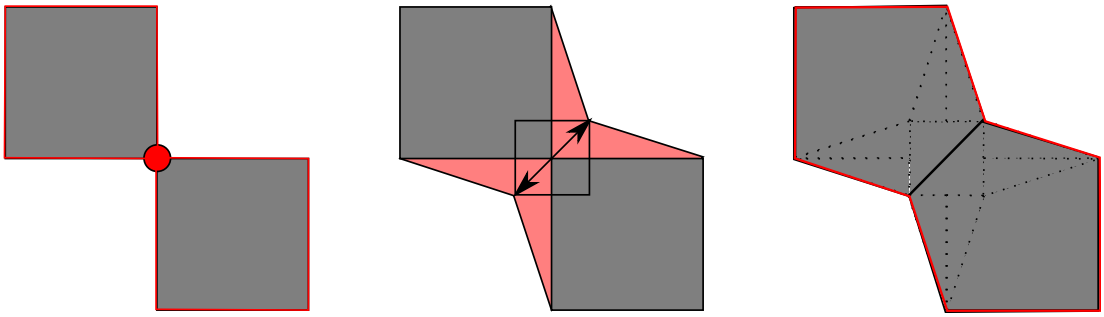

Figure 22.: The equivalent in 2D of the repairing method of Gonzalez-Diaz *et al.*

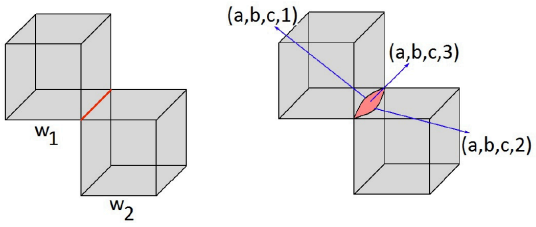

Figure 23.: Repairing of a complex containing a critical edge [67]

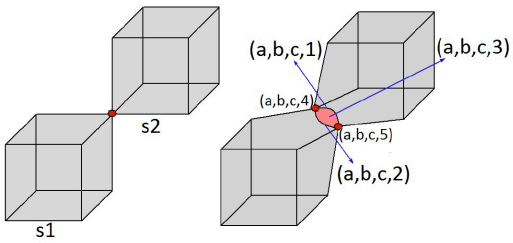

Figure 24.: Repairing of a complex containing a critical vertex [67]

is homotopy preserving, such that the resulting cohomological informations can be used to recognition or characterization tasks.

Their method would be this way in 2D: on a 2D cubical complex, as shown on Figure 22, the aera of the surface of each "critical point" would be "increased" such that there is no more pinch into the boundary of the complex (in dark gray), which would lead to a 2D well-composed polyhedral complex (in dark grey too) whose boundary (in red) is made of simple closed curves.

In 3D, the *critical faces* in the complex, that is, the faces in the combinatorial structure corresponding to the pinch in to the geometrical realization, are "stretched" such that the pinch disappears: Figure 23 shows how a critical edge shared by two edge-adjacent cubes w_1 and w_2 is replaced by a face of dimension 2 plus two bordering edges, and Figure 24 shows how a critical vertex, shared by to vertex-adjacent cubes s_1 and s_2, is replaced by a combinatorial structure made of one 2-face, two bordering edges, and their common vertices. More complicated structures are used to repair the other problematic configurations (see Figure 25). Note that this method is not self-dual.

An efficient coding of this family of polyhedral complexes, called *ECM representation* [63, 66] and using 3D images has been developed to store this family of repaired and well-composed complexes into images.

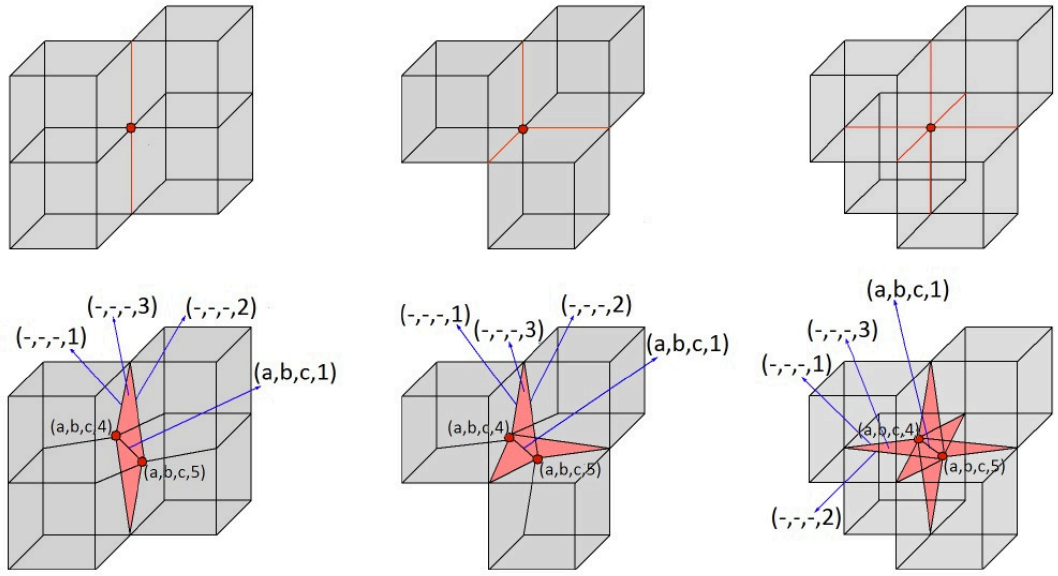

Figure 25.: Repairing of more complex forbidden configurations [67]

Figure 26.: Differents configurations using Majority Interpolation [165]

2.3.2 *Well-composed interpolations*

In 1998, Rosenfeld, Kong and Nakamura [148] developed the first well-composed 2D interpolation, that is a method able to compute an image on a larger domain than that of the initial

image, such that its restriction to the initial domain equals the original image and such that the resulting interpolation is well-composed.

This method can be decomposed in two steps. First an *image magnification* [148], which is equivalent to replacing each pixel of the original image by a set of $(k+1) \times (k+1)$ pixels (where $k \geq 1$ is given) of the same value and which replaces the original pixel. Secondly, a modification step removes the critical configurations of the magnified image by changing one of the values of the 4 points of the critical configuration (from 0 to 1 or the converse). Since the magnification process and the modifications are *simple deformations* [148], they preserve the topology (in the sense that the two images have the same adjacency tree and actually the same homotopy type), and then the final image is a well-composed image topologically equivalent.

Then in 2000, Latecki [100] developed an alternative method to make a 2D binary image well-composed. This new method is based on the *image expansion* of Köthe [93], and consists of doubling the resolution of the square grid of the initial image by adding new pixels (the so-called "secondary" pixels) between the original pixels (the "primary" pixels). A secondary pixel added between two edge-connected pixels will take the value of these primary pixels iff they have the same value. In the contrary case, they will be labeled as "boundary points". A secondary pixel added at the center of a square of 4 vertex-connected pixels will take the value of these pixels iff they all have the same value. In the converse case, they will be labeled boundary points. Finally, we obtain 3 sets, a set of zeros, a set of ones, and a set of boundary points, each of them being well-composed.

We can denote the difference between these two first algorithms: the one of Rosenfeld *et al.* is based on simple deformations, so it ensures topological equivalence, but the one of Latecki is based on a "counting process", which ensures well-composedness but no topological equivalence.

Then in 2006, Stelldinger proposed a method called *Majority Interpolation* [165], shown on Figure 26, which can be seen as a slightly modified 3D extension of the method of Latecki [100], since it is based on a similar counting process. The resulting binary image is always well-composed in the sense that the resulting boundary in the interpolated image is a 2-manifold, but this method is not self-dual.

In 2000, Latecki [100] developed the first gray level well-composed interpolation method in 2D. Starting with the same image expansion as the one used for the binary interpolation, the new pixels are valued based on bilinear interpolation: a pixel added between 2 primary pixels is valued at the mean of these two pixels, and at the center of a square of primary pixel, the new pixel is set a the mean of the values of these 4 pixels if the restriction of the image to these four pixels was well-composed, and at the median of these same values either.

This last method has been slightly modified by Géraud [60] in 2015 where the new pixels added at the center of a square of 4 pixels is always the median of these four primary pixels, since the median is always the good solution in 2D to make an image well-composed. This method does not create any extrema.

We can notice that these gray-level interpolation methods are self-dual in the sense that they do not overemphasize bright components of the dark ones, nor the converse. The counterpart of this powerful property is that the initial images having a integer-based value space, the value space of the new images is $\mathbb{Z}/4$ for the method of Latecki and $\mathbb{Z}/2$ for the method of Géraud.

As we noticed in [28], extending 2D well-composed interpolations to n-D is not so easy when we want to ensure self-duality using a local interpolation with usual constraints. Effectively, Mazo [119] developed a method able to interpolate any image in n-D into a well-composed one, based on the connectivity function where $\varepsilon = 1$ correspond to the *max interpolation* and $\varepsilon = -1$ corresponds to the *min interpolation*. Even if this method is initially for binary images defined on Khalimsky grids, its extension to $\mathbb{Z}^n$ and to gray level images is well-known and frequently used. However this method is not self-dual, contrary to the one we are going to present in this thesis in a next chapter.

Figure 27.: A reconstruction based on cubical grids in 3D leads to critical configurations [166]

2.4 TOPICS RELATED TO WELL-COMPOSEDNESS

Now let us see the numerous topics in image processing and mathematics that are related to well-composedness.

2.4.1 *About digitization of regular images*

In image analysis, many real objects are assumed to be smooth. More exactly, they are assumed to be closed in $\mathbb{R}^2/\mathbb{R}^3$, to have a compact boundary, and such that at each point of their boundary, their tangent line/plane are well-defined [73]. This way, these subsets of $\mathbb{R}^2/\mathbb{R}^3$ are *r-regular*, that is, there exists a value $r > 0$ such that, at each point of their boundary, they admit an inside (respectively an outside) open *osculating disk/ball* of radius greater than or equal to r lying entirely in this set (respectively its complementary). This class of sets has been introduced in 1982 [137, 154] and then used by Latecki *et al.* [101, 98, 102] and by Tajine and Ronse [170].

Then, by *digitization*, some topological properties may be preserved depending on the chosen digitalization (as the *subset digitization* [98], the *Gauss digitization*, the *intersection digitization*, the *threshold-based digitization*, and so on). This also depends on the chosen *reconstruction method* following the digitization process used to reproduce the shape of the original object as good as possible thanks to *continuous analogs* like Voronoï cells, cubes, or balls (centered at the voxels of the digitization and *tessellating* $\mathbb{R}^n$).

Then, the real object and its reconstruction can be homeomorphic (in the sense of the topological equivalence of Pavlidis [137]), or *homotopy equivalent*, or they can have the same *homotopy tree*, they can bee *strongly r-similar* (that is their *morphing distance* [164] is lower than or equal to r), and so on.

A set $X \subset \mathbb{Z}^n$, $n \in \{2,3\}$, is said to be *well-composed* iff its reconstruction using unitary centered cubic voxels has a boundary which is made of a 1-manifold in the 2D case, and is made of a 2-manifold in the 3D case. In other words, manifoldness of the boundary of a real-object is preserved iff its digitization is well-composed, assuming that we used unitary centered cubes for the reconstruction step.

Let be an object in $\mathbb{R}^2$. Now let us assume that $\mathbb{R}^2$ is tessellated with squares of diameter $r > 0$ such that the barycenters of the squared pixels whose interior intersect this object are set at 1 and the barycenters of the other pixels are set at 0. This procedure is called *2D digitization by intersection*, and its *digitization step* is equal to r. According to Gross and Latecki [73], digitizations by intersection of r-regular objects are well-composed sets when using a digitization step lower than or equal to r. This way, manifoldness of the object is preserved using this digitization.

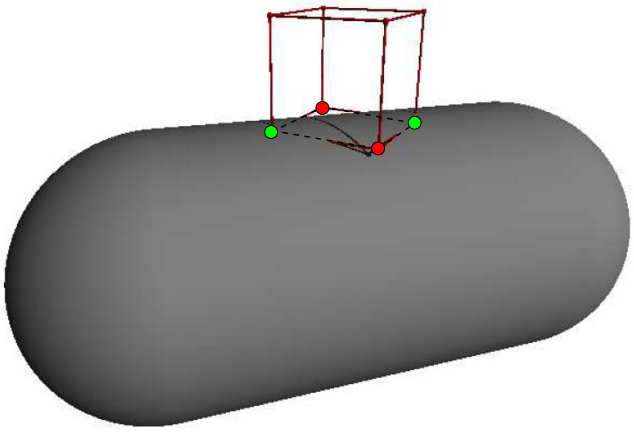

Figure 28.: Even the digitization of a smooth bordered 3-manifold can contain a 2D critical configuration [166]: the two red points at the bottom of the cube lie outside the object when the two green points at the bottom of the cube lie inside the object, which leads to a 2D critical configuration by digitization.

In 3D, it has been shown by Stelldinger *et al.* in [166, 164] that using cubical grids, whatever the regularity of the initial object and the digitization step, we cannot ensure that the reconstructed object is well-composed (see Figure 27).

Effectively, even digitizations of very regular objects can contain some particular configurations, the famous "critical configurations" of Latecki, which result in pinches in the reconstruction using cubic centered voxels (see Figure 27). The same reasoning can be extended to greater dimensions.

Since r-regularity is a very strong constraint, we could imagine that some other kinds of geometric/topological constraints could allow to obtain well-composedness; however it has been shown than r-regularity is a very good assumption to model real objets, since it is a necessary and sufficient condition for many topology preserving theorems [164].

The only possibility seems then to be to change either the grid where the digitization is realized (1), or the digitization itself (2), or the reconstruction procedure (3). In the first case, we can refer to the works of Stelldinger and Strand [167] which show that any digitization on a *body-centered-cubic* (BCC) or *face-centered-cubic* (FCC) grid ensures topology preservation if the digitization is dense enough, and then that the boundary of the reconstruction is a 2-manifold. In the second case, only the 2D digitization by intersection seems promising yet to ensure well-composedness, while the other digitizations do not give any guarantees. In the third case, many efficient techniques exist and ensure that the resulting boundary is a manifold whatever the given input (see Figure 29: *majority interpolation* [165], *ball union* [166], the *Marching Cubes algorithm* [113] (under some constraints), the *trilinear interpolation* [166], the *smooth surface representation* [166]. Note that this list may be not exhaustive.

2.4.2 *Rigid transformations and preservation of well-composedness*

In the continuous world, topological properties are preserved by *rigid transformations*, that is, compositions of a translation and a rotation. They are much used in *remote sensing* [161], *medical imaging* [138, 151], *image registration* [12], and *image warping* [55]. This is not anymore the case in the discrete world [132, 133]: starting from a binary image defined on a square grid, it is often mandatory to discretize the result of a continuous rigid transformation of this image since its domain must belong to $\mathbb{Z}^2$ (see Figure 30).

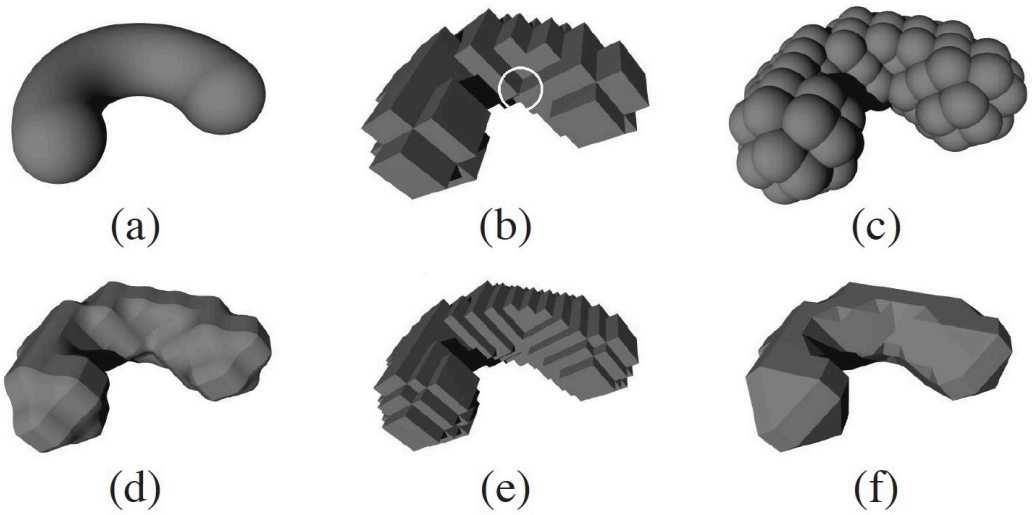

Figure 29.: A r-regular object and its reconstructions [166]: (a) the r-regular object, (b) its reconstruction using a cubic $\frac{r}{2}$-grid, (c) ball union, (d) trilinear interpolation, (e) Majority Interpolation, (f) MMC (modified marching cubes).

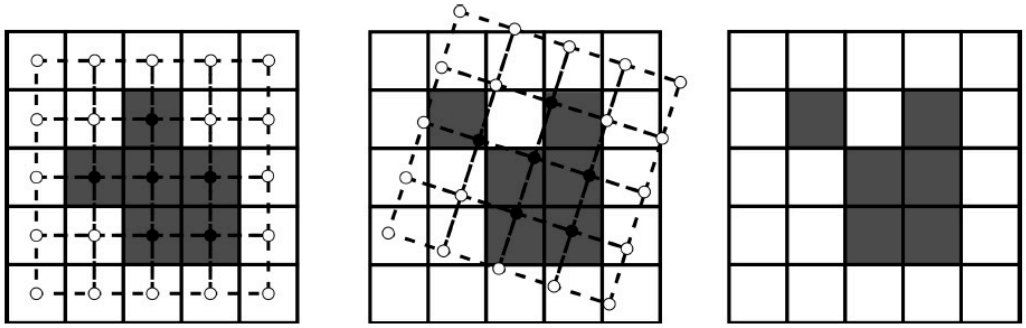

Figure 30.: An image and its rigid transformation [135]

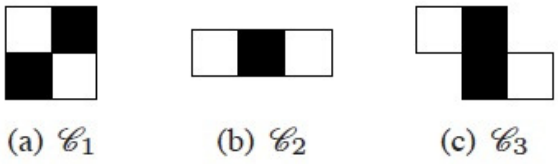

Figure 31.: Forbidden pattern in regular images [135]

This results in the loss of digital topological properties, especially based on connectivities, like the well-composedness or the adjacency tree [141] (a tree-based representation of the nested relationship between the connected components in the image), which is no longer isomorphic to the one of the original image. This way, the two images cannot be topologically equivalent [148].

Fortunately, Ngo *et al.* [135, 134] proved that if the initial image is *regular* (a criterion based on some forbidden patterns described on Figure 31) including the usual critical configurations of Latecki [102]), then the resulting rigid transformation is well-composed and the adjacency trees of the two images are isomorphic. In that sense, they are "topologically equivalent".

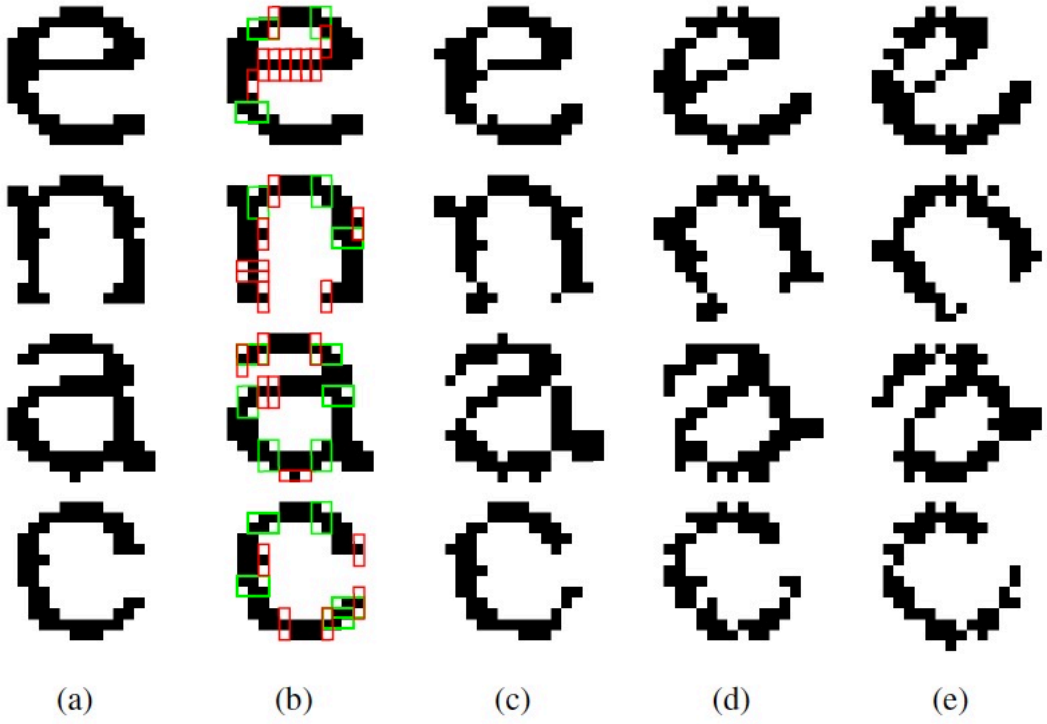

Figure 32.: Patterns that are completely destructured by the rigid transformation [134]

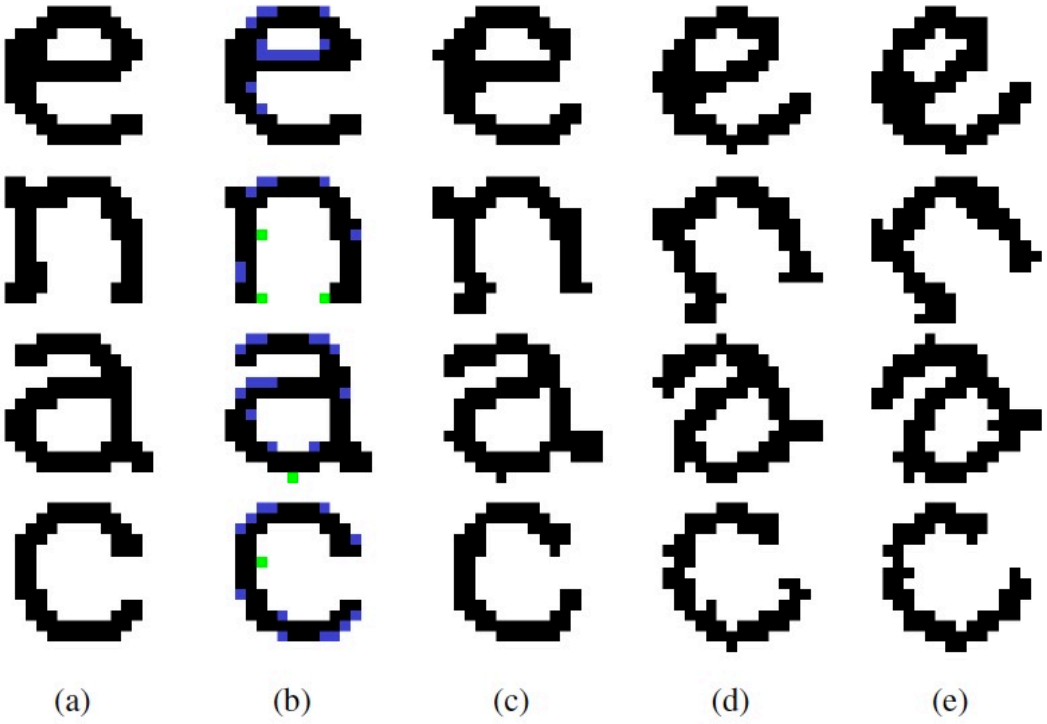

Figure 33.: Modified patterns whose topology is preserved under the rigid transformation [134]

Making regular any image is then straightforward, using for example a super-resolution strategy [135] able to make any well-composed image regular. Figure 32 shows letters whose topology is lost under rigid transformation due to the local critical patterns depicted in red:

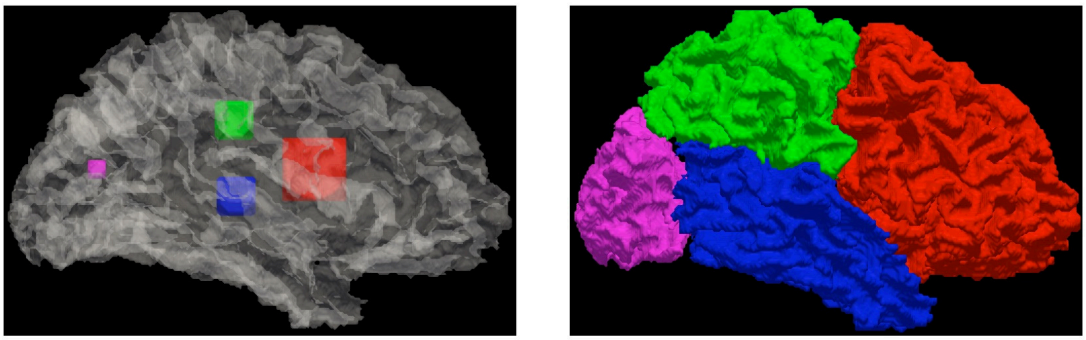

Figure 34.: From seeds to well-composed regions

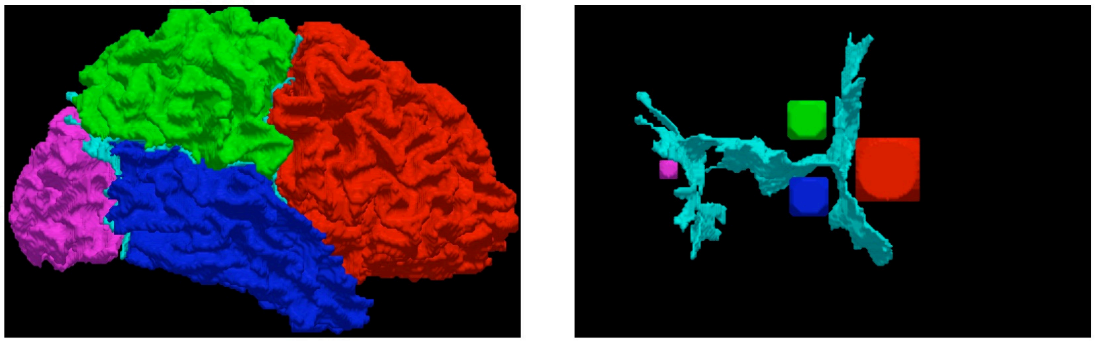

Figure 35.: Glamorous glue applied to regions results in a well-composed region

4-connected components are decomposed into several other 4-connected components, and the 8-components corresponding to the holes are merged with the background. Figure 33 shows the same letters, modified such that no critical pattern occurs, the rigid transformation preserves well-composedness and the adjacency tree. Nowadays, no result about the 3D case has been published.

2.4.3 *Front propagation and well-composed segmentations*

Among the family of topology constrained front propagation methods [33, 6, 169, 103, 75, 153], the works in [75] and in [153] rely on *simple points* [16, 89, 14], that is, points such that their addition or removal to the component will not change the topology of the image. They start from initial seeds distributed in the areas of interest in the space of the image, and then modify these (connected) components by adding/removing simple points. It can also be interesting to use *multisimple points* [153], that is points such that their addition/removal do not create/delete handles in the image.

Tustison proposed in [172] a new method based on two simultaneous criteria: the preservation of the topology, but also the preservation of the well-composedness [102, 97, 98] of the seeds. This procedure is based on the identification using *topological numbers* [19] of points, which preserve the well-composedness and the topology of the image: these *topological well-composed points* are then the only points allowed to be added to the front to make it evolve. This results in a set of connected components and in an interface which are well-composed (see Figure 34): the adjacency relations are then (4,4) in 2D and (6,6) in 3D.

Since the interface between two near components will satisfy the Digital Jordan Separation Theorem [130, 98] (DJST) thanks to their well-composedness, these components can be iteratively *glued* together by adding elegantly the part of the Jordan surface separating them to constitute a final segmentation which is well-composed (see Figure 35). Then, they can be visualized using the MC algorithm [113]: the use of the CCMC (Connectivity-Consistent Marching Cubes) algorithm [74] generally used to resolve the ambiguous cases is not required anymore.

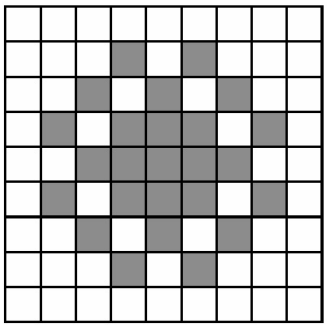

Figure 36.: The irreducible thick configuration [8]

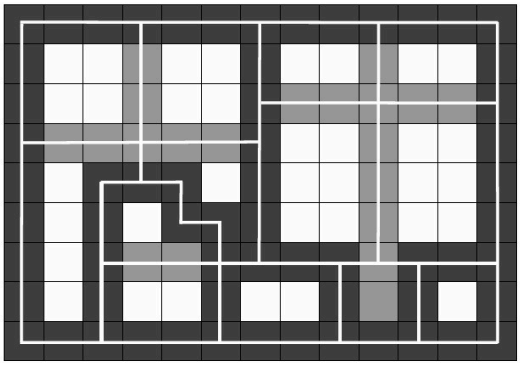

Figure 37.: An irreducible gray-level well-composed image and its crest network [116]

2.4.4 *Thin topological maps thanks to well-composedness*

A discrete image can be seen as the digitization of a piecewise continuous function. This way, we can represent the underlying piecewise continuous function of a discrete image using a topological map where faces correspond to the smooth regions and where the contours made of edges and vertices correspond to the discontinuities of this underlying function. Note that this representation using faces, edges and vertices is not new [58, 94]. However, *consistency problems*, like the "irreducible thick configuration" of [8] on Figure 36 or [17, 89], are encountered when we work on cubical grids in this context: there is then no guarantee that the extracted crest network is thin.

To obviate this problem, Marchadier *et al.* [116] propose to use well-composedness [102, 18, 100] to avoid the connectivity problem and to obtain a coherent topological map where the resulting *crest network* [116] is thin. The proposed method is the following. Starting from a given 2D grayscale image, they compute the gradient that they make well-composed using some topological repairing method [116]. Then they apply a *leveling method* of Bertrand [17] which combines the well-composed-preserving thinning of Latecki [102] and deletion of the *peaks*, to obtain finally an *irreducible well-composed gray level image* (see Figure 37).

In fact, we can see this resulting image as a *watershed transform* [20, 126, 128, 139] of the gradient of the initial image. Effectively, the *quasi-minima* of this gradient represent the *catchment bassins*. Then, by a case-by-case study, a thin crest network is computed on the complement of these quasi-minima, using a linking method [121, 45], with no ambiguities since this image is well-composed. This way, Marchadier obtains a coherent topological map [29, 57] (see Figure 38) representing the underlying piecewise continuous function of the given discrete image.

Figure 38.: The initial image, the reduced gradient, and the resulting watershed [116].

2.4.5 *Locally computable Euler characteristic thanks to well-composedness*

The *Euler number/characteristic* [89] or *genus* is a topological invariant used in many applications [114, 179]: *computer graphics*, *image analysis*, object counting, *visual inspection* [108, 183], *license plates characters and numbers recognition tasks* [1], and *real-time thresholding* [159].

A subset X of the plane or of the 3D space is said to be *simplicial* iff it is expressible as a finite union of vertices (0-faces), edges (1-faces), triangles (2-faces), and tetrahedra (3-faces). We also say that C is the *simplicial decomposition* of X. The *Euler characteristic* is defined by the following axioms:

- $\xi(\emptyset) = 0$,
- $\xi(S) = 1$ if S is non-empty and convex,
- for any simplicial sets S^1, S^2, $\xi(S^1 \cup S^2) = \xi(S^1) + \xi(S^2) - \xi(S^1 \cap S^2)$,

and does not depend on the triangulation C of X.

According to [171, 89], the *(face) Euler number* of the simplicial set S can be formulated such that:

$$\xi(S) = n_0 - n_1 + n_2 - n_3,$$

where n_k, $k \in [\![0,3]\!]$, denotes the number of k-faces in the simplicial decomposition. Note that the value of the face Euler number depends on the chosen connectivity [171].

By the *Euler-Poincaré Formula*, we obtain the formula of the *volume Euler number*:

$$\varepsilon = b_0 - b_1 + b_2,$$

where b_k is the *k-dimensional Betti number*. In fact, b_0 equals the number of connected components of the object, b_1 equals the number of holes in all these components, and b_2 equals the number of cavities in all these components. For a given binary image F, the sum of the volume Euler numbers of all connected components in F is called the *volume Euler number* of the image F.

In fact, in the case of a planar simplicial set, the Euler characteristic is equal to the number of connected components minus the number of holes, which permits to define easily the Euler characteristic of a 2D image where the continuous analog of the ones is represented by its corresponding planar simplicial set, which is always possible on a rectangular grid for a digital, and then finite, set (which is detailed hereafter).

Assume that any 2D binary digital (m,n)-image P, where (m,n) belongs to $\{(4,8),(8,4)\}$, is given, and that we define, as in [89], C_0 as the black point set in the image, C_1 as the union of the black segments whose endpoints are m-adjacent black points. If $(m,n) = (4,8)$ (respectively if $(m,n) = (8,4)$), we define C_2 as the union of the unit squares (respectively the $(1,1,\sqrt{2})$ triangles) whose sides are contained in C_1. Then we obtain $C(P) = C_0 \cup C_1 \cup C_2$,

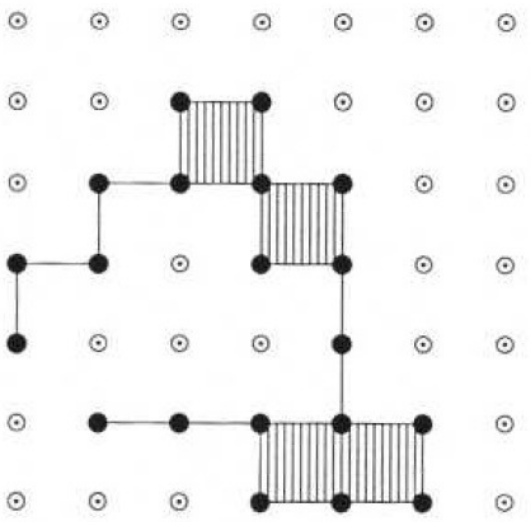

Figure 39.: Simplicial set of a $(4,8)$ digital picture whose Euler characteristic is equal to 1

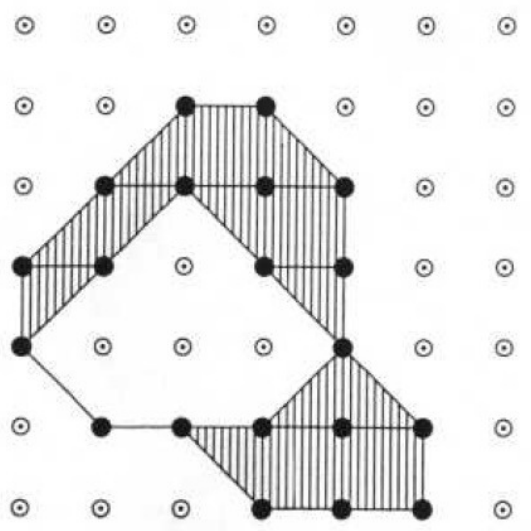

Figure 40.: Simplicial set of a $(8,4)$ digital picture whose Euler characteristic is equal to 0

that is, the simplicial set of the image P. The Euler characteristic of P is then obtained by computing the number of connected components of $C(P)$ minus the number of holes in $C(P)$.

Figure 39 and Figure 40 depict two binary images with the same set of points. Figure 39 depicts an image whose Euler characteristic is equal to one, when Figure 40 depicts an image whose Euler characteristic is equal to zero. Effectively, the Euler characteristic depends on the chosen connectivity. For this reason, if the given digital picture is well-composed, the choice of the adjacencies does not import, and the Euler characterisitic is unique.

Furthermore, it has been observed that using dual adjacencies on arbitrary binary digital image, this characteristic can be computed locally [136, 90] by an enumeration of some local patterns (see also [71, 162] for different approaches). Since using any pair of dual adjacencies on a well-composed image leads to the same result, Latecki deduced then in [102] that the Euler characteristic is also locally computable on well-composed sets. This results in much faster algorithms, which shows one more time powerfulness of well-composedness.

The 3D case is obviously also important and have been treated in [35, 46, 34, 176, 48, 22, 104]. In particular, in [105], the used method is local.

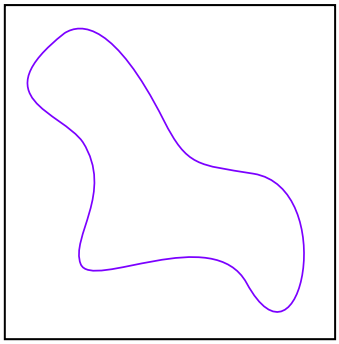

Figure 41.: A simple closed curve in $\mathbb{R}^2$ is a Jordan curve

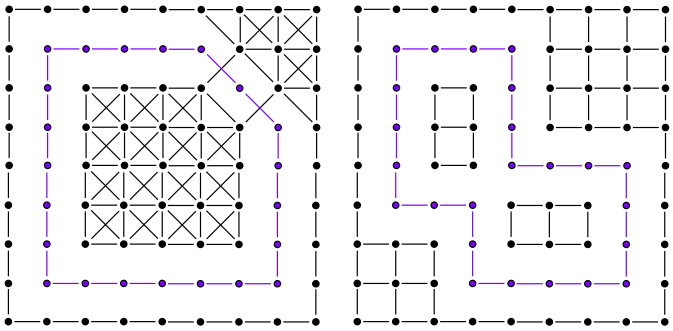

Figure 42.: 8-curves and 4-curves are not always Jordan curves in $\mathbb{Z}^2$

Benefits of well-composedness come mainly from the fact that the number of possible configurations is reduced, and then the calculus is simplified and computation is faster.

2.4.6 *Well-composed Jordan curves separate the plane*

The Jordan Separation Theorem [131] (JST) states that a simple closed curve S in the continuous plane $\mathbb{R}^2$ separates this plane into two components, a bounded part that we call the "interior" and a unbounded part that we call the "exterior", and that this curve is the common boundary of these two parts (see Figure 41). In this case, S is said to be a *Jordan curve*. However it is well-known that when we work into the discrete analog of the plane, like on *rectangular grids*, we loose some topological properties of the continuous world.

For example, a simple closed curve based on *digital connectivity* [71, 81, 124, 125, 141, 145, 147, 146, 185], does not always separate the space into two components anymore: Figure 42 shows on the left a curve based on the 8-connectivity and on the right a curve based on the 4-connectivity; none of them separates the digital plane $\mathbb{Z}^2$.

In fact, this is related to the connectivity paradox of Rosenfeld [150], developed in Subsection 2.1.2, which can happen when we choose the same connectivity in $\mathbb{Z}^n$ for a set and its complement. To obviate this problem, we can use dual pair of connectivities, and then we obtain the Digital Jordan Separation Theorem [168, 144, 142, 143] which states that a *digital 4-connected simple closed curve* (whose each point has two 4-neighbors in the curve) separates the plane into two 8-connected components. Conversely a *digital 8-connected simple closed curve* (whose each point has two 8-neighbors in the curve) separates the plane into two 4-components.

Another way to obviate the connectivity paradox is to use *well-composed simple closed curves*, for which 4-connectivity and 8-connectivity are equivalent: in this manner, no ambiguity is possible and the connectivity paradox cannot occur anymore. Figure 43 shows an example of well-composed simple closed curve, which is then a Jordan curve in the sense that it separates the digital plane into two components.

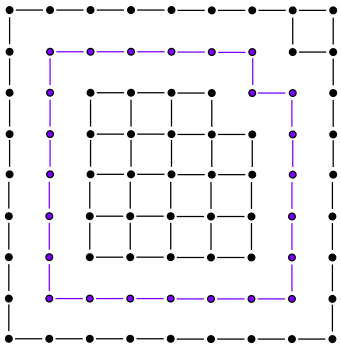

Figure 43.: A well-composed curve is always a Jordan curve in $\mathbb{Z}^2$

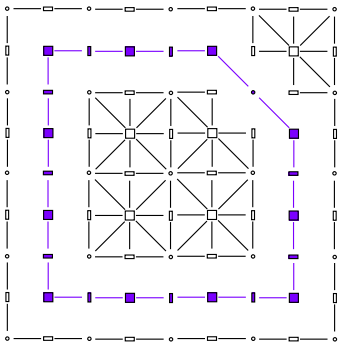

Figure 44.: A simple closed curve in $\mathbb{H}^2$ is a Jordan curve

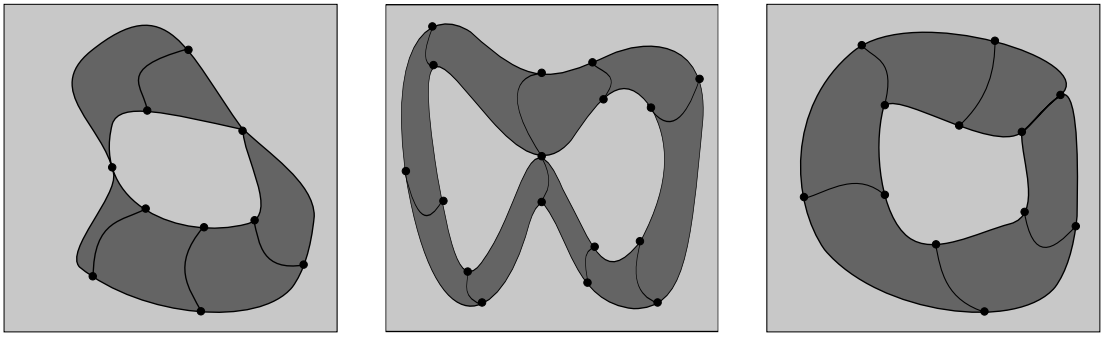

Figure 45.: Different kinds of simple closed curves according to Wang and Battacharya

Note that another way to preserve the separation property proper to the plane is to work in *Khalimsky Grids* [85, 86, 87] (see Figure 44), where simple closed curves, also called 1-*surfaces* [91, 53], separate the Khalimsky grid $\mathbb{H}^2$. However in this case, the neighborhood of a point in $\mathbb{H}^2$ depends on its coordinates, and then the grid structure of $\mathbb{H}^2$ is different from the usual ones of $\mathbb{Z}^2$.

On arbitrary grids, Wang and Battacharya [178] proposed an interesting generalization of the DJST, considering that two pixels are *direct edge-connected* if they share an edge, *direct vertex-connected* if they share a vertex, and *direct mix-connected* if they share an edge or a vertex. This way, their equivalent of the Jordan Separation Theorem on arbitrary grids is the following: a finite *edge-connected* simple closed curve (of pixels) separates the plane into two mix-connected (respectively edge-connected) components. Furthermore, a *well-composed simple closed curve* (of pixels) in the sense of [178], that is, such that *(direct) vertex-connectedness* implies *(direct) edge-connectedness*, separates $\mathbb{R}^2$ into two edge-connected components. Figure 45 shows on the left a mix-connected simple closed curve, separating the plane into two edge-connected parts, the curve in the middle is an edge-connected simple closed curve separating the plane into two mix-connected components, and on the right, we can see a well-composed simple closed

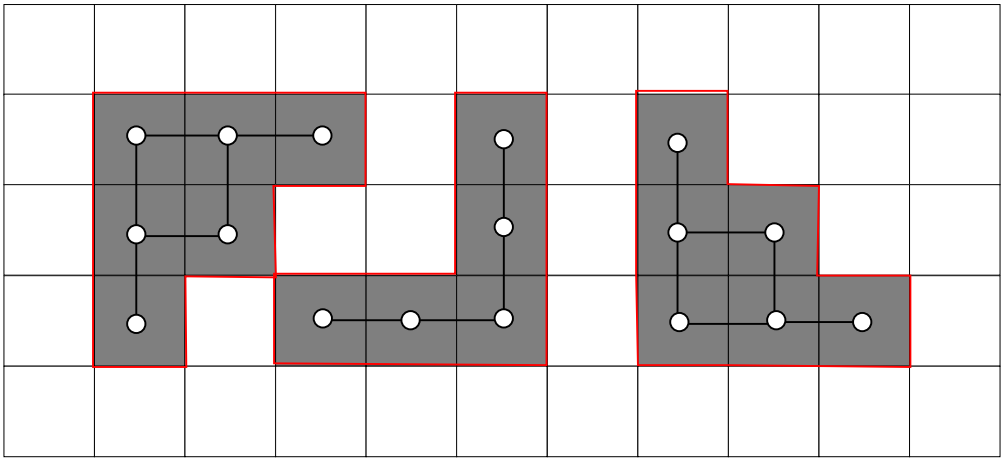

Figure 46.: The continuous analog of a set which is not well-composed

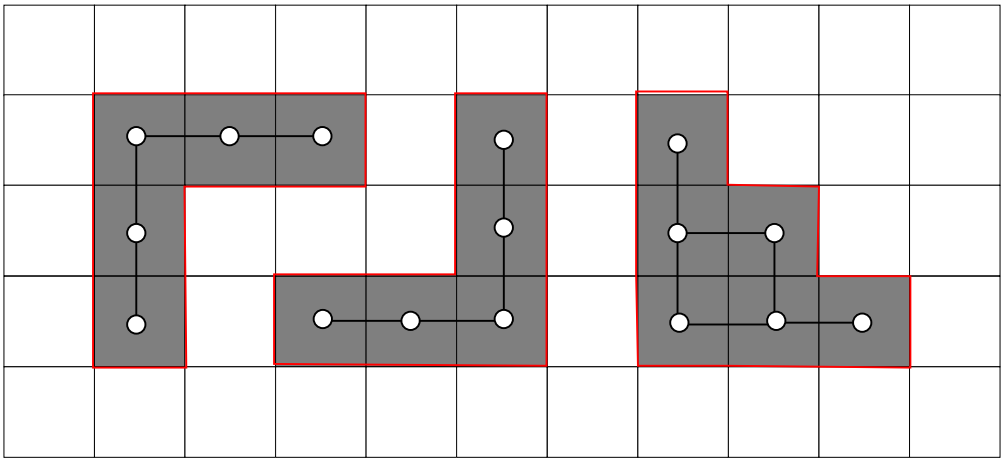

Figure 47.: The continuous analog of a well-composed set

curve which separates the plane into two components, whatever the chosen connectivity. Well-composedness is then used here to give back to the JST the "natural" topological property verified in the continuous plane.

2.4.7 *Jordan separation theorem and well-composedness*

Well-composedness is deeply related to *Jordan curves* and *Jordan surfaces*.

We recall that the *Jordan curve theorem* [82, 13, 173, 23] (resp. the *Jordan-Brouwer Separation theorem* [3, 72, 112, 92]) states that a simple closed curve (resp. a simple closed surface) in the continuous plane $\mathbb{R}^2$ (resp. in the continuous space $\mathbb{R}^3$) separates the plane (resp. the space) into two components, one which is bounded, called the *interior*, and one which is unbounded, called the *exterior*, and that their common boundary is this curve (resp. this surface). In the first case, we call it a *Jordan curve*, and in the second case, we call it a *Jordan surface*.

Effectively, as stated in [100], it is equivalent to say that a 2D subset X of $\mathbb{Z}^2$ is *well-composed* or to say that the boundary of its *continuous analog* is a 1-manifold, which means that it is made of disjoint simple closed curves. Figure 46 shows a set which is not well-composed, since one of the connected components of its boundary is not a simple closed curve, and Figure 47 shows a well-composed set, since each connected component of its boundary is a simple closed curve.

Note that the fact that a simple closed curve is well-composed is different from the fact that the boundary of a 2D set is a simple closed curve. The first concept is a property of

well-composed curves as a set (in this case, the whole set is a Jordan curve), when the second correspond to the property of any boundary of any 2D well-composed set (in this case, the Jordan curves are the boundaries).

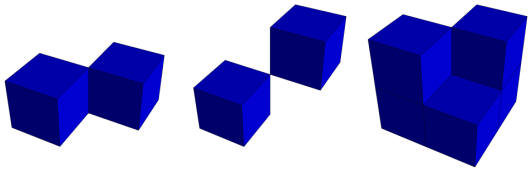

Figure 48.: Non-Jordan surfaces

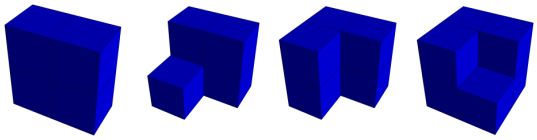

Figure 49.: Jordan surfaces

Also, a digital 3D set $X \subset \mathbb{Z}^3$ said *well-composed* [97, 100] iff the boundary of its continuous analog is a 2-manifold, that is, is made of disjoint simple closed surfaces, which strongly relates the Jordan-Brouwer separation theorem to well-composedness. Figure 48 shows the boundaries of continuous analogs which are not Jordan surfaces, and Figure 49 shows at the contrary boundaries of continuous analogs of well-composed sets which are then 2-manifolds.

3 GENERALIZATION OF WELL-COMPOSEDNESS TO DIMENSION n

In this chapter, we expose our contributions in matter of well-composedness. In particular, we explain how we renamed the different kinds of well-composednesses: since they are not always equivalent, this justifies the terminology we introduced to differentiate them. Also we will study how they are related, and how we propose to extend these definitions to gray-level/real-valued images. We will also show how we propose to characterize real-valued digitally well-composed images in n-D, extending the 2D characterization of Latecki in [100]. We will end with the computation of the complexity of this verification process, able to check if an image is digitally well-composed or not. Note that the dimension $n \in \mathbb{N}^*$ of the space we are working in is assumed to be greater than or equal to 2 and finite.

3.1 THE DIFFERENT FLAVOURS OF n-D WCNESSES IN BRIEF

As we have seen in Section 2.2, Latecki introduced in 2D well-composedness for sets such that a set is well-composed iff its connectivities are equivalent, that is to say, such that we have the same sets of components whatever the chosen connectivity for this set and its complement in $\mathbb{Z}^2$. However, in 3D, the definition of well-composedness is not the natural extension of the 2D one: a 3D set is said well-composed iff the boundary of the continuous analog is a 2-manifold. This is a stronger condition since it implies that a 3D set and its complement in $\mathbb{Z}^n$ have their connectivities equivalent, but the converse is not true (see Figure 15). Furthermore, alternative definitions of well-composednesses appeared in 1997 in 2D arbitrary grids [178], in 2008 in [163] in the cellular complexes, and in 2013 in [127] in Alexandrov spaces (like the *Khalimsky grids*). Since in our case, we were mainly interested in cubical grids, we renamed these definitions and properties in the following manner:

- A digital set $X \subset \mathbb{Z}^n$ is said *EWC* or *well-composed based on the equivalence of its connectivities* iff any $(3^n - 1)$ component of X (respectively of X^c) is a $2n$-component and *vice versa*.

- A digital set $X \subset \mathbb{Z}^n$ is said *CWC* or *well-composed in the continuous sense* iff the (topological) boundary of its continuous analog is a $(n-1)$-manifold.

- A digital set $X \subset \mathbb{Z}^n$ is said *DWC* or *well-composed in the digital sense* iff it does not contain any *k-D critical configuration*, with $k \in [\![2, n]\!]$.

- A digital set $X \subset \mathbb{Z}^n$ is said *AWC* or *well-composed in the Alexandrov sense* iff the connected components of the topological boundary of its immersion $\mathcal{IMM}(X)$ in the Khalimsky grids $\mathbb{H}^n$ are discrete $(n-1)$-surfaces (see Chapter D for more details). By identification, we will say equivalently that $\mathcal{IMM}(X)$ is AWC or that X is AWC.

Notice that we did not take into account well-composedness on arbitrary grids or arbitrary cellular complexes, since we are mainly interested in cubical grids. Also, we generalized these notions to n-D, since we focus on n-D signals, $n \geq 2$.

Let $n \geq 2$ be a (finite) integer called the *dimension*. Now, let $\mathbb{B} = \{e^1, \ldots, e^n\}$ be the (orthonormal) canonical basis of $\mathbb{Z}^n$. We use the notation x_i, where i belongs to $[\![1, n]\!]$, to determine the i^{th} coordinate of the vector $x \in \mathbb{Z}^n$. We recall that the L^1*-norm* of a point $x \in \mathbb{Z}^n$ is denoted by $\|.\|_1$ and is equal to $\sum_{i \in [\![1,n]\!]} |x_i|$ where $|.|$ is the *absolute value*. Also, the L^∞*-norm* is denoted by $\|.\|_\infty$ and is equal to $\max_{i \in [\![1,n]\!]} |x_i|$.

For a given point $x \in \mathbb{Z}^n$, the $2n$*-neighborhood* in $\mathbb{Z}^n$ is noted $\mathcal{N}_{2n}(x)$ and is equal to $\{y \in \mathbb{Z}^n \ ; \ \|x - y\|_1 \leq 1\}$. In other words,

$$\mathcal{N}_{2n}(x) = \{x\} \cup \{x - e^1, x + e^1, \ldots, x - e^n, x + e^n\}.$$

The *starred* $2n$*-neighborhood* of $x \in \mathbb{Z}^n$ is noted $\mathcal{N}^*_{2n}(x)$ and is equal to $\mathcal{N}_{2n}(x) \setminus \{x\}$. An element of the starred $2n$-neighborhood of $x \in \mathbb{Z}^n$ is called a $2n$*-neighbor* of x in $\mathbb{Z}^n$.Two points $x, y \in \mathbb{Z}^n$ such that $x \in \mathcal{N}^*_{2n}(y)$ or equivalently $y \in \mathcal{N}^*_{2n}(x)$ are said to be $2n$*-adjacent*.

For a given point $x \in \mathbb{Z}^n$, the $(3^n - 1)$*-neighborhood* in $\mathbb{Z}^n$ is noted $\mathcal{N}_{3^n-1}(x)$ and is equal to $\{y \in \mathbb{Z}^n \ ; \ \|x - y\|_\infty \leq 1\}$. In other words, $\mathcal{N}_{3^n-1}(x)$ equals:

$$\left\{ x + \sum_{i \in [\![1,n]\!]} \lambda_i e^i \ ; \ \lambda_i \in \{-1, 0, 1\}, \forall i \in [\![1, n]\!] \right\}.$$

The *starred* $(3^n - 1)$*-neighborhood* of $x \in \mathbb{Z}^n$ is noted $\mathcal{N}^*_{3^n-1}(x)$ and is equal to $\mathcal{N}_{3^n-1}(x) \setminus \{x\}$. An element of the starred $(3^n - 1)$-neighborhood of $x \in \mathbb{Z}^n$ is called a $(3^n - 1)$*-neighbor* of x in $\mathbb{Z}^n$. Two points $x, y \in \mathbb{Z}^n$ such that $x \in \mathcal{N}^*_{3^n-1}(y)$ or equivalently $y \in \mathcal{N}^*_{3^n-1}(x)$ are said to be $(3^n - 1)$*-adjacent*.

Let x, y be two points in $\mathbb{Z}^n$ and X be a subset of $\mathbb{Z}^n$. A $2n$*-path* (respectively a $(3^n - 1)$*-path*) joining x to y into X is a finite sequence $(p^0 = x, p^1, \ldots, p^{k-1}, p^k = y)$ such that for any $i \in [\![0, k]\!]$, p^i belongs to X, and such that for any $i \in [\![0, k - 1]\!]$, $p^{i+1} \in \mathcal{N}^*_{2n}(p^i)$ (respectively $p^{i+1} \in \mathcal{N}^*_{3^n-1}(p^i)$). Such paths are said to be of *length* k.

A subset X of $\mathbb{Z}^n$ such that its cardinal $\mathrm{Card}(X)$ is finite is said to be a *digital set*. A digital set $X \subset \mathbb{Z}^n$ is said $2n$*-connected* (respectively $(3^n - 1)$-connected) iff for any couple of points $x, y \in X$, there exists a $2n$-path (respectively a $(3^n - 1)$-path) joining them into X. A subset C of X which is $2n$-connected (respectively $(3^n - 1)$-connected) and which is *maximal in the inclusion sense*, that is, there is no subset of X which is greater than C and which is $2n$-connected (respectively $(3^n - 1)$-connected), is said to be a $2n$*-component* (respectively a $(3^n - 1)$*-component*) of X.

A point $x \in \mathbb{Z}^n$ is said to be $2n$*-connected* (respectively $(3^n - 1)$*-connected*) to a set $Y \subseteq \mathbb{Z}^n$ iff there exists a point $y \in Y$ such that x and y are $2n$-neighbors (respectively $(3^n - 1)$-neighbors) or equal. Two sets $X, Y \subseteq \mathbb{Z}^n$ are said to be $2n$*-connected* (respectively $(3^n - 1)$*-connected*) iff there exists $x \in X$ such that x and Y are $2n$-connected (respectively $(3^n - 1)$-connected).

Let ξ be an element of $\{2n, 3^n - 1\}$. The set of ξ-components of a set $X \subset \mathbb{Z}^n$ in $\mathbb{Z}^n$ is denoted by $\mathcal{CC}_\xi(X)$. Now let x be an element of $\mathbb{Z}^n$ and X be a subset of $\mathbb{Z}^n$, then two cases are possible: either $x \in X$ and then we define $\mathcal{CC}_\xi(X, x)$ such that it is equal to the ξ-component of X in $\mathbb{Z}^n$ containing x, or $x \notin X$ and then we define $\mathcal{CC}_\xi(X, x)$ such that it is equal to $\emptyset$.

3.3 n-D EWCNESS AND n-D DWCNESS

In this section, we extend naturally the seminal definition of EWCness to n-D. Then, we define DWCness in n-D and we show how we can characterize a DWC set using $2n$-connectivity. Finally, we study the correlation between EWCness and DWCness.

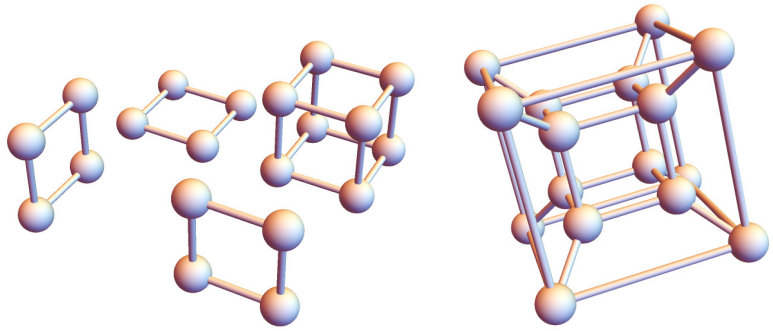

Figure 1.: 2D, 3D and 4D blocks

3.3.1 *n-D EWCness*

Now that we have defined the basics in matter of connectivity in digital topology, we can define well-composedness based on the equivalence of connectivities.

Definition 8. *Let X be a digital set in $\mathbb{Z}^n$. X is said to be* EWC *or* well-composed *based on the equivalence of its connectivities iff the two following conditions hold:*

- *any of its $2n$-component is also one of its (3^n-1)-components and vice versa.*
- *any $2n$-component of X^c is also a (3^n-1)-component of X^c and vice versa.*

We can underline that this definition is clearly self-dual, and since the connectivity does not matter for this class of sets, we will sometimes say that their connectivities (and the ones of their complement in $\mathbb{Z}^n$) are *equivalent*. Also, this definition is the "natural" extension of the one of Latecki in [102] for 2D sets.

3.3.2 *n-D DWCness*

In this subsection, we introduce a notion of *digital well-composedness* for sets in $\mathbb{Z}^n$, that we call in this way because it is based on patterns called "k-dimensional critical configurations", $k \in [\![2, n]\!]$, and these patterns can only occur in subsets of $\mathbb{Z}^n$. So let us introduce the basic mathematical background which will allow us to generalize the notion of well-composedness based on critical configurations to dimension $n \geq 2$.

As usual, $\mathbb{B} = \{e^1, \ldots, e^n\}$ is the canonical basis of $\mathbb{Z}^n$.

Definition 9. *Given a point $z \in \mathbb{Z}^n$ and a family of vector $\mathcal{F} = (f^1, \ldots, f^k) \subseteq \mathbb{B}$, we define the* block *associated to the couple $(z, \mathcal{F})$ in this way:*

$$S(z, \mathcal{F}) = \left\{ z + \sum_{i \in [\![1,k]\!]} \lambda_i f^i \;\middle|\; \lambda_i \in \{0,1\}, \forall i \in [\![1,k]\!] \right\}.$$

A subset $S \subset \mathbb{Z}^n$ is called a *block* iff there exists a couple $(z, \mathcal{F}) \in \mathbb{Z}^n \times \mathcal{P}(\mathbb{B})$ such that $S = S(z, \mathcal{F})$. Note that a block which is associated to a family $\mathcal{F} \in \mathcal{P}(\mathbb{B})$ of cardinal $k \in [\![0, n]\!]$ is said to be of *dimension* k, what will be denoted by $\dim(S) = k$. Figure 1 shows 2D, 3D and 4D blocks. We will denote the set of blocks of $\mathbb{Z}^n$ by $\mathcal{B}(\mathbb{Z}^n)$.

Using this notion of blocks, we can define *antagonism*. Two points p, q belonging to a block $S \in \mathcal{B}(\mathbb{Z}^n)$ are said to be *antagonist* in S iff their distance equals the maximal distance using the L^1 norm between two points into S. In other words, two points p and q in $\mathbb{Z}^n$ are antagonist in $S \in \mathcal{B}(\mathbb{Z}^n)$ iff $p, q \in S$ such that:

$$\|p - q\|_1 = \max\{\|x - y\|_1 \; ; \; x, y \in S\},$$

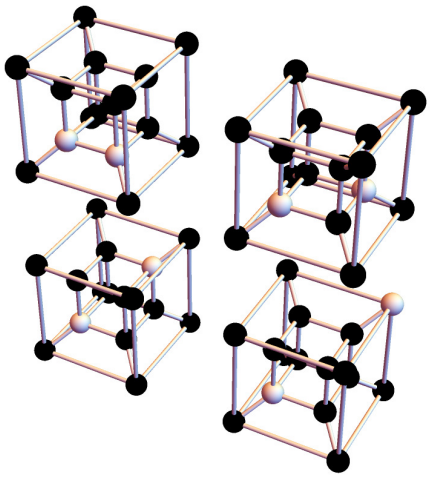

Figure 2.: In the raster scan order: the white points are 1-antagonists, 2-antagonists, 3-antagonists, and 4-antagonists

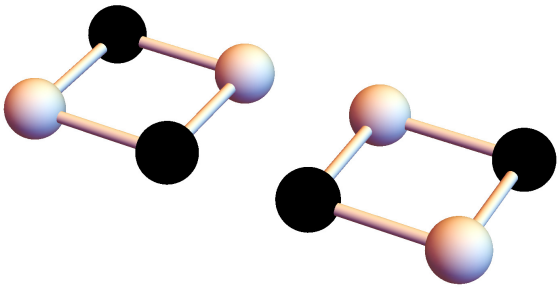

Figure 3.: The white points on the left draw a 2D primary critical configuration, and the white points on the right draw a secondary 2D critical configuration.

and in this case we write that $q = \mathrm{antag}_S(p)$ or equivalently $p = \mathrm{antag}_S(q)$. The antagonist of a point p in a block $S \in \mathcal{B}(\mathbb{Z}^n)$ containing p exists and is unique. Sometimes we will use the notation $S(p, q)$ where $p, q \in \mathbb{Z}^n$ are $(3^n - 1)$-neighbors to indicate the block in $\mathcal{B}(\mathbb{Z}^n)$ such that p and q are antagonist in this block.

Also, two points which are antagonist in a block of dimension $k \in [\![0, n]\!]$ are said *k-antagonist*. In this case, k of their coordinates differ, and they differ from a value 1, the other coordinates being equal. Two points which are 0-antagonist are equal, two points which are 1-antagonist in a block of $\mathbb{Z}^n$ are $2n$-neighbors in $\mathbb{Z}^n$, and two points which are n-antagonist in a block $S \in \mathcal{B}(\mathbb{Z}^n)$ are $(3^n - 1)$-neighbors in $\mathbb{Z}^n$ or equal. See Figure 2 for different possible couple of antagonists (in white) in a 4D space.

Now, we are able to define *critical configurations* of dimension $k \in [\![2, n]\!]$ in a n-D space:

Definition 10. *Let $X \subset \mathbb{Z}^n$ be a digital set, and let $S \in \mathcal{B}(\mathbb{Z}^n)$ be a block of dimension $k \in [\![2, n]\!]$. We say that X contains a* primary critical configuration *of dimension k in the block S iff $X \cap S = \{p, p'\}$ with $p, p' \in S$ two points that are antagonist into S. We say that X contains a* secondary critical configuration *of dimension k in the block S iff $X \cap S = S \setminus \{p, p'\}$ with $p, p' \in S$ two points that are antagonist into S. More generally, a* critical configuration *of dimension $k \in [\![2, n]\!]$ is either a primary or a secondary critical configuration of dimension k.*

Figures 3, 4 and 5 depict 2D, 3D, and 4D critical configurations.

There comes our definition of digitally well-composed sets:

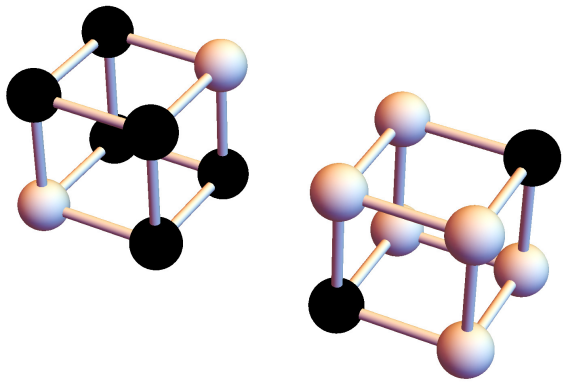

Figure 4.: The white points on the left draw a 3D primary critical configuration, and the white points on the right draw a secondary 3D critical configuration.

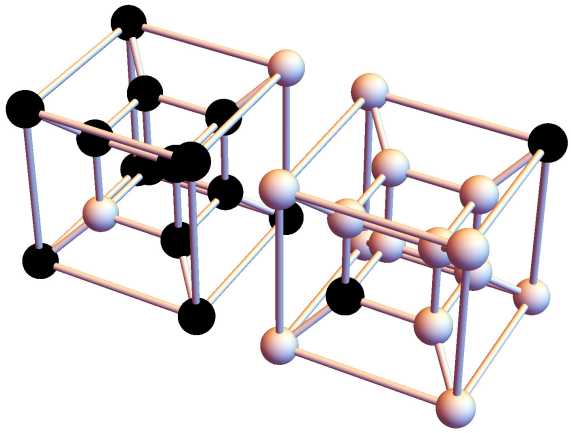

Figure 5.: The white points on the left draw a 4D primary critical configuration, and the white points on the right draw a secondary 4D critical configuration.

Definition 11. *A digital set $X \subset \mathbb{Z}^n$ is said* digitally well-composed *or* DWC *iff it does not contain any critical configurations, that is, for any block $S \in \mathcal{B}(\mathbb{Z}^n)$, the restriction $X \cap S$ is neither a primary nor a secondary critical configuration.*

Obviously, this definition is self-dual, since a set $X \subset \mathbb{Z}^n$ contains a primary (respectively a secondary) critical configuration in the block $S \in \mathcal{B}(\mathbb{Z}^n)$ iff its complement X^c contains a secondary (respectively a primary) critical configuration in this same block S.

Note that this definition is based on local patterns, by contrast to well-composedness based on the equivalence of connectivities which is based on connected components, and then is global.

Also, Latecki remarked that in 2D and 3D, we can express well-composedness using $2n$-paths in restricted areas. Effectively, we can reformulate digital well-composedness based on $2n$-paths in dimension 2, 3, but also in dimension $n \geq 4$ as showed by our n-D theorem:

Theorem 2. *A set $X \subset \mathbb{Z}^n$ is digitally well-composed iff, for any block $S \in \mathcal{B}(\mathbb{Z}^n)$ and for any couple of points $(p, \mathrm{antag}_S(p))$ such that they belong to $X \cap S$ (resp. $S \setminus X$), p and $\mathrm{antag}_S(p)$ are $2n$-connected in $X \cap S$ (resp. in $S \setminus X$).*

Proof: Let us begin by the converse implication. If X is not digitally well-composed, there exists some block $S \subset \mathbb{Z}^n$ such as $X \cap S$ is a primary or a secondary critical configuration in $\mathbb{Z}^n$. In the primary case, $\mathrm{Card}(X \cap S) = 2$, what contradicts that $\mathrm{Card}(X \cap S) \geq k + 1$ due

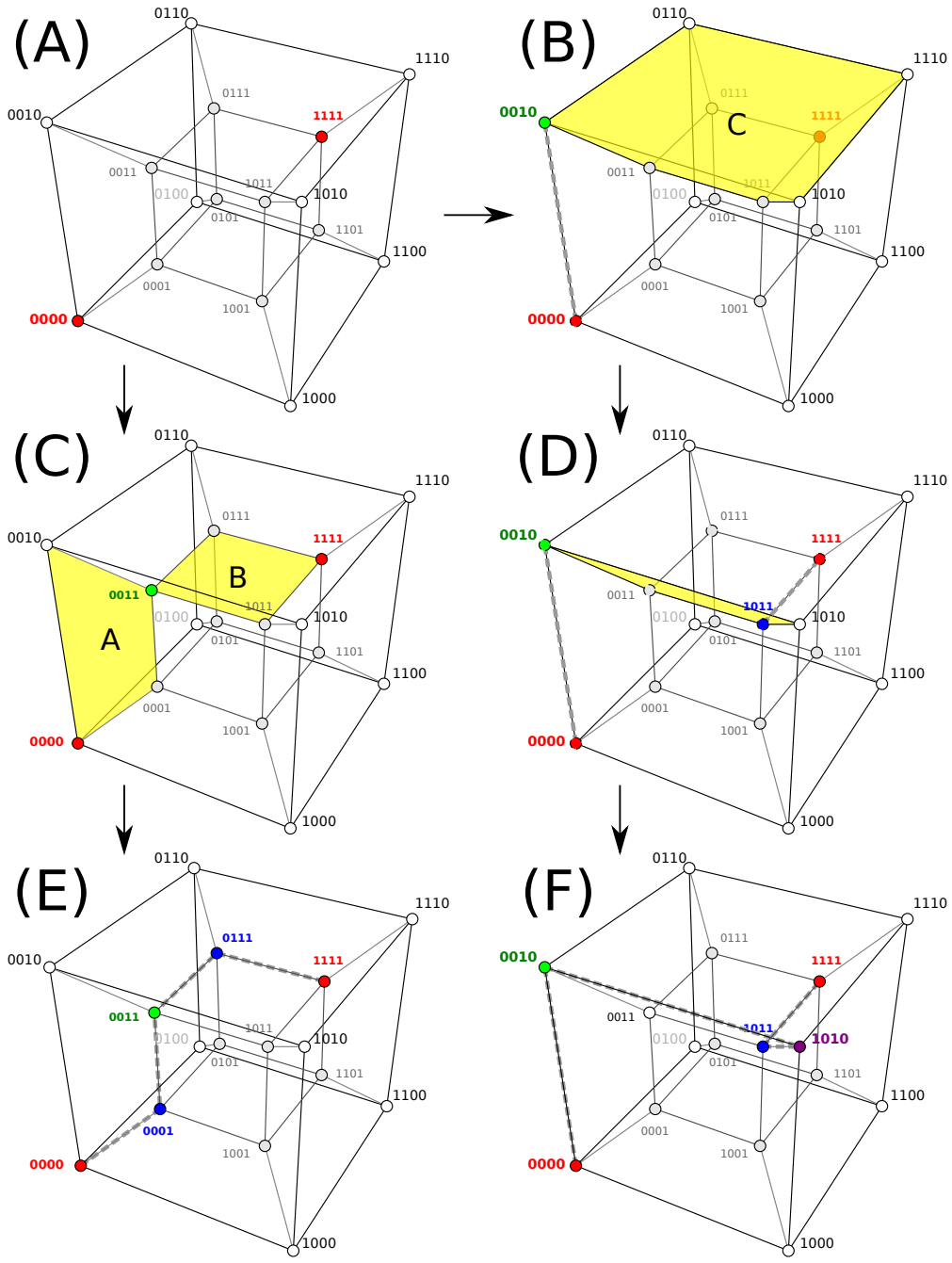

Figure 6.: Step-by-step construction of the $2n$-path joining the two (red) antagonists into $X \cap S$ into $\mathbb{Z}^n$

to the fact that every couple of antagonists (p, p') in this block is connected by a $2n$-path in S. In the secondary case, $\mathrm{Card}(X^c \cap S) = 2$, what contradicts that $\mathrm{Card}(X^c \cap S) \geq k + 1$ for the same reason.

Concerning the direct implication, let us prove firstly that for two antagonists p and p' in some block $S \in \mathcal{B}(\mathbb{Z}^n)$ of dimension $k \in [\![1, n]\!]$ such that $p, p' \in X$, there exists a $2n$-path in $X \cap S$ joining them when X is digitally well-composed. Let us proceed by induction.

Initialization $(k = 1)$: the $2n$-path joining p and p' into $X \cap S$ is simply $\pi = (p, p')$.

Heredity $(k \in [\![2, n-1]\!])$: let us assume that this property is true for every $l \in [\![1, k]\!]$. Now, let us assume that there exists a couple of points p and p' of X such as they are antagonist in a block $S \in \mathcal{B}(\mathbb{Z}^n)$ of dimension $(k + 1)$. We know that X is digitally well-composed and

then does not contain any primary critical configuration. Consequently, there exists one point $q \in X \cap S$ such that $q \neq p$ and $q \neq p'$. That means that p and q are antagonist in some block $S' \in \mathcal{B}(\mathbb{Z}^n)$ of dimension l strictly lower than $k+1$, and then they are connected by a $2n$-path $\pi_{pq} = (p, \ldots, q)$ in $X \cap S' \subset X \cap S$. For the same reason, q and p' are connected by a $2n$-path $\pi_{qp'} = (q, \ldots, p') \subseteq X \cap S$. Consequently, by joining the two paths π_{pq} and $\pi_{qp'}$ we obtain a $2n$-path $\pi_{pp'}$ in $X \cap S$ joining p and p'.

A similar reasoning will prove that the non existence of secondary critical configurations in X (and then the non existence of primary critical configurations in X^c) implies that for any couple of points (p, p') of X^c and antagonist in some block $S \in \mathcal{B}(\mathbb{Z}^n)$, there exists some $2n$-path joining them in $X^c \cap S$. □

This proof is illustrated on Figure 6: two antagonists, depicted in red in the block S (the tesseract), are assumed to belong to a digitally well-composed set $X \subset \mathbb{Z}^n$, which is shown on Subfigure (A). Since the two red points $(0,0,0,0)$ and $(1,1,1,1)$ belong to X and are 4-antagonist in S, there exists at least one more point in the block S belonging to X (in the contrary case, X contains a critical configuration, which is impossible by hypothesis). A first possibility is shown on Subfigure (B), and a second possiblity is shown on Subfigure (C), where the green point depicts this additional point. Let us treat first the case corresponding to Subfigure (B): since the points $(0,0,1,0)$ and $(1,1,1,1)$ are 3-antagonist in the 3D block C depicted in yellow, there must be at least one more point in this block which belongs to X (for the same reason as before), and then we obtain that the blue point $(1,0,1,1)$ belongs to X, which is shown on Subfigure (D). Applying recursively the reasoning until X does not contain any critical configuration, we obtain that the point $(1,0,1,0)$ also belongs to X, which is shown in purple on Subfigure (F). Finally, we obtain a $2n$-path joining the two red points $(0,0,0,0)$ to $(1,1,1,1)$ into $X \cap S$. Let us now treat the case corresponding to Subfigure (C): if $(0,0,0,0)$ and $(0,0,1,1)$, which are 2-antagonist, are the only points of X in the block A, $X \cap A$ is a critical configuration, then there exists an additional point among $(0,0,1,0)$ and $(0,0,0,1)$ which belongs to X. The same happens in the block B where at least $(0,0,1,1)$ and $(1,1,1,1)$ belongs to X: at least $(0,1,1,1)$ or $(1,0,1,1)$ must belong to X. Let us assume that $(0,0,0,1)$ and $(0,1,1,1)$ belong to X, we obtain Subfigure (E) where a $2n$-path joins the two red points $(0,0,0,0)$ to $(1,1,1,1)$ in $X \cap S$. Obvioulsy, the reasoning is similar when $(0,0,0,0)$ and $(1,1,1,1)$ belong to X^c. In this case, we obtain that a $2n$-path joins these two points in $X^c \cap S$, thanks to self-duality of digital well-composedness.

3.3.3 *Link between EWCness and DWCness*

Let us recall that EWCness is a global property, since it is based on connected components, and that DWCness is based on local properties, that is, there is no critical configurations. That shows that the link between DWCness and EWCness is not so obvious. Before proving that DWCness implies EWCness in any (finite) dimension n, $n \geq 2$, let us announce some lemmas.

Lemma 1. *Let $X \subset \mathbb{Z}^n$ be a digitally well-composed set. Then the (3^n-1)-components of X, respectively of X^c, are digitally well-composed.*

Proof: Let us to prove that any element of $\mathcal{CC}_{3^n-1}(X)$ is DWC. Let C be an element of $\mathcal{CC}_{3^n-1}(X)$. Assume that C is not digitally well-composed, that means that there exists a block $S \in \mathcal{B}(\mathbb{Z}^n)$ of dimension $k \geq 2$ such that $C \cap S$ is either a primary critical configuration or a secondary critical configuration. Let us begin with the primary case: there exists $p \in S$ such that $C \cap S = \{p, \mathrm{antag}_S(p)\}$. Then we remark that any point different from p or $\mathrm{antag}_S(p)$ belonging in S is a (3^n-1)-neighbour of both p and p'. In other words, if there exists $q \in S$, $q \notin \{p, \mathrm{antag}_S(p)\}$, belonging to X, it belongs also to C since this is a (3^n-1)-component of X. Then $X \cap S = C \cap S = \{p, \mathrm{antag}_S(p)\}$, which means that X contains a critical configuration, which is impossible. The reasoning is the same for the secondary case. We have proven that the (3^n-1)-connected components of a DWC set are DWC. Now we need to prove that any element of $\mathcal{CC}_{3^n-1}(X^c)$ is DWC. Since X digitally well-composed in $\mathbb{Z}^n$ implies that X^c is digitally well-composed in $\mathbb{Z}^n$, the proof is done. □

Lemma 2. *Let $p, p' \in \mathbb{Z}^n$ be two points in a digitally well-composed set $X \subset \mathbb{Z}^n$. If p and p' are $(3^n - 1)$-connected into X, they are also $2n$-connected into X.*

Proof: Let p, p' be two points in $X \subset \mathbb{Z}^n$ which is digitally well-composed. Assuming that p and p' are $(3^n - 1)$-connected into X, there exists a $(3^n - 1)$-path $\pi = (q^0 = p, q^1, \ldots, q^{k-1}, q^k = p')$ of length $k \geq 0$ joining them into X. For any $i \in [\![0, k-1]\!]$, q^i and q^{i+1} are $(3^n - 1)$-adjacent, and then antagonist in a block $S(q^i, q^{i+1})$. Since X is digitally well-composed in $\mathbb{Z}^n$ and q^i and q^{i+1} belong to X, by Theorem 2, there exists a $2n$-path joining q^i and q^{i+1} into $X \cap S(q^i, q^{i+1})$ as a subset of $\mathbb{Z}^n$, such that these two points are $2n$-connected into X as a subset of $\mathbb{Z}^n$. By transitivity, p and p' are then $2n$-connected into X. □

Note that the converse is true, as stated by the following proposition.

Proposition 12. *Let $X \subset \mathbb{Z}^n$ be a digital set. Let us assume that each element of $\mathcal{CC}_{3^n-1}(X)$ and each element of $\mathcal{CC}_{3^n-1}(X^c)$ are digitally well-composed. Then, X is digitally well-composed.*

Proof: Let us assume that X is not digitally well-composed. There exists some block $S \in \mathcal{B}(\mathbb{Z}^n)$ of dimension $k \in [\![2, n]\!]$ such that $X \cap S$ is a critical configuration of dimension k. Let us treat first the primary case. If $X \cap S = \{p, p'\}$ with $p' = \mathrm{antag}_S(p)$, obviously p and p' are $(3^n - 1)$-neighbors since $\|p - p'\|_\infty = 1$, and then the connected component $C_X = \mathcal{CC}_{3^n-1}(X, p)$ contains also p'. This way, $C_X \cap S \supseteq \{p, p'\}$, and since $C_X \subseteq X$, $C_X \cap S = \{p, p'\}$, which contradicts that C_X is digitally well-composed. Now let us proceed to the secondary case. If X contains a secondary critical configuration in S, it means that $X^c \cap S = \{p, p'\}$ with $p' = \mathrm{antag}_S(p)$. One more time, p and p' are $(3^n - 1)$-neighbors, and then the connected component $C_{X^c} = \mathcal{CC}_{3^n-1}(X^c, p)$ contains also p'. Then, $C_{X^c} \cap S \supseteq \{p, p'\}$, and since $C_{X^c} \subseteq X^c$, $C_{X^c} \cap S = \{p, p'\}$, which contradicts that C_{X^c} is digitally well-composed. □

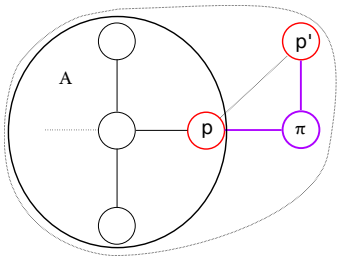

(a) If A is a $2n$-component of a DWC set X, then each point $p' \in X$ which is $(3^n - 1)$-connected to any point p element of X belongs to A since $(3^n - 1)$-connectivity implies $2n$-connectivity in a DWC set.

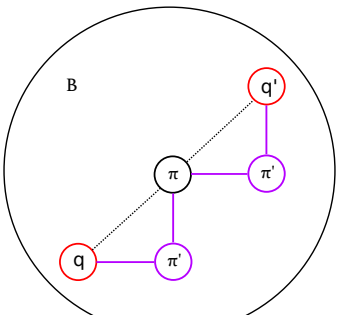

(b) If B is a $(3^n - 1)$-component of a DWC set X, each couple of points $q, q' \in B$ are also $2n$-connected into X since $(3^n - 1)$-connectivity implies $2n$-connectivity in a DWC set.

Figure 7.: DWCness implies EWCness

Theorem 3 (DWC ⇒ EWC)**.** *Let $X \subset \mathbb{Z}^n$ be a digitally well-composed set. Then, X and X^c are well-composed based on the equivalence of connectivities (EWC).*

Proof: By Lemma 2, it is obvious that each $2n$-component in $\mathbb{Z}^n$ of a set $X \subset \mathbb{Z}^n$ which is digitally well-composed is also a $(3^n - 1)$-component of X (see Figure 7a).

Let us now proceed to the converse implication. By Lemma 2, it is also obvious that each $(3^n - 1)$-component of a set $X \subset \mathbb{Z}^n$ which is digitally well-composed is also a $2n$-component of X (see Figure 7b).

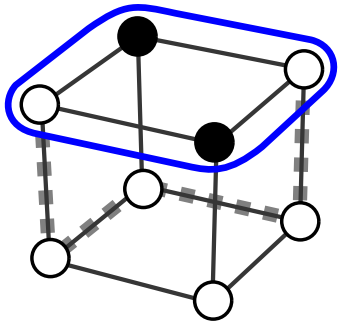

Figure 8.: EWCness does not imply DWCness in n-D ($n \geq 3$)

The same reasoning holds for the components of X^c since DWCness is a self-dual property. X is then well-composed based on the equivalence of connectivities. EWCness being a self-dual property like DWCness, X^c is EWC too. □

Now that we know that each $(3^n - 1)$-component of a set which is digitally well-composed is also one of its $2n$-component and conversely, we can deduce easily the following corollary.

Corollary 1. *Let $X \subset \mathbb{Z}^n$ be a digitally well-composed set. Then we have:*

$$\mathcal{CC}_{2n}(X) = \mathcal{CC}_{3^n-1}(X),$$

and

$$\mathcal{CC}_{2n}(X^c) = \mathcal{CC}_{3^n-1}(X^c).$$

Recall that the converse of Theorem 3 is not true in 3D (and in higher dimensions) (see Figure 8): a 3D subset of $\mathbb{Z}^n$ can be EWC whithout being DWC, since the $(3^n - 1)$-components and the $2n$-components of this set are equal, but it contains a 2D critical configuration at the top and then is not DWC (the reasoning holds for any $n \geq 3$).

Lemma 3. *Let $X \subset \mathbb{Z}^n$ be a digitally well-composed set. Then the $2n$-components of X, respectively of X^c, are digitally well-composed.*

Proof: Since X is digitally well-composed, its $(3^n - 1)$ components and the ones of its complement X^c are digitally well-composed by Lemma 1. Then, by Corollary 1, each $(2n)$-component of X or X^c is digitally well-composed. This concludes the proof. □

Finally, for sets which are digitally well-composed, it does not care if we consider either the $(3^n - 1)$-components or the $2n$-components of this set (respectively of its complement) since they are the same. Furthermore, these components are digitally well-composed.

3.3.4 *Well-composed gray-level n-D images*

In [100], Latecki defines a digital binary image $(\mathbb{Z}^2, X)$ such that the set $X \subset \mathbb{Z}^2$ is finite or its complement is finite. Then, we can easily store this image into a matrix made of zeros and ones on a computer. However, for any gray-level image defined on $\mathbb{Z}^2$, such a procedure is not possible; an infinite amount of data can be necessary to store the image. We propose then to work with images defined on finite domains; more exactly, we will define images on *bounded hyperrectangles* (see the definition below). Then, we will be able to define the different kinds of *well-composednesses* for graylevel images. But let us come back to some basics.

Let $n \geq 2$ be an integer. From now on, we will say that a 4-uple $(A, \mathcal{D}, \mathbb{V}, u)$, representing the mapping $u : \mathcal{D} \subseteq A \to \mathbb{V}$, is an *image* defined on $\mathcal{D} \subseteq A$. In this case, A is called the *space* of the image, $\mathcal{D} \subseteq A$ is called the *domain* of the image, and $\mathbb{V} \subseteq \mathbb{R}$ is the *value space* of the image. Note that $(A, \mathcal{D}, \mathbb{V}, u)$ will be generally identified to u. Also, u will be said to be a *digital image* iff its space is equal to $\mathbb{Z}^n$ and if its domain $\mathcal{D} \subset \mathbb{Z}^n$ is finite. Moreover,

$(A, \mathcal{D}, \mathbb{V}, u)$ will be called a *digital gray-level* image if it is a digital image and if $\mathbb{V}$ is a (finite) set or totally ordered values.

Also we will use the following notation where A denotes any space and $\mathbb{V}$ denotes any value space:

$$\mathbb{Im}(A, \mathcal{D}, \mathbb{V}) = \{u : \mathcal{D} \subseteq A \to \mathbb{V}\},$$

and:

$$\mathbb{Im}(A, \mathbb{V}) = \{u : \mathcal{D} \subseteq A \to \mathbb{V} \ ; \ \mathcal{D} \subseteq A\}.$$

Now let us recall the definition of *threshold sets*, coming from the cross-section topology [121, 21, 18, 17]. Let $u \in \mathbb{Im}(\mathbb{Z}^n, \mathcal{D}, \mathbb{R})$ be an image and let $\lambda \in \mathbb{R}$ be a given threshold, a *large upper threshold set* is defined as:

$$[u \geq \lambda] = \{x \in \mathcal{D} \ ; \ u(x) \geq \lambda\},$$

a *strict upper threshold set* is defined as:

$$[u > \lambda] = \{x \in \mathcal{D} \ ; \ u(x) > \lambda\},$$

a *large lower threshold set* is defined as:

$$[u \leq \lambda] = \{x \in \mathcal{D} \ ; \ u(x) \leq \lambda\},$$

and a *strict lower threshold set* is defined as:

$$[u < \lambda] = \{x \in \mathcal{D} \ ; \ u(x) < \lambda\}.$$

Also, a *bounded hyperrectangle* in $\mathbb{Z}^n$ is defined as the *Cartesian product*, denoted by $\prod$, of the discrete intervals $[\![m_i, M_i]\!]$ for all $i \in [\![1, n]\!]$ denoted by:

$$\prod_{i \in [\![1,n]\!]} [\![m_i, M_i]\!],$$

where $m = (m_i)_{i \in [\![1,n]\!]} \in \mathbb{Z}^n$, its *lower bound*, and $M = (M_i)_{i \in [\![1,n]\!]} \in \mathbb{Z}^n$, its *upper bound*, are given such that $\forall i \in [\![1, n]\!], m_i \leq M_i$.

Definition 12 (Well-composedness(es) of graylevel n-D images)**.** *A digital image $u : \mathcal{D} \subseteq \mathbb{Z}^n \to \mathbb{R}$ is said X-WC, where X belongs to $\{E, D, C, A\}$, iff for every threshold $\lambda \in \mathbb{R}$, all the threshold sets of u are X-WC sets. This same image is said X-WC, where X belongs to $\{E, D, C, A\}$, on a domain $\mathcal{D}' \subseteq \mathcal{D}$ iff for every threshold $\lambda \in \mathbb{R}$, all the threshold sets of u restricted to the domain $\mathcal{D}'$ are X-WC sets in $\mathbb{Z}^n$.*

Note that our restriction of graylevel images to bounded hyperrectangles is due to the fact that n-D images which are defined on cubical grids are generally defined on rectangular domains.

3.3.5 *Characterizing DWC real-valued n-D images*

Now let us remark that in the case of a real-valued image defined on a bounded hyperrectangle, we are able to detect the digital well-composedness of this image only using the upper (respectively lower) threshold sets, as proved using the following lemmas.

Lemma 4. *Let $u \in \mathbb{Im}(\mathbb{Z}^n, \mathcal{D}, \mathbb{R})$ be a gray-level image such that $\mathrm{Card}(\mathcal{D}) < +\infty$. Then u is digitally well-composed on $\mathcal{D}$ iff for any $\lambda \in \mathbb{R}$, $[u \leq \lambda]$ and $[u > \lambda]$ are both digitally well-composed (or equivalently iff $[u \geq \lambda]$ and $[u < \lambda]$ are both digitally well-composed).*

Proof: The direct implication is obvious. For the converse implication, let us proceed in two parts. Let us define $\mathbb{V}(u) = \{u(z) \mid z \in \mathcal{D}\}$ and:

$$\varepsilon = \min\{|u(p) - u(q)| \mid p, q \in \mathcal{D}, \ u(p) \neq u(q)\}.$$

Firstly, we can observe that for any $\lambda \in \mathbb{R}$, every threshold set $[u < \lambda]$ can be rewritten $[u \leq f(\lambda)]$ with $f : \mathbb{R} \to \mathbb{R}$ defined such that:

$$f(\lambda) = \begin{cases} \lambda - \varepsilon/2 & \text{if } \lambda \in \mathbb{V}(u), \\ \lambda & \text{otherwise.} \end{cases}$$

That means that every threshold set $[u < \lambda]$ is equal to $[u \leq \lambda']$ for some $\lambda' \in \mathbb{R}$.

Secondly, we can observe that every threshold set $[u \geq \lambda]$ can be rewritten $[u > f(\lambda)]$ using this same function f. That means that every threshold set $[u \geq \lambda]$ is equal to $[u > \lambda']$ for some $\lambda' \in \mathbb{R}$.

Finally, all the threshold sets $[u \leq \lambda]$ and $[u > \lambda]$ are digitally well-composed, then u is digitally well-composed. The reasoning is dual for the proposition in brackets. □

We have previously defined blocks of $\mathbb{Z}^n$. The extension to *blocks of a domain* $\mathcal{D} \subseteq \mathbb{Z}^n$ is straightforward. For a given domain $\mathcal{D} \subset \mathbb{Z}^n$, the *set of blocks of* $\mathcal{D}$ is denoted $\mathcal{B}(\mathcal{D})$ and is such that:

$$\mathcal{B}(\mathcal{D}) = \{S \in \mathcal{B}(\mathbb{Z}^n) \; ; \; S \subseteq \mathcal{D}\}.$$

Lemma 5. *Let $n \geq 2$ be an integer, and let H be a bounded hyperrectangle. Let X and Y be two sets of $\mathbb{Z}^n$ such as: $X \cap Y = \emptyset$ and $X \cup Y = H$ (i.e., (X, Y) is a* partition of H*). Then, X is digitally well-composed iff Y is digitally well-composed.*

Proof: Let us assume that X contains a primary critical configuration. It means that there exists some block $S \in \mathcal{B}(H)$ such that $X \cap S = \{p, p'\}$ with p and p' antagonist in S. Because X and Y are complementary in H, $X \cap S$ and $Y \cap S$ are complementary in $S \subseteq H$. The consequence is that $Y \cap S = S \setminus \{p, p'\}$, i.e., Y contains a secondary critical configuration in S.

So, we have proven that X contains a primary critical configuration iff Y contains a secondary critical configuration. That finally means that X is digitally well-composed iff Y is digitally well-composed. □

Lemma 6. *Let $n \geq 2$ be an integer, and let H be a bounded hyperrectangle. Let $u : \mathcal{D} \to \mathbb{R}$ be a gray-level image. Then, u is digitally well-composed iff for any $\lambda \in \mathbb{R}$ the threshold set $[u \leq \lambda]$ is digitally well-composed (or equivalently iff for any $\lambda \in \mathbb{R}$ the threshold set $[u \geq \lambda]$ is digitally well-composed).*

Proof: Using Lemma 4 and because the cardinal of H is finite, we know that u is digitally well-composed iff for any $\lambda \in \mathbb{R}$, $[u \leq \lambda]$ and $[u > \lambda]$ are digitally well-composed. Furthermore, using Lemma 5, and because $[u \leq \lambda] \cap [u > \lambda] = \emptyset$ and $[u \leq \lambda] \cup [u > \lambda] = H$ (with H a bounded hyperrectangle), we know that $[u \leq \lambda]$ is digitally well-composed iff $[u > \lambda]$ is digitally well-composed. We can conclude that u is digitally well-composed iff $[u \leq \lambda]$ is digitally well-composed. □

Like exposed in [26], there exists a characterization for gray-level digitally well-composed images defined on bounded hyperrectangles. It is the natural extension of the characterization of Latecki for 2D images in [100].

Proposition 13. *Let $n \geq 2$ be an integer, and let H be a bounded hyperrectangle. A real-valued image $u : \mathcal{D} \subset \mathbb{Z}^n \to \mathbb{R}$ is digitally well-composed iff for any block $S \in \mathcal{B}(\mathcal{D})$ such that $\dim(S) \geq 2$ and for any couple of points $(p, p') \in S \times S$ such that $p' = \text{antag}_S(p)$, the following relation is true:*

$$\text{intvl}(u(p), u(p')) \; \cap \; \text{Span}\{\, u(p'') \;\big|\; p'' \in S \setminus \{p, p'\}\,\} \; \neq \; \emptyset.$$

Proof: Effectively, let us assume that there exists a block $S \in \mathcal{B}(\mathcal{D})$ and a couple of points $(p, p') \in S \times S$ such that this intersection is empty, then either:

$$\max\{\, u(p'') \;\big|\; p'' \in S \setminus \{p, p'\}\,\} < \min(u(p), u(p')),$$

and in this case $[u \geq \min(u(p), u(p'))] \cap S$ is equal to $\{p, p'\}$ which is a primary critical configuration, or:

$$\max(u(p), u(p')) < \min\{\, u(p'') \;\big|\; p'' \in S \setminus \{p, p'\}\,\},$$

Algorithm 1: An algorithm able to check the digital well-composedness of a n-D image

```
CheckImage (n, u, D) : isDWC;
begin
    for S ∈ B(D) s.t. dim(S) ≥ 2 do
        for p ∈ S do
            p' ← antag_S(p);
            m1 ← min(u(p), u(p'));
            M1 ← max(u(p), u(p'));
            m2 ← min{ u(p'') | p'' ∈ S \ {p, p'} };
            M2 ← max{ u(p'') | p'' ∈ S \ {p, p'} };
            if (M1 < m2) || (M2 < m1) then
                return false;
    return true;
```

and:

$$[u \geq \min\{\, u(p'') \mid p'' \in S \setminus \{p,\, p'\}\,\}] \cap S = S \setminus \{p,\, p'\},$$

which is a secondary critical configuration. In both cases, u is obviously not digitally well-composed. Conversely, if there exists a value $\lambda \in \mathbb{R}$ such that $[u \geq \lambda]$ contains a critical configuration in a block $S \in \mathcal{B}(\mathcal{D})$, either $[u \geq \lambda] \cap S$ is a primary critical configuration (1), or it is a secondary critical configuration (2). In case (1), there exists $p, p' \in S$ such that $p' = \text{antag}_S(p)$ and $[u \geq \lambda] \cap S = \{p, p'\}$, which means that $\min\{u(p), u(p')\} \geq \lambda$, and in parallel we have $[u < \lambda] \cap S = S \setminus \{p, p'\}$, which means that $\max\{\, u(p'') \mid p'' \in S \setminus \{p,\, p'\}\} < \lambda$, and then the intersection we are looking for is empty. In case (2), we can proceed to a dual reasoning to obtain the same result. This concludes the proof. □

Practically, this characterization means that for a given and finite dimension $n \geq 2$, we can check if an image defined on a domain $\mathcal{D}$ is digitally well-composed or not by a very simple algorithm by checking at each block $S \in \mathcal{B}(\mathcal{D})$ if the image is digitally well-composed. Furthermore, the complexity of this algorithm is for a fixed dimension in linear time relatively to the number of blocks in the domain $\mathcal{D}$, which means that it is very fast, in particular for small dimensions.

We propose Algorithm 1 which works in n-D and verifies that a given image does not contain any critical configurations.

Let us begin with the 2D case: if we assume that we have a real-valued image u defined on a rectangular domain $\mathcal{D} = [\![0, s_1]\!] \times [\![0, s_2]\!] \subset \mathbb{Z}^2$, we have a total number of $s_1 \times s_2$ 2D blocks in $\mathcal{D}$. In each block, we have a total of $\text{Card}(S)$ possible points p. Then, for each p, we compute in constant time its antagonist p' in the block. The computation of m_1, m_2, M_1, M_2 are each one in $O(\text{Card}(S))$. The comparison $(M_1 < m_2) \,||\, (M_2 < m_1)$ is in constant time. Finally, we obtain a complexity in $O(s_1 \times s_2 \times \text{Card}(S)^2) = O(s_1 \times s_2)$ since the size of the block is a constant in this context.

Now, let us consider that the dimension is a parameter that we have to take into account for the computation of the complexity. Assuming that the given image u if of dimension $n \geq 2$, then its domain can be written $\mathcal{D} = \prod_{i=1}^{n} [\![0, s_i]\!]$ where s_i is a non-null integer for any $i \in [\![1, n]\!]$. Then we have a total number of C_n^k families of k vectors among n (with $k \in [\![2, n]\!]$). For each family of dimension $k \in [\![2, n]\!]$, we have a total number of associated blocks (of dimension k) which is lower than $\prod_{i=1}^{n}(s_i + 1)$. For each block, we have a total number of 2^{k-1} couples of antagonists, and for each couple, we have to compute m_1 and M_1, which can be computed simultaneously with only one comparison, and m_2 and M_2, which need each $2^k - 3$ comparisons. Also, the comparisons $M_1 < m_2$ and $M_2 < m_1$ constitute 2 operations. We obtain that we need less than 2^{k+1} comparisons for each couple of antagonists, which means

less than 4^k comparisons for each block, and then less than $\prod_{i=1}^{n}(s_i+1)\times 4^k$ for each family. We obtain then a total complexity equal to:

$$T(n,\{s_i\}) \leq \prod_{i=1}^{n}(s_i+1) \times \sum_{k=2}^{n} C_n^k 4^k.$$

Using the binomial formula $\sum_{k=0}^{n} C_n^k x^k = (1+x)^n$, we obtain finally:

$$T(n,\{s_i\}) \leq 5^n \times \prod_{i=1}^{n}(s_i+1).$$

3.3.6 *DWCness for interval-valued maps*

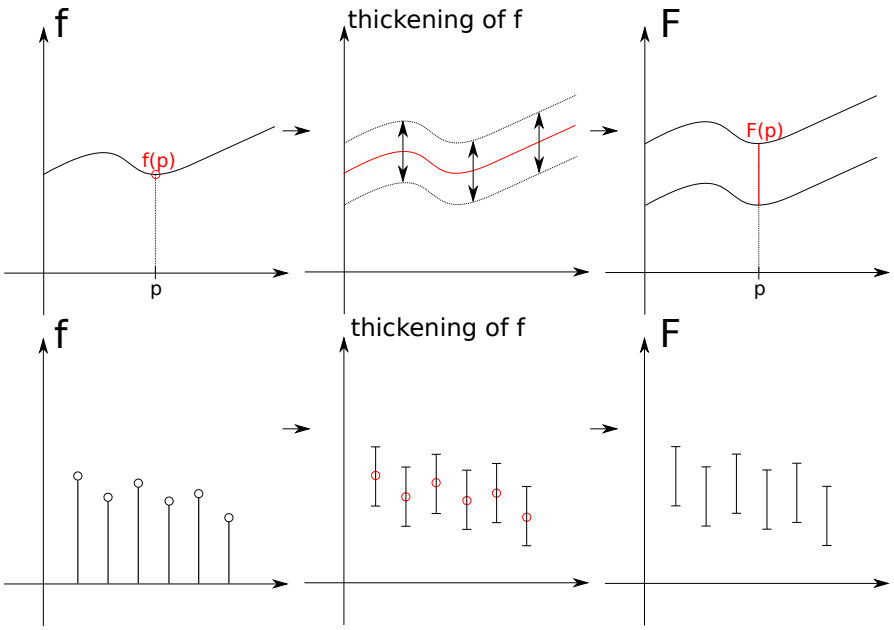

Figure 9.: From single-valued functions to set-valued/interval-valued functions (continuous and discrete cases)

We have seen what means digital well-composedness for single-valued maps, that is, maps such that for a point p belonging to their domain $\mathcal{D}$, the value at p is a real value belonging to $\mathbb{R}$. However, as seen in [10], which introduces *set-valued analysis*, we can define *set-valued maps*, that is, maps such that for a point p belonging to their domain $\mathcal{D}$, the value at p is a subset of $\mathbb{R}$. We will be particularly interested in *interval-valued maps*, a class of set-valued maps such that the value at each point of the domain is an interval $[a,b] \subset \mathbb{R}$.

These set-valued maps can be interpreted in the following manner: let us imagine we have a single-valued function $f : \mathcal{D} \to \mathbb{R}$. By stretching/thickening the function as depicted on top of Figure 9, we obtain a new function $F : \mathcal{D} \to 2^{\mathbb{R}}$ (also written $F : \mathcal{D} \rightsquigarrow \mathbb{R}$), that is, a function such that at each point $p \in \mathcal{D}$, $F(p)$ is a set and then has potentially a thickness not equal to zero. For this reason, F is said to be a *set-valued function*. We can easily extend this thickening to discrete images, as shown on the bottom of Figure 9, to obtain discrete set-valued images.

Let us now introduce digital well-composedness for interval-valued images [26] defined on discrete spaces as $\mathbb{Z}^n$, where $n \geq 2$ is the dimension.

Definition 13. *A* set-valued map $U : \mathcal{D} \subseteq X \rightsquigarrow Y$ *is a function from a topological space X to a topological space Y such that for any $p \in X$, $p \in \mathcal{D} \Leftrightarrow U(p) \neq \emptyset$ ($\mathcal{D}$ is called the* domain *of U) and such that $\forall p \in \mathcal{D}, U(p) \subseteq Y$.*

Definition 14. *An* interval-valued map $U : \mathcal{D} \subseteq X \rightsquigarrow Y$ *is a set-valued map such that for any* $p \in \mathcal{D}$, $U(p)$ *is an* interval *of the topological space* $Y \subseteq \mathbb{R}^n$, *that is,* $U(p)$ *can be written* $[a, b] \cap Y$ *for some* $a, b \in \mathbb{R}$ *such that* $a \leq b$.

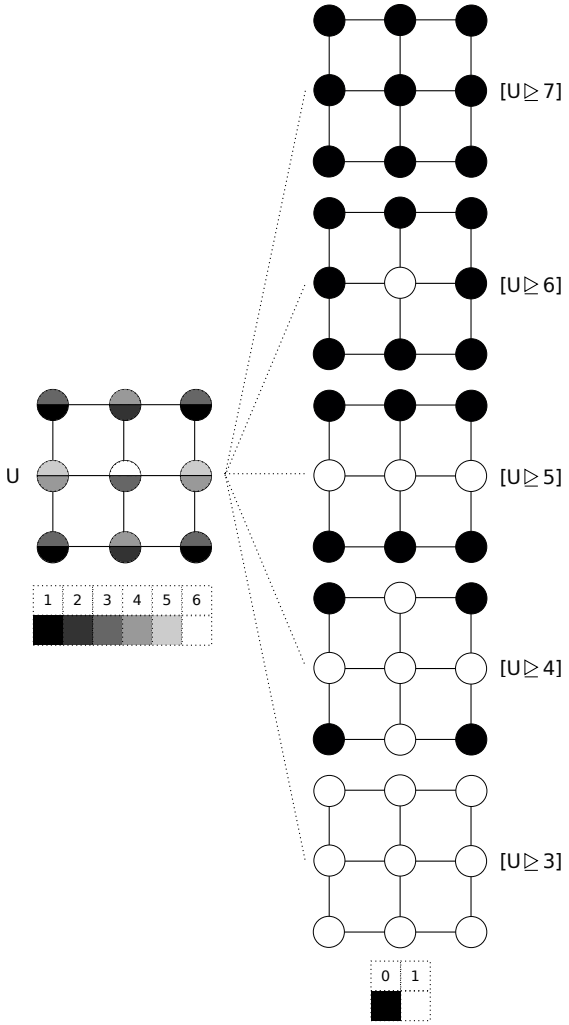

Figure 10.: A family of (large upper) threshold sets $\{[U \trianglerighteq \lambda]\}_\lambda$ of an interval-valued image U. We can remark the straightforward inclusion relationship $[U \trianglerighteq \lambda] \subseteq [U \trianglerighteq \lambda - \varepsilon]$ for any $\lambda \in \mathbb{R}$ and $\varepsilon > 0$.

Now that we have defined interval-valued maps, we can define their *threshold sets* (see Figures 10 and 11).

Definition 15. *For a given interval-valued map* $U : \mathcal{D} \subseteq \mathbb{Z}^n \rightsquigarrow \mathbb{R}$, *we define for any* $\lambda \in \mathbb{R}$ *respectively the* large upper, the strict upper, the strict lower, the large lower threshold sets *as well:*

$$
\begin{aligned}
[U \trianglerighteq \lambda] &= \{ z \in \mathcal{D} \mid \exists v \in U(z), v \geq \lambda \}, \\
[U \triangleright \lambda] &= \{ z \in \mathcal{D} \mid \forall v \in U(z), v > \lambda \}, \\
.[U \triangleleft \lambda] &= \{ z \in \mathcal{D} \mid \forall v \in U(z), v < \lambda \}, \\
[U \trianglelefteq \lambda] &= \{ z \in \mathcal{D} \mid \exists v \in U(z), v \leq \lambda \}.
\end{aligned}
$$

Using the threshold sets like in [127], we can define digital well-composedness on $\mathbb{Z}^n$:

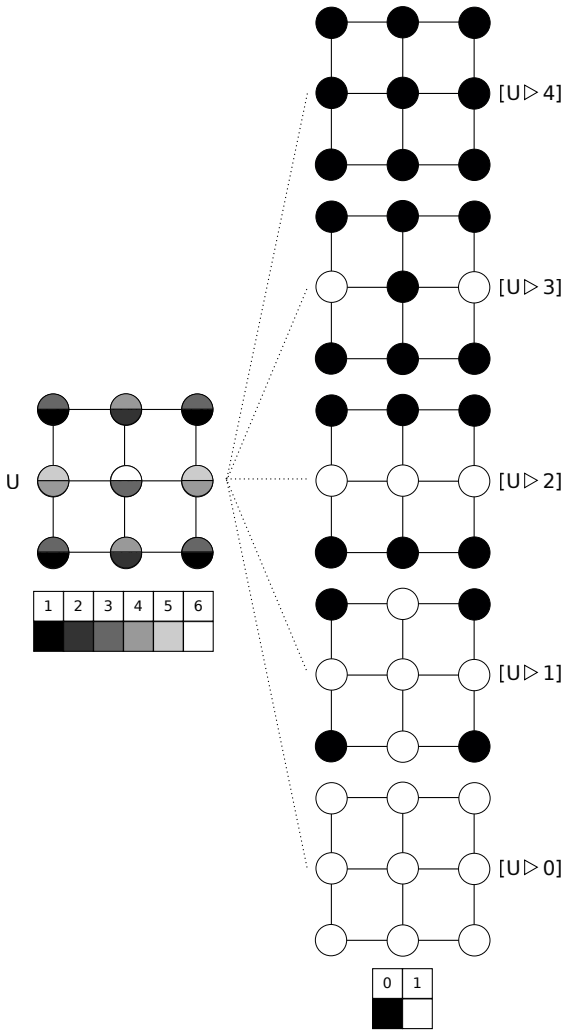

Figure 11.: A family of (strict upper) threshold sets $\{[U \rhd \lambda]\}_\lambda$ of an interval-valued image U. We can remark the straightforward inclusion relationship $[U \rhd \lambda] \subseteq [U \rhd \lambda - \varepsilon]$ for any $\lambda \in \mathbb{R}$ and $\varepsilon > 0$.

Definition 16. *An n-D interval-valued map $U : \mathcal{D} \subseteq \mathbb{Z}^n \to \mathbb{I}_\mathbb{R}$, where $\mathbb{I}_\mathbb{R}$ is the set of intervals of $\mathbb{R}$, is said* digitally well-composed *iff all its threshold sets are digitally well-composed.*

Note that there exists a similar definition of interval-valued maps into [127], but these functions, also called *plain maps*, are defined in Alexandrov spaces.

Now, let us define the *upper/lower bounds* of an interval-valued map. They will be useful to characterize interval-valued digitally well-composed maps.

Definition 17. *For an n-D interval-valued map $U : \mathcal{D} \subseteq \mathbb{Z}^n \to \mathbb{I}_\mathbb{R}$, the* upper bound $\lceil U \rceil$ *and the* lower bound $\lfloor U \rfloor$ *are defined such that for any $p \in \mathcal{D}$, $\lceil U \rceil(p) = \max(U(p))$ and $\lfloor U \rfloor(p) = \min(U(p))$.*

Then a simple characterization follows.

Proposition 14. *An n-D interval-valued map $U : \mathcal{D} \subseteq \mathbb{Z}^n \to \mathbb{I}_\mathbb{R}$ defined on a bounded hyperrectangle $\mathcal{D}$ is digitally well-composed iff both $\lceil U \rceil : \mathcal{D} \to \mathbb{R}$ and $\lfloor U \rfloor : \mathcal{D} \to \mathbb{R}$ are n-D images which are digitally well-composed.*

Proof: Effectively, for any $\lambda \in \mathbb{R}$, we have the remarkable equalities:

$$\begin{cases} [U \rhd \lambda] = [\lfloor U \rfloor > \lambda], & (1) \\ [U \lhd \lambda] = [\lceil U \rceil < \lambda], & (2) \\ [U \trianglerighteq \lambda] = [\lceil U \rceil \geq \lambda], & (3) \\ [U \trianglelefteq \lambda] = [\lfloor U \rfloor \leq \lambda]. & (4) \end{cases}$$

This way, if U is digitally well-composed, then for any $\lambda \in \mathbb{R}$, $[U \trianglerighteq \lambda]$ and $[U \trianglelefteq \lambda]$ are digitally well-composed, and then by (3) and (4), $\lceil U \rceil$ and $\lfloor U \rfloor$ are digitally well-composed. Conversely, if both $\lceil U \rceil$ and $\lfloor U \rfloor$ are digitally well-composed, then for any $\lambda \in \mathbb{R}$, $[\lfloor U \rfloor > \lambda]$, $[\lceil U \rceil < \lambda]$, $[\lceil U \rceil \geq \lambda]$, and $[\lfloor U \rfloor \leq \lambda]$ are digitally well-composed and then by (1) to (4), U is digitally well-composed. □

3.4 RELATIONS BETWEEN AWCNESS, DWCNESS, AND CWCNESS ON CUBICAL GRIDS

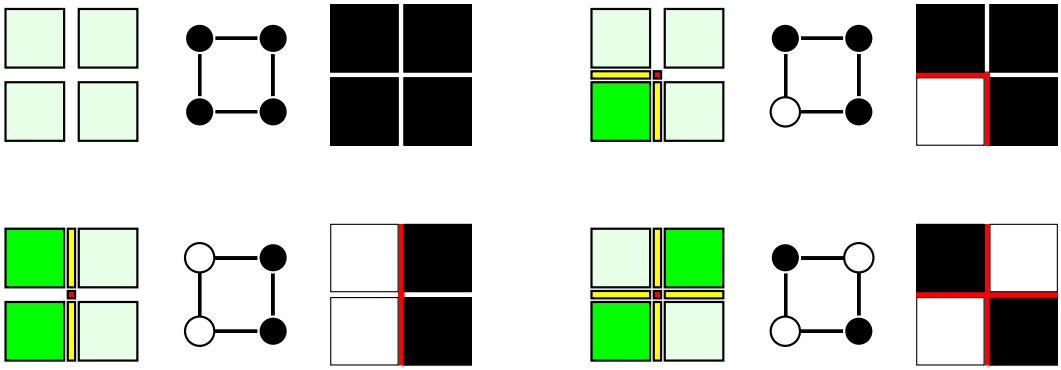

Figure 12.: Possible set configurations in 2D

The proof of the equivalence between EWCness, CWCness, and DWCness in 2D being already in [102, 100], let us expose briefly why AWCness and DWCness are equivalent (a study of the equivalence between AWCness and DWCness in n-D, $n \geq 2$, is provided in Chapter D).

On Figure 12, the middle of the subfigure represents the restriction of a set to a 2D block in $\mathbb{Z}^2$ (the white points correspond to the foreground), the left of the subfigures represents the representation in Khalimsky Grids of this same set up to an isomorphism (the foreground is depicted by the green squares and the boundary is depicted by the yellow edges and the red point), and the right of the subfigures represents the continuous analog of the restriction of this set in $\mathbb{R}^2$ (the foreground is in white and the boundary in red).

In the raster scan order, we observe then the following possibilities by comparing the first two columns of the subfigures:

1. if the restriction of the set is made of four black points, that is, no point of X belongs to the block, and then there is no boundary in this part of the Khalimsky grid, we have then nothing to prove,

2. if the restriction of the set is made of only one point, we can observe that the red point belonging to the discrete boundary has only two neighbors into the boundary: the two yellow edges,

3. if this resctriction is made of two 4-adjacent white points, the red point belonging to the discrete boundary has one more time two yellow edges as neighbors into the boundary,

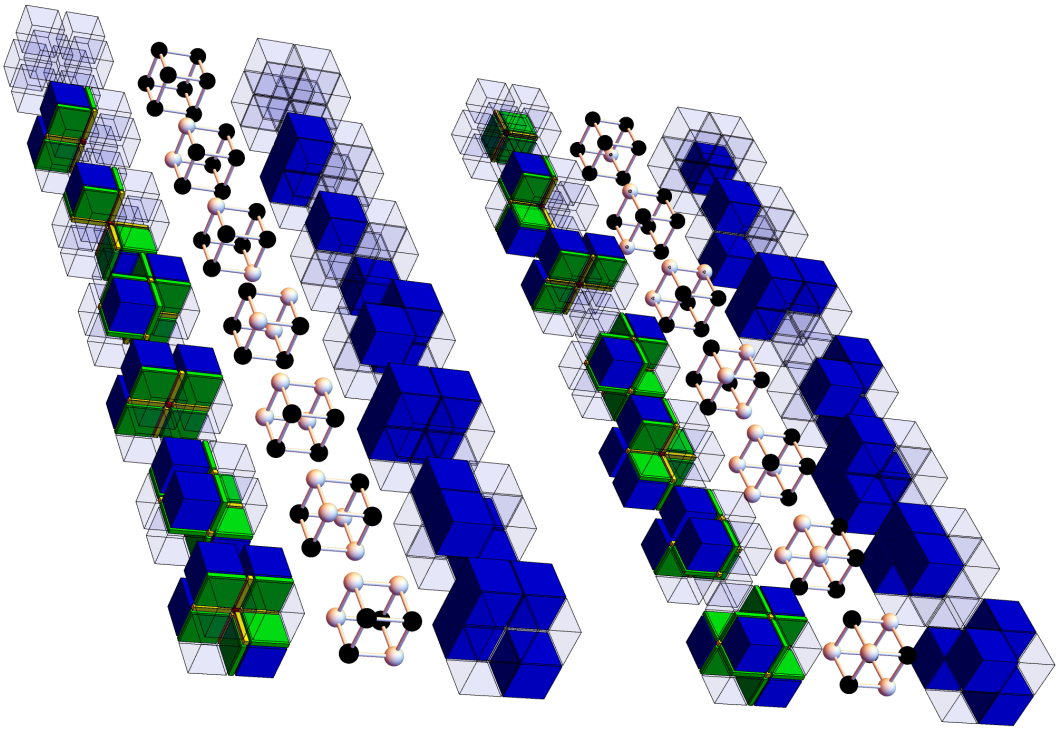

Figure 13.: Possible set configurations in 3D

4. if this restriction is made of two white points which are 8-adjacent but not 4-adjacent, that is, when we have a critical configuration, then we obtain that the red point has four neighbors, the four yellow edges.

Then the red points of the boundary of the representation of the set in Khalimsky grids admit only two neighbors iff the set is digitally well-composed. Since the yellow edges admit always two neighbors, because a boundary is closed (and then contains its vertices in the Khalimsky grid) by construction, we obtain finally that every set which is AWC is DWC and conversely in 2D.

Note that Figure 12 shows also the equivalence between DWCness and CWCness in 2D.

Also, since it is well-known that EWCness, DWCness, AWCness and CWCness are equivalent for digital sets in $\mathbb{Z}^2$, they are also equivalent for 2D digital binary or gray-level images.

In 3D, Latecki has proven that DWCness and CWCness are equivalent, and has also shown that they imply EWCness. However the proof of the equivalence of AWCness and DWCness in 3D, even if well-known and admitted in the community of digital topology, has not been published to our knowledge. That is why we propose to recall in brief why it is true (the detailed study in n-D, $n \geq 2$, is in Chapter D).

Looking at Figure 13, with the same reasoning as for the 2D case, we obtain that there is no critical configurations in the restriction $X \cap S$, where S is a 3D block, if and only if the boundary $\partial\mathcal{IMM}(X)$ (made of green squares, yellow edges, and red points) of the *immersion* $\mathcal{IMM}(X)$ (such that white points in $\mathbb{Z}^3$ become blue cubes) of X is locally a simple closed curve. At the contrary, in the cases containing one or more 2D critical configurations or a 3D critical configuration, $\partial\mathcal{IMM}(X)$ is not locally a simple closed curve: it contains a "pinch" at a yellow edge in the case of a 2D critical configuration and at a red point in the case of a 3D critical configuration. Note that the cases that we can obtain by complementarity have been omitted since well-composedness is self-dual. This gives the intuition of why AWCness and DWCness are equivalent in 3D.

2D:	**EWC** **1995** [102]	$\Leftrightarrow$	DWC	$\Leftrightarrow$	AWC	$\Leftrightarrow$	CWC
3D:	EWC	$\Leftarrow$	DWC	$\Leftrightarrow$	AWC	$\Leftrightarrow$	**CWC** **1997** [97]
n-D:	**EWC** **2015** [26]	$\Leftarrow$	**DWC** **2015** [26]	$\overset{?}{\Leftrightarrow}$	**AWC** **2013** [127]	$\overset{?}{\Leftrightarrow}$	**CWC** 2000 [100]

Table 1.: The different "flavors" of well-composedness and their relationship on cubical grids (our contributions are emphasized in yellow).

Obviously, the equivalence between AWCness, DWCness, and CWCness in 3D is also true for digital binary or gray-level images by extension.

Finally, thanks to Latecki, 3D CWCness implies 3D EWCness (for sets), and then each kind of WCness among AWCness, CWCness, and DWCness implies in 3D EWCness for sets, binary images, and gray-level images.

In n-D, it is more complicated, because the case-by-case study is impossible: the different possible cases depend on the given n. However, we have proven that DWCness in n-D implies EWCness for digital sets and then for binary and gray-level images.

We summarized all these relations in Table 1. Note that the relation between n-D DWCness, AWCness and CWCness has a "?" on the equivalence relationships because the proof of the equivalence between AWCness and DWCness remains not verified at this moment, and because the equivalence between AWCness and CWCness (exposed later) is a conjecture.

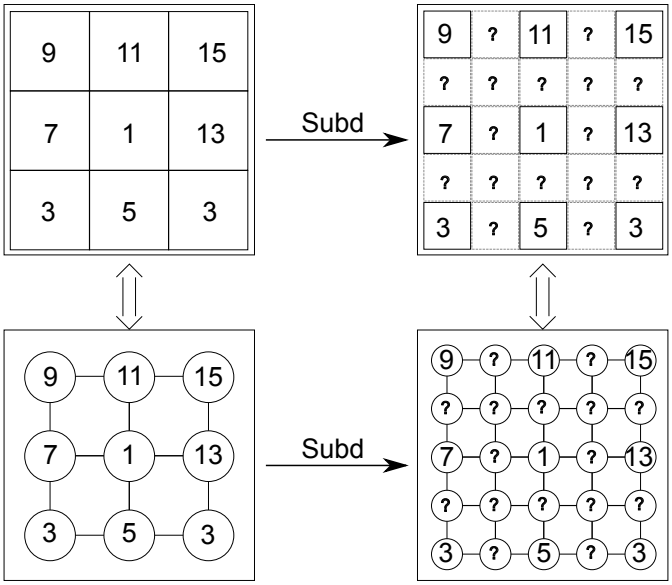

Figure 1.: Subdividing the domain $\mathcal{D}$ into $\mathcal{D}'$ to interpolate

4 DIGITALLY WELL-COMPOSED INTERPOLATIONS IN n-D

Let us begin with the definition of the interpolation of a digital image.

Definition 18. *An* interpolation *of an image* $(\mathbb{R}^n, \mathcal{D}, \mathbb{R}, u)$ *defined on a (bounded hyperrectangular) domain* $\mathcal{D} \subset \mathbb{Z}^n$ *is an image* $(\mathbb{R}^n, \mathcal{D}', \mathbb{R}, u')$ *such that its domain* $\mathcal{D}'$ *contains* $\mathcal{D}$ *and such that the restriction of the interpolation* u' *to the domain* $\mathcal{D}$ *of the initial image* u *is equal to* u *(see Figure 1).*

In this chapter, we are going to show that making an interpolation is not so easy when some criterias are required: digital well-composedness, *self-duality*, n-dimensionality, *in-betweeness*, and so on. In particular, we are going to show in Section 4.1 that *local interpolations* fail to produce 3D digitally well-composed interpolations satisfying all these constraints, and that another approach has to be found. In Section 4.2, we will expose the interpolation that we propose to this aim.

Note that, in the sequel, we will always assume that the given images are defined on a bounded hyperrectangular domain, that is, on sets that can be written:

$$\prod_{i \in [\![1,n]\!]} [\![m_i, M_i]\!],$$

where $\prod$ is the *Cartesian product* and where m, M are the *minimal bound* and *maximal bound* of the domain respectively; their interpolations will be defined on *subdivisions* of these domains, that is, on sets that can be written such as:

$$\prod_{i \in [\![1,n]\!]} [m_i, M_i] \cap \left(\frac{\mathbb{Z}}{2}\right)^n.$$

Also, the topological notions that have been presented before are naturally extended from $\mathbb{Z}^n$ to $(\mathbb{Z}/s)^n$, with $s \in \mathbb{N}^*$ the *subdivision factor*, in the following manner: two points $p, q \in (\mathbb{Z}/s)^n$ are said to be $2n$-neighbours respectively (3^n-1)-neighbours) in $(\mathbb{Z}/s)^n$ iff $||p-q||_1 = 1/s$ (respectively if $||p-q||_\infty = 1/s$), the $2n$-neighborhood (respectively the (3^n-1)-neighborhood) of a point $p \in (\mathbb{Z}/s)^n$ is the set $\mathcal{N}_{2n}(p, (\mathbb{Z}/s)^n) = \{q \ ; \ ||p-q||_1 \leq 1/s\}$ (respectively $\mathcal{N}_{3^n-1}(p, (\mathbb{Z}/s)^n) = \{q \ ; \ ||p-q||_\infty \leq 1/s\}$), from which we deduce their starred versions which are respectively $\mathcal{N}^*_{2n}(p, (\mathbb{Z}/s)^n) = \mathcal{N}_{2n}(p, (\mathbb{Z}/s)^n) \setminus \{p\}$ and $\mathcal{N}^*_{3^n-1}(p, (\mathbb{Z}/s)^n) = \mathcal{N}_{3^n-1}(p, (\mathbb{Z}/s)^n) \setminus \{p\}$. For $\xi \in \{2n, 3^n-1\}$, the ξ-connectivity and then the ξ-components are computed based on the ξ-neighborhood relationship in $(\mathbb{Z}/s)^n$. In the same manner, blocks in $(\mathbb{Z}/s)^n$ are defined such that, given a point $z \in (\mathbb{Z}/s)^n$ and a family of vector:

$$\mathcal{F} = (f^1, \ldots, f^k) \subseteq \mathbb{B},$$

the *block* associated to the couple $(z, \mathcal{F})$ in $(\mathbb{Z}/s)^n$ is such that:

$$S_s(z, \mathcal{F}, (\mathbb{Z}/s)^n) = \left\{ z + \sum_{i \in [\![1,k]\!]} \lambda_i f^i \ \middle| \ \lambda_i \in \{0, 1/s\}, \forall i \in [\![1,k]\!] \right\},$$

and the set of blocks in $(\mathbb{Z}/s)^n$ are denoted by $\mathcal{B}((\mathbb{Z}/s)^n)$. Based on this definition, we obtain easily that two points $p, q \in (\mathbb{Z}/s)^n$ are *antagonist* in a block of $(\mathbb{Z}/s)^n$ iff they maximise the L^1-distance between two points into this block. Then, let $X \subset (\mathbb{Z}/s)^n$ be a digital set, and let $S \in \mathcal{B}((\mathbb{Z}/s)^n)$ be a block of dimension $k \in [\![2, n]\!]$. We say that X contains a *primary critical configuration* of dimension k in the block S as a subset of $(\mathbb{Z}/s)^n$ iff $X \cap S = \{p, p'\}$ with $p, p' \in S$ two points that are antagonist into S. We say that X contains a *secondary critical configuration* of dimension k in the block S as a subset of $(\mathbb{Z}/s)^n$ iff $X \cap S = S \setminus \{p, p'\}$ with $p, p' \in S$ two points that are antagonist into S. As usual, a critical configuration in $(\mathbb{Z}/s)^n$ is either a primary or a secondary critical configuration in $(\mathbb{Z}/s)^n$. A subset X of $(\mathbb{Z}/s)^n$ is then said *digitally well-composed (DWC)* iff it does not contain any primary or secondary critical configuration in $(\mathbb{Z}/s)^n$. Also, a subset X of $(\mathbb{Z}/s)^n$ is said *well-composed based on the equivalence of connectivities (EWC)* iff the connected components of X (respectively of $(\mathbb{Z}/s)^n \setminus X$) in $(\mathbb{Z}/s)^n$ do not depend on the chosen connectivity.

4.1 SELF-DUAL LOCAL INTERPOLATIONS

After having recalled some preliminary vocabulary related to *cubical subdividions*, the usual process used to subdivide $\mathbb{Z}^n$ into $\left(\frac{\mathbb{Z}}{2}\right)^n$, we will show that an "usual" interpolation of a digital image is simply a numerical scheme with some constraints. In particular, when we combine *orderedness*, invariance by 90 degrees rotations, translations and axial symmetries, *in-betweenness*, and digital well-composedness, we can characterize our interpolation method by a set of "interpolating functions" that are used one by one to construct the interpolation in such a way that it is digitally well-composed on all its domain at the end of the interpolation (if no impossible case is encountered). Finally we will observe that our counter-example shows that every self-dual interpolation verifying the above properties fail in 3D and higher dimensions.

4.1.1 *Subdivisions and interpolations*

A block of $\mathbb{Z}^n$ can be *subdivided* into blocks of $(\mathbb{Z}/s)^n$, where s belongs to $\mathbb{N}^*$, using the following procedure:

Definition 19 (Cubical subdivision of a block)**.** *Let us assume that a value $s \in \mathbb{N}^*$ is given. Let $S \in \mathcal{B}(\mathbb{Z}^n)$ be a block of dimension $k \geq 0$ associated to a point $z \in \mathbb{Z}^n$ and the family of*

vectors $\mathcal{F} = (f^1, \ldots, f^k) \subseteq \mathbb{B}$ *associated to* S*. Then the* cubical subdivision *of* S *is denoted by* $\mathrm{Subd}_s(S)$ *and is equal to:*

$$\left\{ z + \sum_{i \in [\![1,k]\!]} \lambda_i f^i ; \forall i \in [\![1,k]\!], \lambda_i \in \{0, \frac{1}{s}, \frac{2}{s}, \ldots, 1\} \right\}.$$

In the case where s is even, like when $s = 2$, we will sometimes speak about the *center* of a subdivided block. For a given block $S \in \mathcal{B}(\mathbb{Z}^n)$, the *center* of the block S is defined as $(p+q)/2$ where p and q are two antagonists in this block. Obviously, this point belongs to $\left(\frac{\mathbb{Z}}{2}\right)^n$ and is unique (in the sense that it does not depend on the couple of antagonists that has been chosen to compute it).

Let us define now the *cubical subdivision* of a domain:

Definition 20 (Cubical subdivision of a bounded hyperrectangle)**.** *Let us assume that a value* $s \in \mathbb{N}^*$ *is given. Let* $\mathcal{D} \subseteq \mathbb{Z}^n$ *be a bounded hyperrectangle. Then the* cubical subdivision *of this domain is the union of the subdivision of the blocks of* $\mathbb{Z}^n$ *that are subset of this domain:*

$$\mathrm{Subd}_s(\mathcal{D}) = \bigcup_{S \in \mathcal{B}(\mathcal{D})} \mathrm{Subd}_s(S).$$

Obviously, $\mathrm{Subd}_s(\mathcal{D}) \subseteq (\mathbb{Z}/s)^n$.

Note that, from now on, we will omit the term s in Subd_s to represent the operator Subd_2, corresponding to the cubical subdivision with $s = 2$.

Now that we have defined the cubical subdivision of a domain, we can define an interpolation of an image defined on a cubical grid.

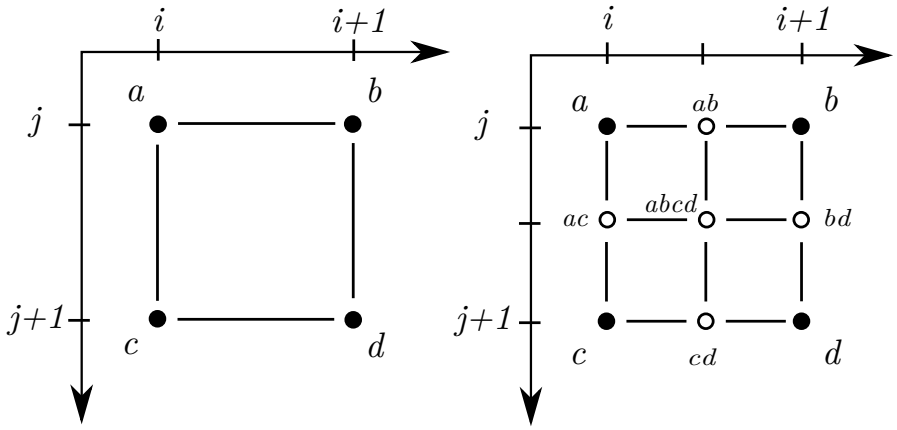

Figure 2.: Illustration of the cubical subdivision process on a block S

Definition 21 (Interpolations)**.** *Let* $(\mathbb{Z}^n, \mathcal{D}, \mathbb{R}, u)$ *be a given image (with* $\mathcal{D}$ *a bounded hyperrectangle). We call* real-valued digital interpolation of u *any image* $\left(\left(\frac{\mathbb{Z}}{2}\right)^n, \mathrm{Subd}(\mathcal{D}), \mathbb{R}, u'\right)$ *such that its restriction to* $\mathcal{D}$ *is equal to* u*:*

$$u'\big|_{\mathcal{D}} = u.$$

For example, on Figure 2, we can see an image defined on a 2D block and that can be represented as a 2D matrix by $\begin{pmatrix} a & b \\ c & d \end{pmatrix}$. On its right side, we can observe the interpolation of this image:

$$\begin{pmatrix} a & ab & b \\ ac & abcd & bd \\ c & cd & d \end{pmatrix},$$

where the pixels $(i, j, u(i, j) = a)$, $(i+1, j, u(i+1, j) = b)$, $(i, j+1, u(i, j+1) = c)$, and $(i+1, j+1, u(i+1, j+1) = d)$, the *primary pixels*, preserved their positions, and where $(i+1/2, j, ab)$, $(i, j+1/2, ac)$,$(i+1, j+1/2, bd)$, $(i+1/2, j+1, cd)$, and $(i+1/2, j+1/2, abcd)$, the *secondary pixels*, are "inserted" between the primary ones.

Now let us observe that the cubical subdivision (of a block) of $\mathbb{Z}^n$ when $s = 2$ induces an *relation order*, that is, a binary relation $R : \left(\frac{\mathbb{Z}}{2}\right)^n \to \{0, 1\}$ which is *reflexive* ($\forall a, a R a$), *antisymmetrical* ($\forall a, b, a R b \wedge b R a \Rightarrow a = b$), and *transitive* ($\forall a, b, c, a R b \wedge b R c \Rightarrow a R c$).

For that, let us define the mapping $\mathfrak{o} : \left(\frac{\mathbb{Z}}{2}\right)^n \to \mathbb{N}$, called the *order*, defined such that $\forall p \in \mathbb{Z}^n, \mathfrak{o}(p) = 0$, such that for each point $q \in \left(\frac{\mathbb{Z}}{2}\right)^n$ inserted at $\frac{q^1+q^2}{2}$ where $q^1, q^2 \in \left(\frac{\mathbb{Z}}{2}\right)^n$ are two points of order o such that $||q^1 - q^2||_1 = 1$, $\mathfrak{o}(q) = 1$, such that for each point $q \in \left(\frac{\mathbb{Z}}{2}\right)^n$ inserted at $\frac{q^1+q^2}{2}$ where $q^1, q^2 \in \left(\frac{\mathbb{Z}}{2}\right)^n$ are two points of order 1 such that $||q^1 - q^2||_1 = 1$, $\mathfrak{o}(r) = 2$, and so on until the order n.

This way, we can define the binary relation $R : \left(\frac{\mathbb{Z}}{2}\right)^n \to \{0, 1\}$ such that $p, q \in \left(\frac{\mathbb{Z}}{2}\right)^n$ verify $p R q$ which is said "p is *parent* of q" iff $\mathfrak{o}(p) \leq \mathfrak{o}(q)$ and $\|p - q\|_\infty \leq 1/2$. The couple $(\mathbb{Z}^n, R)$ which represents $\mathbb{Z}^n$ supplied with the order relation R is called a *partial order* or *poset*. Also, a point $p \in \left(\frac{\mathbb{Z}}{2}\right)^n$ is said to be a *direct parent* of $q \in \left(\frac{\mathbb{Z}}{2}\right)^n$ iff $p R q$ and there exists no point into $\left(\frac{\mathbb{Z}}{2}\right)^n \setminus \{p, q\}$ such that $p R r$ and $r R q$.

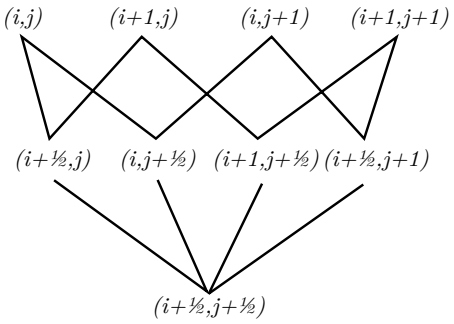

Figure 3.: $\mathrm{Subd}(S) \subseteq \left(\frac{\mathbb{Z}}{2}\right)^n$ as a poset

Figure 3 shows this parenthood relationship between the points of a 2D block $S((i, j), (e^1, e^2))$ by linking a point of the 2D block and its direct parent(s) in this block. Based on this figure, we can also obtain the following matrix of orders corresponding to this subdivided block:

$$\begin{pmatrix} 0 & 1 & 0 \\ 1 & 2 & 1 \\ 0 & 1 & 0 \end{pmatrix}.$$

A generalization to dimension $n \geq 2$ is proposed in the next subsection.

Note that a similar relation exists using the Khalimsky grids, where the order relation is based on the inclusion, but we do not have any inclusion right here since we are working on graphs made of vertices and edges.

4.1.2 *Notations specific to cubical subdivisions*

As we have seen before, we can associate an order to a position in $\left(\frac{\mathbb{Z}}{2}\right)^n$ assuming that this space results from the subdivision of $\mathbb{Z}^n$. Let us define this notion more formally.

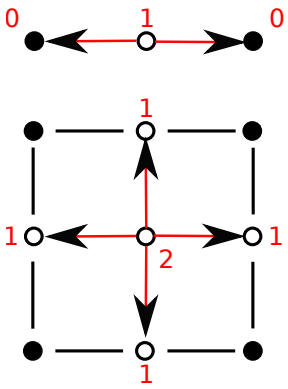

Figure 4.: Parenthood relationship in the graph of a subdivided block

Definition 22. *We denote by* $\frac{1}{2}(z)$ *the set of the coordinates of the point* $z \in \left(\frac{\mathbb{Z}}{2}\right)^n$ *such that they are not integers:*

$$\frac{1}{2}(z) = \left\{ i \in [\![1, n]\!] \; ; \; z_i \in \frac{\mathbb{Z}}{2} \setminus \mathbb{Z} \right\}.$$

This notation, even if looking much simple, will be very useful in the following, because it permits to classify the points of $\left(\frac{\mathbb{Z}}{2}\right)^n$ just based on the number of integral coordinates.

Definition 23 (Order)**.** *We denote by* $\mathbb{E}_k$ *with* $k \in [\![0, n]\!]$ *the set of points in* $\left(\frac{\mathbb{Z}}{2}\right)^n$ *such that they have* $(n - k)$ *integral coordinates:*

$$\mathbb{E}_k = \left\{ z \in \left(\frac{\mathbb{Z}}{2}\right)^n \; ; \; \mathrm{Card}\left(\frac{1}{2}(z)\right) = k \right\}.$$

Then, we call order *of a point* $z \in \left(\frac{\mathbb{Z}}{2}\right)^n$ *the value* k *such that* $z \in \mathbb{E}_k$.

The sets of parents can then be defined very easily:

Definition 24 (Parents)**.** *Let* z *be an element of* $\left(\frac{\mathbb{Z}}{2}\right)^n \setminus \mathbb{Z}^n$*. The set of* (direct) parents *(see Figure 4) of* z *is denoted by* $\mathbb{P}(z)$ *and equal to:*

$$\mathbb{P}(z) = \bigcup_{i \in \frac{1}{2}(z)} \left\{ z + \frac{e^i}{2}, z - \frac{e^i}{2} \right\}.$$

With z *an element of* $\left(\frac{\mathbb{Z}}{2}\right)^n$*, we define the* 0^{th} *order parents of* z *denoted* $\mathbb{P}^0(z)$ *and equal to* $\{z\}$*. Also, we define recursively, for any* z *element of* $\left(\frac{\mathbb{Z}}{2}\right)^n \setminus \mathbb{Z}^n$*, and for* $k \geq 1$*:*

$$\mathbb{P}^k(z) = \bigcup_{p \in \mathbb{P}(z)} \mathbb{P}^{k-1}(p).$$

Note that a point of $\mathbb{Z}^n$ does not have parents if it corresponds to a primary pixel. However points of order 1 have parents of order 0, points of order 2 have parents of order 1, and so on. Also we can remark that $\{\mathbb{E}_k\}_{k \in [\![0,n]\!]}$ represents a partition of $\left(\frac{\mathbb{Z}}{2}\right)^n$.

Now we define a category of points that we call *ancesters* (of a point $p \in \left(\frac{\mathbb{Z}}{2}\right)^n$). They are very useful because they represent the set of positions of the pixels of which directly depends the value of the interpolation at p (see Figure 5) when using *local interpolations*.

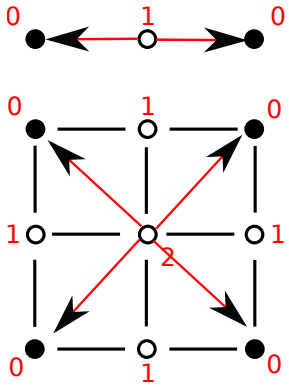

Figure 5.: Ancesters of the point z at the center of the subdivided block

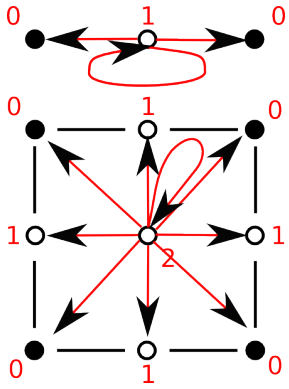

Figure 6.: Groups of the point z at the center of the subdivided block

Definition 25 (Ancesters). *Let z be an element of $\left(\frac{\mathbb{Z}}{2}\right)^n$. The set of the* ancesters of p *is denoted by $\mathbb{A}(p)$ and is defined such that:*

$$\mathbb{A}(p) = \mathbb{P}^{\mathfrak{O}(z)}(z).$$

Note that $\mathbb{A}(p)$ is a subset of $\mathbb{Z}^n$.

Definition 26 (Groups). *Let z be an element of $\left(\frac{\mathbb{Z}}{2}\right)^n$. The* group of p *denoted by $\mathcal{G}(p)$ is defined such that:*

$$\mathcal{G}(p) = \bigcup_{k \in [\![0, \mathfrak{O}(z)]\!]} \mathbb{P}^k(z),$$

and represents the set of all the parents of any order of z in $\left(\frac{\mathbb{Z}}{2}\right)^n$.

The usefulness of *groups* (see Figure 6) of a point $z \in \left(\frac{\mathbb{Z}}{2}\right)^n$ will be seen later.

A last notation is useful when we work with *in-between interpolations*.

Definition 27 (Opposites). *Let z be an element of $\left(\frac{\mathbb{Z}}{2}\right)^n \setminus \mathbb{Z}^n$. The set of* opposites *of z is the family of pairs or points:*

$$\mathrm{opp}(z) = \bigcup_{i \in \frac{1}{2}(z)} \left\{ \left\{ z - \frac{e^i}{2}, z + \frac{e^i}{2} \right\} \right\}.$$

Let a, b, z be three points of $\left(\frac{\mathbb{Z}}{2}\right)^n$, we say that a is opposite to b relatively to z *iff $\{a, b\} \in \mathrm{opp}(z)$.*

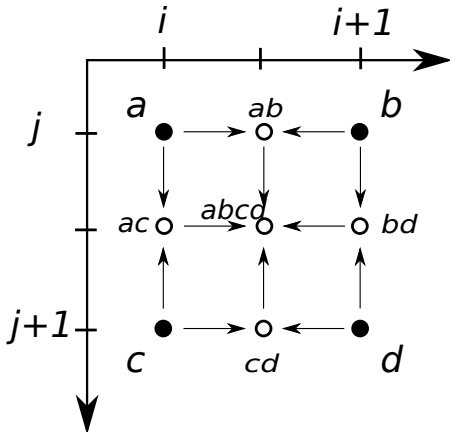

Figure 7.: Ordered computing of the values of the interpolation

Now that we have defined the mathematical basics in matter of cubical subdivisions, we are able to define the different properties that an "usual" local interpolation has to satisfy on a cubical grid.

4.1.3 *"Usual" local interpolations*

We have seen that an image $u' \in \mathbb{I}\mathrm{m}(\left(\frac{\mathbb{Z}}{2}\right)^n, \mathbb{R})$ defined on a domain $\mathcal{D}' \subset \left(\frac{\mathbb{Z}}{2}\right)^n$ is an interpolation of an image $u \in \mathbb{I}\mathrm{m}(\mathbb{Z}^n, \mathbb{R})$ defined on a given domain $\mathcal{D} \subset \mathbb{Z}^n$ iff $\mathcal{D} \subseteq \mathcal{D}'$ and the restriction of u' to $\mathcal{D}$, noted $u'\big|_{\mathcal{D}}$, is equal to u, that is, for any $p \in \mathcal{D}$, $u'(p) = u(p)$.

Definition 28. *An operator $\mathcal{I} : \mathbb{I}\mathrm{m}(\mathbb{Z}^n, \mathbb{R}) \to \mathbb{I}\mathrm{m}(\left(\frac{\mathbb{Z}}{2}\right)^n, \mathbb{R})$ is said to be a* cubical (real-valued) interpolation method *iff for any image $u \in \mathbb{I}\mathrm{m}(\mathbb{Z}^n, \mathbb{R})$ defined on a bounded hyperrectangle $\mathcal{D} \subseteq \mathbb{Z}^n$, $\mathcal{I}(u) : \mathrm{Subd}(\mathcal{D}) \to \mathbb{R}$ is an interpolation of u.*

Definition 29 (Self-duality)**.** *A cubical real-valued interpolation method $\mathcal{I} : \mathbb{I}\mathrm{m}(\mathbb{Z}^n, \mathbb{R}) \to \mathbb{I}\mathrm{m}(\left(\frac{\mathbb{Z}}{2}\right)^n, \mathbb{R})$ is said* self-dual *iff for any image $u \in \mathbb{I}\mathrm{m}(\mathbb{Z}^n, \mathbb{R})$, we have the relation:*

$$\mathcal{I}(-u) = -\mathcal{I}(u)$$

In other words, if we denote by u'_+ the interpolation by $\mathcal{I}$ of u and by u'_- the interpolation by $\mathcal{I}$ of $(-u)$, both of domain $\mathcal{D}' \subseteq \left(\frac{\mathbb{Z}}{2}\right)^n$, we have for any $p \in \mathcal{D}'$ the relation:

$$u'_+(p) = -u'_-(p).$$

Self-duality is much important to us, and in image analysis in general, because it represents that an image will be treated in the same manner whatever if it contains bright components over a dark background or dark components over a bright background.

Definition 30 (Ordered)**.** *Let $\mathcal{D}$ be a bounded hyperrectangle in $\mathbb{Z}^n$. A cubical real-valued interpolation method:*

$$\mathcal{I} : \mathbb{I}\mathrm{m}(\mathbb{Z}^n, \mathcal{D}, \mathbb{R}) \to \mathbb{I}\mathrm{m}(\left(\frac{\mathbb{Z}}{2}\right)^n, \mathrm{Subd}(\mathcal{D}), \mathbb{R})$$

is said ordered *iff for any image $u \in \mathbb{I}\mathrm{m}(\mathbb{Z}^n, \mathbb{R})$, at each point $p \in \mathrm{Subd}(\mathcal{D})$, the value $u'(p)$ of the interpolation $\mathcal{I}(u)$ at p is computed based only on the values of u at the parents of p in $\left(\frac{\mathbb{Z}}{2}\right)^n$. In other words, the values at the centers of the subdivided "edges" depend only on the values at the vertices of the initial edges, the values at the center of the subdivided "squares" depend only on the values at the centers of its edges, and so on.*

As depicted on Figure 7 illustrating orderedness of an interpolation method, on the image $\begin{pmatrix} a & ab & b \\ ac & abcd & bd \\ c & cd & d \end{pmatrix}$, ab is a function of a and b, ac is a function of a and c, bd is a function of b and d, cd is a function of c and d, and $abcd$ is a function of ab, ac, bd and cd, and then also a function of a,b,c and d. In other words, the values of the secondary pixels depend on the value of their ancesters. In this manner, an interpolation method which is ordered is also *local*:

Definition 31 (Local). *Let $\mathcal{D}$ be a bounded hyperrectangle in $\mathbb{Z}^n$. A cubical real-valued interpolation method $\mathcal{I} : \mathbb{Im}(\mathbb{Z}^n, \mathcal{D}, \mathbb{R}) \to \mathbb{Im}(\left(\frac{\mathbb{Z}}{2}\right)^n, \mathrm{Subd}(\mathcal{D}), \mathbb{R})$ is said* local *iff for any image $u \in \mathbb{Im}(\mathbb{Z}^n, \mathcal{D}, \mathbb{R})$, at each point $p \in \mathrm{Subd}(\mathcal{D})$, the value $u'(p)$ of the interpolation $\mathcal{I}(u)$ at p is computed based only on the values $u\big|_{\mathbb{A}(p)}$.*

Definition 32 (In-between). *A cubical real-valued interpolation method $\mathcal{I} : \mathbb{Im}(\mathbb{Z}^n, \mathbb{R}) \to \mathbb{Im}(\left(\frac{\mathbb{Z}}{2}\right)^n, \mathbb{R})$ is said* in-between *iff for any image $u \in \mathbb{Im}(\mathbb{Z}^n, \mathbb{R})$ defined on a domain $\mathcal{D} \subseteq \mathbb{Z}^n$ which is a bounded hyperectangle, its interpolation $u' = \mathcal{I}(u)$ defined on the domain $\mathcal{D}' = \mathrm{Subd}(\mathcal{D})$ is such that at each point $p \in \mathcal{D}' \setminus \mathcal{D}$, the value $u'(p)$ satisfies the relation:*

$$u'(p) \in \bigcap_{\{z^-, z^+\} \in \mathrm{opp}(p)} \mathrm{intvl}(u'(z^+), u'(z^-)).$$

Note that this relation is recursive. Also, this property is very interesting because it implies that we do not create any extrema in the image when we proceed to the interpolation.

Definition 33 (DWC interpolations). *A cubical real-valued interpolation method $\mathcal{I} : \mathbb{Im}(\mathbb{Z}^n, \mathbb{R}) \to \mathbb{Im}(\left(\frac{\mathbb{Z}}{2}\right)^n, \mathbb{R})$ is said* digitally well-composed (DWC) *iff for any image $u \in \mathbb{Im}(\mathbb{Z}^n, \mathbb{R})$ defined on a domain $\mathcal{D} \subseteq \mathbb{Z}^n$ which is a bounded hyperrectangle, its interpolation $u' = \mathcal{I}(u)$ defined on the domain $\mathcal{D}' = \mathrm{Subd}(\mathcal{D})$ is digitally well-composed.*

Note that we make the difference between an interpolation, which is a digitally well-composed image, and an interpolation method, which is an operator which produces digitally well-composed images.

Now we can express the set of properties that "usual" local interpolations on cubical grids satisfy in general. We call this set of properties $(\mathcal{P})$.

Notations 1.

$$(\mathcal{P}) \equiv \begin{cases} \mathcal{I} \text{ is a cubical real-valued interpolation} \\ \mathcal{I} \text{ is invariant by translations, } \frac{\pi}{2}\text{'s rotations and axial symmetries} \\ \mathcal{I} \text{ is ordered} \\ \mathcal{I} \text{ is in-between} \\ \mathcal{I} \text{ is self-dual} \\ \mathcal{I} \text{ is digitally well-composed} \end{cases}$$

Note that there exist other manners to subdivide the domain before proceeding to the interpolation. Effectively, the interpolation could be done on a domain such that we added more than one pixel between each pixel. Also, we could imagine a "double" interpolation, that is, made of two succesive interpolations, which could lead to primary, secondary, and then ternary pixels. See Figure 8 for an illustration of these two methods. In our study, we will limit ourselves to "simple" interpolations which subdivide only once the original domain, as described for the cubical real-valued interpolation methods using the operator Subd.

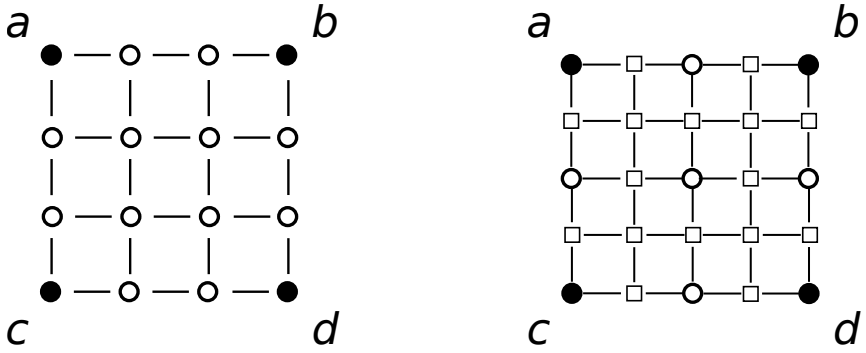

(a) Atypic subdivision. (b) Double interpolation.

Figure 8.: Other kinds of subdivisions/interpolations

4.1.4 *Constrained interpolation methods*

We are going to show in this subsection that taking into account the set of properties $(\mathcal{P})$ for an interpolation method is equivalent to solve a system of equations.

Lemma 7. *Any cubical real-valued interpolation method* $\mathcal{I} : \mathbb{I}\mathrm{m}(\mathbb{Z}^n, \mathbb{R}) \to \mathbb{I}\mathrm{m}(\left(\frac{\mathbb{Z}}{2}\right)^n, \mathbb{R})$ *verifying* $(\mathcal{P})$ *can be characterized by a set of functions* $\{f_k\}_{k\in[\![1,n]\!]}$ *constraining* $u' = \mathcal{I}(u)$ *such that:*

$$\forall\, z \in \left(\frac{\mathbb{Z}}{2}\right)^n,\ u'(z) = \begin{cases} u(z) & \text{if } z \in \mathbb{E}_0 \\ f_k(u|_{\mathbb{A}(z)}) & \text{if } z \in \mathbb{E}_k,\ k \in [1,n] \end{cases}$$

We denote such an interpolation method $\mathcal{I}_{f_1,\dots,f_n}$.

Proof: The interpolation u' at the center of a subdivided 1D block depends only on the values of u at the points of $\mathbb{E}_0$. Furthermore, this method has to be invariant by translations, 90 degrees rotations and then does not depend on the position or on the orientation of the 1D block. It does not depend neither on the order of these two values because the process is invariant by symmetries. Hence, there is an unique function f_1 characterizing this method on subdivisions of 1D blocks, and this function must be symmetrical. On a subdivision of a 2D block, the only unknown value is at its center, since the values belonging to $\mathbb{E}_0$ or $\mathbb{E}_1$ in the subdivided domain are already valued. Since the method in invariant by translations and 90 degrees rotations, the function that value the center of the subdivided 2D block does not depend on the position or on the rotation, and then there exists only one function f_2 used to compute this value. We can follow iteratively the reasoning for the subdivisions of blocks of greater dimensions until n. □

Notice that this Lemma is an implication and not an equivalence: an interpolation verifying this numerical scheme does not always verify all the properties in $(\mathcal{P})$.

Definition 34 (I_0)**.** *Let* $(\mathbb{Z}^n, \mathcal{D}, \mathbb{R}, u)$ *be an image and let* $\mathcal{I} : \mathbb{I}\mathrm{m}(\mathbb{Z}^n, \mathbb{R}) \to \mathbb{I}\mathrm{m}(\left(\frac{\mathbb{Z}}{2}\right)^n, \mathbb{R})$ *be a cubical real-valued interpolation method, such that we obtain the interpolation* $u' = \mathcal{I}(u)$ *defined on the domain* $\mathcal{D}' = \mathrm{Subd}(\mathcal{D})$*. In this case, we can define the set* $I_0(u', z)$ *representing the set of possible values* $u'(z)$ *at* $z \in \mathcal{D}' \setminus \mathcal{D}$ *such that* $\mathcal{I}$ *is in-between:*

$$I_0(u', z) = \bigcap_{\{z^-, z^+\} \in \mathrm{opp}(z)} \mathrm{intvl}(u'(z^+), u'(z^-)).$$

In this manner, $\mathcal{I}$ *is in-between iff* $\forall z \in \mathcal{D}' \setminus \mathcal{D},\ u'(z) \in I_0(u', z)$.

Definition 35 (I_{WC})**.** *Let* $(\mathbb{Z}^n, \mathcal{D}, \mathbb{R}, u)$ *be an image and let be a cubical real-valued interpolation method* $\mathcal{I} : \mathbb{I}\mathrm{m}(\mathbb{Z}^n, \mathbb{R}) \to \mathbb{I}\mathrm{m}(\left(\frac{\mathbb{Z}}{2}\right)^n, \mathbb{R})$ *such that we obtain the interpolation* $u' = \mathcal{I}(u)$ *defined on*

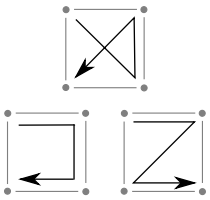

Figure 9.: The 3 possible configurations in 2D (modulo reflections and rotations)

the domain $\mathcal{D}' = \mathrm{Subd}(\mathcal{D})$. *In this case, we define the set* $I_{WC}(u', z)$ *such that for any* $z \in \mathbb{E}_1 \cap \mathcal{D}'$, $I_{WC}(u', z) = \mathbb{R}$ *and for any* $z \in \mathbb{E}_k \cap \mathcal{D}'$ *with* $k \in [\![2, n]\!]$*:*

$$I_{WC}(u', z) \;=\; \{\, v \in \mathbb{R} \;\mid\; u'(z) = v \;\Rightarrow\; u'|_{\mathcal{G}(z)} \text{ is DWC} \,\}$$

Now, we can see that the restriction of u' to $\mathcal{G}(z) \setminus \{z\}$ makes the algorithm able to decide how to value $u'(z)$ such that the restriction of u' will be DWC on $\mathcal{G}(z)$. This way, if no unsolvable case is encountered, u' will be digitally well-composed on the whole domain $\mathcal{D}'$ as a subset of $\left(\frac{\mathbb{Z}}{2}\right)^n$ at the end of the interpolation.

Definition 36 (I_{sol})**.** *Let* $(\mathbb{Z}^n, \mathcal{D}, \mathbb{R}, u)$ *be an image and let be a cubical real-valued interpolation method* $\mathcal{I} : \mathbb{Im}(\mathbb{Z}^n, \mathbb{R}) \to \mathbb{Im}(\left(\frac{\mathbb{Z}}{2}\right)^n, \mathbb{R})$ *such that we obtain the interpolation* $u' = \mathcal{I}(u)$ *defined on the domain* $\mathcal{D}' = \mathrm{Subd}(\mathcal{D})$. *In this case, we define the set* $I_{sol}(u', z)$ *such that for any* $z \in \mathcal{D}' \setminus \mathcal{D}$*:*

$$I_{sol}(u', z) \;=\; I_0(u', z) \cap I_{WC}(u', z).$$

The set $I_{sol}(u', z)$ takes into account at the same time the fact that $\mathcal{I}$ must be digitally well-composed in $\left(\frac{\mathbb{Z}}{2}\right)^n$, in-between, and ordered.

Proposition 15. *Let* $(\mathbb{Z}^n, \mathcal{D}, \mathbb{R}, u)$ *be an image and let be a cubical real-valued interpolation method* $\mathcal{I} : \mathbb{Im}(\mathbb{Z}^n, \mathbb{R}) \to \mathbb{Im}(\left(\frac{\mathbb{Z}}{2}\right)^n, \mathbb{R})$ *such that we obtain the interpolation* $u' = \mathcal{I}(u)$ *defined on the domain* $\mathcal{D}' = \mathrm{Subd}(\mathcal{D})$. *In this case, if* $\mathcal{I}$ *satisfies* $(\mathcal{P})$*, then we have:*

$$\forall z \in \left(\frac{\mathbb{Z}}{2}\right)^n, u'(z) = \begin{cases} u(z) & \text{if } z \in \mathbb{E}_0, \\ f_k(u|_{\mathbb{A}(z)}) \in I_{sol}(u, z) & \text{if } z \in \mathbb{E}_k, k \in [1, n]. \end{cases}$$

Proof: It is the direct consequence of Lemma 7 and Definition 36. □

Notice that, this way, such a local interpolation method $\mathcal{I}$ is ordered, in-between, digitally well-composed, but not necessarily self-dual, and then this numerical scheme is not sufficient to ensure that $\mathcal{I}$ satisfies $(\mathcal{P})$.

Now that we have proven that the set of functions $\{f_1, \ldots, f_n\}$ is characteristic of such interpolations, let us determine them.

4.1.5 *Determining* f_1

Let us begin with the study of f_1, *i.e.*, the function setting the values at the centers of the subdivided blocks of dimension 1. This function has to be self-dual, symmetrical, and in-between due to $(\mathcal{P})$. We choose one of the most common function satisfying these constraints: the mean operator $f_1 : \mathbb{R}^2 \mapsto \mathbb{R} : (v_1, v_2) \mapsto f_1(v_1, v_2) = (v_1 + v_2)/2$.

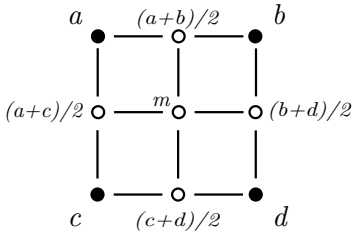

Figure 10.: $u'\big|_{\mathcal{G}(z)}$ for $z \in \mathbb{E}_2$ for any self-dual local interpolation after the application of f_1 (with m any value $\in \mathbb{R}$).

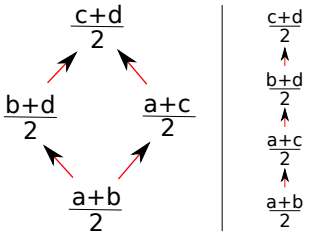

Figure 11.: The Hasse diagrams for the α- and the U-configurations (left) and for the Z-configuration (right)

4.1.6 *Equations of f_2*

Concerning f_2, *i.e.*, the function which sets the values of u' at the centers of the subdivided blocks of dimension 2, let us compute $I_0(u', z)$ and $I_{WC}(u', z)$ for any given $z \in \mathbb{E}_2$ to deduce $I_{sol}(u', z)$.

However, since their values depend on the configurations of $u\big|_{\mathbb{A}(z)}$, let us examine which configurations are possible in the 2D case. Let us assume that $u\big|_{\mathbb{A}(z)} = \begin{pmatrix} a & b \\ c & d \end{pmatrix}$. Then a total of $4! = 24$ configurations are possible. Modulo 90 degrees rotations, axial symmetries and reflections, it remains only 3 possible configurations: the *α-configurations* which correspond to the relation $a \leq d < b \leq c$, the *U-configurations* which corresponds to $a \leq b \leq d \leq c$, and the *Z-configurations* which corresponds to $a \leq b \leq c \leq d$ (see Figure 9).

Proposition 16. *Let $\left(\left(\frac{\mathbb{Z}}{2}\right)^n, \mathcal{D}, \mathbb{R}, u\right)$ be a given real-valued image, and let z be a point in $z \in \mathbb{E}_2 \cap \mathrm{Subd}(\mathcal{D})$. Modulo 90 degrees rotations and symmetries, an α-configuration implies that $u\big|_{\mathbb{A}(z)}$ is not digitally well-composed in $\mathbb{Z}^n$, whereas a U- or Z-configuration implies that $u\big|_{\mathbb{A}(z)}$ is digitally well-composed in $\mathbb{Z}^n$.*

Proof: Let us assume that an image $u : \mathcal{D} \subseteq \mathbb{Z}^n \to \mathbb{R}$ is given. For the given $z \in \mathbb{E}_2 \cap \mathrm{Subd}(\mathcal{D})$, let us denote by $u\big|_{\mathbb{A}(z)} = \begin{pmatrix} a & b \\ c & d \end{pmatrix}$ the restriction of u to the 2D block $\mathbb{A}(z)$ in $\mathbb{Z}^n$. If this restriction corresponds to an α-configuration, that is, $a \leq d < b \leq c$ (next to a 90 degrees rotation or axial symmetry), then clearly $[u \geq b] \cap \mathbb{A}(z)$ is a critical configuration in $\mathbb{Z}^n$ and then the restriction of u to $\mathbb{A}(z)$ is not digitally well-composed in $\mathbb{Z}^n$. If we have an U-configuration, we have $a \leq b \leq d \leq c$ (next to a 90 degrees rotation or axial symmetry) and then $\mathrm{intvl}(a, d) \cap \mathrm{intvl}(b, c) = \mathrm{intvl}(b, d) \neq \emptyset$, and then the restriction of u to $\mathbb{A}(z)$ is digitally well-composed in $\mathbb{Z}^n$. And if we have a Z-configuration, we have $a \leq b \leq c \leq d$ (next to a 90 degrees rotation or axial symmetry), and then $\mathrm{intvl}(a, d) \cap \mathrm{intvl}(b, c) = \mathrm{intvl}(b, c) \neq \emptyset$ and the restriction of u to $\mathbb{A}(z)$ is digitally well-composed in $\mathbb{Z}^n$. □

Theorem 4. *Given an image $u : \mathcal{D} \subseteq \mathbb{Z}^n \to \mathbb{R}$, any cubical real-valued interpolation $\mathcal{I}_{f_1,\ldots,f_n}$ satisfying $(\mathcal{P})$ and such that f_1 is the mean operator is such that $\forall\, z \in \mathrm{Subd}(\mathcal{D}) \cap \mathbb{E}_2$:*

$$\begin{cases} f_2(u|_{\mathbb{A}(z)}) & = \mathrm{med}\{u|_{\mathbb{A}(z)}\} & \text{if } u|_{\mathbb{A}(z)} \text{ is not DWC,} \\ f_2(u|_{\mathbb{A}(z)}) & \in I_0(u,z) & \text{otherwise.} \end{cases}$$

Proof: Let us begin with the computation of $I_0(u',z)$ for $z \in \mathbb{E}_2$. From the values already set in u' on $\mathbb{P}(z) \subseteq \mathbb{E}_1$ by f_1 during the recursive process (see Figure 10), we can compute $I_0(u',z)$ using the Hasse diagram of each configuration (see Figure 11). Recall that a *Hasse diagram* is a representation of a finite partially ordered set where greater elements are at a higher position in the diagram. We obtain then $I_0(u',z) = \mathrm{intvl}(\frac{a+c}{2}, \frac{b+d}{2})$ for the three configurations, with one remarkable property: the median value of $u|_{\mathbb{A}(z)}$, equal to $\frac{b+d}{2}$ for the α- and for the U-configurations and equal to $\frac{b+c}{2}$ for the Z-configuration, always belongs to $I_0(u',z)$.

Let us follow with the computation of $I_{WC}(u',z)$, where $u'|_{\mathcal{G}(z)}$ (see Figure 10) satisfies the four conditions:

$$\begin{cases} \mathrm{intvl}(a,m) \cap \mathrm{intvl}((a+b)/2,(a+c)/2) & \neq \emptyset, \quad (1) \\ \mathrm{intvl}((a+b)/2,(b+d)/2) \cap \mathrm{intvl}(m,b) & \neq \emptyset, \quad (2) \\ \mathrm{intvl}((a+c)/2,(c+d)/2) \cap \mathrm{intvl}(m,c) & \neq \emptyset, \quad (3) \\ \mathrm{intvl}(m,d) \cap \mathrm{intvl}((c+d)/2,(b+d)/2) & \neq \emptyset. \quad (4) \end{cases}$$

In the case of the α-configuration in $\mathbb{Z}^n$, $(2) \Rightarrow m \leq \frac{b+d}{2}$ and $(4) \Rightarrow m \geq \frac{b+d}{2}$. That implies that $m = \frac{b+d}{2}$, which also satisfies (1) and (3). Consequently, $I_{WC}(u',z) = \{\mathrm{med}\{u|_{\mathbb{A}(z)}\}\}$, and because $I_{WC}(u',z) \subseteq I_0(u',z)$, $I_{sol}(u',z) = \{\mathrm{med}\{u|_{\mathbb{A}(z)}\}$ in the not digitally well-composed case.

In the cases of the U- and the Z-configurations in $\mathbb{Z}^n$, we obtain that $I_{WC}(u',z) = [\frac{a+b}{2}, \frac{c+d}{2}] \supseteq I_0(u',z)$, so we conclude that $I_{sol}(u',z) = I_0(u',z)$. □

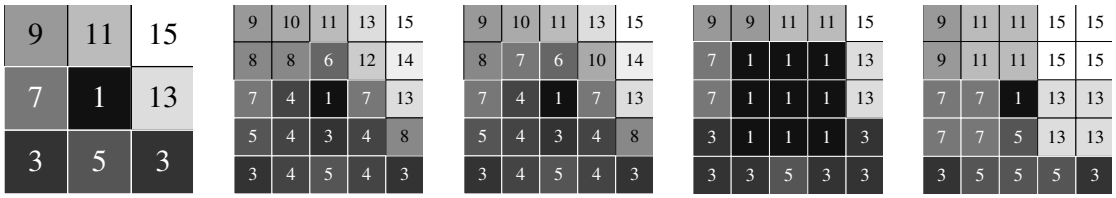

Figure 12.: An image, and its interpolations using the *median*, the *mean/median*, the *min* and the *max* operators respectively (see Definition 37 for more details).

Let us remark that all the well-known self-dual interpolations making 2D images well-composed are particular cases of interpolations characterized by the first two interpolation functions f_1 and f_2. They all use the mean operator for f_1. Furthermore, let z be a point in $\mathbb{E}_2$ belonging to the subdivision of the domain of the original image. The *median method* (see Figure 12), consists in setting the value $u'(z)$ at $\mathrm{med}\{u|_{\mathbb{A}(z)}\}$. The *mean/median method of Latecki* [100] consisting in setting the value $u'(z)$ at $\mathrm{mean}\{u|_{\mathbb{A}(z)}\}$ if the restriction of the image to the 2D block is digitally well-composed and to $\mathrm{med}\{u|_{\mathbb{A}(z)}\}$ otherwise. Finally, the *min/max method* consists in setting the value $u'(z)$ at $\frac{1}{2}(\min\{u|_{\mathbb{A}(z)}\} + \max\{u|_{\mathbb{A}(z)}\})$ in the digitally well-composed case and to $\mathrm{med}\{u|_{\mathbb{A}(z)}\}$ otherwise. Take care not to confuse the min method, the max method and the min/max method.

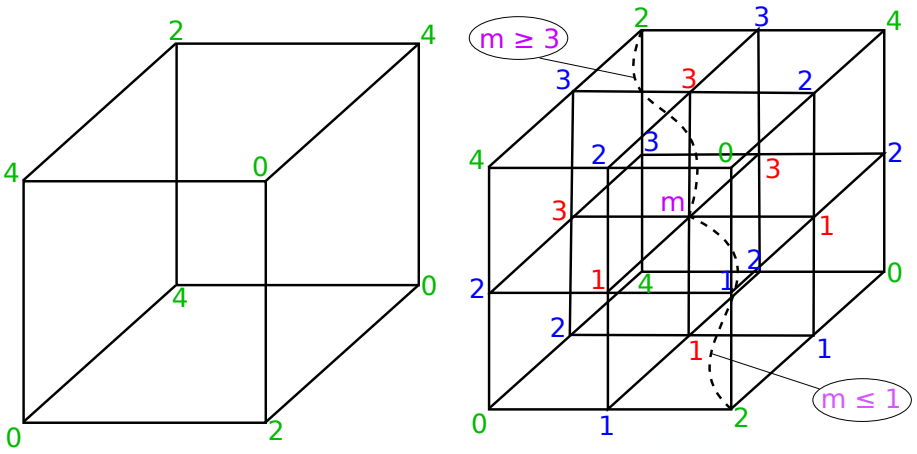

Figure 13.: A counter-example proving that an interpolation satisfying $(\mathcal{P})$ (with only one subdivision and with f_1 the mean operator) cannot ensure digital well-composedness (the values of u' on $\mathbb{E}_0$ are in green, those on $\mathbb{E}_1$ are in blue, those on $\mathbb{E}_2$ are in red, and those on $\mathbb{E}_3$ are in purple).

4.1.7 *Equations of f_3 for local self-dual interpolations*

Theorem 5. *No local interpolation satisfies $(\mathcal{P})$ for $n \geq 3$ with one subdivision when we choose the mean operator to interpolate in 1D.*

Proof: Let $S^0 \in \mathcal{B}(\mathbb{Z}^n)$ be a block of dimension 3 such that we have $u'|_{S^0}$ as in Figure 13: the initial valued 3D block is on the left, its "in-process interpolation" is on the right. We apply the first interpolating function f_1, *i.e.*, we set the values of u' at the centers of the 1D blocks at the mean of the values of the initial block. Then we apply the second interpolating function f_2, which fixes the values of u' at the centers of the subdivided 2D blocks at the median of the values of u' at the initial 2D blocks because u is not digitally well-composed on them. Finally, since we want u' to be digitally well-composed on the 3D blocks of $\mathcal{B}(\text{Subd}(S^0), \left(\frac{\mathbb{Z}}{2}\right)^n)$, we need to have for any of these blocks $S \in \mathcal{B}(\text{Subd}(S^0), \left(\frac{\mathbb{Z}}{2}\right)^n)$ and for any point $p \in S$ and $p' = \text{antag}_S(p)$:

$$\text{intvl}(u'(p), u'(p')) \cap \text{Span}\{\, u'(p'') \mid p'' \in S \setminus \{p, p'\} \,\} \neq \emptyset.$$

This results in a set of two inequations $m \geq 3$ and $m \leq 1$, where $m \in \mathbb{R}$ is the value of u' at the center of the 3D block, that are impossible to satisfy simultaneously. Then, no interpolation can satisfy the set of constraints $(\mathcal{P})$ as soons as we reach $n \geq 3$. □

Finally, assuming that an *usual interpolation* is a cubic real-valued interpolation method that starts from an image defined on a bounded hyperectangle in $\mathbb{Z}^n$, such that it satisfies the set of properties $(\mathcal{P})$, and such that its function f_1 is the mean operator, we have shown that no usual local interpolation is able to make digitally well-composed images in 3D (and higher dimensions) in $\left(\frac{\mathbb{Z}}{2}\right)^n$.

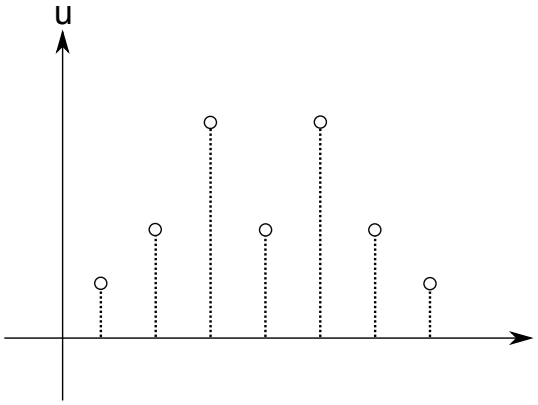

Figure 14.: The initial image u

4.2 A NEW SELF-DUAL n-D DWC INTERPOLATION

In Section 3.1, we have seen that it is usual to develop cubical real-valued digitally well-composed interpolation methods $\mathcal{I}$ such that:

$$\begin{cases} \mathcal{I} \text{ is self-dual} & (1) \\ \mathcal{I} \text{ is in-between} & (1) \\ \mathcal{I} \text{ subdivides the domain only once} & (3) \\ \mathcal{I} \text{ has a subdivision factor of 2} & (4) \\ \mathcal{I} \text{ is invariant by translations, } \frac{\pi}{2}\text{'s rotations and axial symmetries} & (5) \\ \mathcal{I} \text{ is ordered} & (6) \\ \mathcal{I} \text{ is local} & (7) \\ \mathcal{I} \text{ uses the mean operator at the centers of edges} & (8) \end{cases}$$

These properties are listed by order of priority. Effectively self-duality is mandatory because it is our main objective: as we have seen, min- and max-interpolations already exist, and they favorize bright components over dark ones or the converse. In-betweeness is important too, because it ensures that we preserve the contours in the image in the sense that we do not create new extrema. The third and fourth constraints are not necessary but they mean that we interpolate the image by adding the minimal number of pixels in the new image (assuming we want a regular grid as output and that we want that the domain of the interpolation does not depend on the input image). The fifth condition means that we want that the result does not depend on a possible translation/rotation/symmetry. The sixth, seventh, eighth conditions are finally of low priority: effectively life is easier when we proceed to an ordered interpolation, because we know in advance the order at which we value the domain of the interpolation; it is more "systematic". But as we will see, there exists (at least) an interpolation that verifies the constraints (1) to (5) without being ordered, since this interpolation is even not local.

4.2.1 *A front-propagation algorithm*

Effectively, if we consider that orderednes and locality are not so much necessary, we can use a front-propagation algorithm (FPA); in this case, our approach is then global.

So, let us proceed in two steps. First, we make the input image u depicted on Figure 14 "continuous" by using the *span-based interpolation* (detailed later); the values of the new image are not single values but intervals, as depicted on Figure 15. We call this new map the *interval-valued interpolation* U.

Then, we use the FPA to "flatten" this function into a third map $u^\flat$, which is then single-valued. Moreover, this new map $u^\flat$ will have new topological properties thanks to the "regularization" properties of the FPA. The whole process is developed later.

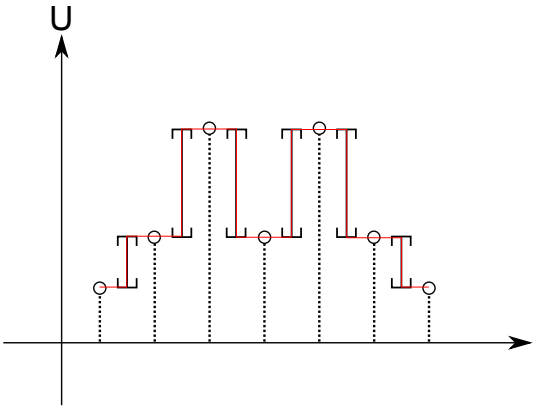

Figure 15.: The "continuous" interpolation U

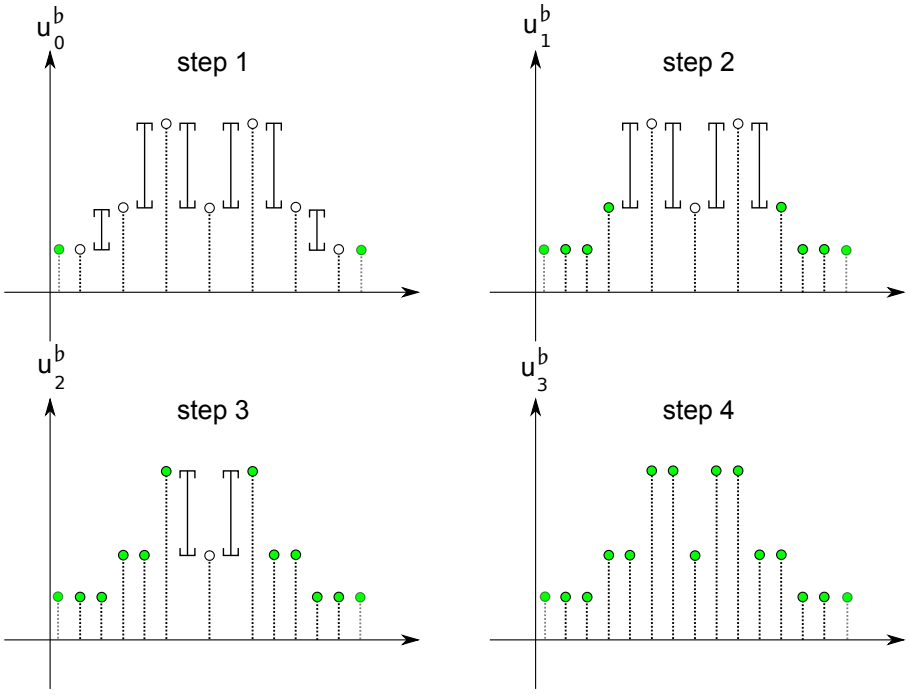

Figure 16.: Flattening process

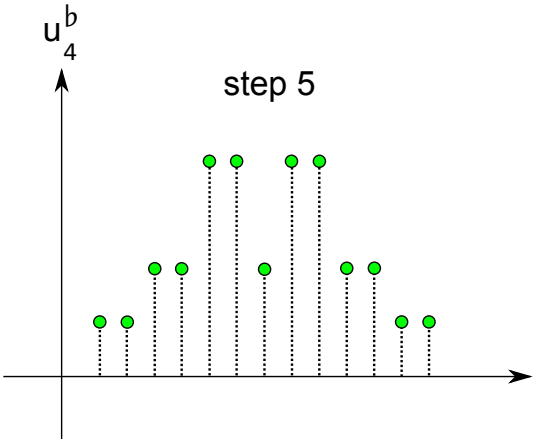

Figure 17.: The interpolation of u

We depicted the details of the flattening process on Figure 16: starting from the interval-valued interpolation U, we add a border that we consider as being the initial front (for this

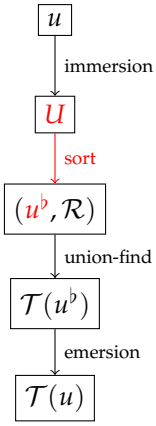

Figure 18.: Computation of the tree of shapes

reason, we depict it using green points), to ensure that the propagation starts from the contour. Then we propagate the front deeper and deeper in the image until the front, made of the green points, covers the whole domain of U. The new image is called $u^\flat$ because it correspond to U which has been flattened. Then, we remove the temporary border (see Figure 17) to obtain an interpolation which is "smoother" than the original image u.

Applying this algorithm in n-D, $n \geq 2$, leads to digitally well-composed images, as we are going to prove in the following subsections.

4.2.2 *Origin of the FPA*

The front propagation algorithm studied in the next subsection is related to the algorithm proposed in [61, 41], which computes in quasi-linear time the morphological tree of shapes [31] of a n-D image. Schematically, the tree of shapes computation algorithm is composed of 4 steps as depicted in Figure 18. The input is an integer-valued image u, defined on the n-D cubical grid. First an immersion step creates an interval-valued map U, defined on a larger space $\mathcal{K}$. A front propagation step, based on a hierarchical queue, takes U and produces two outputs: an image $u^\flat$ and an array $\mathcal{R}$ containing the elements of $\mathcal{K}$. In this array, the elements are sorted so that the next step, an union-find-based tree computation, produces $\mathcal{T}(u^\flat)$ the tree of shapes of $u^\flat$. Actually $u^\flat|_{\mathbb{Z}^n} = u$ and $\mathcal{T}(u^\flat)|_{\mathbb{Z}^n} = \mathcal{T}(u)$. The last step, the emersion, removes from $\mathcal{T}(u^\flat)$ all the elements of $\mathcal{K} \setminus \mathbb{Z}^n$, and also performs a canonicalization of the tree. So $\mathcal{T}(u)$, the tree of shapes of u, is obtained [61].

The front propagation step (highlighted in red in the schematic description) acts as a *flattening* of an interval-valued map U into a function $u^\flat$, because we have $\forall z,\ u^\flat(z) \in U(z)$ [61]. In the following, we will denote by $\mathfrak{FP}$ both the front propagation algorithm (the part highlighted in red in Figure 18) and the mathematical operator $\mathfrak{FP} : U \mapsto u^\flat$.

Last, let us give two important remarks. **1.** We are going to reuse the front propagation algorithm $\mathfrak{FP}$, yet in a *very different* way than it is used in the tree of shapes computation algorithm. Indeed, its input U will be different (both the structure and the values of U will be different), and its purpose also will be different (flattening versus sorting). **2.** Actually, the front propagation algorithm is *just a part* of the solution that we present to make n-D functions digitally well-composed.

4.2.3 *An explanation of the FPA*

Let us now explain shortly the $\mathfrak{FP}$ algorithm, which is recalled in Algorithm 3. The basic procedures used to handle the hierarchical queue are recalled in Algorithm 2 . The reader can also refer to [61] for the original version. This algorithm uses a classical front propagation on the definition domain of U. This propagation is based on a hierarchical queue, denoted by

Algorithm 2: Handling of a hierarchical queue is ensured thanks to PRIORITY_PUSH and PRIORITY_POP.

```
PRIORITY_PUSH(Q, h, U, ℓ)
/* modifies Q */
begin
    [lower, upper] ← U(h)
    if lower > ℓ then
        ℓ' ← lower
    else if upper < ℓ then
        ℓ' ← upper
    else
        ℓ' ← ℓ
    PUSH(Q[ℓ'], h)

PRIORITY_POP(Q, ℓ) : H
/* modifies Q, and sometimes ℓ */
begin
    if Q[ℓ] is empty then
        ℓ' ← level next to ℓ such as Q[ℓ'] is not empty
        ℓ ← ℓ'
    return POP(Q[ℓ])
```

Q and the current (queue) level is denoted by ℓ. There are two notable differences with the well-known hierarchical-queue-based propagation. First the values of U are interval-valued so we have to decide at which (single-valued) level to enqueue the domain points. The solution is to enqueue a point h at the value of the interval $U(h)$ that is the closest to ℓ (see the procedure PRIORITY_PUSH). The image $u^\flat$ actually stores the *enqueuing level* of the points. Second, when the queue at the current level, $Q[\ell]$, is empty (and when the hierarchical queue Q is not yet empty), we shall decide what is the next current level. We have the choice of taking the next level, either less or greater than ℓ, such that the queue at that level is not empty (see the procedure PRIORITY_POP). Practically, choosing going up or down the levels does not change the resulting image $u^\flat$. The neighborhood $\mathcal{N}_{2n}$ used by the propagation corresponds to the $2n$-connectivity into $(\mathbb{Z}/s)^n$.

Like in [61], the initialization of the front propagation relies on the definition of a point, p_∞ (first point enqueued), and of a value $\ell_\infty \in U(p_\infty)$, which is the initial value of the current level ℓ. Similarly to the case of the tree of shapes computation, p_∞ is taken in the outer boundary of the definition domain of U. The initial level ℓ_∞ is set at the median value of the points belonging to the inner boundary of the definition domain of U; more precisely, when the interval-valued U is constructed from an integer-valued function u, ℓ_∞ is computed from the values of the inner boundary of u. Using the median operator ensures that ℓ_∞ is set in a self-dual way: schematically $\ell_\infty(-u) = -\ell_\infty(u)$.

Note that a first example of propagation, without outer boundary, will be given in Section 4.2.4, to explain how works the flattening process step-by-step; a second example, with an outer boundary, will be given in Section 4.2.8 to show how the front starts its propagation from the outer boundary to end by covering the whole domain of the image.

4.2.4 *An illustration of the FPA*

Let us now illustrate this algorithm on a simple run, depicted in Figure 19. The initial interval-valued image U is displayed in (i). Squares filled in gray indicate the points that have already been processed at previous iterations. A circle filled in orange indicates the point h being processed, and the value displayed in the circle is the current level ℓ; it means that we have just executed the line "$u^\flat(h) \leftarrow \ell$" of the algorithm. A dashed circle filled in green, say at a point p, indicates that this point is in the hierarchical queue Q; the value displayed in this

Algorithm 3: Computation of the function $u^\flat$ from an interval-valued map U defined on $(\mathbb{Z}/s)^n$, $s \in \mathbb{N}^*$.

```
𝔉𝔓(U) : Image ;
/* computes u^♭ */ ;
begin
    for all h ∈ (ℤ/s)^n do
        deja_vu(h) ← false;
    PUSH(Q[ℓ_∞], p_∞);
    deja_vu(p_∞) ← true;
    ℓ ← ℓ_∞   /* start from root level */ ;
    while Q is not empty do
        h ← PRIORITY_POP(Q, ℓ);
        u^♭(h) ← ℓ;
        for all n ∈ 𝒩_2n(h, (ℤ/s)^n) such as deja_vu(n) = false do
            PRIORITY_PUSH(Q, n, U, ℓ);
            deja_vu(n) ← true;
    return u^♭
```

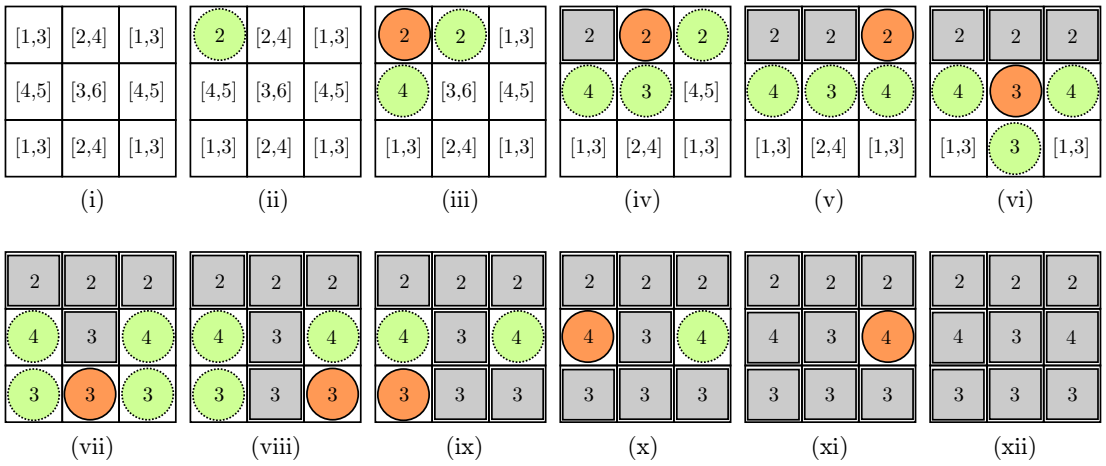

Figure 19.: The front propagation algorithm applied on a digitally well-composed interval-valued image U

circle, say v, is the queue level of this point, i.e., we have $p \in Q[v]$. When no symbol is displayed at a point, it means that this point is not yet processed and is not in Q; we then depict its value in U.

The input interval-valued image U is shown in (i). In the following, the point coordinates are $(row, column)$; for instance we have $U(2,1) = U(2,3) = [4,5]$.

The initialization step is depicted by (ii). We assume that we have $p_\infty = (1,1)$ and $\ell_\infty = 2$. The initialization thus adds p_∞ in $Q[2]$, and sets $\ell \leftarrow \ell_\infty$, so the current level ℓ is 2.

The first iteration of the 'while' loop is depicted by (iii). It pops the point $h = (1,1)$, and performs the assignment $u^\flat(h) \leftarrow \ell$, precisely $u^\flat(1,1) \leftarrow 2$. It then pushes its neighboring points $(1,2)$ and $(2,1)$ into Q, respectively with level **2** and **4**. Indeed, we have $U(1,2) = [\mathbf{2},4]$ and $U(2,1) = [\mathbf{4},5]$ so PRIORITY_PUSH respectively chooses in these intervals the levels that are the closest to the current level $\ell = 2$.

The second iteration is depicted by (iv). Since the queue $Q[\ell]$ is not empty, the current level does not change, and the point $h = (1,2)$ is popped. $u^\flat(h) \leftarrow \ell$ is performed; precisely $u^\flat((1,2)) \leftarrow 2$. Then the points $(1,3)$ and $(2,2)$ are pushed respectively in $Q[\mathbf{2}]$ and $Q[\mathbf{3}]$ since $\ell = 2$, $U(1,3) = [1,3] = \{1,\mathbf{2},3\}$, and $U(2,2) = [\mathbf{3},6]$.

The third iteration is depicted by (v), popping $(1,3)$ from $Q[2]$ (the current level does not change), and pushing $(2,3)$ in $Q[\mathbf{4}]$ since $U(2,3) = [\mathbf{4},5]$.

For the fourth iteration, depicted by (vi), the current level is $\ell = 2$, and the queue corresponding to the current level, namely $Q[\mathbf{2}]$, is empty. Indeed, the hierarchical queue is only composed of $Q[\mathbf{3}] \cup Q[4]$; the four points depicted with circles in (vi) only contains the values 3 and 4. The procedure PRIORITY_POP thus changes the current level to the closest level whose queue is not empty, so $\ell \leftarrow 3$. The point $h = (2,2)$ is then popped from $Q[3]$, the assignment $u^\flat(2,2) \leftarrow 3$ is performed, and the neighbor point $(3,2)$ of h is pushed in $Q[\mathbf{3}]$ since $U(3,2) = [2,4] = \{2,\mathbf{3},4\}$.

The following iterations, depicted by the sub-figures (vii) to (xi), lead to the final integer-valued image $u^\flat$, depicted by (xii). This resulting image is such as:

$$\forall\, z \in \mathcal{D},\ \ u^\flat(z) \in U(z).$$

This front propagation algorithm thus flattens an interval-valued map U into the integer-valued image $u^\flat = \mathfrak{FP}(U)$.

4.2.5 *Intrinsic continuity properties of the FPA*

Two main continuity properties of the FPA are of major interest for the sequel. Both properties relate the values of the flattened image $u^\flat$ at two pixels p and q of the domain $\mathcal{D}' \subset (\mathbb{Z}/s)^n$ of U which are neighbors in $(\mathbb{Z}/s)^n$ depending on the values $U(p)$ and $U(q)$. We say that these properties are *intrinsic* in the sense that they are a direct result of the internal functioning of the algorithm. But let us introduce first some additional notations concerning the FPA.

We define $\ell : \mathcal{D}' \to \mathbb{R}$ as the real-valued *map of levels*: for a given point $z \in \mathcal{D}'$, $\ell(z) \in \mathbb{R}$ is the value of ℓ when we enqueue z into the hierarchical queue Q during the front propagation. Note that it is different from the "enqueuing level" ℓ' presented just before in the algorithm. Also, we define the *enqueuing time map* $t : \mathcal{D}' \to \mathbb{N}$ such that, for any point $z \in \mathcal{D}'$, $t(z)$ is the time at which the point z has been enqueued into Q during the front propagation. We say that a position $p \in \mathcal{D}'$ is being *processed* while the current position h is equal to p. Obviously, for any $p \in \mathcal{D}'$, we use the notation $u^\flat(p)$ assuming that this pixel has been valued yet by the front propagation algorithm (we recall that each pixel of $u^\flat$ is valued only once).

Now let us begin with a preliminary lemma which correlates the values of the initial interval-valued image U, the interpolation $u^\flat$ and the map of levels $\ell : \mathcal{D}' \to \mathbb{R}$. This lemma will be necessary to prove the first main intrinsic continuity property detailed after.

Lemma 8. *Let $U : \mathcal{D}' \subseteq (\mathbb{Z}/s)^n \rightsquigarrow \mathbb{R}$ be an n-D interval-valued map, and let $u^\flat = \mathfrak{FP}(U) : \mathcal{D}' \to \mathbb{R}$ be the real-valued function resulting from the front propagation algorithm applied on U. Now, let r be a point of $\mathcal{D}'$. We can observe the two following implications:*

$$\begin{cases} u^\flat(r) < \lceil U \rceil(r) \Rightarrow \ell(r) \leq u^\flat(r) & (1) \\ \\ u^\flat(r) > \lfloor U \rfloor(r) \Rightarrow \ell(r) \geq u^\flat(r) & (2) \end{cases}$$

Proof: By a case-by-case study, we can establish a correlation between $\ell(r)$ and $u^\flat(r)$ for any given point $r \in \mathcal{D}'$. The possible cases are $\ell(r) < \lfloor U \rfloor(r)$ (1), $\ell(r) \in U(r)$ (2), and $\ell(r) > \lceil U \rceil(r)$ (3):

1. we obtain that $\ell(r) < u^\flat(r)$ because $u^\flat(r) \in U(r)$, and at the same time, $u^\flat(r)$ is equal to $\lfloor U \rfloor(r)$ because it is the nearest value to $\ell(r)$ in $U(r)$;
2. we obtain that $u^\flat(r) = \ell(r)$ because the nearest value to $\ell(r)$ in $U(r)$ is $\ell(r)$ itself, and at the same time we obtain simply the initial property $u^\flat(r) \in U(r)$ (no additional assumption is possible);
3. we obtain that $\ell(r) > u^\flat(r)$ because $u^\flat(r) \in U(r)$, and at the same time $u^\flat(r) = \lceil U \rceil(r)$ because this is the nearest value to $\ell(r)$ into $U(r)$.

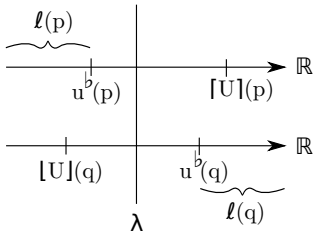

Figure 20.: A situation impossible to obtain with $p, q \in \mathcal{D}$ being $2n$-neighbors in $(\mathbb{Z}/s)^n$

Finally, we obtain this table:

Case	Relation 1	Relation 2
(1) : $\ell(r) < \lfloor U \rfloor(r)$	$\ell(r) < u^\flat(r)$	$u^\flat(r) = \lfloor U \rfloor(r)$
(2) : $\ell(r) \in U(r)$	$\ell(r) = u^\flat(r)$	$u^\flat(r) \in U(r)$
(3) : $\ell(r) > \lceil U \rceil(r)$	$\ell(r) > u^\flat(r)$	$u^\flat(r) = \lceil U \rceil(r)$

Then we can observe that if $u^\flat(r) < \lceil U \rceil(r)$, that is, if $u^\flat(r) \neq \lceil U \rceil(r)$, we are then either in the case (1) or in the case (2) and then we obtain that $\ell(r) \leq u^\flat(r)$.

Conversely, if $u^\flat(r) > \lfloor U \rfloor(r)$, that is, if $u^\flat(r) \neq \lfloor U \rfloor(r)$, we are then either in the case (2) or in the case (3) and then we obtain that $\ell(r) \geq u^\flat(r)$.

□

There follows a lemma that we call *the first intrinsic property of the FPA*. Note that this is the key to understand why a digitally well-composed interval-valued image results in a digitally well-composed single-valued image.

Lemma 9. *Let $U : \mathcal{D}' \subseteq (\mathbb{Z}/s)^n \rightsquigarrow \mathbb{R}$ be an n-D interval-valued map, and let $u^\flat = \mathfrak{FP}(U) : \mathcal{D}' \to \mathbb{R}$ be the real-valued function resulting from the front propagation algorithm applied on U. Let $p, q \in \mathcal{D}'$ be two $2n$-neighbors in $(\mathbb{Z}/s)^n$ and $\lambda \in \mathbb{R}$. Then, it is impossible to get the following set of properties together:*

$$\begin{cases} u^\flat(p) & \leq & \lambda, & (\mathcal{H}1) \\ \lceil U \rceil(p) & > & \lambda, & (\mathcal{H}2) \\ u^\flat(q) & > & \lambda, & (\mathcal{H}3) \\ \lfloor U \rfloor(q) & \leq & \lambda. & (\mathcal{H}4) \end{cases}$$

Proof: Now, let p, q be two $2n$-neighbors in $\mathcal{D}'$ and let us assume that there exists a value $\lambda \in \mathbb{R}$ verifying $(\mathcal{H}1)$, $(\mathcal{H}2)$, $(\mathcal{H}3)$ and $(\mathcal{H}4)$.

We can observe easily thanks to $(\mathcal{H}1)$ and $(\mathcal{H}2)$ that $u^\flat(p) < \lceil U \rceil(p)$ and then by Lemma 8, we obtain:

$$\ell(p) \leq u^\flat(p) \quad (\mathcal{H}5).$$

Also, thanks to $(\mathcal{H}3)$ and $(\mathcal{H}4)$, we obtain $u^\flat(q) > \lfloor U \rfloor(q)$ and using Lemma 8, this results in:

$$\ell(q) \geq u^\flat(q) \quad (\mathcal{H}6).$$

Taking into consideration the two $2n$-neighbors p and q, we have 4 possible scenarii as depicted on Figure 21:

1. either p is enqueued before q, then two subcases are possible:
   a) either q is enqueued when p is the current position,
   b) or q is enqueued before p is the current position.

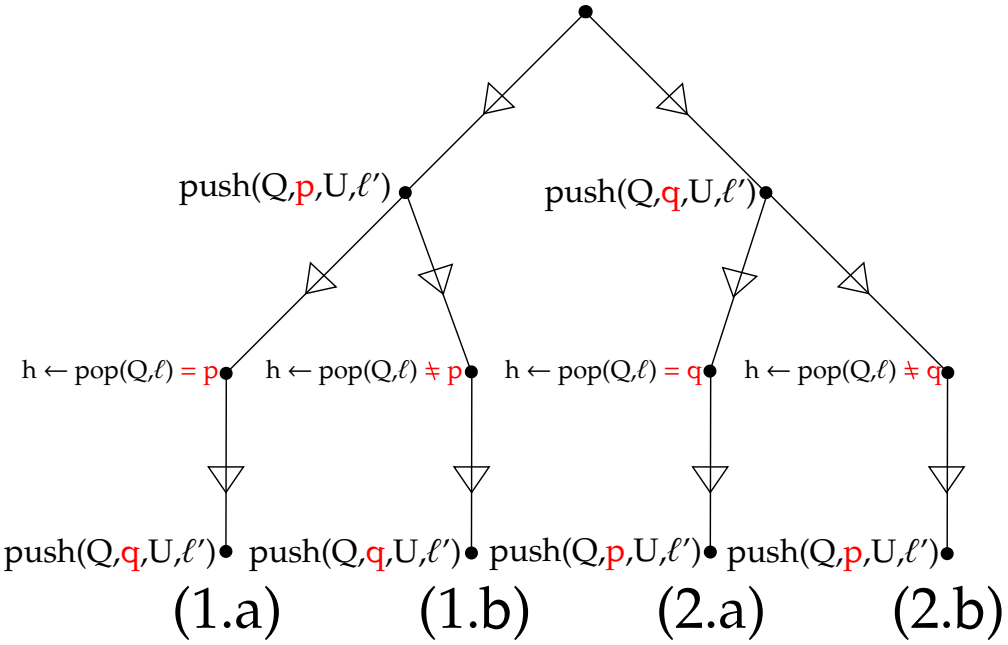

Figure 21.: The 4 possible scenarii when only two $2n$-neighbors p and q in $\mathcal{D}'$ are considered

2. either q is enqueued before p, then two subcases are possible:
   a) either p is enqueued when q is the current position,
   b) or p is enqueued before q is the current position.

Let us notice that since p and q are $2n$-neighbors, q cannot be enqueued after p is the current position, and similarly p cannot been enqueued after q is the current position (all the $2n$-neighbors of the current position will have been enqueued when it has been processed).

Now let us show that whatever the scenario we choose, we always obtain a contradiction.

$(1.a)$: p is enqueued before q, and then q is enqueued when p is the current position. It means that $\ell(q) = u^\flat(p)$. However, we have seen that $u^\flat(p) \leq \lambda$ by $(\mathcal{H}1)$, and that $\ell(q) \geq u^\flat(q) > \lambda$ by $(\mathcal{H}6)$ and $(\mathcal{H}3)$. This leads to a contradiction.

$(1.b)$: p is enqueued before q, and q is enqueued before the current position is set at p. This way, since the current level ℓ at $t(p)$ is equal to $\ell(p) \leq u^\flat(p)$, it is equal to $\ell(q) \leq u^\flat(p)$ at $t(q)$ (no jump of the non-empty queue level $Q[u^\flat(p)]$ is allowed by the algorithm). This means by $(\mathcal{H}1)$ that $\ell(q) \leq \lambda$. However, by $(\mathcal{H}6)$ and $(\mathcal{H}3)$, $\ell(q) > \lambda$. This leads to a contradiction.

$(2.a)$ is the symmetrical case of $(1.a)$ and $(2.b)$ is the one of $(1.b)$ and then they lead also to contradictions.

The conclusion is that whatever the scenario (and one of these scenarii happens during the computation of the interpolation), the combination of hypotheses $(\mathcal{H}1)$, $(\mathcal{H}2)$, $(\mathcal{H}3)$ and $(\mathcal{H}4)$ leads to a contradiction. These hypotheses are then incompatible.

□

Now, let us expose the *second intrinsic continuity property of the FPA* that we will use later to prove that the interpolation method used in this thesis is *in-between*.

Lemma 10. *Let $U : \mathcal{D}' \subseteq (\mathbb{Z}/s)^n \rightsquigarrow \mathbb{R}$ be an n-D interval-valued map, and let $u^\flat = \mathfrak{FP}(U) : \mathcal{D}' \to \mathbb{R}$ be the real-valued function resulting from the front propagation algorithm applied on U. Now, let $a, m \in \mathcal{D}'$ be $2n$-neighbors in $(\mathbb{Z}/s)^n$ such that $U(a) \subseteq U(m)$. Then $u^\flat(m) < u^\flat(a)$ implies that $u^\flat(a) = \lfloor U \rfloor(a)$ and $u^\flat(m) > u^\flat(a)$ implies that $u^\flat(a) = \lceil U \rceil(a)$.*

Proof: Let us begin with the case $t(a) < t(m)$, that is, a has been enqueued before m. Three cases are possible.

The first subcase corresponds to $\ell(a) > \lceil U \rceil(a)$. Then $u^\flat(a) = \lceil U \rceil(a)$, $Q[u^\flat(a)] \supseteq \{a\}$ at $t = t(a)$, and the current level ℓ remains greater than or equal to $u^\flat(a)$ until a has been processed, because no jump of non-empty queue level is allowed. Since m is enqueued after a (by hypothesis) and at the latest during the processing of a (because a and m are $2n$-neighbors), $\ell(m) \geq u^\flat(a)$. Since $\lceil U \rceil(m) \geq \lceil U \rceil(a) \geq u^\flat(a)$, we obtain finally the relation $u^\flat(m) \geq u^\flat(a)$ (Case 1.1).

The second subcase corresponds to $\ell(a) \in U(a)$. In this subcase, $u^\flat(a) = \ell(a)$, $Q[u^\flat(a)] \supseteq \{a\}$ at time $t = t(a)$, and the current level ℓ stays at the value $u^\flat(a)$ until a is processed (at least). Since a and m are $2n$-neighbors, and since m is enqueued after a, m is enqueued after $t(a)$ and at the latest while a is processed. This way, $\ell(m) = u^\flat(a)$ and then $u^\flat(m) = u^\flat(a)$ since $U(a) \subseteq U(m)$ (Case 1.2).

The third subcase corresponds to $\ell(a) < \lfloor U \rfloor(a)$. We reason by symmetry and we obtain that $u^\flat(a) = \lfloor U \rfloor(a)$ and $u^\flat(m) \leq u^\flat(a)$ (Case 1.3).

Let us follow with the case $t(a) > t(m)$. Then five subcases are possible.

If $\ell(m) > \lceil U \rceil(m)$, then $u^\flat(m) = \lceil U \rceil(m)$, $Q[u^\flat(m)] \supseteq \{m\}$ at $t = t(m)$, and the current level ℓ remains greater than or equal to $u^\flat(m)$ until m has been processed, because no jump of non-empty queue level is allowed. Since a is enqueued after m (by hypothesis) and at the latest during the processing of m (because a and m are $2n$-neighbors), $\ell(a) \geq u^\flat(m)$. Then two subcases are possible: either $\lceil U \rceil(m) > \lceil U \rceil(a)$ and $u^\flat(a) = \lceil U \rceil(a) < u^\flat(m)$ (Case 2.1.a), or $\lceil U \rceil(m) = \lceil U \rceil(a)$ and $u^\flat(a) = \lceil U \rceil(a) = u^\flat(m)$ (Case 2.1.b).

If $\ell(m) \in]\lceil U \rceil(a), \lceil U \rceil(m)]$, assuming that $\lceil U \rceil(a) < \lceil U \rceil(m)$, $u^\flat(m) = \ell(m)$, $Q[u^\flat(m)] \supseteq \{m\}$ at $t = t(m)$, and the current level ℓ stays at the value $u^\flat(m)$ until m is processed (at least). Since a and m are $2n$-neighbors, and since a is enqueued after m, a is enqueued after $t(m)$ and at the latest while m is processed. This way, $\ell(a) = u^\flat(m)$, and then $u^\flat(a) = \lceil U \rceil(a) < u^\flat(m)$ (Case 2.2).

If $\ell(m) \in U(a)$, $u^\flat(m) = \ell(m)$ (since $U(a) \subseteq U(m)$) and $Q[u^\flat(m)] \supseteq \{m\}$ at $t = t(m)$. Then the current level ℓ stays at the value $u^\flat(m)$ until m is processed (at least). Since a and m are $2n$-neighbors, and since a is enqueued after m, a is enqueued after $t(m)$ and at the latest while m is processed. This way, $\ell(a) = u^\flat(a)$ and then $u^\flat(a) = u^\flat(m)$ (Case 2.3).

If $\ell(m) \in [\lfloor U \rfloor(m), \lfloor U \rfloor(a)[$ (assuming that $\lfloor U \rfloor(m) < \lfloor U \rfloor(a)$), we reason by symmetry and we obtain that $u^\flat(a) = \lfloor U \rfloor(a) > u^\flat(m)$ (Case 2.4).

If $\ell(m) < \lfloor U \rfloor(m)$, we reason again by symmetry and we obtain that either $\lfloor U \rfloor(m) < \lfloor U \rfloor(a)$ and $u^\flat(a) = \lfloor U \rfloor(a) > u^\flat(m)$ (Case 2.5a), or $\lfloor U \rfloor(m) = \lfloor U \rfloor(a)$ and $u^\flat(a) = \lfloor U \rfloor(a) = u^\flat(m)$ (Case 2.5b).

Let us summarize the different cases:

Case	Relation 1	Relation 2	Relation 3
(1.1)	$t(a) < t(m)$	$u^\flat(a) = \lceil U \rceil(a)$	$u^\flat(m) \geq u^\flat(a)$
(1.2)	$t(a) < t(m)$	$u^\flat(a) \in U(a)$	$u^\flat(m) = u^\flat(a)$
(1.3)	$t(a) < t(m)$	$u^\flat(a) = \lfloor U \rfloor(a)$	$u^\flat(m) \leq u^\flat(a)$
(2.1.a)	$t(m) < t(a)$	$u^\flat(a) = \lceil U \rceil(a)$	$u^\flat(m) > u^\flat(a)$
(2.1.b)	$t(m) < t(a)$	$u^\flat(a) = \lceil U \rceil(a)$	$u^\flat(m) = u^\flat(a)$
(2.2)	$t(m) < t(a)$	$u^\flat(a) = \lceil U \rceil(a)$	$u^\flat(m) > u^\flat(a)$
(2.3)	$t(m) < t(a)$	$u^\flat(a) \in U(a)$	$u^\flat(m) = u^\flat(a)$
(2.4)	$t(m) < t(a)$	$u^\flat(a) = \lfloor U \rfloor(a)$	$u^\flat(m) < u^\flat(a)$
(2.5.a)	$t(m) < t(a)$	$u^\flat(a) = \lfloor U \rfloor(a)$	$u^\flat(m) < u^\flat(a)$
(2.5.b)	$t(m) < t(a)$	$u^\flat(a) = \lfloor U \rfloor(a)$	$u^\flat(m) = u^\flat(a)$

We obtain finally that $u^\flat(a) < u^\flat(m)$ implies that we are in Case 1.1, 2.1.a, or 2.2 and then $u^\flat(a) = \lceil U \rceil(a)$, and that $u^\flat(a) > u^\flat(m)$ implies that we are in Case 1.3, 2.4, or 2.5.a, and then $u^\flat(a) = \lfloor U \rfloor(a)$. This concludes the proof. □

4.2.6 *Fundamental properties of the FPA*

Thanks to Lemma 9, the FPA presents a very strong property: if the input image U is a digitally well-composed interval-valued image, the output image $u^\flat = \mathfrak{FP}(U)$ is digitally well-composed, whatever the chosen value ℓ_∞ at which is set the inner boundary of the definition domain of U before the front propagation. This result can be observed on Figure 19.

Theorem 6 ($\mathfrak{FP}(U)$ is DWC if U is DWC)**.** *If the n-D interval-valued map $U : \mathcal{D}' \subset \left(\frac{\mathbb{Z}}{2}\right)^n \rightsquigarrow \mathbb{R}$, defined on a bounded hyperrectangle $\mathcal{D}'$, is digitally well-composed, the resulting n-D function $u^\flat = \mathfrak{FP}(U)$ is digitally well-composed.*

Proof: Let us assume that $u^\flat$ is not digitally well-composed. Then, there exists some $\lambda \in \mathbb{R}$ such that $[u^\flat \geq \lambda]$ contains a critical configuration of primary or secondary type. Let us begin with the primary case.

If $[u^\flat \geq \lambda]$ contains a critical configuration of primary type, that means that there exists some block $S \subseteq \mathcal{D}'$ of dimension k (with $2 \leq k \leq n$) such that $[u^\flat \geq \lambda] \cap S = \{p, p'\}$ where p and p' are two antagonists in S. In other words, we have:

$$\begin{cases} u^\flat(p) & \geq & \lambda \\ u^\flat(p') & \geq & \lambda \\ u^\flat(p'') & < & \lambda, \ \forall\, p'' \in S \setminus \{p, p'\}. \end{cases}$$

We know that $u^\flat(p'') < \lambda$ implies that $\lfloor U \rfloor(p'') < \lambda, \ \forall\, p'' \in S \setminus \{p, p'\}$. This way, we obtain the following relation:

$$\max\{\, \lfloor U \rfloor(p'') \mid p'' \in S \setminus \{p, p'\} \,\} \ < \ \lambda.$$

Moreover, $\lfloor U \rfloor$ is digitally well-composed (since U is digitally well-composed) by Proposition 14. The characterization of a digitally well-composed single-valued function implies that intvl$(\lfloor U \rfloor(p), \lfloor U \rfloor(p'))$ intersects Span$\{\lfloor U \rfloor(p'') \mid p'' \in S \setminus \{p, p'\}\}$, so there exists some $p_* \in \{p, p'\}$ such that:

$$\lfloor U \rfloor(p_*) < \lambda.$$

Also, we have:

$$\begin{cases} \lceil U \rceil(p_*) \geq \lambda, \\ \lceil U \rceil(\mathrm{antag}_S(p_*)) \geq \lambda. \end{cases}$$

This means that these two antagonists in S belong to the set $[\lceil U \rceil \geq \lambda]$ which is digitally well-composed. Then, there exists a $2n$-path connecting them into $[\lceil U \rceil \geq \lambda] \cap S$. Consequently, there exists some point $p'_* \in \mathcal{N}_{2n}(p_*) \cap S$ such that:

$$\lceil U \rceil(p'_*) \geq \lambda.$$

We thus end up with the four properties: $u^\flat(p_*) \geq \lambda$, $\lfloor U \rfloor(p_*) < \lambda$, $u^\flat(p'_*) < \lambda$, and $\lceil U \rceil(p'_*) \geq \lambda$ with p_*, p'_* $2n$-neighbors in $\mathcal{D}'$ (see Figure 22). Thanks to Lemma 9, we obtain a contradiction.

For the secondary case, the hypothesis such as $[u^\flat \geq \lambda]$ contains a secondary critical configuration is equivalent to have $[u^\flat < \lambda]$ containing a primary critical configuration. With a symmetrical reasoning, we obtain that $u^\flat(p_*) < \lambda$, $\lceil U \rceil(p_*) \geq \lambda$, $u^\flat(p'_*) \geq \lambda$, and $\lfloor U \rfloor(p'_*) < \lambda$, which is impossible too.

□

Since we are much interested in self-duality, there is another fundamental property of our algorihm.

Conjecture 1. *For any n-D interval-valued map U, and whatever p_∞ and $\ell_\infty \in U(p_\infty)$ now considered as parameters, we have:*
$\mathfrak{FP}_{(p_\infty, \ell_\infty)}(U) \ = \ -\,\mathfrak{FP}_{(p_\infty, -\ell_\infty)}(-U)$, *so $\mathfrak{FP}$ is* self-dual.

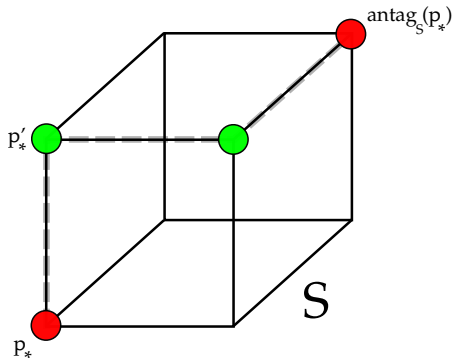

Figure 22.: Assuming U is digitally well-composed and $u^\flat$ is not digitally well-composed, we obtain the four properties: $u^\flat(p_*) \geq \lambda$, $\lfloor U \rfloor(p_*) < \lambda$, $u^\flat(p'_*) < \lambda$, and $\lceil U \rceil(p'_*) \geq \lambda$ with p_*, p'_* $2n$-neighbors in $\mathcal{D}'$, which lead to a contradiction.

The fact that this algorithm is self-dual is part of the proof that the tree of shapes computation algorithm is self-dual. It is not published yet.

Now, there is a property of Algorithm 3, which is related to the determinism of the FPA.

Conjecture 2. *Once given p_∞ and ℓ_∞, the front propagation algorithm $\mathfrak{FP}$ (Algorithm 3) is deterministic with respect to its input, the n-D interval-valued map U.*

The fact that this algorithm is deterministic is part of the proof that the tree of shapes computation algorithm is correct. It is not published yet.

4.2.7 *Making an n-D function digitally well-composed*

In this subsection, we explain the full process which starts from a given single-valued image and ends up with a digitally well-composed interpolation of this image.

Our interpolation in details

We start from a gray-level image $u : \mathcal{D} \subset \mathbb{Z}^n \to \mathbb{Z}$ defined on a bounded hyperrectangle $\mathcal{D}$. We *subdivide* the domain of the image by computing the smallest hyperrectangle $\mathcal{D}' \subset \left(\frac{\mathbb{Z}}{2}\right)^n$ containing $\mathcal{D}$ and we define a new function on the domain $\mathcal{D}'$ such that the restriction of this function to $\mathcal{D}$ is equal to u, that is, this function *interpolates* u. With $B = \{-\frac{1}{2}, 0, \frac{1}{2}\}^n$, where B_z is the translation of B by z, and with "op" an operator on (finite) subsets of $\mathbb{R}$, we define the following interpolation:

Definition 37. *Let $u : \mathcal{D} \to \mathbb{R}$ with $\mathcal{D} \subset \mathbb{Z}^n$ a bounded hyperrectangle. We define the* operator-based interpolation $\mathcal{I}_{\text{op}}(u) : \mathcal{D}' = \text{Subd}(\mathcal{D}) \to \mathbb{R}$ *such that, for any $z \in \mathcal{D}'$:*

$$\left(\mathcal{I}_{\text{op}}(u)\right)(z) \;=\; \begin{cases} \text{op}\{\, u(z) \,\} & \text{if } z \in \mathcal{D}, \\ \text{op}\{\, u(z'),\ z' \in B_z \cap \mathcal{D} \,\} & \text{otherwise.} \end{cases}$$

This interpolation is said *local* since it is computed at each point $p \in \mathcal{D}'$ using only the nearest neighbors of p in $\left(\frac{\mathbb{Z}}{2}\right)^n$.

Proposition 17. *For any $u : \mathcal{D} \subset \mathbb{Z}^n \to \mathbb{Z}$, the n-D real-valued functions $\mathcal{I}_{\min}(u)$ and $\mathcal{I}_{\max}(u)$ are digitally well-composed, and the interpolation operators $\mathcal{I}_{\min}$ and $\mathcal{I}_{\max}$ are dual* (i.e. $\forall\, u,\ \mathcal{I}_{\min}(u) = -\mathcal{I}_{\max}(-u)$).

Proof: The proof is in Chapter A, but could also be derived from [119]. □

Let us recall the definition of the Span operator: $\forall\, V \subset \mathbb{V}$,

$$\mathrm{Span}(V) \;=\; [\,\min(V),\, \max(V)\,] \;\cap\; \mathbb{V}.$$

Using this operator on the interpolations $\mathcal{I}_{\min}(u)$ and $\mathcal{I}_{\max}(u)$, we obtain the following *span-based interpolation* of u that we call $\mathcal{I}_{\mathrm{Span}}(u)$, defined such that:

$$\left\{ \begin{array}{rcl} \lfloor \mathcal{I}_{\mathrm{Span}}(u) \rfloor & = & \mathcal{I}_{\min}(u) \\ \lceil \mathcal{I}_{\mathrm{Span}}(u) \rceil & = & \mathcal{I}_{\max}(u). \end{array} \right.$$

Since this interpolation is interval-valued, we say it is an *immersion* of u. The property of $\mathcal{I}_{\mathrm{Span}}(u)$ is then obvious:

Proposition 18. *For any $u : \mathcal{D} \subset \mathbb{Z}^n \to \mathbb{Z}$, the n-D interval-valued function $\mathcal{I}_{\mathrm{Span}}(u) : \mathcal{D}' \subset \left(\frac{\mathbb{Z}}{2}\right)^n \rightsquigarrow \mathbb{Z}$ is digitally well-composed, and the interpolation operator $\mathcal{I}_{\mathrm{Span}}$ is self-dual (it verifies $\forall\, u,\, \mathcal{I}_{\mathrm{Span}}(u) = -\mathcal{I}_{\mathrm{Span}}(-u)$).*

Proof: It follows from the fact that the two functions $\mathcal{I}_{\min}(u)$ and $\mathcal{I}_{\max}(u)$ are (single-valued) digitally well-composed images and that an interval-valued is digitally well-composed iff its upper and lower bounds are digitally well-composed by Proposition 14.

□

Then, starting from $\mathcal{I}_{\mathrm{Span}}(u) : \mathcal{D}' \subset \left(\frac{\mathbb{Z}}{2}\right)^n \rightsquigarrow \mathbb{Z}$ as developed above, we add an outer border to the hyperrectangle $\mathcal{D}'$, which becomes $\mathcal{D}'_+$, and we define $U_+ : \mathcal{D}'_+ \rightsquigarrow (\mathbb{Z}/2)$ such that $\forall p \in \mathcal{D}'$, $U_+(p) = (\mathcal{I}_{\mathrm{Span}}(u))(p)$, and $\forall p \in \mathcal{D}'_+ \setminus \mathcal{D}', U(p) = \{\ell_\infty(u)\}$. This way, we preserved digital well-composedness of the interpolation, since adding an outer border valued by a constant to an image defined on a bounded hyperrectangle preserves digital well-composedness. Effectively, we have the following proposition.

Proposition 19 (Adding a constant-valued border preserves DWCness)**.** *Let $U_0 : \mathcal{D} \subset \left(\frac{\mathbb{Z}}{2}\right)^n \rightsquigarrow \mathbb{Z}$ be a DWC set-valued map defined on a bounded hyperrectangle $\mathcal{D}$ in $\left(\frac{\mathbb{Z}}{2}\right)^n$. Now, let $U_1 : \mathcal{D}' \rightsquigarrow \mathbb{Z}$ be another set-valued map defined on a bounded hyperrectangle $\mathcal{D}' = \delta(\mathcal{D}, \mathrm{se})$ (where δ is the dilation operator and* se *is the structuring element defined such that $\{p \in \left(\frac{\mathbb{Z}}{2}\right)^n \;;\; ||p||_\infty \leq 1/2\}$), such that $U_1|_{\mathcal{D}} = U_0$ and for any $p \in \mathcal{D}' \setminus \mathcal{D}$, $U'(p) = \{c\}$ (where c in a given constant in $\mathbb{R}$). Then, U_1 is a DWC set-valued map.*

Proof: First let us introduce some notations. Let $(\mathrm{se}^k)_{k \in [\![1,2n]\!]}$ be a sequence of structuring elements defined s.t. $\forall k \in [\![1, 2n]\!]$:

$$\mathrm{se}^k = \left\{ \mathbf{0}, \frac{1}{2}\,(-1)^k\, e_{\lfloor \frac{(k+1)}{2} \rfloor} \right\},$$

and let $(\mathcal{D}_k)_{k \in [\![0,2n]\!]}$ be a sequence of domains s.t. $\mathcal{D}_0 = \mathcal{D}$ and s.t., $\forall k \in [\![1, 2n]\!]$:

$$\mathcal{D}_k = \delta(\mathcal{D}_{k-1}, \mathrm{se}^k).$$

In this manner, $\mathcal{D}_{2n} = \delta(\mathcal{D}, \mathrm{se}) = \mathcal{D}'$.

We want to show that U_1 is digitally well-composed on $\mathcal{D}'$, and for that we are going to show by an induction process that, $\forall k \in [\![0, 2n]\!]$, $U_1\big|_{\mathcal{D}_k}$ is digitally well-composed.

Initialization ($k = 0$): $U_1\big|_{\mathcal{D}_0} = U_0$ which is DWC by hypothesis.

Heredity ($k \in [\![1, 2n]\!]$): assuming that $U_1\big|_{\mathcal{D}_{k-1}}$ is DWC, let us show that $U_1\big|_{\mathcal{D}_k}$ is DWC too. Two cases are then possible.

- either k is odd, then $\mathrm{se}^k = \{\mathbf{0}, -\frac{1}{2}\, e_{\frac{k+1}{2}}\}$, and then we obtain the configuration depicted on Figure 23 (Case 1),

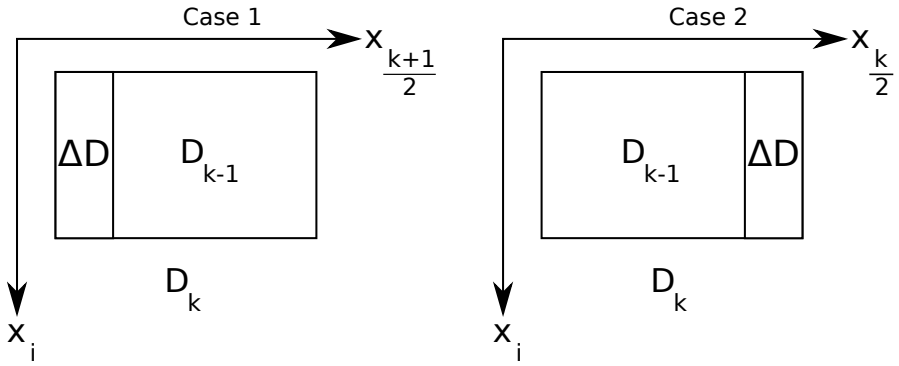

Figure 23.: Two possible configurations when dilating the domain $\mathcal{D}_{k-1}$ into $\mathcal{D}_k$ with our structuring elements.

- either k is even, then $\text{se}^k = \{\mathbf{0}, \frac{1}{2}\, e_{\frac{k}{2}}\}$, and then we obtain the configuration depicted on Figure 23 (Case 2).

Let us now denote $\Delta\mathcal{D}$ the set equal to $\mathcal{D}_k \setminus \mathcal{D}_{k-1}$. Let us remark that this set is also an hyperrectangle. Also, let us denote by u_k^+, u_k^-, u_{k-1}^+ and u_{k-1}^- the images $\lceil U_1 \rceil\big|_{\mathcal{D}_k}$, $\lfloor U_1 \rfloor\big|_{\mathcal{D}_k}$, $\lceil U_1 \rceil\big|_{\mathcal{D}_{k-1}}$, $\lfloor U_1 \rfloor\big|_{\mathcal{D}_{k-1}}$ respectively. We can say that $U_1\big|_{\mathcal{D}_k}$ is DWC iff $\forall S \in \mathcal{B}(\mathcal{D}_k, \left(\frac{\mathbb{Z}}{2}\right)^n)$ s.t. $\dim(S) \geq 2$, $\forall p, p' \in S$ s.t. $p' = \text{antag}_S(p)$, we have the following relations:

$$\begin{cases} \text{intvl}(u_k^+(p), u_k^+(p')) \cap \text{Span}\{u_k^+(q)\ ;\ q \in S \setminus \{p, p'\}\} \neq \emptyset, & (A) \\ \\ \text{intvl}(u_k^-(p), u_k^-(p')) \cap \text{Span}\{u_k^-(q)\ ;\ q \in S \setminus \{p, p'\}\} \neq \emptyset. & (B) \end{cases}$$

So let S be such a block of $\mathcal{D}_k$ into $\left(\frac{\mathbb{Z}}{2}\right)^n$, and let $p^{\min}$ and $p^{\max}$ be two elements of S such that, for any $i \in [\![1, n]\!]$,

$$\begin{cases} p_i^{\min} = \min\{p_i\ ;\ p \in S\}, \\ \\ p_i^{\max} = \max\{p_i\ ;\ p \in S\}. \end{cases}$$

In this manner, $p^{\min}$ and $p^{\max}$ are antagonist in S. Then, 4 cases are possible:

1. either $p^{\min}$ and $p^{\max}$ belong to $\mathcal{D}_{k-1}$, then $S \subseteq \mathcal{D}_{k-1}$, and in this way, $\forall p \in S$, $u_k^+(p) = u_{k-1}^+(p)$ and $u_k^-(p) = u_{k-1}^-(p)$, which implies that the intersections in (A) and (B) are non empty since u_{k-1}^+ and u_{k-1}^- are DWC and since $\dim(S) \geq 2$,
2. or $p^{\min}$ and $p^{\max}$ belong to $\Delta\mathcal{D}$, then $S \subseteq \Delta\mathcal{D}$, and then $\forall p \in S$, $u_k^+(p) = u_k^-(p) = c$, which means that (A) and (B) are true since $\dim(S) \geq 2$,
3. or $p^{\min} \in \mathcal{D}_{k-1}$ and $p^{\max} \in \Delta\mathcal{D}$. Then we are in the second case of Figure 23. In other words,

$$\begin{cases} S \cap \mathcal{D}_{k-1} = \{p \in S\ ;\ p_{k/2} = p_{k/2}^{\min}\}, \\ \\ S \cap \Delta\mathcal{D} = \{p \in S\ ;\ p_{k/2} = p_{k/2}^{\max}\}, \end{cases}$$

   which means that S can decomposed into two blocks of dimension $\dim(S) - 1 \geq 1$, the first being $S \cap \mathcal{D}_{k-1}$ and the second being $S^* = S \cap \Delta\mathcal{D}$. Since S^* verifies that $\forall p \in S^*$, $u_k^+(p) = u_k^-(p) = c$ and that $\dim(S^*) \geq 1$, there exist two points $p, q \in S^*$ which are not antagonist into S and such that $u_k^+(p) = u_k^+(q)$ and $u_k^-(p) = u_k^-(q)$, then (A) and (B) are both true,
4. or $p^{\max} \in \mathcal{D}_{k-1}$ and $p^{\min} \in \Delta\mathcal{D}$. Then we are in the first case of Figure 23. A dual reasoning leads to the fact that (A) and (B) are both true.

We can then conclude by induction that U_1 is DWC. □

Then we proceed to the front propagation on U_+ with p_∞ belonging to the outer border of $\mathcal{D}'_+$. We obtain the single-valued image $u^\flat : \mathcal{D}'_+ \to \mathbb{Z}/2$, which is digitally well-composed, at which we remove the border. Since removing the outer border preserves digital well-composedness, we obtain the final interpolation $u_{\text{DWC}} : \mathcal{D}' \to \mathbb{Z}/2$ of u, which is digitally well-composed too.

With $\alpha \in \mathbb{R}$, let us denote by b_α the operator which adds an outer border set at $\{\alpha\}$ to a interval-valued image defined on an hyperrectangle, and b^- the operator which removes the outer border to a single-valued image defined on an hyperrectangle. We can then define our interpolation in this way:

$$u_{\text{DWC}} = \mathfrak{I}_{\text{DWC}}(u),$$

where the *digitally well-composed interpolation operator* is defined such that:

$$\mathfrak{I}_{\text{DWC}} = b^- \circ \mathfrak{FP} \circ b_{\ell_\infty(.)} \circ \mathcal{I}_{\text{Span}}.$$

u_{DWC} is digitally well-composed

Combining the properties of the immersion and of the FPA, we obtain the following proposition:

Proposition 20. *Let $u : \mathcal{D} \subset \mathbb{Z}^n \to \mathbb{Z}$ be a given image. Then the image $u_{\text{DWC}} = \mathfrak{I}_{\text{DWC}}(u)$ is digitally well-composed.*

u_{DWC} interpolates u

Since for each $p \in \mathcal{D}$, $U_+(p) = (\mathcal{I}_{\text{Span}}(u))(p) = \{u(p)\}$, the FPA cannot choose another value than $u(p)$ at the point p during the flattenning process, and then $u_{\text{DWC}}(p) = u^\flat(p) = u(p)$. This way, the following proposition is straightforward:

Proposition 21. *Let $u : \mathcal{D} \subset \mathbb{Z}^n \to \mathbb{R}$ be a given image. Then the image $u_{\text{DWC}} = \mathfrak{I}_{\text{DWC}}(u)$ interpolates u.*

u_{DWC} is self-dual

Since the immersion step and the front propagation are self-dual, the complete process is self-dual, and then we obtain the following statement:

Conjecture 3. *Let $u : \mathcal{D} \subset \mathbb{Z}^n \to \mathbb{R}$ be a given image. Then the image $u_{\text{DWC}} = \mathfrak{I}_{\text{DWC}}(u)$ interpolates u in a self-dual way.*

u_{DWC} is in-between

Let us recall the Definition 32 establishes what is an in-between interpolation. This notion is much important because it represents that the interpolation method outputs an image with no new extrema compared to the input image.

Proposition 22. *Let $u : \mathcal{D} \subset \mathbb{Z}^n \to \mathbb{Z}$ be a given image. Then the image $u_{\text{DWC}} : \mathcal{D}' \subset \left(\frac{\mathbb{Z}}{2}\right)^n \to \mathbb{Z}/2$ defined such that $u_{\text{DWC}} = \mathfrak{I}_{\text{DWC}}(u)$ is an in-between interpolation of u.*

Proof: Let $u : \mathcal{D} \to \mathbb{Z}$ be a given image, and $u_{\text{DWC}} = \mathfrak{I}_{\text{DWC}}(u)$ be its interpolation. This way, we know that $\forall z \in \mathcal{D}$, $u_{\text{DWC}}(p) = u(p)$. Let us assume now that u_{DWC} is not in-between. Then there exists some point $m \in \text{Subd}(\mathcal{D}) \setminus \mathcal{D}$ such that:

$$u_{\text{DWC}}(m) \notin \cap_{\{p^-,p^+\} \in \text{opp}(m)} \text{intvl}(u_{\text{DWC}}(p^-), u_{\text{DWC}}(p^+)).$$

In other words, there exists two points $a, b \in \text{Subd}(\mathcal{D})$ such as $\{a, b\} \in \text{opp}(m)$ and:

$$u_{\text{DWC}}(m) \notin \text{intvl}(u_{\text{DWC}}(a), u_{\text{DWC}}(b)).$$

Two situations are then possible:

- either $u_{\mathrm{DWC}}(m) < \min(u_{\mathrm{DWC}}(a), u_{\mathrm{DWC}}(b))$ (Case 1)
- or $u_{\mathrm{DWC}}(m) > \max(u_{\mathrm{DWC}}(a), u_{\mathrm{DWC}}(b)$ (Case 2).

Since these two relations are dual, we will study only the first case, the reasoning being the same for the second.

By hypothesis, $u_{\mathrm{DWC}}(m) < u_{\mathrm{DWC}}(a)$, and then:

$$u^\flat(m) < u^\flat(a), \quad (1).$$

Also, we know that a and m are $2n$-neighbors in $\mathcal{D}'$ (2). Finally, since $a \in \mathbb{P}(m)$, $U_+(a) = (\mathcal{I}_{\mathrm{Span}}(u))(a) \subseteq (\mathcal{I}_{\mathrm{Span}}(u))(m) = U_+(m)$ (3). This way, we have the three properties of Lemma 10 and we can conclude that $u_{\mathrm{DWC}}(a) = u^\flat(a) = \lfloor U_+ \rfloor(a)$.

With the same reasoning applied to b, we obtain that $u_{\mathrm{DWC}}(b) = \lfloor U_+ \rfloor(b)$, which leads to:

$$u_{\mathrm{DWC}}(m) < \min(\lfloor U_+ \rfloor(a), \lfloor U_+ \rfloor(b)).$$

By construction,

$$\lfloor U_+ \rfloor(a) = \min\{u(p)\ ;\ p \in \mathbb{A}(a)\},$$

and

$$\lfloor U_+ \rfloor(b) = \min\{u(p)\ ;\ p \in \mathbb{A}(b)\}.$$

This implies that $u^\flat(m) < \min\{u(p)\ ;\ p \in \mathbb{A}(m)\}$ (since $\mathbb{A}(a) \cup \mathbb{A}(b) = \mathbb{A}(m)$), which is equal to $\lfloor U_+ \rfloor(m)$. However $u_{\mathrm{DWC}}(m) < \lfloor U \rfloor(m)$ is impossible by construction. This concludes the proof.

□

Invariance of u_{DWC}

Note that u_{DWC} should be invariant by translations, $\frac{\pi}{2}$'s rotations and axial symmetries, since the propagation of the front begins at the boundary of the domain of the interval-valued interpolation of the input image, which justifies the following conjecture:

Conjecture 4. *Following the complete process detailed in this section, the interpolation u_{DWC} of the image u is invariant by translations, $\frac{\pi}{2}$'s rotations and axial symmetries.*

4.2.8 *An illustration of the complete process*

An example of the span-based interpolation is depicted in Figure 24. We start from an image u that we interpolate using the digitally well-composed interval-valued interpolation $\mathcal{I}_{\mathrm{Span}}(u)$ at which we add a border to obtain U_+ which is still digitally well-composed. This boundary is displayed in light gray and is filled with a single value $\ell_\infty(u)$, which is actually the median value of the set of values of the boundary of the definition domain of u. We have:

$$\ell_\infty(u) = \mathrm{med}\{3, 3, 5, 7, 9, 11, 13, 15\} = 8.$$

When we take U_+ as input to the FPA, p_∞ can be any point of its boundary. This way, which is similar to [61], we ensure that the propagation starts from the outer boundary of U_+, and that all the points of the inner boundary of u are enqueued. Having $\ell_\infty(-u) = -\ell_\infty(u)$ guarantees that U_+ remains self-dual with respect to u. Then the flattenning process is applied on U_+ and results in a digitally well-composed image $u^\flat$.

Figure 25 depicts the propagation steps: we start from Subfigure (a) where p_∞ is the only point to be enqueued in $Q[\ell_\infty(u)] = Q[8]$. Then, until $Q[8]$ is empty, the propagation continues across the domain of the image, which contains (at least) the ounter boundary, as shown

9	11	15
7	1	13
3	5	3

(a) u

$\{\mathbf{9}\}$	$[\![9,11]\!]$	$\{\mathbf{11}\}$	$[\![11,15]\!]$	$\{\mathbf{15}\}$
$[\![7,9]\!]$	$[\![1,11]\!]$	$[\![1,11]\!]$	$[\![1,15]\!]$	$[\![13,15]\!]$
$\{\mathbf{7}\}$	$[\![1,7]\!]$	$\{\mathbf{1}\}$	$[\![1,13]\!]$	$\{\mathbf{13}\}$
$[\![3,7]\!]$	$[\![1,7]\!]$	$[\![1,5]\!]$	$[\![3,13]\!]$	$[\![3,13]\!]$
$\{\mathbf{3}\}$	$[\![3,5]\!]$	$\{\mathbf{5}\}$	$[\![3,5]\!]$	$\{\mathbf{3}\}$

(b) $U = \mathcal{I}_{\text{Span}}(u)$

$\{8\}$	$\{8\}$	$\{8\}$	$\{8\}$	$\{8\}$	$\{8\}$	$\{8\}$
$\{8\}$	$\{\mathbf{9}\}$	$[\![9,11]\!]$	$\{\mathbf{11}\}$	$[\![11,15]\!]$	$\{\mathbf{15}\}$	$\{8\}$
$\{8\}$	$[\![7,9]\!]$	$[\![1,11]\!]$	$[\![1,11]\!]$	$[\![1,15]\!]$	$[\![13,15]\!]$	$\{8\}$
$\{8\}$	$\{\mathbf{7}\}$	$[\![1,7]\!]$	$\{\mathbf{1}\}$	$[\![1,13]\!]$	$\{\mathbf{13}\}$	$\{8\}$
$\{8\}$	$[\![3,7]\!]$	$[\![1,7]\!]$	$[\![1,5]\!]$	$[\![3,13]\!]$	$[\![3,13]\!]$	$\{8\}$
$\{8\}$	$\{\mathbf{3}\}$	$[\![3,5]\!]$	$\{\mathbf{5}\}$	$[\![3,5]\!]$	$\{\mathbf{3}\}$	$\{8\}$
$\{8\}$	$\{8\}$	$\{8\}$	$\{8\}$	$\{8\}$	$\{8\}$	$\{8\}$

(c) U_+

8	8	8	8	8	8	8
8	**9**	9	**11**	11	**15**	8
8	8	8	8	8	13	8
8	**7**	7	**1**	8	**13**	8
8	7	7	5	8	8	8
8	**3**	5	**5**	5	**3**	8
8	8	8	8	8	8	8

(d) $u^\flat$

9	9	**11**	11	**15**
8	8	8	8	13
7	7	**1**	8	**13**
7	7	5	8	8
3	5	**5**	5	**3**

(e) u_{DWC}

Figure 24.: The complete process in detail

on Subfigure (b) in light gray. The green pixels correspond to the points which have been enqueud during the propagation, and that are not valued yet. Then ℓ is set at 9, and the same process reiterates, until the whole domain of the image has been enqueued and valued, which results in $u^\flat$ on Subfigure (j).

The final result u_{DWC} which corresponds to $u^\flat$ minus its boundary is digitally well-composed and computed in a self-dual way.

4.2.9 *Conclusions about* u_{DWC}

We finally have the following properties for our interpolation:

$$\begin{cases} u_{\text{DWC}} \text{ is self-dual (conjecture)} \\ u_{\text{DWC}} \text{ is in-between} \\ u_{\text{DWC}} \text{ subdivides the domain only once} \\ u_{\text{DWC}} \text{ has a subdivision factor of 2} \\ u_{\text{DWC}} \text{ is deterministic (conjecture)} \end{cases}$$

Obviously, u_{DWC} is neither ordered nor local, but this methods works in n-D, $n \geq 2$.

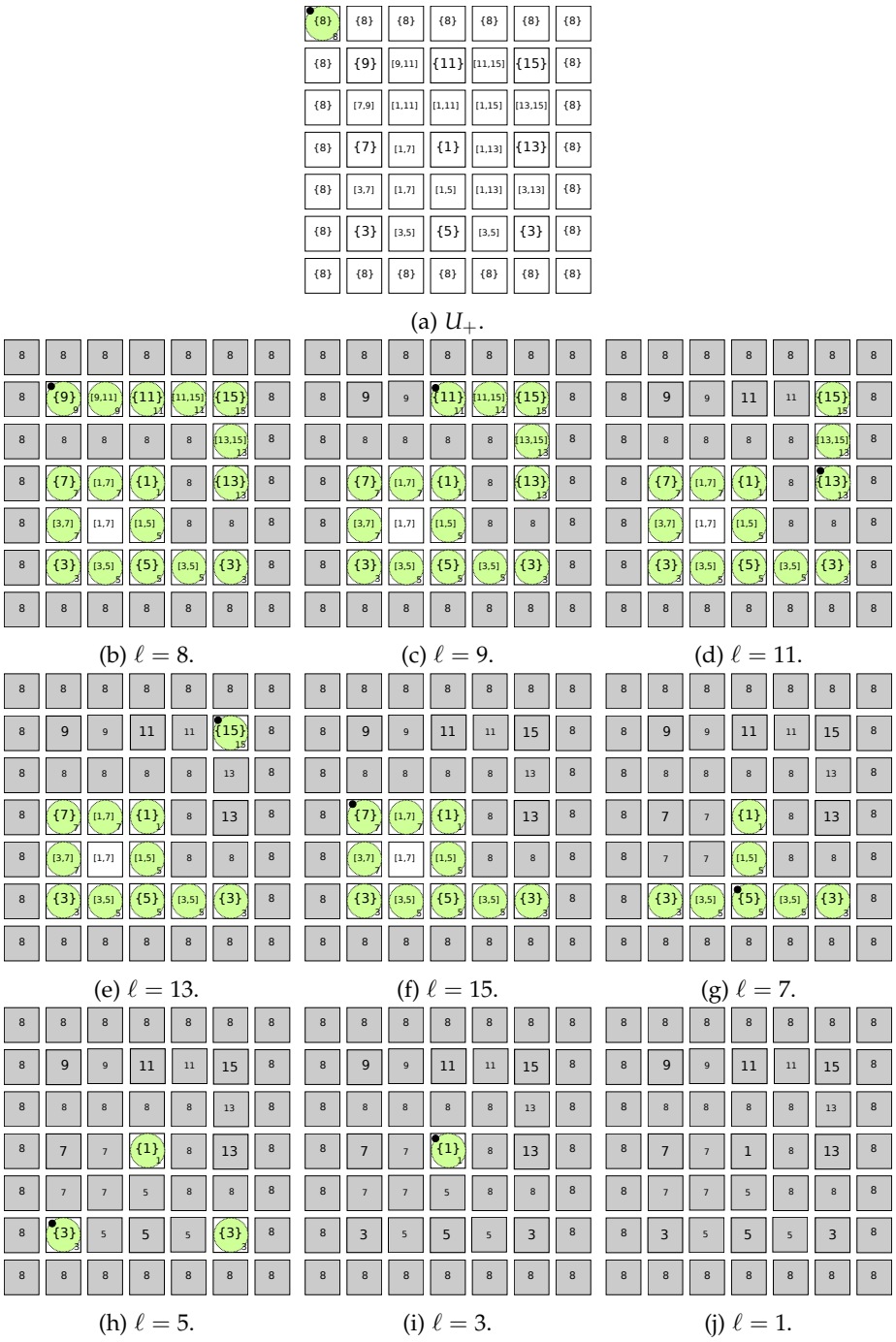

(a) U_+.

(b) $\ell = 8$.

(c) $\ell = 9$.

(d) $\ell = 11$.

(e) $\ell = 13$.

(f) $\ell = 15$.

(g) $\ell = 7$.

(h) $\ell = 5$.

(i) $\ell = 3$.

(j) $\ell = 1$.

Figure 25.: From U_+ to $u^\flat$

4.2.10 *From $\mathcal{D} \to \mathbb{Z}$ to $\mathcal{D}' \to (\mathbb{Z}/2)$*

We can notice that in practice, we will have an integer-valued map u whose values are defined into $\mathbb{Z}$, and then its immersion U will be also defined into $\mathbb{Z}$. When we add a border to the domain of U, we obtain a new function U_+, which is no more defined into $\mathbb{Z}$ but into $\mathbb{Z}/2$, since the median at which we set the border belongs to $\mathbb{Z}/2$. The use of a generic library is then necessary [110] (or we can round the value of ℓ_∞ but we can loose *perfect* self-duality). The consequence is that $u^\flat$ and the final image u_{DWC} will be defined into $\mathbb{Z}/2$. According to us, it is a nice way (and perhaps the only way) to ensure self-duality to an interpolation method starting from an image whose values are defined into $\mathbb{Z}$.

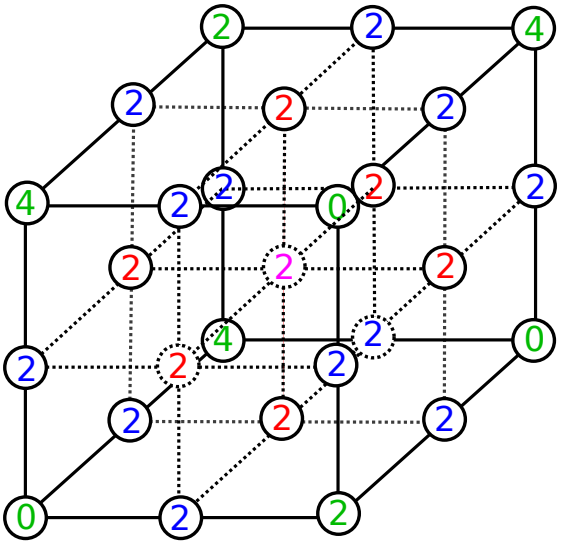

Figure 26.: A self-dual digitally well-composed interpolation of image of Figure 13

4.2.11 *The FPA succeeds where local methods fail*

We showed in the chapter before that no self-dual local interpolation with usual constraints can make any 3D image digitally well-composed with one subdivision. However, our self-dual non-local FPA succeeds in making any n-D image digitally well-composed thanks to its process in 2 steps: the immersion U and the propagation u_{DWC} (see Figure 26).

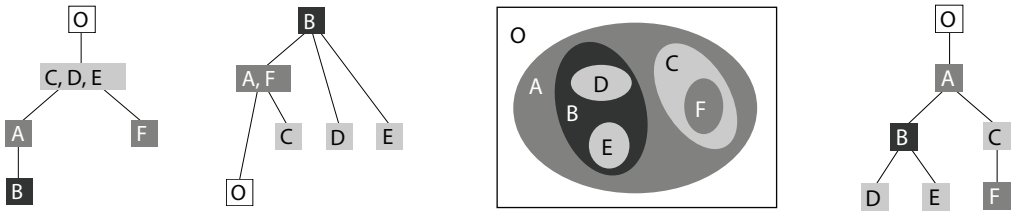

Figure 1.: A gray-level image (in the middle), its min-tree and its max-tree (on the left), and its tree of shapes [61] (on the right).

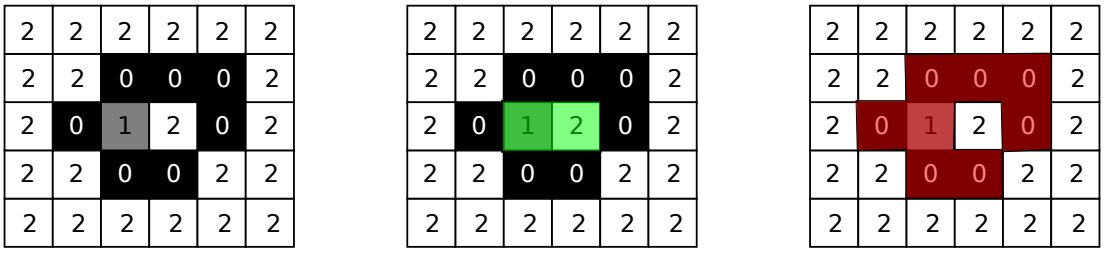

Figure 2.: Incoherences using 4-connectivity for both upper and lower threshold sets: some shapes intersect but are not nested the one in the other one

5 SOME CONSEQUENCES AND APPLICATIONS

In this chapter, we explain how we can use the tools we have developed in this thesis to reach our aims: we see in a first time how the self-dual interpolation u_{DWC} of a given image u can be used to obtain pure self-duality using a given self-dual operator, and in a second time, we explain how we can combine this same interpolation and the conjecture that AWCness and DWCness are equivalent on cubical grids to obtain finally a plain map with strong topological properties such as AWCness and continuity. We also show that thanks to the local equivalence of connectivities in a DWC image defined on a cubical grid, the underlying structure of the graph of a well-composed image does not depend anymore on the values in this image. Finally, we observe we have no "ambiguity cases" using the Marching Cubes algorithm on a DWC image, and we conjecture that this property is true in n-D.

5.1 PURE SELF-DUALITY

A very powerful hierarchical representation, based on the inclusion relationship of the components of an image, exists in mathematical morphology: the tree of shapes [123, 61, 41] (see [120, 180, 181, 182] for some possible applications). It is sometimes seen as the fusion of the *min-tree*, made of the connected components of the lower threshold sets (leaves are the regional minima in the image), and its dual, the *max-tree*, which is made of the connected components of the upper threshold sets (leaves are the regional maxima in the image). Figure 1 shows a gray-level image and its component trees.

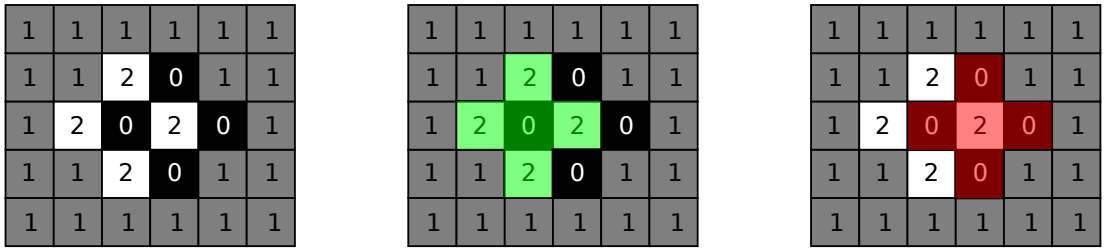

Figure 3.: Incoherences using 8-connectivity for both upper and lower threshold sets: some shapes intersect but are not nested the one in the other one

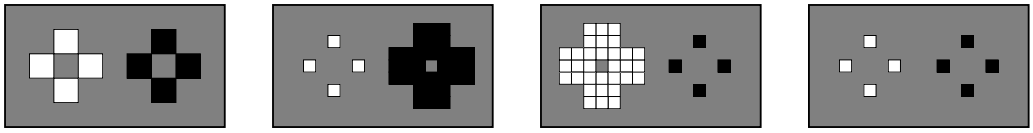

(a) u. (b) u_{min}. (c) u_{max}. (d) u_{DWC}.

Figure 4.: An image u, its min/max interpolations, and u_{DWC} which is self-dual

In fact, this morphological operator is *self-dual* in the sense that it is invariant by contrast: it treats in a similar way bright objects over a dark background or dark objects over a bright background. This is very useful when we do not know a priori the contrast of the object, or if we need to study several objects of different contrasts in the same image.

However, this operator is based on connectivities: we need to associate a connectivity to the upper threshold sets and to the lower threshold sets used to compute the saturated connected components, called "shapes", in the image using a "cavity-fill-in" operator.

Theoretically, a tree of shapes is such that if two components overlap, they are nested the one in the other one; in the contrary case, they are disjoint. However, in practice, it can be observed that by associating the $2n$-connectivity (respectively the $(3^n - 1)$-connectivity) to both upper and lower threshold sets, we obtain some abnormalities: we can see on Figure 2 (respectively Figure 3) that there exist some shapes whose intersection is non-empty and such that they are not included the one in the other one. In these cases, the tree of shapes is a lattice but not a tree: it contains cycles.

To avoid these incoherences, it is common to associate a *Jordan pair of connectivities* [11, 31] to the lower and upper threshold sets. However, the $(4, 8)$- and the $(8, 4)$-trees of shapes of a same 2D image will usually not be exactly the same; in other words, we do not have *unicity* of the tree, which is then ill-defined.

However, using a well-composed image (in the sense that connectivities are equivalent), we can compute the tree of shapes of an image and its negative with exactly the same couple of connectivities (no switch is needed), the result will be the same: Géraud and Najman [61] call this phenomenon "pure self-duality".

Since the front propagation in the computation of the tree of shapes is based on $2n$-connectivity, we can emulate the dual pair of connectivities (c_{2n}, c_{3^n-1}) (which connects the zeros and disconnect the ones) using a min interpolation. In the same way, we can compute the tree of shapes based on the dual pair (c_{3^n-1}, c_{2n}) (which connects the ones and disconnects the zeros) using a max interpolation. So, starting from a given image u, we compute its min, max, and self-dual interpolations as shown on Figure 4. Then we compute their respective trees of shapes $\mathcal{T}(u_{min})$, $\mathcal{T}(u_{max})$, and $\mathcal{T}(u_{\mathrm{DWC}})$ as shown on Figure 5. We can observe that the upper and lower threshold sets are not processed in the same way using the min and max interpolations, contrary to the tree of shapes computed on our self-dual representations u_{DWC} which treats exactly in the same way bright and dark components.

Now, let us show how our self-dual interpolation u_{DWC} deletes the pinches in the image and let us observe the result we obtain on the tree of shapes. We start from an initial 3D image u

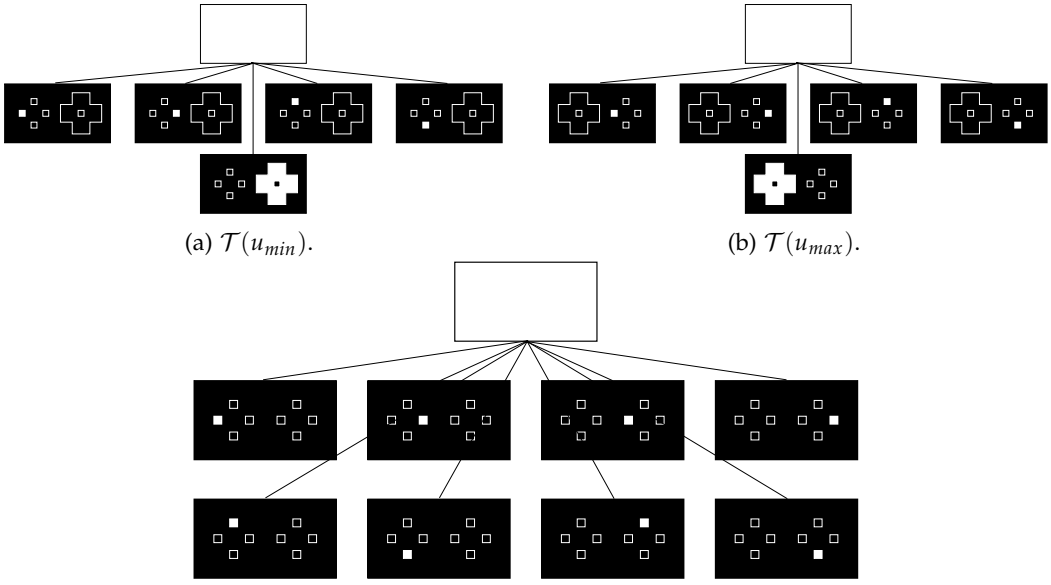

(a) $\mathcal{T}(u_{min})$. (b) $\mathcal{T}(u_{max})$.

(c) $\mathcal{T}(u_{\mathrm{DWC}})$.

Figure 5.: The tree of shapes of the min, max, and self-dual interpolations

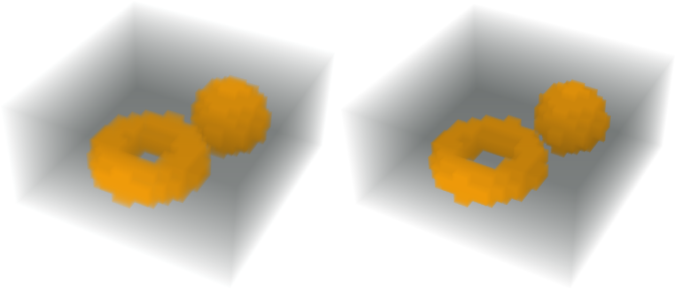

Figure 6.: The initial image u containing a ball and a full torus and its self-dual interpolation

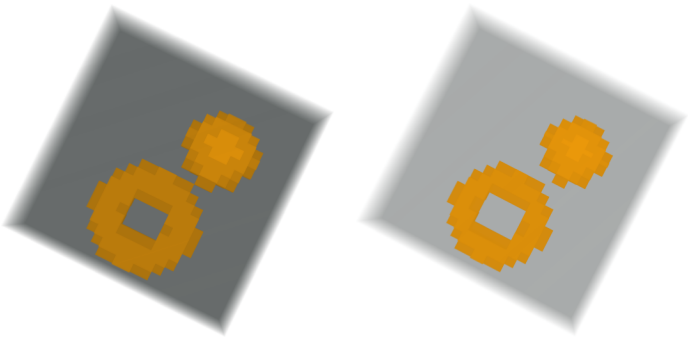

Figure 7.: On the left, u seen from the top, and on the right, u_{DWC} seen from the top

showed on the left of Figure 6 and we compute its self-dual interpolation u_{DWC} showed on the right of the same figure. Figure 7 shows the same images seen from the top to see the "pinch". The final result is that the tree of shapes, showed on Figure 8, expose the same separation as u_{DWC} (since the union-find is applied on it).

Note that any self-dual operator which is based on connectivities, derived [32, 181] from the tree of shape or not, will be purely self-dual on well-composed images. Effectively, an example of self-dual operator derived from the tree of shapes is the *grain filter*, which removes the shapes in the hierarchical representation of an image u whose area is smaller than a given threshold. We can remark easily on Figure 9 that using the connectivities (c_4, c_8) or (c_8, c_4)

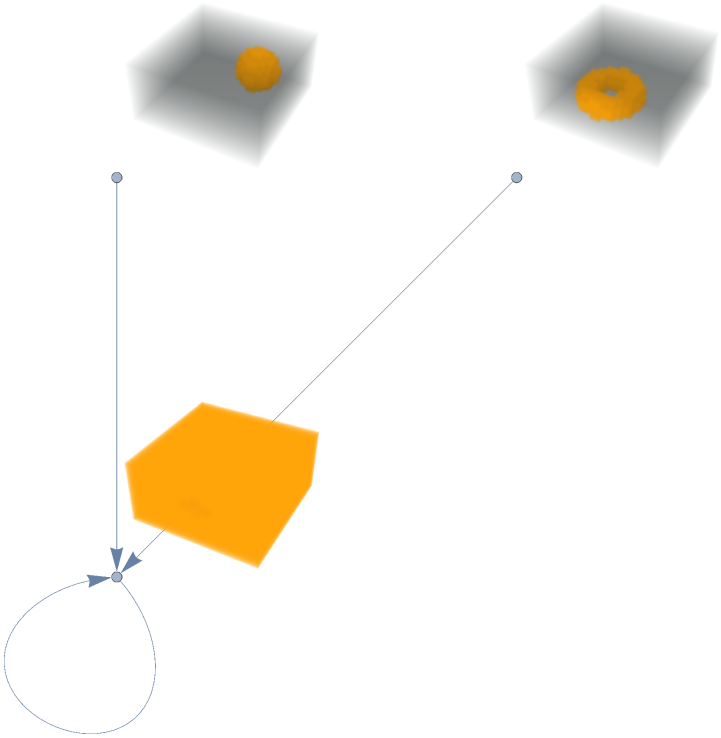

Figure 8.: The tree of shapes of u

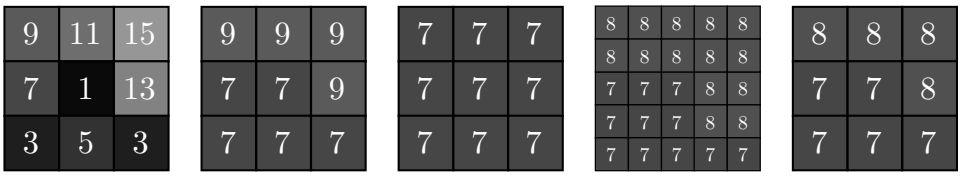

(a) u. (b) $G_{c_4,c_8}(u)$. (c) $G_{c_8,c_4}(u)$. (d) $G(u_{\mathrm{DWC}})$. (e) Emersion of $G(u_{\mathrm{DWC}})$.

Figure 9.: Grain filtering on an image u: our self-dual representation leads to "pure" self-duality

does not lead to the same result. Furthermore, the use of our self-dual representation gives a result which is between the two before, and then shows how our self-dual representation u_{DWC} is "purely" self-dual.

In the same manner, in digital topology, we assume that a Jordan pair of adjacencies, such as (c_{2n}, c_{3^n-1}), is associated to a binary or gray-level image, that is, we associate $2n$-adjacency to the ones (or the upper threshold sets), and $(3^n - 1)$-adjacency to the zeros (or the lower threshold sets). Note that some other Jordan pairs of adjacencies can be considered, as its dual pair (c_{3^n-1}, c_{2n}), depending on the application. In this manner, we obviate connectivity paradoxes. The resulting problem is then that a specific adjacency is considered depending on the values of the pixels in the image, and then the underlying structure of the graph (corresponding to the domain of the image) depends on the location (see Figure 10). However, DWC images have their connectivities locally equivalent, and then they can be seen as $(2n, 2n)$ images. This way, the underlying graph of the image becomes simpler, regular, 90-degrees-rotation- and translation-invariant, and is not anymore correlated to the values in the image.

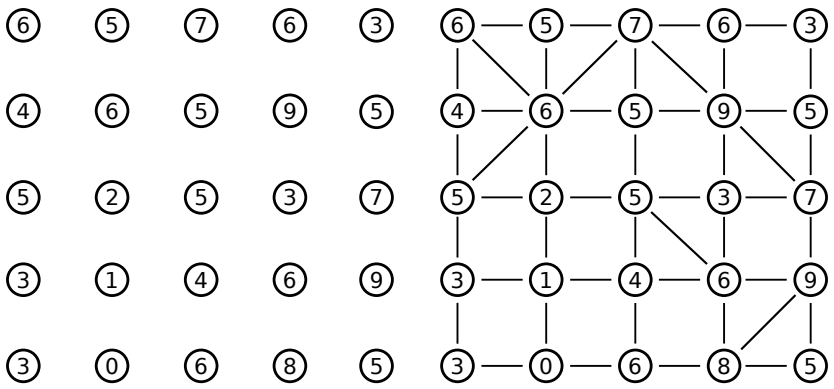

(a) u. (b) Underlying graph structure.

Figure 10.: From u to its underlying graph structure using the dual pair (c_8, c_4): we connect couples of diagonal pixels whose values are greater than the two other diagonal values.

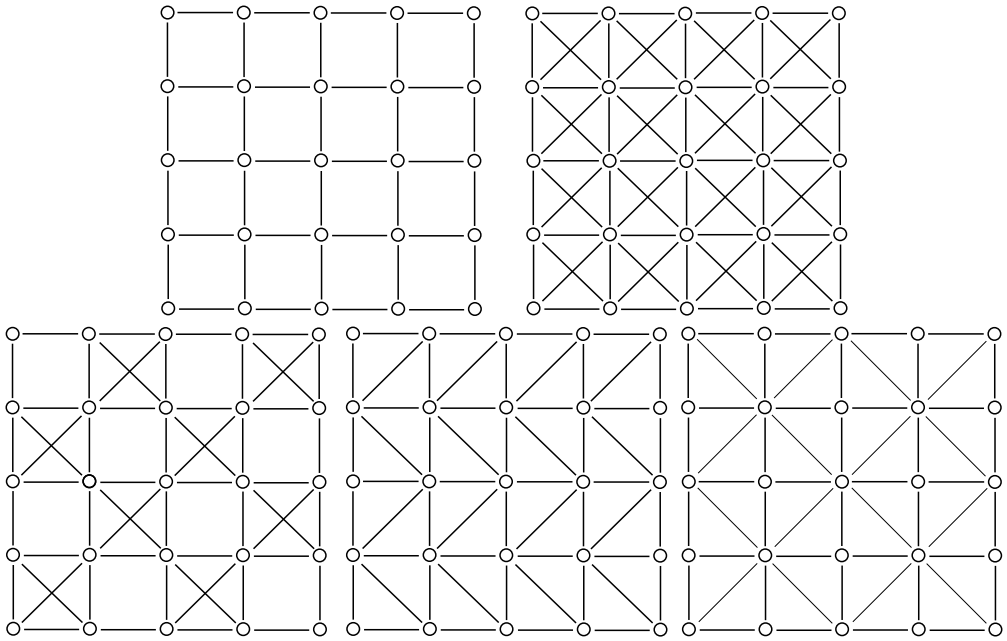

Figure 11.: All the possible cubical connectivity grids are equivalent on a digitally well-composed image. In the raster scan order, the 4-connectivity grid, the 8-connectivity grid, the perfect fusion grid, a 6-connectivity grid, and the Khalimsky grid.

In fact, since any chosen connectivity for the ones and for the zeros will lead to the same result, we can associate any graph structure to the image. This way, the *perfect fusion grid* [39, 40], the Khalimsky grid [86], and so on, can be associated to a DWC image (see Figure 11).

5.2 A NEW REPRESENTATION OF DIGITAL IMAGES

Note that this section needs some prerequisites of Chapters C, D, and E.

Since we work with images defined on bounded hyperrectangles in a space of finite dimension $n \geq 0$, we can assume that we start from an image $u : \mathcal{D} \to \mathbb{R}$ where $\mathcal{D} = \otimes_{i \in [\![1,n]\!]} [\![k_i^{\min}, k_i^{\max}]\!]$, with $k^{\min}, k^{\max} \in \mathbb{Z}^n$ the lower and upper bounds of the domain $\mathcal{D}$ of u respectively.

Also, since we are working with subsets of **finite** spaces, we do not use the topological boundary ∂ but the border Δ instead. We recall that the *border* of a subset X in any Alexandrov

space of finite rank $n \geq 0$ (as an order) is the union of the closures of the $(n-1)$-faces that have one n-face as coface.

FROM $(\mathbb{Z}/2)^n$ TO $\mathbb{H}^n$ Now let us define the isomorphism between $(\mathbb{Z}/2)^n$ and $\mathbb{H}^n$ we use to immerse u into any cubical complex subset of $\mathbb{H}^n$. We define the application $\mathcal{H} : (\mathbb{Z}/2) \to \mathbb{H}^1$ such that:

$$\forall z \in (\mathbb{Z}/2), \mathcal{H}(z) = \begin{cases} \{z + 1/2\} & \text{if} \quad z \in (\mathbb{Z}/2) \setminus \mathbb{Z}, \\ \{z, z+1\} & \text{if} \quad z \in \mathbb{Z}, \end{cases} \tag{1}$$

from which we deduce using the Cartesian product the application $\mathcal{H}_n : \left(\frac{\mathbb{Z}}{2}\right)^n \to \mathbb{H}^n$ such that:

$$\forall z \in (\mathbb{Z}/2)^n, \mathcal{H}_n(z) = \otimes_{i \in [\![1,n]\!]} \mathcal{H}(z_i).$$

We will denote by $\mathcal{Z}_n$ the inverse of the bijection $\mathcal{H}_n$.

SPAN-BASED IMMERSIONS ARE CONTINUOUS BUT NOT AWC Then, a first idea could be to immerse u into $\mathrm{Imm}_u : \alpha(\mathcal{H}_n(\mathcal{D})) \rightsquigarrow \mathbb{R}$, where α is the closure operator, such that $\forall z \in \alpha(\mathcal{H}_n(\mathcal{D}))$:

$$\mathrm{Imm}_u(h) = \begin{cases} \{u(\mathcal{Z}_n(h))\} & \text{if } h \in \mathbb{H}^n_n, \\ \mathrm{Span}\{u(\mathcal{Z}_n(q)) \ ; \ q \in \beta(h) \cap \mathbb{H}^n_n\} & \text{either.} \end{cases}$$

Note that $\alpha(\mathcal{H}_n(\mathcal{D}))$ is a cubical complex (see Definition 70), since it is closed by inclusion, and that any face of any face of this set belongs to this set.

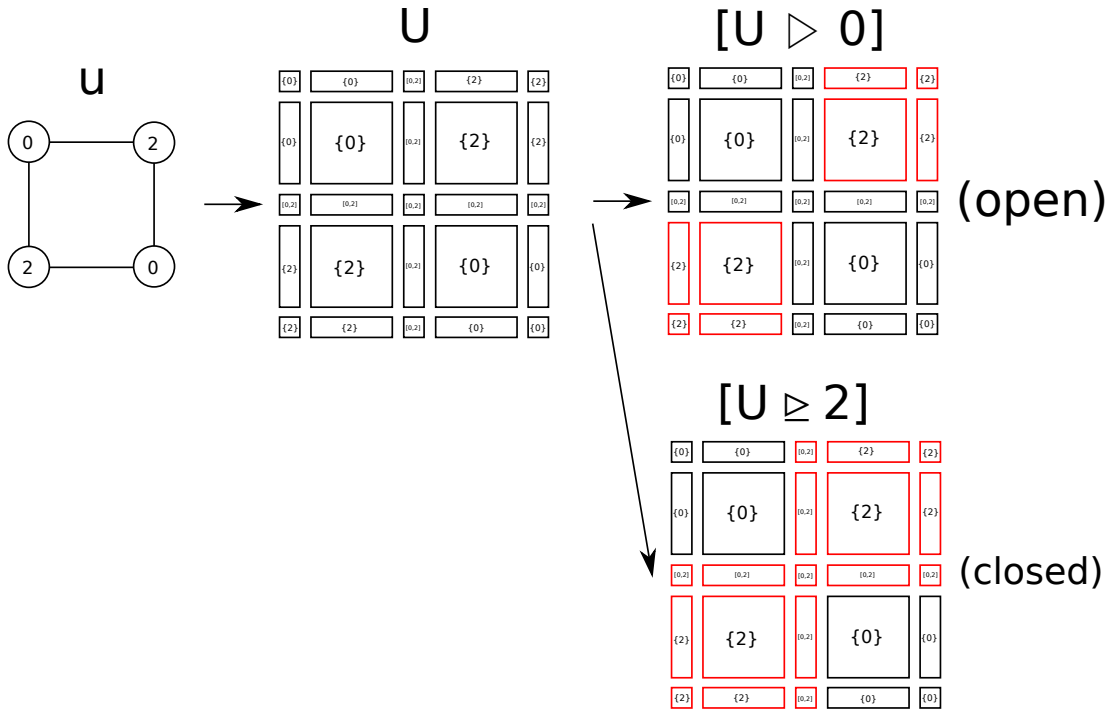

Figure 12.: Span-based immersion of $u : [\![0,1]\!] \times [\![0,1]\!] \to \mathbb{R}$ into a cubical complex provides continuity properties to the new representation U of u.

This way, we obtain an USC map as showed on Figure 12: the strict upper/lower threshold sets are open and the upper/lower threshold sets are closed.

However, this map is not AWC, as showed on Figure 13, in the sense that its *border* in not a disjoint union of $(n-1)$-surfaces.

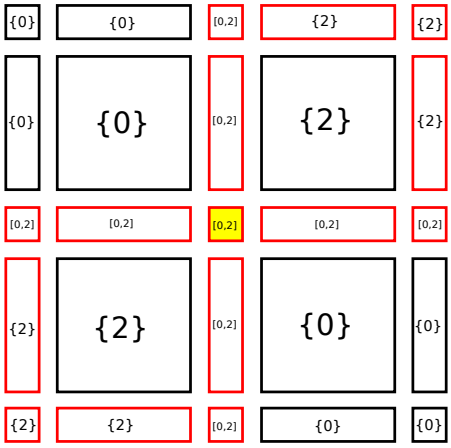

Figure 13.: $\Delta[U \trianglerighteq 2]$, depicted in red, contains a pinch (in yellow)

AN AWC CONTINUOUS REPRESENTATION ON $\mathbb{H}^n$ Note that this section requires the content of Chapter D containing the sketch of the proof that immersions of DWC images on the Khalimsky grids are AWC interval-valued maps.

For this reason, we propose the following numerical scheme (see Figure 14): we start from an image $u : \mathcal{D} \to \mathbb{R}$ where $\mathcal{D}$ is defined such that:

$$\mathcal{D} = \otimes_{i \in [\![1,n]\!]} [\![2k_i^{\min}, 2k_i^{\max}]\!] \cap (2\mathbb{Z})^n,$$

we compute its span-based interpolation $U : \mathcal{D}_2 \rightsquigarrow \mathbb{R}$ with $\mathcal{D}_2$ defined such that:

$$\mathcal{D}_2 = \otimes_{i \in [\![1,n]\!]} [\![2k_i^{\min}, 2k_i^{\max}]\!],$$

we apply the front propagation $\mathfrak{FP}$ on it to obtain $u_{\mathrm{DWC}} : \mathcal{D}_2 \to \mathbb{R}$, and then we use u_{DWC} to compute its immersion U_{AWC} defined onto $\alpha(\mathcal{H}_n(\mathcal{D}_2)) \subseteq \mathbb{H}^n$ such that, $\forall h \in \alpha(\mathcal{H}_n(\mathcal{D}_2))$:

$$U_{\mathrm{AWC}}(h) = \begin{cases} \{u_{\mathrm{DWC}}(\mathcal{Z}_n(h))\} & \text{if } z \in \mathcal{H}_n(\mathcal{D}_2), \\ \mathrm{Span}\,\{u_{\mathrm{DWC}}(\mathcal{Z}_n(q)) \;;\; q \in \beta(z) \cap \mathcal{H}_n(\mathcal{D}_2)\} & \text{otherwise.} \end{cases}$$

We obtain finally U_{AWC} which is AWC in the sense that the border of its threshold sets are either disjoint union of $(n-1)$-surfaces or empty sets (at least in 2D and in 3D, the n-D case, $n \geq 4$, being still not verified).

Following the same idea as Najman and Géraud in [127], and considering that the value image of U is supplied with the usual Euclidian distance, the properties of our self-dual interpolation U_{AWC} will be the following:

- U_{AWC} is AWC,
- U_{AWC} is USC,
- for any $\lambda \in \mathbb{R}$, the threshold sets $[U_{\mathrm{AWC}} \lhd \lambda]$ and $[U_{\mathrm{AWC}} \rhd \lambda]$ are open sets,
- for any $\lambda \in \mathbb{R}$, the threshold sets $[U_{\mathrm{AWC}} \trianglelefteq \lambda]$ and $[U_{\mathrm{AWC}} \trianglerighteq \lambda]$ are closed sets (since $\alpha(\mathcal{H}_n(\mathcal{D}_2))$ is closed by construction),
- U_{AWC} satisfies the *intermediate value theorem*,
- when $\alpha(\mathcal{H}_n(\mathcal{D}_2))$ is *unicoherent*[1], the set of *shapes* [127] $\mathfrak{T}$ of U_{AWC} is a *tree*, that is, two components of $\mathfrak{T}$ are either nested or disjoint; in other words, the tree of shapes is well-defined.

1 A topological space is said to be *unicoherent* iff it is connected and for any two closed connected sets such that their union equals the whole space, their intersection is also connected.

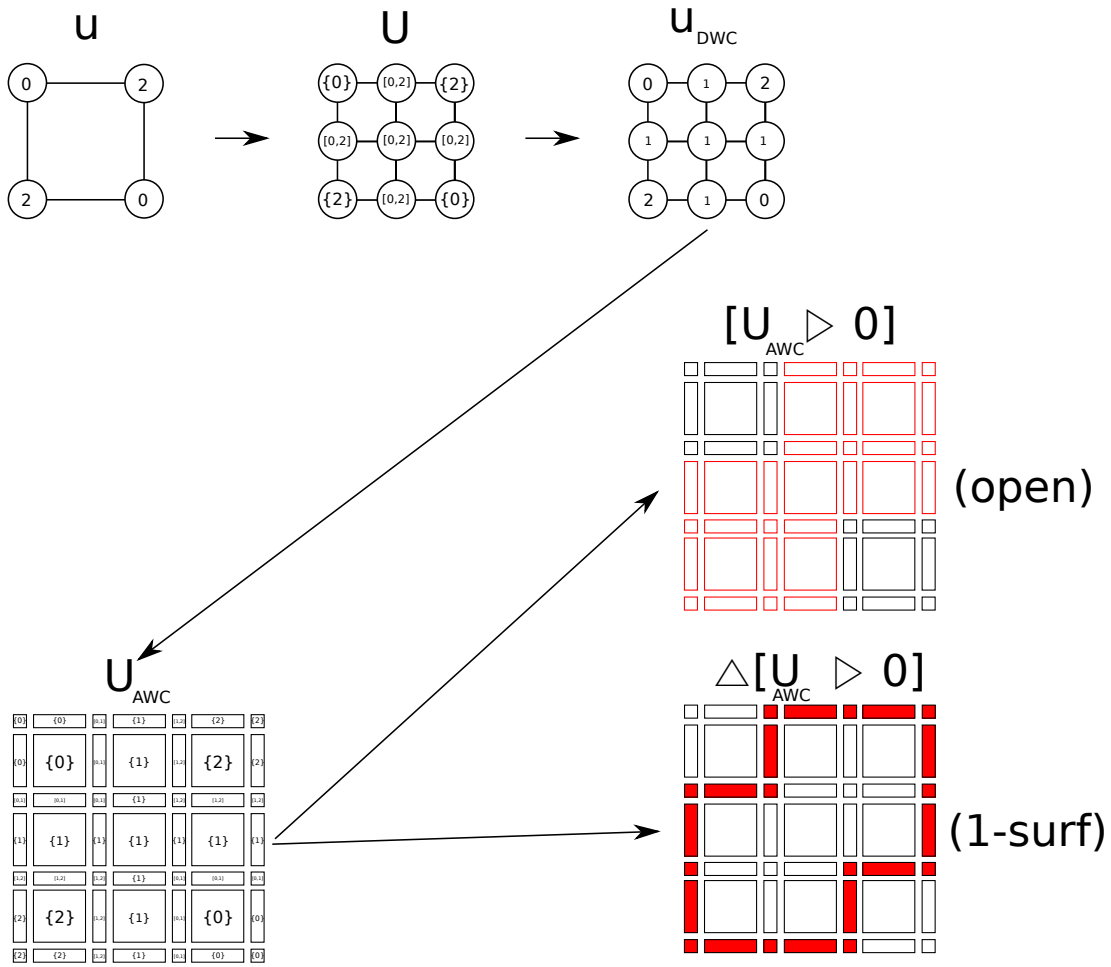

Figure 14.: Our method to obtain an AWC plain map

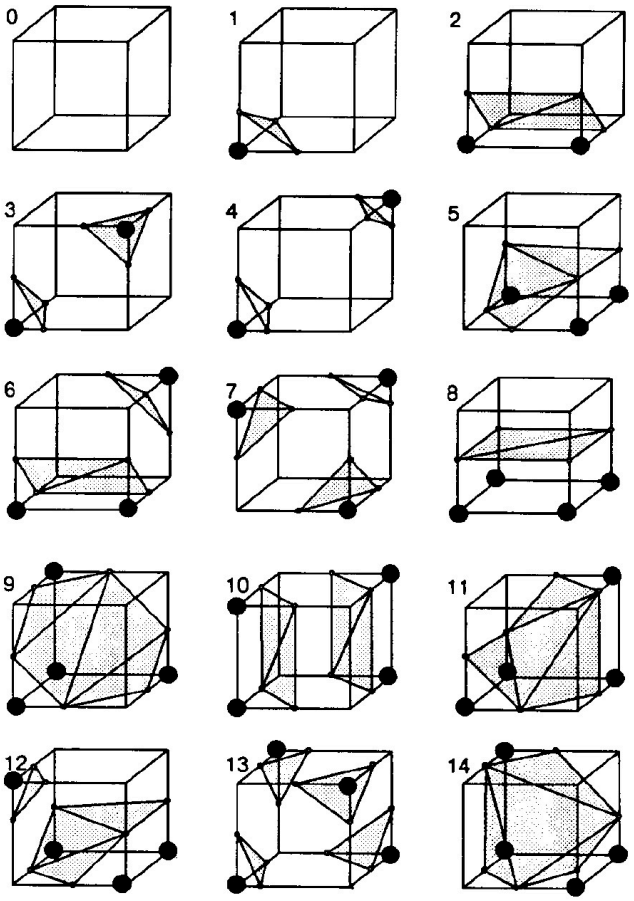

Figure 15.: Lorensen's Marching Cubes Lookup Table [113]

Note: Obviously, a span-based immersion applied on the AWC interpolations described in Chapter E will also lead to AWC continuous maps with these same properties.

5.3 n-D MARCHING-CUBES-LIKE ALGORITHMS

We propose here the conjecture that any n-D MC-like algorithm has no ambiguity cases when the digital gray-level image we are working with is DWC.

The main reference in matter of scientific and experimental visualization of scalar field data on 3D cubical grids is the *Marching Cubes (MC)* algorithm of Lorensen [113]. Assuming that we have a continuous scalar field f whose values are known on the lattice points of a cubical grid, we can visualize the approximate of the implicit surface $[f = \alpha]$ (usually assumed to be a topological 2-manifold), $\alpha \in \mathbb{R}$, using a *triangular mesh*, that is, a simplicial complex, also called the *surface tiling* of the iso-surface. This algorithm computes the triangulation cube by cube in this way: each corner c of the cube (the lattice points of the cubical grid) whose value $f(c)$ is superior or equal to the given threshold α is said to be *positive* (they correspond to the inside part of the object), and the other corners of the cubes are said to be *negative* (they correspond to the outside part of the object). A *boundary point* is then created on each edge of the cube using a (trivial or non-trivial) interpolation such that one of its vertices is positive and the other is negative. Then, using a lookup table proper to the MC algorithm [113] as shown on Figure 15, boundary points are connected with one or several triangles, making a triangular mesh, connected or not, depending on the configuration of points in the cube. Then the "local" meshes are grouped together to make the final mesh in $\mathbb{R}^3$.

We would then hope that the resulting mesh is an union of disjoint simplical surfaces [24] which separates the positive vertices to the negative vertices. However some *holes/cracks* can

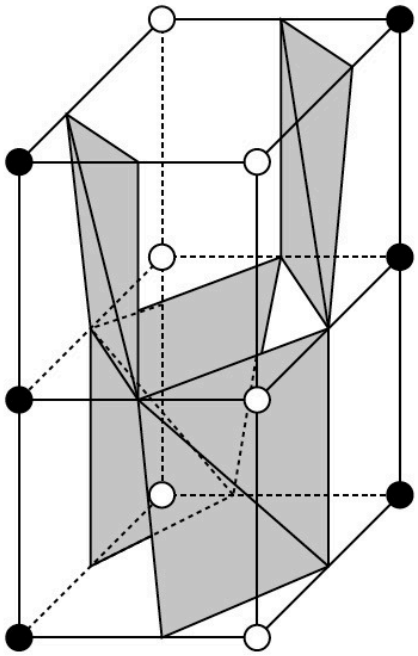

Figure 16.: The "hole problem" using Marching Cubes ([157])

appear as shown on Figure 16, due to *ambiguities* in some configurations. In this case, the algorithm fails to produce a piecewise linear manifold: some edges are the face of only one triangle, which means that they draw together the boundary of a hole in the surface. To obviate these ambiguities, Han *et al* [74] use *digital topology*: a couple of connectivities (among the 8-,18-, and 26-connectivities) is then associated to the positive/negative lattice points, to be able to decide which surface tiling has to be drawn (at each cube separatly). As usual, this couple must be a Jordan pair to avoid the connectivity paradox of Rosenfeld. Then there is only one possible tiling at each cube and positive and negative vertices are separated in each cube by the local tiling surface. The resulting mesh is *"digitally" topologically correct* in the sense that the surface tiling correctly reflects the topology of the initial isosurface $[f = \alpha]$ if the connectedness is well chosen. This algorithm is called *connectivity-consistent marching cubes* (CCMC).

Be careful not to amalgamate the topological correctness in the context of digital topology and the *topological correctness* used in isosurface extraction and which means that the approximating isosurface is homeomorphic to piecewise trilinear interpolation of the digitization of the given continuous scalar field.

However it is sometimes difficult to choose which connectivity is the best suited to a given application, and then we would avoid to choose a connectivity, since the resulting mesh depends strongly on this choice. *Digital well-composedness* (in the sense that the sets and its complement do not contain any *critical configurations*) is then salutary: it has been stated in [88] that a cubic cell is unambiguous iff there exists a 6-path of positive (respectively negative) vertices in this cube connecting each pair of positive (respectively negative) vertices of this same cube, which is equivalent to well-composedness in 3D. This way, no choice of connectivity is needed anymore, since whatever the chosen connectivities the result will be the same. Moreover, $[f = \alpha]$ is a PL (*Piecewise Linear*) 2-manifold with no hole, and then its boundary is contained in the boundary of the cubical grid, what is called *topological consistency*.

Furthermore, Siqueira *et al.* proved in [157] that the isosurface resulting from the MC algorithm may reflect the topology of the initial continuous scalar field when the given binary

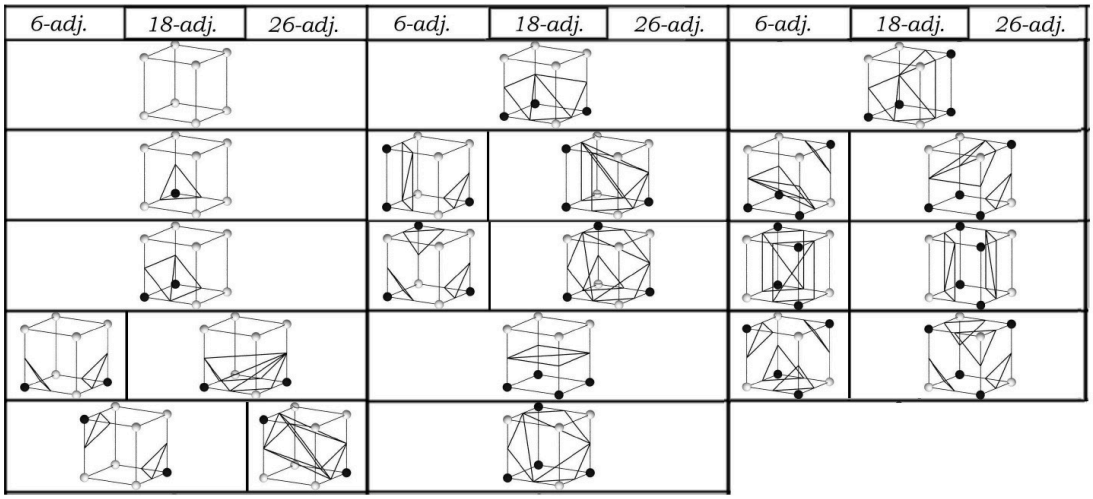

Figure 17.: Lookup tables of Daragon [44, 43] in the 3D case

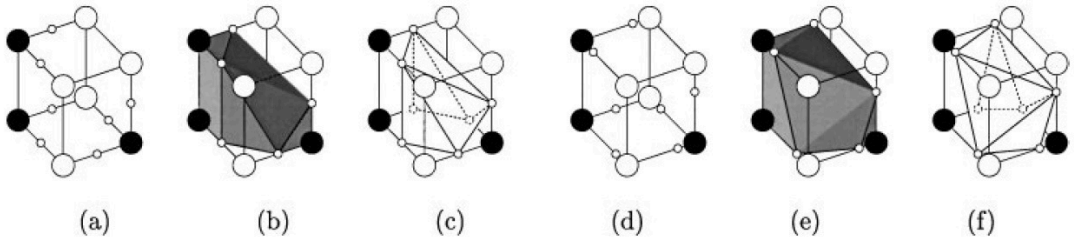

Figure 18.: n-D approach of Lachaud [96], based on the convex hull

image is well-composed. If for some reason, we are not able to make any well-composed interpolation or to use any topological repairing method, the use of the *Modified Marching Cubes algorithm (MMC)* [165] is a good choice, but it assumes that the digitized object is r-regular and that the sampling grid has a sufficient resolution.

Note that some very powerful MC-like methods exist for the n-dimensional case, $n \geq 2$, as the *frontier orders* of Daragon [44, 43] based on combinatorial topology and the *continuous analog of the digital boundary* of Lachaud and Montanvert [96] based on digital topology. Both obtain the same surface tilings in the 3D case, as shown on Figure 17, showing each possible configuration in the 3D case, assuming that we use 6-,18-, or 26-connectivity for the black points (and a dual connectivity for the white points). In other words, $(6, 18)$-connectivity will join the black points which are 6-connected, and will separate the black points which are only 18- or 26-connected. In the same time, it will join the white points which are 6- or 18-connected, and it will separate the white points which are only 26-connected. Note that the n-D approach of Lachaud is depicted on Figure 18, and consists in computing in each cube separatly the boundary of the convex hull of the set of points made with the black points plus the boundary points (see (a), (b), and(c)). An equivalent approach but using a non trivial interpolating function is showed from (d) to (f). Under reasonable constraints, these two methods provide simplicial surfaces with no "holes", at least in the 3D case.

Finally, we can mention the existence of isosurface simplification algorithms [156, 83] used to reduce the excessive number of triangles produced by the MC algorithm in practice. These methods works particularly well with well-composed images since they preserve the topology of the boundary of the continuous analog of the foreground of a well-composed digital image [157].

Finally, we strongly think that a n-D image which is DWC has no possible local ambiguity. Effectively, assuming that we want to extract the isosurface of a set $X \subset \mathbb{Z}^n$, an ambiguity

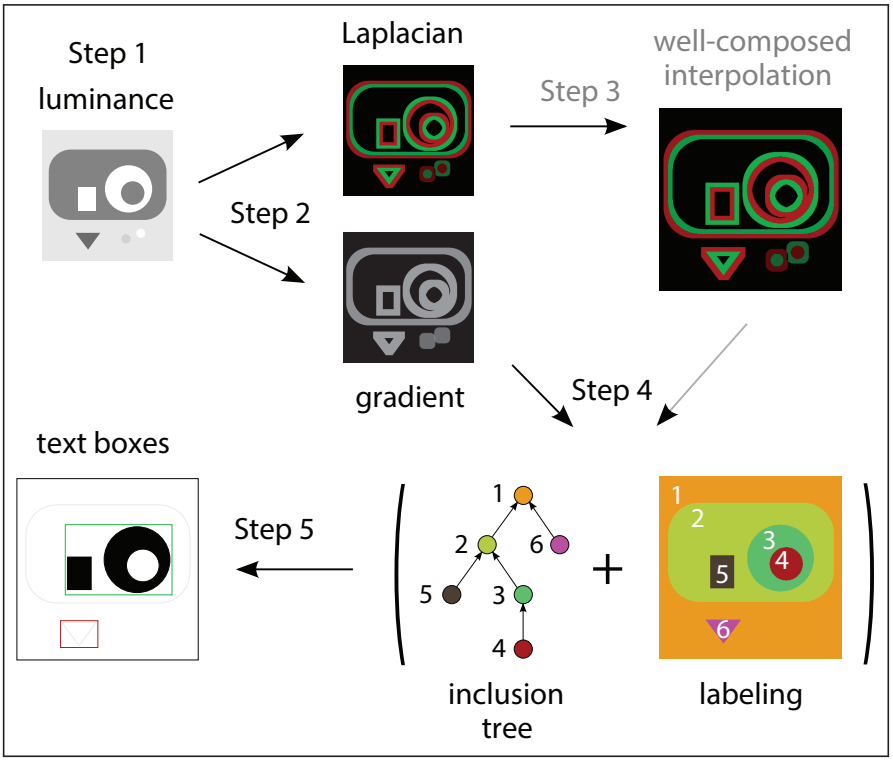

Figure 19.: Summary of the method used by Huyhn *et al.* [80]

appears in a block $S \in \mathcal{B}(\mathbb{Z}^n)$ if and only if there exists two points p, p' in $X \cap S$ (respectively in $X^c \cap S$) which are α-connected but not β-connected, where α-connectivity and β-connectivity are two connectivities both implied by $2n$-connectivity, and such that they both imply $(3^n - 1)$-connectivity. However, if the set X is DWC, $(3^n - 1)$-connectivity in S of X (respectively of X^c) implies $2n$-connectivity. In other words, α-connectivity will imply $(3^n - 1)$ connectivity, which implies $2n$-connectivity, which implies β-connectivity, and conversely. In that sense, any pair of connectivities is be equivalent in any block S, and then no ambiguity is possible on the domain of the image. This reasoning leads us to the following conjecture:

Conjecture 5. *Let $u : \mathcal{D} \to \mathbb{R}$ be a real-valued DWC image defined on a domain $\mathcal{D}$. Then, u does not have any ambiguous cases. In other words, no "hole problem" is possible in n-D using DWC images.*

5.4 TREE OF SHAPES OF THE SIGN OF THE DWC MORPHOLOGICAL LAPLACIAN

In this section, we present some results of Huyhn *et al.* [80] obtained thanks to the computation of the tree of the sign of the (DWC) morphological Laplacian in a self-dual way. Even if it is used here for text detection, this approach can easily be extended to treat n-D signals, such as M.R images, videos, or CT-scans.

Nowadays, text detection methods [54, 184, 186] are widely used, especially on mobile devices, for recognition tasks. They are generally classified into *connected-components-based approaches*, like *FASText* [30], the *SWT* (Stroke Width Transform) [52], the *TMMS* (Toggle Mapping Morphological Segmentation), and the *MSER* (Maximally Stable Extremal Regions), or into sliding-windows approaches using *SVM* (Support Vector Machines) [36], *AdaBoost* [107], or *CNN* (Convolutional Neural Networks) [177] as classifiers.

The one presented by Huyhn *et al.* [80] is part of the connected-components-based approaches, and consists in transforming an image into a tree-based hierarchical representation (see Figure 19), based on adjacency and inclusion relationship between the components in the image.

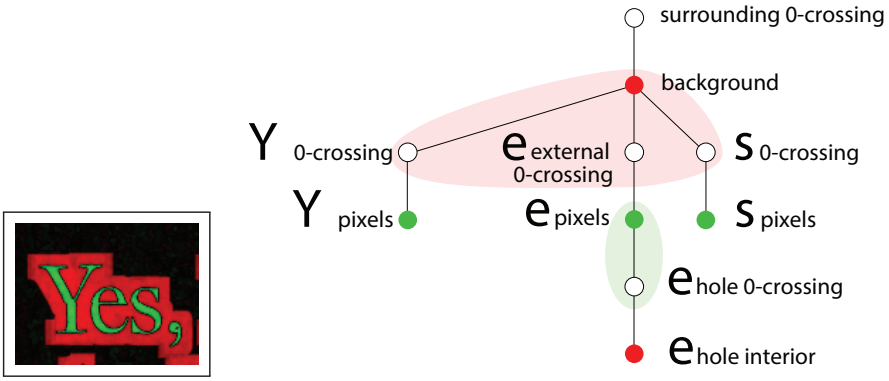

(a) $\Delta^{wc}(u)$. (b) Tree $\mathfrak{S}(\operatorname{sign}(\Delta^{wc}(u)))$.

Figure 20.: An inclusion tree and its corresponding image [80]

To proceed, they compute the Laplacian of a given image using a *morphological Laplacian operator* [175, 160, 129], whose *zero-crossings* are known to be very precise contour estimations of the initial image. Using a large-sized structuring element relatively to the size of the text to detect, spurious contours are easily eliminated and salient contours preserved, thanks to the non-linearity of the operator. After that, a self-dual well-composed interpolation (like the one we presented in this thesis) of this Laplacian is computed; this way, the zero-crossings of this interpolation are simple closed curves. Using these separated Jordan curves, we can naturally induce a hierarchy [27] in the image: saturation of these curves (whatever the chosen connectivity) are either nested or disjoint. A component labeling of the sign of the Laplacian and the generation of the inclusion tree are then straightforward and very fast (a classical blob labeling algorithm is sufficient).

Thanks to this tree-based representation of the image, they can extract text candidates: a hole of a character or a solid character are leafs of the tree (ss Figure 20), and so on. Text grouping is then simply a subtree of this inclusion tree, since characters must be grouped iff they belong to the same background.

Finally, in this context, well-composedness gave access to a very fast (linear time) and efficient self-dual text detection algorithm thanks to the hierarchy induced by the Jordan curves extracted from the well-composed Laplacian.

6 PERSPECTIVES

In this chapter, we present some future works that seem promising and that are related to well-composedness.

6.1 ABOUT THE EQUIVALENCE BETWEEN AWCNESS AND CWCNESS ON CUBICAL GRIDS

In digital topology, its is generally admitted that in 2D and 3D a finite set $X \subseteq \mathbb{Z}^n$ is continuous well-composed, that is, the boundary of its continuous analog $\mathrm{bdCA}(X)$ is a $(n-1)$-manifold, iff its immersion $\mathcal{IMM}(X) = \mathrm{Int}(\alpha(\mathcal{H}_n(X)))$ in the Khalimsky grids $\mathbb{H}^n$ is well-composed in the sense of Alexandrov, that is, its boundary is a disjoint union of discrete $(n-1)$-surfaces.

Starting from a finite subset $\mathcal{IMM}(X) \subseteq \mathbb{H}^n$, let us recall how we can proceed to build its *underlying polyhedron* into $\mathbb{R}^n$.

Definition 38 (Underlying Polyhedron)**.** *Let h_1 be an element of $\mathbb{H}^1$. We call* underlying polyhedron *of h_1 the set denoted by $\mathrm{Poly}(h_1)$ and defined such that:*

$$\mathrm{Poly}(h_1) = \begin{cases} \{a_1\} & \text{if } \exists a_1 \in \mathbb{Z} \text{ s.t. } h_1 = \{a_1\}, \\ [a_1, a_1+1] & \text{if } \exists a_1 \in \mathbb{Z} \text{ s.t. } h_1 = \{a_1, a_1+1\}. \end{cases}$$

In other words, a 0-face becomes a point in $\mathbb{R}$ and a 1-face becomes a closed unitary interval in $\mathbb{R}$. Then, for any face $h \in \mathbb{H}^n$, we define the underlying polyhedron *of the face h as the Cartesian product of the underlying polyhedron of its coordinates:*

$$\mathrm{Poly}(h) = \otimes_{i \in [\![1,n]\!]} \mathrm{Poly}(h_i).$$

Finally, let $X \subseteq \mathbb{H}^n$ be a set of faces; then its underlying polyhedron *is defined as the union of the underlying polyhedra of its elements:*

$$\mathrm{Poly}(X) = \bigcup_{h \in X} \mathrm{Poly}(h).$$

Note that any of these underlying polyhedra are closed into $\mathbb{R}^n$.

This construction seems equivalent to construct the continuous analog in $\mathbb{R}^n$ with unitary n-cubes centered at the points of the set $\mathcal{Z}_n(\mathcal{X})$. Then we propose the following conjecture:

Conjecture 6. *Let X be a finite subset of $\mathbb{Z}^n$ and let $\mathcal{IMM}(X)$ be its immersion in $\mathbb{H}^n$. Then, $\mathcal{IMM}(X)$ is well-composed in the sense of Alexandrov iff X is continuous well-composed, that is, the boundary $\mathfrak{N}$ of $\mathcal{IMM}(X)$ is a disjoint union of (discrete) $(n-1)$-surfaces iff the topological boundary $\partial\mathrm{Poly}(\mathcal{IMM}(X)) = \mathrm{bdCA}(X)$ is a $(n-1)$-manifold.*

As for the equivalence between AWCness and DWCness, we believe that the Cartesian product is a property which is essential to prove that CWCness and AWCness are equivalent. Furthermore, we can easily feel that the decomposition of $\mathbb{R}^n$ into $\{\mathrm{Poly}(h)\ ;\ h \in \mathbb{H}^n\}$ has the same structure as $\mathbb{H}^n_n$ whatever the dimension. For these reasons, we think that CWCness and AWCness are equivalent on cubical grids.

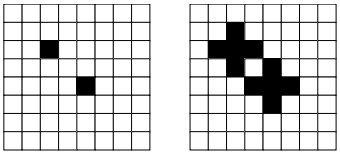

Figure 1.: Morphological dilation does not preserve digital well-composedness using a structuring element based on 4-connectivity

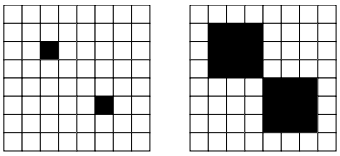

Figure 2.: Morphological dilation does not preserve digital well-composedness using a structuring element based on 8-connectivity

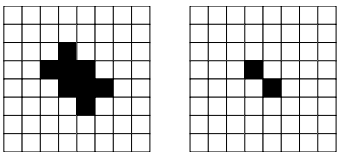

Figure 3.: Morphological erosion does not preserve digital well-composedness using a structuring element based on 4-connectivity

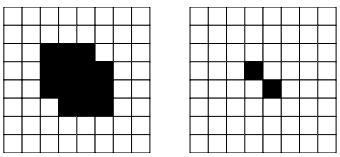

Figure 4.: Morphological erosion does not preserve digital well-composedness using a structuring element based on 8-connectivity

6.2 PRESERVATION OF DIGITAL WELL-COMPOSEDNESS

In mathematical morphology, digital well-composedness is not usually "stable": even the simplest morphological operators like the dilation (see Figure 1 and Figure 2) and the erosion (see Figure 3 and Figure 4) do not preserve digital well-composedness. It is even worst with second order operators like the morphological Laplacian.

However, we are going to show that there exist some classes of morphological operators that preserve digital well-composedness. Among them, there exist the monotone plannings, a transformation which preserves the order between neighbouring pixels, and the grain filters, a transformation which removes components of small size in the hierarchical representation of the image (computed using the tree of shapes).

6.2.1 *Monotone plannings*

In [122], Meyer and Maragos present a strong morphological filter, the *levelings*, whose definition is the following:

Definition 39 (Levelings)**.** *An image* $g : \mathcal{D} \subseteq \mathbb{Z}^n \to \mathbb{R}$ *is a* leveling *of the image* $f : \mathcal{D} \to \mathbb{R}$ *iff* $\forall (p, q)$ *2n-neighbors in* $\mathbb{Z}^n$*:*

$$\{g(p) > g(q)\} \Rightarrow \{f(p) \geq g(p) \text{ and } g(q) \geq f(q)\}.$$

The meaning of this definition is that if there exists a difference between two neighboring pixels in the leveling g, there exists an even greater difference in the original image f: "to any contour of a function g corresponds a stronger contour in the function f at the very same location, and the localisation of this contour is exactly the same".

Levelings correspond to a particular case of *monotone plannings* [122]:

Definition 40 (Monotone plannings). *An image $g : \mathcal{D} \subseteq \mathbb{Z}^n \to \mathbb{R}$ is a* monotone planning *of the image $f : \mathcal{D} \to \mathbb{R}$ iff $\forall (p, q)$ $2n$-neighbors in $\mathbb{Z}^n$:*

$$\{g(p) > g(q)\} \Rightarrow \{f(p) > f(q)\}.$$

This definition called us to mind because monotone plannings constitute a class of transformations which preserves the relation order between neighboring pixels in an image, which is very close to digital well-composedness: if we assume that a 2D image g contains a critical configuration, it means that there exist two points p, p' which are antagonist in a 2D block S such that their corresponding values $g(p)$ and $g(p')$ are strictly lower than the two other values of g in S. By definition of monotone plannings, the original image f satisfies then this same order relation, and then the critical configuration is preserved from g to f. That means that, in 2D, the monotone planning of a digitally well-composed image is digitally well-composed. We can even announce that this property is true in n-D, $n \geq 2$. To prove that, let us introduce some additional material.

Definition 41. *Let z be a point in $\mathbb{Z}^n$. We define the* $2n$-neigborhood of order l, $l \geq 1$, *such that $\mathcal{N}^1_{2n}(x) = \mathcal{N}_{2n}(x)$, and:*

$$\mathcal{N}^l_{2n}(x) = \bigcup_{v \in \mathcal{N}^{l-1}_{2n}(x)} \mathcal{N}_{2n}(v),$$

when $l \geq 2$. For sake of simplicity, we will also denote for $l \geq 2$:

$$\delta\mathcal{N}^l_{2n}(p) = \mathcal{N}^l_{2n}(p) \setminus \mathcal{N}^{l-1}_{2n}(p).$$

Lemma 11. *Let $u : \mathcal{D} \subset \mathbb{Z}^n \to \mathbb{R}$ be a real-valued image defined on a bounded hyperrectangle $\mathcal{D}$ in $\mathbb{Z}^n$. Now, let $S^k \in \mathcal{B}(\mathcal{D})$ be a block of dimension $k \geq 2$, and p be a point in S^k such that $\forall n^1 \in S^k \cap \mathcal{N}_{2n}(p)$, $u(p) < u(n^1)$ (case 1), or such that $\forall n^1 \in S^k \cap \mathcal{N}_{2n}(p)$, $u(p) > u(n^1)$ (case 2). Let us assume that the restriction of u to S^k is digitally well-composed. Then, for any $l \in [\![2, k]\!]$, and for any $n^l \in S^k \cap \delta\mathcal{N}^l_{2n}(p)$, there exists a block S^l of dimension l included in S_k, such that there exists a $2n$-path $\pi = (p, n^1, \ldots, n^l) \subseteq S^l$ such that $\forall i \in [\![1, l]\!]$:*

$$n^i \in \delta\mathcal{N}^i_{2n}(p),$$

and:

$$u(p) < u(n^1) \leq \cdots \leq u(n^l), \qquad \textit{(Case 1)}$$

or:

$$u(p) > u(n^1) \geq \cdots \geq u(n^l). \qquad \textit{(Case 2)}$$

Proof: Let us proceed by induction on $l \in [\![2, k]\!]$ to prove Case 1, the proof of Case 2 being its dual.

Initialization ($l = 2$): Let $n^2 \in S^k \cap \delta\mathcal{N}^2_{2n}(p)$ be a point. n^2 is then antagonist of p in a 2D block $S^2 \subseteq S^k$. Since the restriction of u to S^2 is digitally well-composed, we have:

$$\text{intvl}(u(p), u(n^2)) \cap \text{Span}\{u(q)\ ;\ q \in S^2 \setminus \{p, n^2\}\} \neq \emptyset,$$

and then $u(n^2) \geq \min\{u(q)\ ;\ q \in S^2 \setminus \{p, n^2\}\}$. This way,

$$\pi = (p,\ \underset{q \in S^2 \setminus \{p, n^2\}}{\arg\min}\ (v(q)), n_2)$$

is the $2n$-path we are looking for.

Induction ($l \in [\![3, k]\!]$): we assume that the property is true for $(l-1)$. In other words, we assume that for any $n^{l-1} \in S^k \cap \delta\mathcal{N}_{2n}^{l-1}(p)$, there exists $S^{l-1} \in \mathcal{B}(S^k)$ and a $2n$-path in $\mathbb{Z}^n$:

$$\pi = (p, n^1, \ldots, n^{l-1}) \subseteq S^{l-1} \subset S^k$$

such that $u(p) < u(n^1) \leq u(n^2) \leq \cdots \leq u(n^{l-1})$ with $n^i \in S^{l-1} \cap \delta\mathcal{N}_{2n}^i(p)$ for any $i \in [\![1, l-1]\!]$. Then the following property comes out: $\forall q \in S^k \cap \mathcal{N}_{2n}^{l-1}(p) \setminus \{p\}, u(p) < u(q)$. Let be now $n^l \in S^l \cap \delta\mathcal{N}_{2n}^l(p)$. If we assume that for any $r \in S^l \cap \mathcal{N}_{2n}(n^l)$, we have $u(n^l) < u(r)$, then by the induction hypothesis, and following the same reasoning as for p in S^{l-1}, we obtain that there exists S_*^l of dimension l such that $p \in S_*^l$ and such that for all $s \in S_*^l \cap \mathcal{N}_{2n}^{l-1}(n^l) \setminus \{n^l\}$, $u(n^l) < u(s)$. In fact, $S^l = S(p, n^l) = S(n^l, p) = S_*^l$, and then we have that:

$$\max(u(p), u(n^l)) < \min\{u(q)\ ;\ q \in S^l \setminus \{p, n^l\}\},$$

which would imply that u contains a critical configuration into $S^l \subset S^k$, which is impossible. Then there exists $r^* \in S^l \cap \mathcal{N}_{2n}(n^l)$ such that $u(r^*) \leq u(n^l)$. Since r^* is a $2n$-neighbor of n^l such that it belongs to S^l, $r^* \in S^l \cap \mathcal{N}_{2n}^{l-1}(p)$, and then $(p, n^1, \ldots, n^{l-1} = r^*, n^l)$ is a $2n$-path in S^l which satisfies $u(p) < u(n^1) \leq \cdots \leq u(n^l)$. □

Then we can announce our theorem:

Theorem 7. *Let $u : \mathcal{D} \subset \mathbb{Z}^n \to \mathbb{R}$ be a real-valued image defined on a bounded hyperrectangle $\mathcal{D}$, and let be $u' : \mathcal{D} \to \mathbb{R}$ be a monotone planning of u. If u is digitally well-composed, then u' is digitally well-composed too.*

Proof: Let us show that if u' is not digitally well-composed and if u is digitally well-composed, we get a contradiction. If u' is not digitally well-composed, there exists a block $S^k \in \mathcal{B}(\mathcal{D})$ of dimension $k \geq 2$ such that $p, p' \in S^k$ are antagonist in S^k and we have one of these two cases:

$$\begin{cases} \max(u'(p), u'(p')) < \min\{u'(q)\ ;\ q \in S^k \setminus \{p, p'\}\}, & (1) \\ \max\{u'(q)\ ;\ q \in S_k \setminus \{p, p'\}\} < \min(u'(p), u'(p')). & (2) \end{cases}$$

Let us treat the first case, the reasoning being dual for the second case.

From (1), it follows that:

$$\begin{cases} \forall n^1(p) \in \mathcal{N}_{2n}^*(p) \cap S^k, u'(p) < u'(n^1(p)), \\ \forall n^1(p') \in \mathcal{N}_{2n}^*(p') \cap S^k, u'(p') < u'(n^1(p')), \end{cases}$$

and u' being a monotone planning of u, we have also that:

$$\begin{cases} \forall n^1(p) \in \mathcal{N}_{2n}^*(p) \cap S^k, u(p) < u(n^1(p)), & (A) \\ \forall n^1(p') \in \mathcal{N}_{2n}^*(p') \cap S^k, u(p') < u(n^1(p')). & (A') \end{cases}$$

Since u is assumed to be digitally well-composed, we have that the restriction of u to S^k is digitally well-composed. Then (A) implies by Lemma 11 that there exists a $2n$-path $(q^0 = p, \ldots, q^k = p')$ into S^k going from p to p' such that $u(p) < u(q^1) \leq \cdots \leq u(p')$, and then $u(p) < u(p')$. From (A'), we obtain using Lemma 11 that $u(p') < u(p)$, which is impossible. We have a contradiction. Then u is not digitally well-composed. □

Obviously, since we have proven that all kinds of monotone plannings preserve digital well-composedness, it follows that levelings preserve also digital well-composedness.

Figure 5.: The original Barbara image

Figure 6.: The 44417 critical configurations in the original Barbara image

6.2.2 *Grain filters*

We observed that another class of filtering preserves digital well-composedness in morphological analysis: grain filters [32]. The principle is to decompose the image into an hierarchical representations of the shapes in the image, using the tree of shapes [31, 61], and to keep only the components such that their area is greater than a given threshold. Figure 5 shows the original Barbara image, Figure 6 shows the critical configurations contained in this image, and Figure 7 shows our self-dual interpolation of this image.

Our observation is the following: grain filters preserve digital well-composedness, as depicted on Figure 8, Figure 9, Figure 10 corresponding to filtered DWC interpolations with different thresholds. The result is that any of these images is digitally well-composed.

Our explanation of this phenomenon is that the hierarchical representation of the interpolation consists of nested or disjoint connected components such that they do no touch each other, since no critical configurations occur in threshold sets of digitally well-composed images. Then, by applying the grain filter, we juste remove some shapes, and in this manner we

Figure 7.: Our self-dual interpolation of the Barbara image

Figure 8.: A grain filter of the DWC interpolation of the Barbara image with a threshold $\lambda = 10$

just "simplify" the hierarchical representation of the image, and then the reconstructed image must be digitally well-composed.

6.2.3 *Geodesic dilations/erosions*

We remarked that another class of operations preserves digital well-composedness: geodesic dilations and erosions, much used in mathematical morphology. Geodesic dilation basically consists of starting from a given binary image considered as the *mask*, that we associate to a *marker image* representing the "seeds" lying in this subset. Applying the geodesic dilation is then equivalent to dilate progressively the seeds in the space corresponding to the mask, such that they will completely fill the connected components of the initial set, since dilation outside the set is forbidden. In this manner, geodesic dilation simply extracts some connected components of a set depending on the associated initial marker.

Starting from a digitally well-composed binary image where connected components have Jordan curves as boundaries and do not "touch" each other, geodesic dilation chooses among these connected components which ones are kept and which ones are rejected, and in this

Figure 9.: A grain filter of the DWC interpolation of the Barbara image with a threshold $\lambda = 320$

Figure 10.: A grain filter of the DWC interpolation of the Barbara image with a threshold $\lambda = 1280$

manner preserves the digital well-composedness of this binary image; note that this reasoning is similar to the grain filters we have studied in the preceding section.

The geodesic erosion is simply the dual of the geodesic dilation, and the geodesic dilation/erosion for graylevel images is the natural extension of their binary version using cross-section topology. For these reasons, we think that geodesic dilations and erosion preserve digital well-composedness.

6.2.4 *Conclusion*

Finally, as proven by Theorem 7 and showed by the experimental results we obtained with grain filters, the class of transformations which preserve digital well-composedness is much larger than we could believe: monotone plannings, geodesic dilations/erosions, and grain filters, and certainly shapings [181] in general, preserve digital well-composedness in the sense that they only remove shapes in the hierarchical representation of the image.

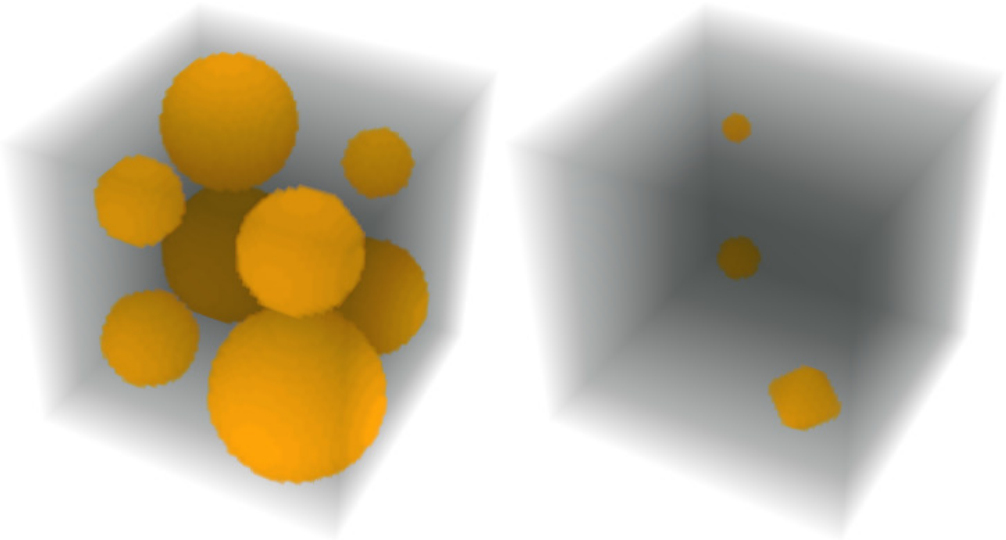

Figure 11.: A 3D digitally well-composed binary image, the mask, and a marker of the same size

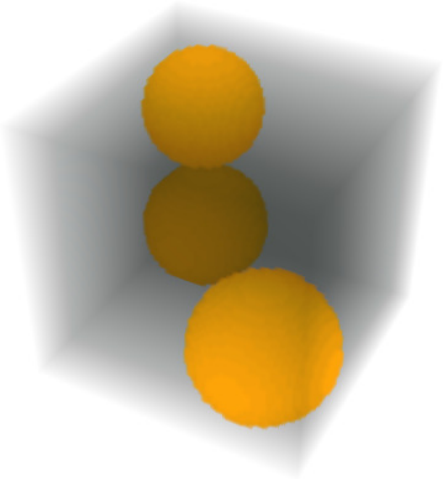

Figure 12.: The geodesic dilation of the marker in the binary image is also digitally well-composed

6.3 GRAPH-BASED CHARACTERIZATIONS OF AWCNESS AND DWCNESS

These approaches are based on *regional minima* and *regional maxima* in graphs, that we define such that:

Definition 42 (Regional extrema)**.** *Let $G = (V, E)$ be a graph valued by a map $u : V \to \mathbb{R}$. We say that a connected component $\mathfrak{P}$ of G is a* plateau *iff there exists $v \in \mathbb{R}$ such that for any element p of $\mathfrak{P}$, the value $u(p)$ is equal to v. We call v the* value *of the plateau. We call a* regional minimum *(respectively a* regional maximum*) a plateau $\mathfrak{P}$ of G (associated to its value) such that for any neighbor q of $\mathfrak{P}$ which does not belong to $\mathfrak{P}$, the value $u(q)$ is strictly lower (respectively strictly greater) than the value of $\mathfrak{P}$. Regional minima and maxima are both said to be* regional extrema*.*

6.3.1 *Graph-based characterization of AWCness*

Note that this section needs some prerequisites presented into Chapters C and E.

We recall that a partially ordered set $|X| = (X, \alpha)$ is said to be a discrete 0-surface if it is made of two points which are not neighbor the one of the other one, and a n-surface, $n \geq 1$,

Figure 13.: A discretized sphere with values on the 2-faces

is defined such as it is connected and for any point z belonging to X, the order $|\theta_X^{\square}(x)|$ is a $(n-1)$-surface. It is therefore easy to check if a set is a n-surface with a recursive program. Hence, it is easy to check whether a digital set is well-composed in the sense of Alexandrov in n-D. However, even if a 0-surface or a 1-surface are easy to interpret, it becomes harder to get the intuition of a 2-surface and higher.

Also, assuming that we are able to check in a short time whether a set in an Alexandrov space is AWC, it seems much longer to check if a real-valued, or even integer-valued, image is AWC, in particular in the dynamic of the image is high or if the quantification has a very high resolution: assuming that the domain $\mathcal{D}$ of the image $u : \mathcal{D} \to \mathbb{R}$, made of n-faces, is finite, whatever if it is cubical or not, we should check if, for any λ belonging to the space of the image, the closures of the threshold sets $[u \geq \lambda]$ and $[u \leq \lambda]$ are AWC. Then it can be much interesting to find a characterization of AWCness, like the one of DWCness on bounded hyperrectangles.

Figure 13 depicts a triangulated sphere whose 2-faces are valued by a real-valued function. The idea is then to find a new method able to check whether this function is AWC without checking the AWCness of the closure of every threshold set.

Let us recall that, for any polyhedral complex $\mathfrak{PC}^n$, the set $\mathfrak{PC}_k^n$ denotes the k-faces of this complex, and that in the polyhedral complexes presented here, the infimum between two faces h^1, h^2, assumed to be well-defined when $\alpha(h^1) \cap \alpha(h^2)$ is non-empty, in this complex is denoted $h^1 \wedge h^2$ and is defined as the supremum of the set $\alpha(h^1) \cap \alpha(h^2)$.

Conjecture 7 (Graph-based Characterization of AWCness)**.** *Let $\mathfrak{PC}^n$ be any polyhedral complex of rank $n \geq 2$ which is a n-surface (bordered or not). Let u be any real-valued map defined on the n-faces of this complex. The real map u is AWC on $\mathfrak{PC}^n$ iff for any $z \in \mathfrak{PC}_k^n$, $k \in [\![0, n-1]\!]$, the valued graph $\mathcal{G}(u, z) = (V, E)$ defined such that the set of vertices is defined such that:*

$$V = \left\{ u(h) \ ; \ h \in \beta^{\square}_{\mathfrak{PC}^n}(z) \cap \mathfrak{PC}_n^n \right\},$$

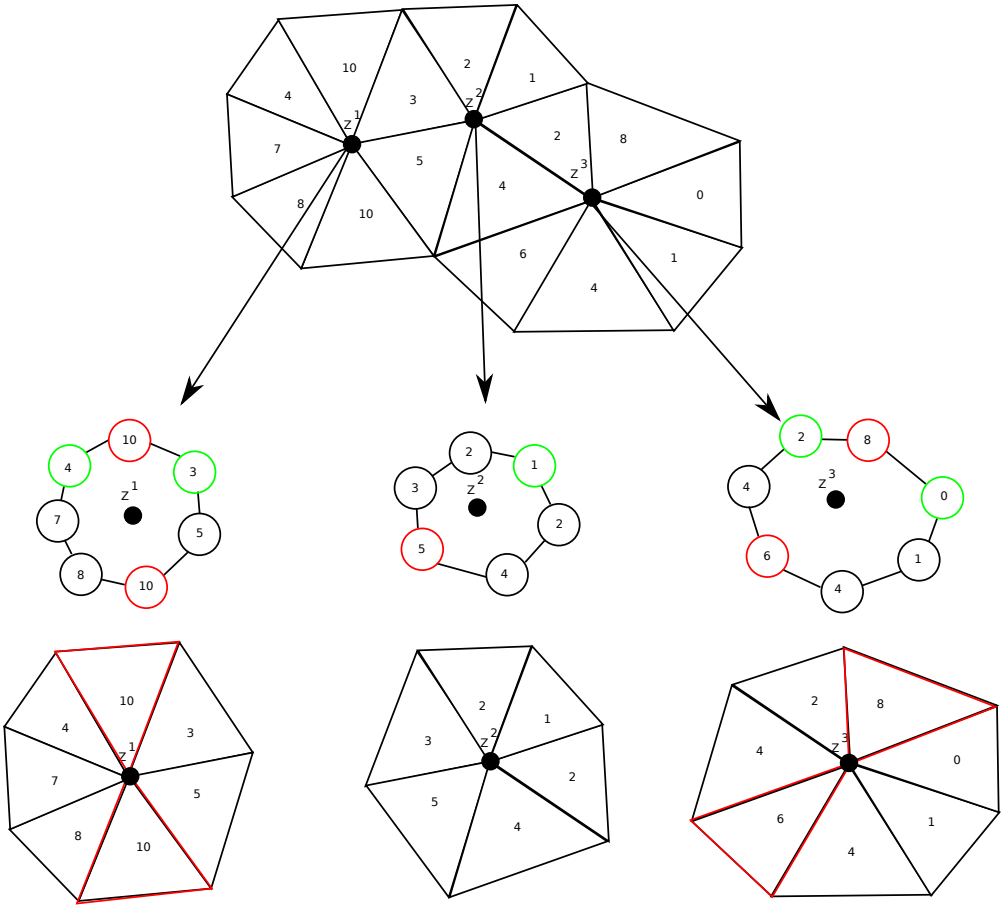

Figure 14.: How to characterize AWCness in 2D

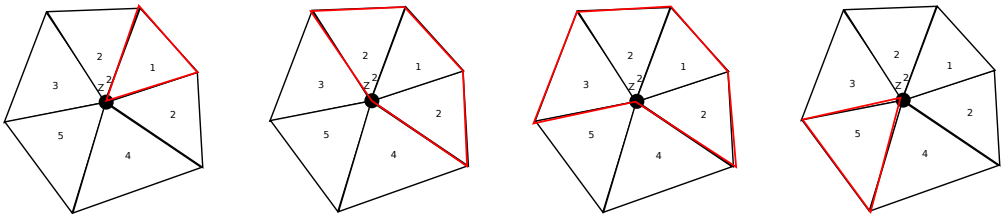

Figure 15.: Boundaries of the different threshold sets around z^2

and such that the set of edges is defined such that:

$$E = \left\{ (h^1, h^2) \in \mathfrak{PC}^n \times \mathfrak{PC}^n \; ; \; h^1 \wedge h^2 \in \mathfrak{PC}^n_{n-1} \right\},$$

admits exactly one regional maximum and one regional minimum.

Figure 14 depicts how we can determine if a 2D image is well-composed in the sense of Alexandrov, and furthermore for which values $\lambda \in \mathbb{R}$ the threshold sets $[u \geq \lambda]$ and $[u \leq \lambda]$ are not well-composed in the sense of Alexandrov: by observing the values of u into the open neighborhood of the 0-face z^1, we can see that the graph $\mathcal{G}(u, z^1)$ contains two maxima, circled in red, and two minima, circled in green. From that, we can respectively deduce that $[u \geq 8]$ and $[u \leq 4]$ are not well-composed in the sense of Alexandrov. Observing the graph $\mathcal{G}(u, z^3)$, we can observe in the same manner that $[u \geq 6]$ and that $[u \leq 2]$ are not well-composed in the sense of Alexandrov.

At the contrary, we can observe that the graph $\mathcal{G}(u, z^2)$ admits one only minimum, which is equal to 1, and one maximum, which is equal to 5. This, way, our conjecture says that this

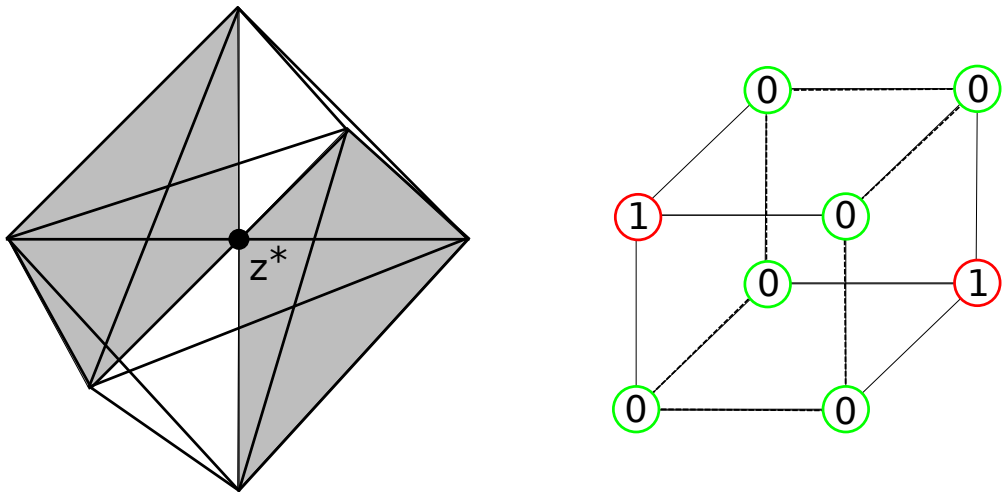

Figure 16.: A 3D image which is not AWC

restriction of u to this subcomplex is well-composed in the sense of Alexandrov, and effectively we can depict that the boundary of each threshold sets is a 1-surface as shown on Figure 15.

As depicted on the octahedron in Figure 16, our method works also in 3D (and more): we have two points in $\mathcal{G}(u,z)$ whose value is one; they are the maxima of $\mathcal{G}(u,z^*)$, and we have only one minimum, the connected component corresponding to the value 0 in $\mathcal{G}(u,z^*)$. This means that u is not AWC. Note that it is crucial to have at the same time one only minimum and only maximum in each graph $\mathcal{G}(u,z)$, since we can have a "pinch" and at the same time one only minimum in $\mathcal{G}(u,z^*)$, where z^* is the point where this pinch occurs.

6.3.2 *Graph-based characterization of DWCness*

Let us show that we can characterize DWC functions defined on bounded hyperrectangles in $\mathbb{Z}^n$ using graphs.

Notations 2 (Graph associated to $u\big|_{\mathbb{A}(z)}$)**.** *Let u be a real-valued function on a bounded hyperrectangle $\mathcal{D} \subset \mathbb{Z}^n$ and let $\mathcal{D}'$ be the smallest hyperrectangle containing $\mathcal{D}$ and subset of $\left(\frac{\mathbb{Z}}{2}\right)^n$. For any element $z \in \mathcal{D}'$, the graph $\mathcal{G}(u,z) = (V,E)$ (corresponding to $u\big|_{\mathbb{A}(z)}$) is defined such that:*

$$V = \{(p, u(p)) \; ; \; p \in \mathbb{A}(z)\},$$

and:

$$E = \{(v^1, v^2) \in V \times V \; ; \; v^1 \in \mathcal{N}_{2n}(v^2)\}.$$

In the sequel, we proceed in two steps: first we show that the digital well-composedness of u is equivalent to the fact that for any threshold $\lambda \in \mathbb{R}$, and for any z belonging to $\mathcal{D}'$, the sets $[u\big|_{\mathbb{A}(z)} \geq \lambda]$, $[u\big|_{\mathbb{A}(z)} \leq \lambda]$, $[u\big|_{\mathbb{A}(z)} > \lambda]$ and $[u\big|_{\mathbb{A}(z)} < \lambda]$ are $2n$-connected, and then we prove that this property is equivalent to have that, for any $z \in \mathcal{D}'$, and for any $\lambda \in \mathbb{R}$, the valued graph $\mathcal{G}(u,z)$ (see Figure 17) admits exactly one maximum and one minimum.

Corollary 2. *Let $u : \mathcal{D} \subset \mathbb{Z}^n \to \mathbb{R}$ be a real-valued image defined on a bounded hyperrectangle $\mathcal{D}$ of $\mathbb{Z}^n$. Then, u is digitally well-composed iff for any value $\lambda \in \mathbb{R}$ and for any block $S \in \mathcal{B}(\mathcal{D}, \mathbb{Z}^n)$, the sets $[u \geq \lambda] \cap S$, $[u \leq \lambda] \cap S$, $[u > \lambda] \cap S$, and $[u < \lambda] \cap S$ are either $2n$-connected or empty sets.*

Proof: This proposition is a direct consequence of Theorem 2. □

For the second step, we need to formulate some definitions and lemmas.

Definition 43. *Let $\mathcal{G} = (V,E)$ be a valued graph whose vertices are valued by a real-valued function u. Now, let us define the set of regional maxima $\{M^i\}_{i \in \mathcal{I}}$ such that their respective values are in*

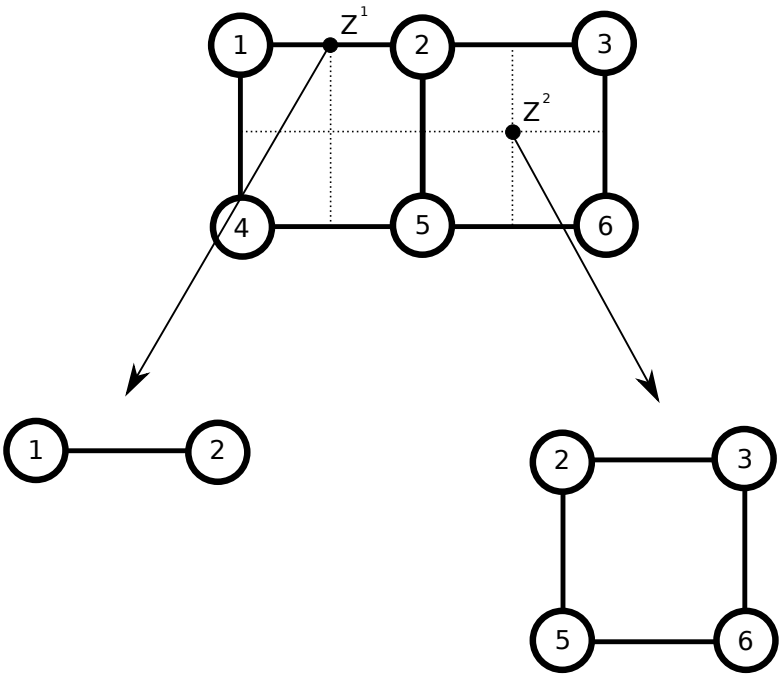

Figure 17.: Some examples of graphs $\mathcal{G}(u, z)$

decreasing order: $\forall i_1, i_2 \in \mathcal{I}, i_1 > i_2 \Rightarrow v_{i_1} \leq v_{i_2}$ *where* v_{i_1} *is the value of* M^{i_1} *and* v_{i_2} *is the one of* M^{i_2}. *Then we say that* M_1 *is the* first regional maximum *of* $\mathcal{G}$. *Also, if* $\text{Card}\,(\mathcal{I}) \geq 2$, *we say that* $\mathcal{G}$ *admits a second maximal region.* M_2 *is then called the* second regional maxima *of* $\mathcal{G}$. *Note that the first and the second regional maxima of a graph can have the same value.*

Definition 44 ($2n$-adjacency)**.** *Let* $A \subset \mathbb{Z}^n$ *be a subset of* $\mathbb{Z}^n$. *We say that* $x \in \mathbb{Z}^n$ *is* $2n$-adjacent *to* A *iff* x *does not belong to* A *and there exists* $q \in A$ *such that* p *and* q *are* $2n$*-neighbors.*

Definition 45 ($2n$-separated)**.** *Let* A, B *be two finite subsets of* $\mathbb{Z}^n$. *We say that* A *and* B *are* $2n$-separated *iff the following relation holds:*

$$(\mathcal{N}_{2n}(A) \cap B) \cup (\mathcal{N}_{2n}(B) \cap A) = \emptyset.$$

Lemma 12. *Let* $\mathcal{G} = (V, E)$ *a graph valued on its vertices* $V \subseteq \mathbb{Z}^n$ *by a real-valued function* $u : V \to \mathbb{R}$, *such that* $\text{Card}\,(V) < \infty$ *and* $\mathcal{G}$ *is connected as a graph. We denote then by* $M^1 \subseteq V$ *the first regional maximum of* $\mathcal{G}$, *by* λ^1 *its value, and by* p^1 *any element of the regional maximum. Then, we obtain:*

$$M^1 = \mathcal{CC}_{2n}([u \geq \lambda^1], p^1).$$

Furthermore, if $\mathcal{G}$ *admits a second regional maximum, we denote respectively by* $M^2 \subset V$,λ^2 *and* p^2 *this regional maximum, its value, and one of its elements, and we define:*

$$M^1_+ = \mathcal{CC}_{2n}([u \geq \lambda^2], p^1).$$

Then we obtain that there exists some $p^2 \in [u \geq \lambda^2] \setminus M^1_+$ *such that:*

$$M^2 = \mathcal{CC}_{2n}([u \geq \lambda^2], p^2),$$

with $\lambda^2 \leq \lambda^1$ *Finally,* M^1_+ *and* M^2 *are* $2n$*-separated.*

Proof: Let $\mathcal{G} = (V, E)$ be a graph and let u be a real-valued function defined on V. Since $\mathcal{G}$ is connected, V is $2n$-connected, and its cardinal is finite. Now let us denote by $(M^i, \lambda^i)_{i \in \mathcal{I}}$ the family of regional maxima of $\mathcal{G}$ sorted by decreasing order of value λ^i.

Let us say that p^1 belongs to the set $\{p \in V \ ; \ u(p) = \max_{v \in V}\{u(v)\}\}$ and let us show that $M^1 = \mathcal{CC}_{2n}([u \geq \lambda^1], p^1)$ is a first regional maximum of u. Firstly, M^1 is connected by

construction. Secondly, the value at each point of M^1 is the same. Thirdly, there does not exist a greater plateau which contains p^1, and this way, any element $q \in V$ which is $2n$-adjacent to M^1 admits a value $u(q)$ which is strictly lower than $u(p^1)$. Then, M^1 is a first regional maximum of $\mathcal{G}$.

Obviously, for $i, j \in \mathcal{I}$ such that $i \neq j$, M^i and M^j are $2n$-separated: if $M^i \cap \mathcal{N}_{2n}(M^j) \neq \emptyset$, there exists $p^i \in M^i$ and $p^j \in M^j$ such that $u(p^i) \geq u(p^j)$ (because p^i belongs to the regional maximum M^i) and such that $u(p^j) \geq u(p^i)$ (because p^j belongs to the regional maximum M^j). This way, $u(p^i) = u(p^j)$ and $M^i = M^j$, which is impossible.

Now let us admit that $\mathcal{G}$ admits at least two regional maxima, it is clear that $\lambda^2 \leq \lambda^1$, due to the sorting of the family $(M^i, \lambda^i)_{i \in \mathcal{I}}$.

Let us now prove that the second regional maximum M^2 can be written $\mathcal{CC}_{2n}([u \geq \lambda^2], p^2)$ for some $p^2 \in [u \geq \lambda^2] \setminus M^1_+$. If p^2 belongs to M^1_+ which is a connected component of $[u \geq \lambda^2]$, then $\mathcal{CC}_{2n}([u \geq \lambda^2], p^2) = M^1_+$, which means that this component contains M^1, which is impossible. Also, let us assume that p^2 belongs to $[u < \lambda^2]$, it is obvious that $\mathcal{CC}_{2n}([u \geq \lambda^2], p^2) = \emptyset$, which is impossible too. Then, p^2 belongs to $[u \geq \lambda^2] \setminus M^1_+$. Let us now show that it is a sufficient condition. Let us assume that p^2 belongs to this set, then $\mathcal{CC}_{2n}([u \geq \lambda^2], p^2)$ is non-empty since $u(p^2) \geq \lambda^2$. Also, this component is a plateau: if there exists a point in this component such that its corresponding value is strictly greater than λ^2, then λ^2 does not correspond to the second regional maxima in V. Also, for any element q of V which is $2n$-adjacent to this component, $u(q) < \lambda$. Then, $M^2 = \mathcal{CC}_{2n}([u \geq \lambda^2], p^2)$. Let us remark that by definition, M^1 and M^2 are $2n$-separated.

Let us show now that M^1_+ and M^2 are effectively $2n$-separated. If the intersection of M^2 and $\mathcal{N}_{2n}(M^1_+, \mathbb{Z}^n)$ is non-empty, there exists $v^2 \in M^2$ and $v^1 \in M^1_+$ such that $v^1 \in \mathcal{N}_{2n}(v^2, \mathbb{Z}^n)$. This way, $\mathcal{CC}_{2n}([u \geq \lambda^2], p^2) = \mathcal{CC}_{2n}([u \geq \lambda^2], v^2)$ contains v^1 (because $u(v^1) \geq \lambda^2$), and then M^2 contains M^1_+, which would imply that M^2 contains M^1, which is impossible since they are disjoint. A same reasoning will show that $\mathcal{N}_{2n}(M^2, \mathbb{Z}^n) \cap M^1_+ \neq \emptyset$ is impossible too, and then M^2 and M^1_+ are $2n$-separated. □

Lemma 13. *Let $\mathcal{G} = (V, E)$ a graph valued on its vertices $V \subseteq \mathbb{Z}^n$ by a real-valued function $u : V \to \mathbb{R}$, such that $\mathrm{Card}\,(V) < \infty$ and G is connected as a graph. We denote then by $m^1 \subseteq V$ the first regional minimum of $\mathcal{G}$, by μ^1 its value, and by p^1 any element of the regional minimum. Then, we obtain:*

$$m^1 = \mathcal{CC}_{2n}([u \leq \mu^1], p^1).$$

Furthermore, if $\mathcal{G}$ admits a second regional minima, we denote respectively by $m^2 \subset V$, μ^2 and p^2 this regional minimum, its value, and one of its elements, and we define:

$$m^1_+ = \mathcal{CC}_{2n}([u \leq \mu^2], p^1).$$

Then we obtain that there exists some $p^2 \in [u \leq \mu^2] \setminus m^1_+$ such that:

$$m^2 = \mathcal{CC}_{2n}([u \leq \mu^2], p^2),$$

with $\mu^2 \geq \mu^1$ Finally, m^1_+ and m^2 are $2n$-separated.

Proof: We can prove this lemma by a reasoning dual to the proof of Lemma 12. □

Notations 3 (Graph associated to $u\big|_S$)**.** *Let u be a real-valued function on a bounded hyperrectangle $\mathcal{D} \subset \mathbb{Z}^n$. For any block $S \in \mathcal{B}(\mathcal{D}, \mathbb{Z}^n)$, the graph $\mathcal{G} = (V, E)$ (corresponding to $u\big|_S$) is defined such that:*

$$V = \{(p, u(p)) \; ; \; p \in S\},$$

and:

$$E = \{(v^1, v^2) \in V \times V \; ; \; v^1 \in \mathcal{N}_{2n}(v^2)\}.$$

Lemma 14. *Let $u : \mathcal{D} \subset \mathbb{Z}^n \to \mathbb{R}$ be a real-valued image defined on a bounded hyperrectangle $\mathcal{D}$, and let be a block $S \in \mathcal{B}(\mathcal{D}, \mathbb{Z}^n)$. If there exists a value $\lambda \in \mathbb{R}$ such that $[u \geq \lambda] \cap S$ is not $2n$-connected, then u admits strictly more than one maximum on the graph corresponding to $u\big|_S$.*

Proof: Let us assume that there exists some λ such that $[u \geq \lambda] \cap S$ is not $2n$-connected. It is sufficient to show that each $2n$-component of $[u \geq \lambda] \cap S$ contains at least one regional maximum of $u\big|_S$. Let $\{M^i_\lambda\}_{i \in \mathcal{I}} = \mathcal{CC}_{2n}([u \geq \lambda] \cap S)$ be the family of connected components of $[u \geq \lambda] \cap S$. Obviously, Card $(\mathcal{I}) \geq 2$. Let i be an index in $\mathcal{I}$, and let λ^i be the value $\max_{p \in S^i}\{u(p)\}$, we can then choose any point p^i in $\{p \in M^i_\lambda \ ; \ u(p) = \lambda^i\}$ and $M^i = \mathcal{CC}_{2n}([u \geq \lambda^i] \cap S, p^i)$. Let us show that M^i is a regional maximum of u in S. Firstly, M^i is $2n$-connected by definition. Secondly, M^i is a plateau (since λ^i is the maximal value of u in this component), and is maximal for the inclusion by construction. Thirdly, any point q of S which is $2n$-adjacent to M^i satisfies $u(q) < \lambda^i$. Each component M^i is then a regional maximum of u into S.

To prove that there exist more than two regional maxima, let us prove for each $i \in \mathcal{I}$, the component M^i is contained into M^i_λ. Effectively, λ^i is greater than or equal to λ by construction, and then $[u \geq \lambda^i] \subseteq [u \geq \lambda]$, which implies that $[u \geq \lambda^i] \cap S \subseteq [u \geq \lambda] \cap S$. Since $u(p^i) = \lambda^i \geq \lambda$ and $p^i \in S$, p^i belongs to $[u \geq \lambda] \cap S$ and then:

$$\mathcal{CC}_{2n}([u \geq \lambda^i] \cap S, p^i) \subseteq \mathcal{CC}_{2n}([u \geq \lambda] \cap S, p^i),$$

which means that M^i is included into M^i_λ. Based on this observation, we obtain that M^1 and M^2 are two separated regional maxima since:

$$\begin{cases} \mathcal{N}_{2n}(M^1) \cap M^2 \subseteq \mathcal{N}_{2n}(M^1_\lambda) \cap M^2_\lambda = \emptyset, \\ \mathcal{N}_{2n}(M^2) \cap M^1 \subseteq \mathcal{N}_{2n}(M^2_\lambda) \cap M^1_\lambda = \emptyset. \end{cases}$$

□

Lemma 15. *Let $u : \mathcal{D} \subset \mathbb{Z}^n \to \mathbb{R}$ be a real-valued image defined on a bounded hyperrectangle $\mathcal{D}$, and let be a block $S \in \mathcal{B}(\mathcal{D}, \mathbb{Z}^n)$. If there exists a value $\lambda \in \mathbb{R}$ such that $[u \leq \lambda] \cap S$ is not $2n$-connected, then u admits strictly more than one minimum on the graph corresponding to $u\big|_S$.*

Proof: This proof is dual to the one of Lemma 14.

Proposition 23. *Let $u : \mathcal{D} \subset \mathbb{Z}^n \to \mathbb{R}$ be a real-valued image defined on a bounded hyperrectangle $\mathcal{D}$ of $\mathbb{Z}^n$. Then, for any $z \in \mathcal{D}'$, the graph $\mathcal{G}(u, z)$ admits exactly one regional maximum and one regional minimum iff for any value $\lambda \in \mathbb{R}$ and for any block $S \in \mathcal{B}(\mathcal{D}, \mathbb{Z}^n)$, the sets $[u \geq \lambda] \cap S$, $[u \leq \lambda] \cap S$, $[u > \lambda] \cap S$ and $[u > \lambda] \cap S$ are $2n$-connected sets.*

Proof: Let us assume that for any value $\lambda \in \mathbb{R}$ and for any block $S \in \mathcal{B}(\mathcal{D})$, the sets $[u \geq \lambda] \cap S$, $[u \leq \lambda] \cap S$, $[u > \lambda] \cap S$ and $[u > \lambda] \cap S$ are $2n$-connected sets, and let us show that for any $z \in \mathcal{D}'$, the graph $\mathcal{G}(u, z)$ corresponding to $u\big|_{\mathbb{A}(z)}$ admits exactly one regional maximum and one regional minimum. For that, let us assume that $\mathcal{G}(u, z)$ admits two regional maxima on the block $S = \mathbb{A}(z)$ of $\mathbb{Z}^n$. Since S is $2n$-connected and finite (because n is finite), and since $u\big|_{\mathbb{A}(z)}$ is a real-valued function, we can apply Lemma 12. This way, we obtain that (M^1, λ^1) is the first regional maximum of $\mathcal{G}(u, z)$ such that $M^1 = \mathcal{CC}_{2n}([u \geq \lambda^1] \cap S, p^1)$ with p^1 an element of V such that $u(p^1) = \lambda^1 = \max_{v \in S}\{u(v)\}$, and (M^2, λ^2) is the second regional maximum of $\mathcal{G}(u, z)$ such that $M^2 = \mathcal{CC}_{2n}([u \geq \lambda^2] \cap S, p^2)$ with p^2 an element of $[u \geq \lambda^2] \setminus M^1_+$, where $M^1_+ = \mathcal{CC}_{2n}([u \geq \lambda^2] \cap S, p^1)$. Furthermore, M^1_+ and M^2 are separated. This means that M^1_+ and M^2 are two disjoint connected components of $[u \geq \lambda^2] \cap S$, which is connected by hypothesis. We obtain a contradiction, and then $u\big|_{\mathbb{A}(z)}$ admits one unique maximum. The same reasoning applies for the minima of $u\big|_{\mathbb{A}(z)}$ by Lemma 13.

Conversely, we assume that for any $z \in \mathcal{D}'$ with $\mathcal{D}'$ the smallest hyperrectangle containing $\mathcal{D}$ in $(\mathbb{Z}/2)^n$, we have that the graph $\mathcal{G}(u, z)$ corresponding to $u\big|_{\mathbb{A}(z)}$ admits one maximum and one minimum. Let us now assume that there exists some $\lambda \in \mathbb{R}$ such that $[u \geq \lambda] \cap \mathbb{A}(z)$ is not $2n$-connected (or equivalently such that $[u > \lambda] \cap \mathbb{A}(z)$ is not $2n$-connected since we work with a finite number of values). Then, by Lemma 14, the restriction of u to $\mathbb{A}(z)$ contains at least two maxima, and then $\mathcal{G}(u, z)$ has at least two maxima too. A dual reasoning using Lemma 15

will show that if $[u \leq \lambda] \cap \mathbb{A}(z)$ is not $2n$-connected (or equivalently if $[u < \lambda] \cap \mathbb{A}(z)$ is not $2n$-connected), the restriction of u to S contains at least two minima, and then $\mathcal{G}(u, z)$ has at least two minima. This proves that for any $\lambda \in \mathbb{R}$, the sets $[u \geq \lambda] \cap \mathbb{A}(z)$, $[u \leq \lambda] \cap \mathbb{A}(z)$, $[u > \lambda] \cap \mathbb{A}(z)$ and $[u < \lambda] \cap V$ are $2n$-connected. □

Theorem 8 (Graph-based characterization of DWCness)**.** *Let $u : \mathcal{D} \subset \mathbb{Z}^n \to \mathbb{R}$ be a real-valued image defined on a bounded hyperrectangle $\mathcal{D}$ of $\mathbb{Z}^n$. Now, let $\mathcal{D}'$ be the smallest hyperrectangle in $(\mathbb{Z}/2)^n$ such that it contains $\mathcal{D}$. Then, u is DWC on $\mathcal{D}$ iff for any element $z \in \mathcal{D}'$, the graph $\mathcal{G}(u, z) = (V, E)$ admits only one regional maximum and only one regional minimum.*

Proof: This is the result of Corollary 2 and Proposition 23. □

6.4 n-D SEGMENTATION AND PARAMETERIZATION

Combining the conjecture that DWCness and CWCness are equivalent on cubical grids in n-D, and the conjecture that geodesic dilation preserves DWCness in n-D, we can segment gray-level images such that the final segmentation result is CWC. This result permits then to (locally) parameterize the topological boundary of the object (thanks to *coordinate charts* [106]), this one being a topological $(n-1)$-manifold.

On Figure 18, we propose to segment the ventricles of the CSF (Cerebro-Spinal Fluid) in a partial MRI (Magnetic Resonance Imaging) of a human brain (see [62, 115, 37, 38] for more details on brain segmentation using mathematical morphology and digital topology).

Firstly, we binarize the original image u with a threshold $\lambda = 0.2$ (where 0 and 1 are the minimal and maximal luminances of the brain image respectively) and we obtain the set $[u \geq \lambda]$. Then, we proceed to a geodesic dilation of this set using a marker made of a full ellipse of radius $(10, 10, 5)$ at the center of the image (where the CSF is located). We compute then the boundaries of the continuous analog of the geodesic dilation of this marker into $[u \geq \lambda]$. Since this image is not digitally well-composed, we obtain a boundary with a lot of "pinches" which can cause topological issues.

Secondly, we repeat the same process but with the self-dual well-composed interpolation u_{DWC} (proposed in this thesis) instead of u: starting from u_{DWC}, we compute $[u_{\mathrm{DWC}} \geq \lambda]$ which is digitally well-composed since the threshold sets of a well-composed image are well-composed. Then we proceed to a geodesic dilation of the (rescaled) marker into $[u_{\mathrm{DWC}} \geq \lambda]$, resulting then into a digitally well-composed image since geodesic dilations in a digitally well-composed mask results in a digitally well-composed image. Since DWCness and CWCness are equivalent on cubical grids in 3D, the boundary of the resulting segmentation is a 2-manifold.

(a) u.

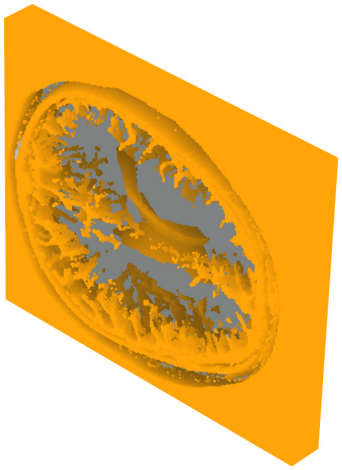

(b) $[u \geq \lambda]$

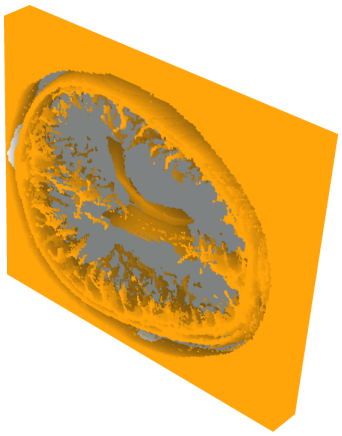

(c) $[u_{\mathrm{DWC}} \geq \lambda]$

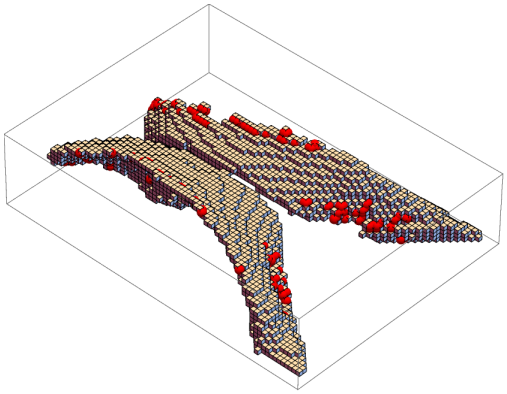

(d) $\partial\delta_{\mathrm{Geod}}[u \geq \lambda]$

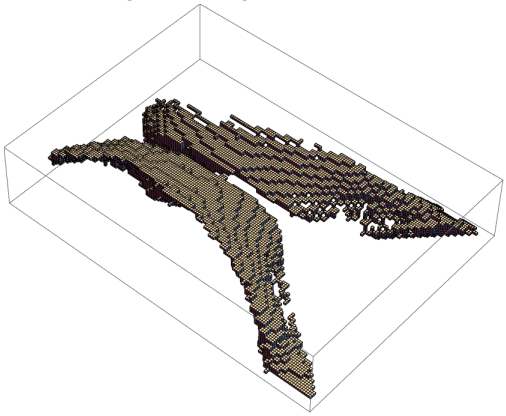

(e) $\partial\delta_{\mathrm{Geod}}[u_{\mathrm{DWC}} \geq \lambda]$

Figure 18.: Boundaries of DWC objects are manifolds in 3D: on the left, the boundary of the continuous analog of an object which is not DWC; the pinches in its boundary are depicted using little red spheres. On the right, the boundary of a DWC interpolation of this same object; this boundary does not own any pinches.

7 CONCLUSION

Our main contributions are the following: after a differentiation of the various kinds of well-composednesses and their extension to n-D gray-level images, we proved that DWCness implies EWCness in n-D, and we conjectured that DWCness is equivalent to AWCness and to CWCness in n-D on cubical grids. Since we are interested about how to make images DWC, we proved that no self-dual local method making images DWC exists in n-D $n \geq 3$, and then we proposed a non-local self-dual methods (based on front-propagation) which makes images DWC in n-D. We also proposed a way to make images defined on a polyhedral complex AWC. Because it is of much interest to be able to test if an image is well-composed or not, we proposed a characterization of n-D DWC images (on cubical grids) based on interval values and spans, and a characterization of AWC images defined on the n-faces of polyhedral complexes based on graphs.

To conclude this thesis, we will end with an open question: we have seen that DWCness, AWCness, and CWCness seem to be equivalent on cubical grids, but how CWCness and AWCness are related in polyhedral complexes? The counter-example of Daragon [42], stated that the chain complex of the order join of a 0-surface and a torus (see Figure 2) is a 3-surface, but not a *combinatorial manifold*[1]. It proves effectively that discrete surfaces are not always (combinatorial) manifolds, but is it enough to ensure that CWCness is stronger than AWCness?

1 We recall that a *combinatorial n-manifold* is a (geometric) simplicial complex C of dimension n and such that for each vertex $\{x\} \in C$, the *link* of $\{x\}$ in C is a *combinatorial* $(n-1)$*-sphere*(see p. 67 of [42] for more details).

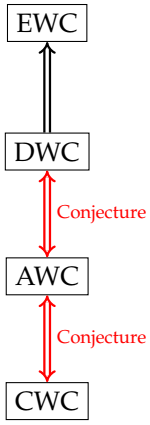

Figure 1.: Links betweens the different flavors of well-composedness on cubical grids

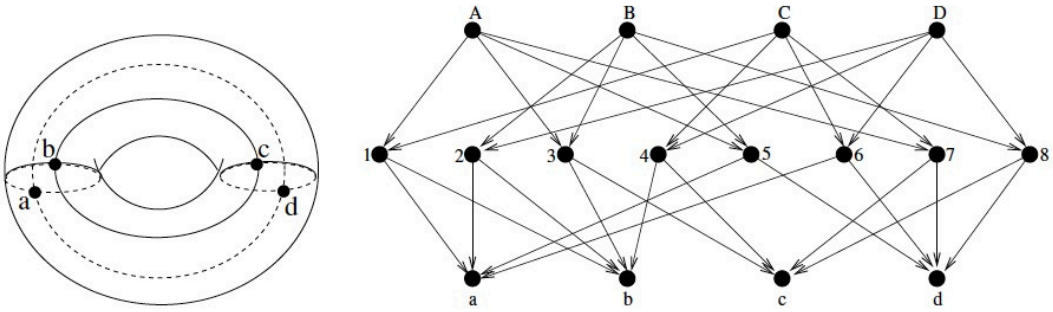

Figure 2.: A (subdivided) torus and its incidence graph [42] (p. 50)

Appendices

A

PROOF THAT $\mathcal{I}_{\min}(u)$ AND $\mathcal{I}_{\max}(u)$ ARE DIGITALLY WELL-COMPOSED

We prove here that Proposition 17 is true, that is, for any real-valued image $u : \mathcal{D} \subset \mathbb{Z}^n \to \mathbb{R}$ defined on a bounded hyperrectangle $\mathcal{D}$ in $\mathbb{Z}^n$, the n-D real-valued images $\mathcal{I}_{\min}(u)$ and $\mathcal{I}_{\max}(u)$ are digitally well-composed (their respective duality is obvious).

But before let us present a simple lemma relative to cubical subdivisions:

Lemma 16. *Let $z \in \left(\frac{\mathbb{Z}}{2}\right)^n \setminus \mathbb{Z}^n$ be a point. Then $\mathbb{A}(\mathbb{P}(z)) = \mathbb{A}(z)$.*

Proof: Let z be a point in $\left(\frac{\mathbb{Z}}{2}\right)^n \setminus \mathbb{Z}^n$, then:

$$\begin{aligned}
\mathbb{A}(\mathbb{P}(z)) &= \bigcup_{p \in \mathbb{P}(z)} \mathbb{A}(p), \\
&= \bigcup_{p \in \mathbb{P}(z)} \mathbb{P}^{\mathfrak{o}(p)}(p), \\
&= \bigcup_{p \in \mathbb{P}(z)} \mathbb{P}^{\mathfrak{o}(z)-1}(p), \\
&= \mathbb{P}^{\mathfrak{o}(z)-1}(\mathbb{P}(z)), \\
&= \mathbb{A}(z).
\end{aligned}$$

□

Then, the interpolation $\mathcal{I}_{\mathrm{op}}(u)$ of Definition 37 can be reformulated as well:

Proposition 24. *Let $u : \mathcal{D} \to \mathbb{R}$ be an image defined on a bounded hyperrectangle $\mathcal{D} \subset \mathbb{Z}^n$. Then the interpolation $u' \equiv \mathcal{I}_{\mathrm{op}}(u) : \mathcal{D}' = \mathrm{Subd}(\mathcal{D}) \to \mathbb{R}$ can be reformulated such that:*

$$\forall z \in \mathcal{D}', \left(\mathcal{I}_{\mathrm{op}}(u)\right)(z) = \begin{cases} \mathrm{op}\{u(z)\} & \text{if } z \in \mathcal{D}, \\ \mathrm{op}\{u(p) \,;\, p \in \mathbb{A}(z)\} & \text{otherwise.} \end{cases}$$

Proof: Let us remark that $\bigcup_{k \in [\![0,n]\!]} \mathbb{E}_k \cap \mathcal{D}' = \mathcal{D}'$, and then we can verify the property for each $z \in \mathbb{E}_k \cap \mathcal{D}'$ with $k \in [\![0, n]\!]$.

The case $z \in \mathbb{E}_0 \cap \mathcal{D}' = \mathcal{D}$ is obvious. For the other points of $\mathcal{D}'$, let us proceed by induction.

Initialization ($k = 1$): let z be a point in $\mathbb{E}_1 \cap \mathcal{D}'$. Then,

$$\begin{aligned}
\mathrm{op}\{u'(p) \,;\, p \in \mathbb{P}(z)\} &= \mathrm{op}\{u(p) \,;\, p \in \mathbb{P}(z)\} \\
&= \mathrm{op}\{u(p) \,;\, p \in \mathbb{A}(z)\}
\end{aligned}$$

Heredity ($k \in [\![2, n]\!]$): we assume that for any $p \in \mathbb{E}_{k'} \cap \mathcal{D}'$, $k' \in [\![1, k-1]\!]$, we have the relation $\mathrm{op}\{u'(q)\ ;\ q \in \mathbb{P}(p)\} = \mathrm{op}\{u(a)\ ;\ a \in \mathbb{A}(p)\}$. Let us prove that this relation is still true for $z \in \mathbb{E}_k \cap \mathcal{D}'$:

$$\begin{aligned}
&\mathrm{op}\{u'(p)\ ;\ p \in \mathbb{P}(z)\}\\
&= \mathrm{op}\{\mathrm{op}\{u'(q)\ ;\ q \in \mathbb{P}(p)\}\ ;\ p \in \mathbb{P}(z)\},\\
&= \mathrm{op}\{\mathrm{op}\{u(a)\ ;\ a \in \mathbb{A}(p)\}\ ;\ p \in \mathbb{P}(z)\},\\
&= \mathrm{op}\{u(a)\ ;\ a \in \mathbb{A}(p)\ ,\ p \in \mathbb{P}(z)\},\\
&= \mathrm{op}\{u(a)\ ;\ a \in \mathbb{A}(\mathbb{P}(z))\},\\
&= \mathrm{op}\{u(a)\ ;\ a \in \mathbb{A}(z)\},
\end{aligned}$$

thanks to Lemma 16. □

This leads to the following proposition:

Proposition 25. *Let $u : \mathcal{D} \to \mathbb{R}$ be an image defined on a bounded hyperrectangle $\mathcal{D} \subset \mathbb{Z}^n$. Then the interpolation $\mathcal{I}_{\min}(u) : \mathcal{D}' = \mathrm{Subd}(\mathcal{D}) \to \mathbb{R}$ (respectively $\mathcal{I}_{\max}(u) : \mathcal{D}' = \mathrm{Subd}(\mathcal{D}) \to \mathbb{R}$) are digitally well-composed.*

Proof: We will treat only the case of $\mathcal{I}_{\max}$, since $\mathcal{I}_{\min}$ and $\mathcal{I}_{\max}$ are dual. Let $S \in \mathcal{B}(\mathcal{D}', \left(\frac{\mathbb{Z}}{2}\right)^n)$ be a block of dimension greater than or equal to 2 in the domain of the interpolation $\mathcal{I}_{\max}$. Then there exists a point $z \in \mathcal{D}'$ and a family of vectors $\mathcal{F} = \{f^1, \ldots, f^k\} = \{e^{j_1}, \ldots, e^{j^k}\}$ such that $S = S_2(z, \mathcal{F})$.

Let group together the indices of the vectors of $\mathbb{B}$ that are in $\mathcal{F}$ by denoting $\mathcal{J} = \{j_1, \ldots, j_k\}$. Let $\pi = (q^0, \ldots, q^k)$ be such that:

$$q^0 = z + \sum_{j \in \mathcal{J} \cap \frac{1}{2}(z)} \frac{e^j}{2},$$

and:

$$\forall l \in [\![0, k-1]\!], q^{l+1} = \begin{cases} q^l - \frac{e^{j_{l+1}}}{2} & \text{if } j_{l+1} \in \frac{1}{2}(z),\\ q^l + \frac{e^{j_{l+1}}}{2} & \text{otherwise .} \end{cases}$$

Obviously, q^0 is by definition the point of minimal order into S. Also we can compute that:

$$q^k = q^0 - \sum_{j \in \mathcal{J} \cap \frac{1}{2}(z)} \frac{e^j}{2} + \sum_{j \in \mathcal{J} \setminus \frac{1}{2}(z)} \frac{e^j}{2} = z + \sum_{j \in \mathcal{J} \setminus \frac{1}{2}(z)} \frac{e^j}{2},$$

which shows that q^k is the point of maximal order in S. We can then observe that q^0 and q^k are antagonist in S.

Also, we can remark that $\forall r \in S$, $q^0 \in \mathbb{P}^{\delta_1}(r)$ and $r \in \mathbb{P}^{\delta_2}(q^k)$ for some $\delta_1, \delta_2 \in [\![0, k]\!]$, $\mathcal{I}_{\max}(q^0) \leq \mathcal{I}_{\max}(r) \leq \mathcal{I}_{\max}(q^k)$, which means that $\mathcal{I}_{\max}(q^0)$ and $\mathcal{I}_{\max}(q^k)$ are respectively the minimal and the maximal values of $\mathcal{I}_{\max}\big|_S$.

Hence, for any $p, p' \in S$ such that they are antagonist in S, we need to prove that:

$$\mathrm{intvl}(\mathcal{I}_{\max}(p), \mathcal{I}_{\max}(p')) \cap \mathrm{Span}\{\, \mathcal{I}_{\max}(p'') \,|\, p'' \in S \setminus \{p, p'\}\,\}$$

is not an empty set. In fact, two cases are possible: either $p \in \{q^0, q^k\}$, and in this case $\{p, p'\} = \{q^0, q^k\}$, and then:

$$\begin{aligned}
\mathrm{intvl}(\mathcal{I}_{\max}(p), \mathcal{I}_{\max}(p')) &= [\mathcal{I}_{\max}(q^0), \mathcal{I}_{\max}(q^k)],\\
&\supseteq \mathrm{Span}\{\, \mathcal{I}_{\max}(p'') \mid p'' \in S \setminus \{p, p'\}\,\},
\end{aligned}$$

and the intersection equals $\mathrm{Span}\{\, \mathcal{I}_{\max}(p'') \mid p'' \in S \setminus \{p,\, p'\}\,\}$, which is not empty since $\dim(S) \geq 2$. Or $p \notin \{q^0, q^k\}$, and then q^0 and q^k belong to $S \setminus \{p,\, p'\}$, which means that we have the converse case:

$$\begin{aligned} \mathrm{Span}\{\, \mathcal{I}_{\max}(p'') \mid p'' \in S \setminus \{p,\, p'\}\,\} &= [\mathcal{I}_{\max}(q^0), \mathcal{I}_{\max}(q^k)], \\ &\supseteq \mathrm{intvl}(\mathcal{I}_{\max}(p),\, \mathcal{I}_{\max}(p')), \end{aligned}$$

and then the intersection equals:

$$\mathrm{intvl}(\mathcal{I}_{\max}(p),\, \mathcal{I}_{\max}(p')),$$

which is not empty. □

B

TOPOLOGICAL REPARATION IN n-D

Two approaches exist to make binary images well-composed. The first is to keep the original space of the image and to change some of the values of the initial image in such a way that the modified image becomes well-composed [158]. The second is to make an interpolation to preserve the topology of the original image [100, 165, 60]. However, this second approach needs a subdivision of the original space and measurably increases the computational costs of the algorithms.

In this section, we propose a fast method that we published in [27] and that produces a digitally well-composed image in n-D, $n \geq 2$, by modifying the original values (see an application in Figure 1). We will also illustrate this algorithm with a 2D application to text detection.

B.1 PRINCIPLE OF THE ALGORITHM

Let $u : \mathcal{D} \subseteq \mathbb{Z}^n \to \mathbb{Z}$ be a given image. We want to find a digitally well-composed image $u^* : \mathcal{D} \subseteq \mathbb{Z}^n \to \mathbb{Z}$ which minimizes the L^1-distance between u and u^*:

$$u^* = \arg\min_v \{\, ||v - u||_1 \mid v \text{ is DWC} \,\} \tag{1}$$

However, to the best of our knowledge, such a combinatorial problem does not have a solution reachable in a reasonable time. To find an approximate solution to this problem, we propose to iteratively select critical configurations and correct them, one by one. To prevent oscillation, we impose that, at each step of the algorithm, the current solution is greater than the previous one. Our process is thus *increasing*.

As we modify a critical configuration, our algorithm is local, in the sense that we only need to look at a block and modify the pixel in the block. However, the modification of the value of a given pixel can create a novel critical configuration in its neighborhood. Hence, there is potentialy a propagation effect, and thus several passes on the image are in principle necessary to achieve convergence.

Due to this propagation effect, the convergence of the algorithm is only ensured if the process is monotone. Indeed, if we allow any modification on the image at each step of the algorithm, then oscillation effects could appear.

B.2 CORRECTION STEP

We want to correct a given critical configuration in the block $S \in \mathcal{B}(\mathcal{D})$. By definition of a critical configuration, there exists two points $p \in S, p' \in S$ with $p' = \text{antag}_S(p)$, verifying:

$$\text{intvl}(u(p), u(p')) \cap \text{Span}\{\, u(q) \mid q \in S \setminus \{p, p'\} \,\} = \emptyset.$$

Then two cases are possible. Either we have:

$$\max(u(p), u(p')) < \min\{\, u(q) \mid q \in S \setminus \{p, p'\} \,\},$$

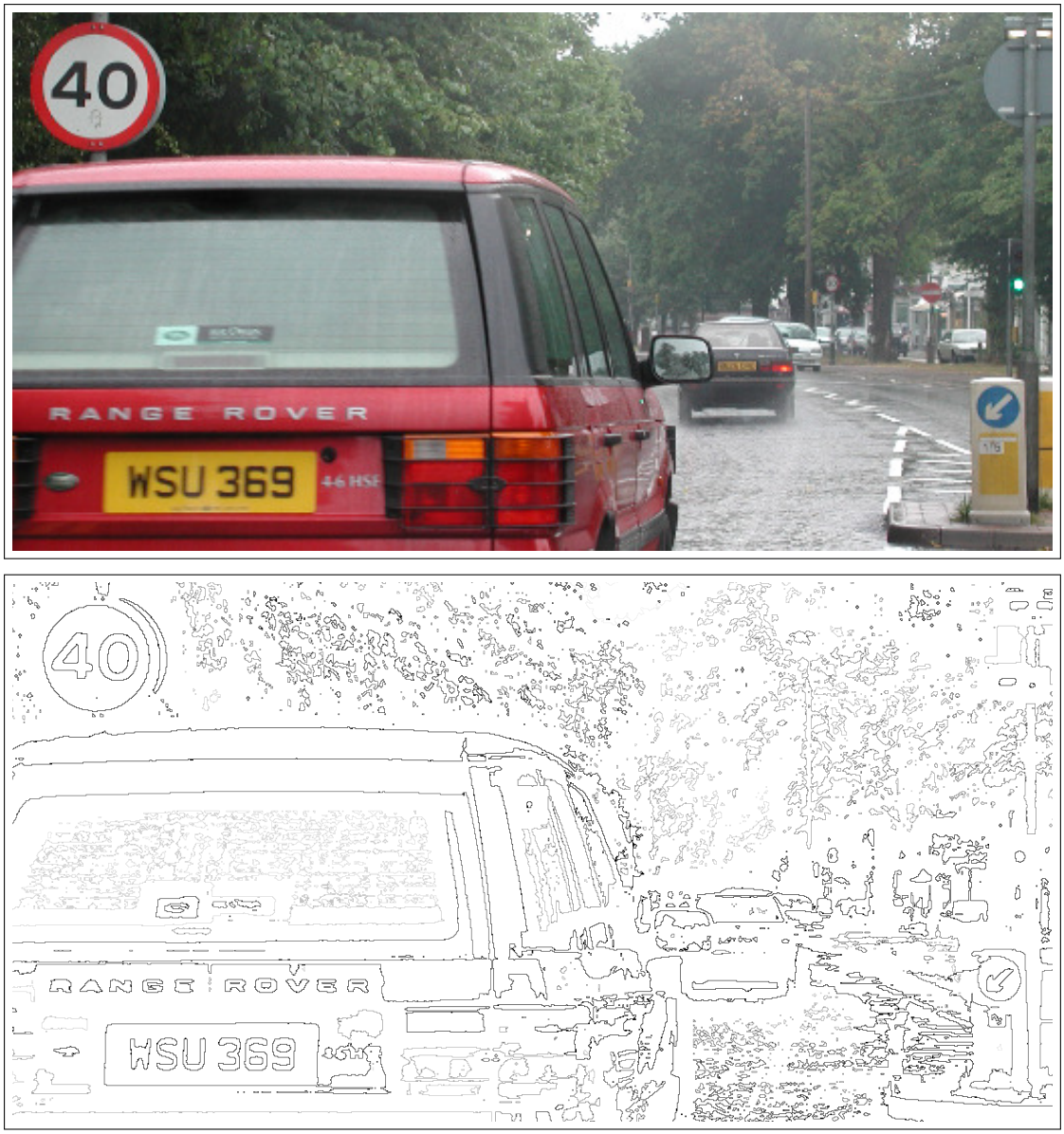

Figure 1.: Hierarchical representation of an image: since component boundaries are simple closed curves on well-composed images, two boundaries are either disjoint or in an inclusion relationship; thus, the delimited regions naturally form a tree. Actually it is a sub-part of the tree of shapes [61].

and we set:

$$\begin{cases} p^* \leftarrow \arg\max_q \{\, u(q) \;\middle|\; q \in \{p, p'\}\,\}, \\ u(p^*) \leftarrow \min\{\, u(q) \;\middle|\; q \in S \setminus \{p, p'\}\,\}, \end{cases}$$

or we have:

$$\max\{\, u(q) \;\middle|\; q \in S \setminus \{p, p'\}\,\} \;<\; \min(u(p), u(p')),$$

then we set:

$$\begin{cases} p^* \leftarrow \arg\max_q \{\, u(q) \;\middle|\; q \in S \setminus \{p, p'\}\,\} \\ u(p^*) \leftarrow \min(u(p), u(p')). \end{cases}$$

In both cases, u has been made digitally well-composed on S.

Algorithm 4: The correction process.

```
SolveCC (u, S) : p
begin
    p' ← antag_S(p)
    m_1 ← min(u(p), u(p'))
    M_1 ← max(u(p), u(p'))
    m_2 ← min{ u(p'') | p'' ∈ S \ {p, p'} }
    M_2 ← max{ u(p'') | p'' ∈ S \ {p, p'} }
     /* Primary case: */
    if M_1 < m_2 then
        p* ← arg max{ u(q) | q ∈ {p, p'} }
        u(p*) ← m_2
     /* Secondary case: */
    if M_2 < m_1 then
        p* ← arg max{ u(p'') | p'' ∈ S \ {p, p'} }
        u(p*) ← m_1
    return p*
```

B.3 CONVERGENCE

The convergence of the method is easy to prove. Indeed, let us define $u_{min} = \min\{ u(p) \,|\, u(p) \in \mathcal{D} \}$ and $u_{max} = \max\{ u(p) \,|\, p \in \mathcal{D} \}$. As the algorithm increases the function u by at least 1 (since we work in $\mathbb{Z}$), we have a maximum of $(u_{max} - u(p))$ corrections for each $p \in \mathcal{D}$. The total number of corrections is then lower than or equal to $\sum_{p \in \mathcal{D}} (u_{max} - u(p)) \leq (u_{max} - u_{min}) \times \mathrm{Card}(\mathcal{D})$. This ensures the convergence of the algorithm, since $\mathrm{Card}(\mathcal{D})$ is finite.

Algorithm 5: The increasing n-D algorithm.

```
Increasing (u) : Image
/* Makes the image DWC */
begin
    /* Initialization of the queue */
    for all S ∈ B(D) do
        if CriticalConfiguration(S, u) then
            push(Q, S)
    while Q ≠ ∅ do
        S ← pop(Q)
         /* Correction process: */
        p ← SolveCC(u, S)
         /* Detection of the direction of the propagation */
        for all S' ∈ B(D) s.t. p ∈ S' do
            if CriticalConfiguration(S', u) then
                push(Q, S')
```

B.4 PROPOSED ALGORITHM

Given the correction step, the algorithm is straightforward; it is detailed in Algorithm 5. It proceeds in two steps. First, the *initialization step* detects all the critical configurations of the threshold sets $\{[u \geq \lambda]\}_\lambda$ on $\mathcal{D}$ and enqueues them into Q. Second, the *correction step* solves one by one the critical configurations listed into Q using Algorithm 4, and enqueues the new critical configurations which appeared in the neighborhood of the modified value.

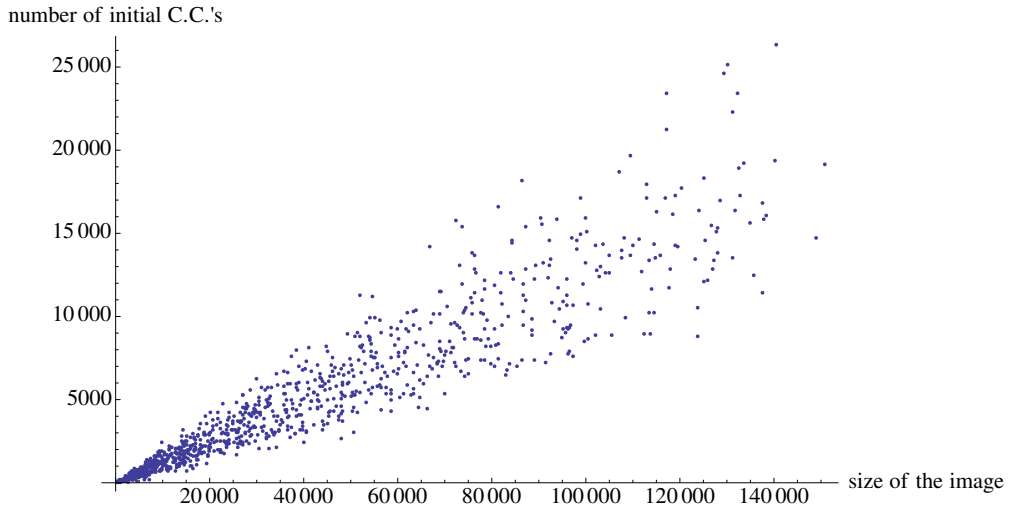

Figure 2.: Number of critical configurations as a function of the size of the image given in number of pixels

This algorithm iterates until there are no longer any critical configurations in $\mathcal{D}$; the resulting image u is then digitally well-composed.

B.5 EXPERIMENTAL RESULTS AND COMPLEXITY OF THE 2D CASE

We used the test set of 100 natural images of the Berkeley image database [117]. Their sizes are $(\mathrm{sx}, \mathrm{sy})$ with $\mathrm{sx} = 481$ and $\mathrm{sy} = 321$ pixels or the converse. We cropped each image with ten different windows (for each image) to obtain images of various sizes. The size $(\mathrm{newsx}, \mathrm{newsy})$ of the window is randomly chosen into $[\![2, \mathrm{sx}]\!] \times [\![2, \mathrm{sy}]\!]$ and its position is randomly chosen into $[\![1, \mathrm{sx} - \mathrm{newsx} + 1]\!] \times [\![1, \mathrm{sy} - \mathrm{newsy} + 1]\!]$.

We experimentally assessed the percentage of critical configurations contained in a given image. Figure 2 shows that up to 24.77% of the domain of the original images is covered by critical configurations. From a statistical point of view, an image contains on average 0.1237 (± 0.0361) critical configuration by pixel. It is rare to have a digitally well-composed image.

Queue initialization. To initialize the queue of critical configurations, we simply have to detect among the $(\mathrm{newsx} - 1) \times (\mathrm{newsy} - 1)$ blocks which one contains a critical configuration, and in this case we insert it in the queue Q. Each detection and each insertion in the queue is in constant time. This implies that the initialization step is in linear time relatively to the size of the image.

Correction process. Concerning the correction step, we had to proceed to c corrections by pixel, with $\mathrm{c} \leq 0.2376$. From a statistical point of view, an average number of 0.1195 (± 0.0346) corrections by pixel has been observed. Numerical experiments show that the correction step is linear on average with respect to the image size.

The number of corrections by initial critical configuration is not a constant: it can be seen on Figure 3 that the number of corrections is between $m = 86.93\%$ and $M = 108.33\%$ of the number of initial critical configurations. Indeed, a given correction can repair several critical configurations at the same time, which explains that m is lower than 100%. Conversely, the propagation effect is responsible for M being greater than 100%. Statistically, we obtain a mean ratio of 0.9659 (± 0.0338) corrections by initial critical configuration.

Detection of the direction of the propagation. For each processed correction, there exists only one position $p \in \mathcal{D}$ such as $u(p)$ is modified in the image, and then the propagation is possible in a bounded number of blocks, *i.e.*, in the blocks containing p. This means that the number of

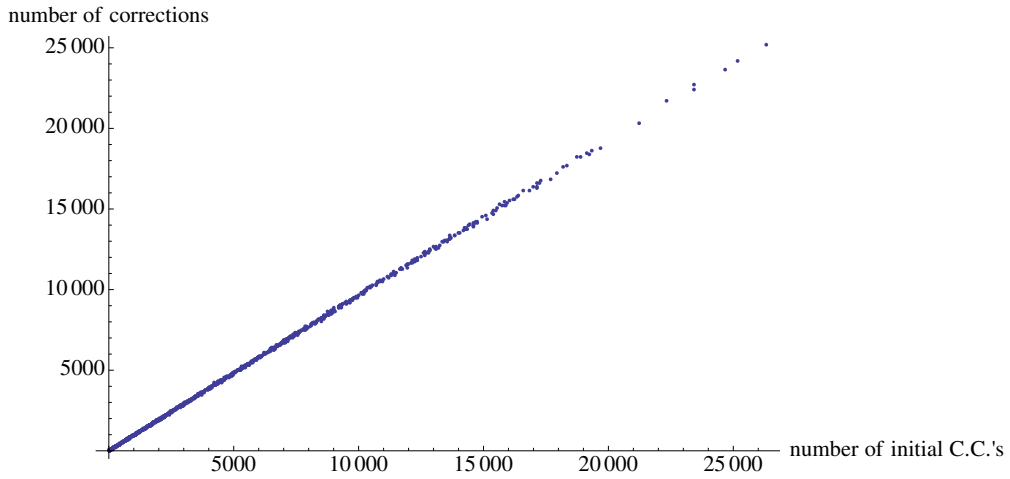

Figure 3.: Number of corrections as a function of the number of initial critical configurations

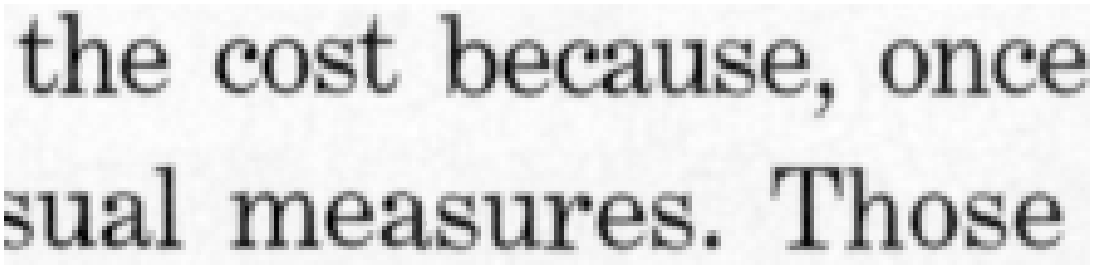

Figure 4.: Original image u

Figure 5.: Zero-crossings of the original Laplacian

blocks processed in the detection step is proportional to the total number of corrections. Since the correction step is in linear time, so is the detection step.

Complexity. Since the 3 steps of the algorithm are in linear time, the complete algorithm is in linear time with respect to the size of the image (in number of pixels).

B.6 ILLUSTRATION

We illustrate the interest of well-composedness to text detection with the morphological Laplacian in 2D. Let us recall that the morphological Laplacian $\mathcal{L}$ of a given image u is defined as $\mathcal{L}_{se}(u) = \delta_{se}(u) + \varepsilon_{se}(u) - 2u$ where se is a given structuring element. The contours of u are the zero-crossing of the Laplacian. As they are boundaries of level-sets of the grayscale image, the zero-crossing are closed curves. We can set the gray-level of a given contour to the mean of the gradient of the original image along the contour.

We start from Figure 4. Without correction, it can be seen on Figure 5 and Figure 7a that some characters are split into several connected components. If we apply the proposed process

Figure 6.: Zero-crossings of the Laplacian modified by the increasing process

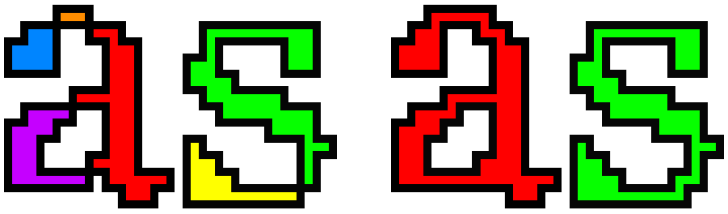

(a) Using the original Laplacian.

(b) Using the DWC Laplacian.

Figure 7.: Text segmentation results

on the Laplacian image, we observe that the contours are simple. In practice, it can be seen on Figure 6 and Figure 7b that the correction repairs many contours.

B.7 CONCLUSION

We have presented a new algorithm that produces digitally well-composed images without interpolation. Compare to the interpolation methods, the proposed algorithm is faster and less memory consuming. It can be seen as a natural extension of the algorithm of topological repairing of Siqueira *et al.* [158] to gray-valued images.

The source code of the proposed algorithm has been implemented using our image processing C++ library "Milena" [109, 110], which is a free software under the GNU Public Licence v2. Since we advocate reproducible research, this source code is released on our web site at: `http://publications.lrde.epita.fr/boutry.15.icip`.

C

AXIOMATIC DIGITAL TOPOLOGY

Our sources in matter of *Combinatorial Topology* and of *Piecewise Linear Topology* in this chapter are mainly: [49, 15, 2, 42, 79, 2, 7, 4, 111, 42].

C.1 TOPOLOGY

Definition 46 (Topological spaces [84, 2])**.** *Let X be a set of points, and let $\mathcal{U}$ be a set of subsets of X such that:*

- $X, \emptyset \in \mathcal{U}$, $(TO1)$
- *any union of any family of elements in $\mathcal{U}$ belongs to $\mathcal{U}$,* $(TO2)$
- *any finite intersection of any family of elements in $\mathcal{U}$ belongs to $\mathcal{U}$.* $(TO3)$

Then $\mathcal{U}$ is said to be a topology*, and the couple $(X,\mathcal{U})$ is called a* topological space*. The elements of X are called the* points *of $(X,\mathcal{U})$, and the elements of $\mathcal{U}$ are called the* open sets *of $(X,\mathcal{U})$. We will abusively say that X is a topological space, assuming it is supplied with its topology $\mathcal{U}$.*

An open set which contains a point of X is said to be a *neighborhood* of this point.

Definition 47 (Closed sets and closure [2])**.** *Let $(X,\mathcal{U})$ be a topological space, and let S be a subset of X. A set $S \subseteq X$ is said* closed *iff it is the complement of an open set in X. The intersection of all the closed sets in X containing M is denoted by $\mathrm{Clo}_{(X,\mathcal{U})}(S)$ and is called the* closure of S*. When no ambiguity is possible, we will abusively denote it $\mathrm{Clo}(S)$.*

Proposition 26 (Properties of the closure [2])**.** *Let $(X,\mathcal{U})$ be a topological space, and let S, T be subsets of X, then:*

- $\mathrm{Clo}(S \cup T) = \mathrm{Clo}(S) \cup \mathrm{Clo}(T)$,
- $S \subseteq \mathrm{Clo}(S)$,
- $\mathrm{Clo}(\emptyset) = \emptyset$.

Definition 48 (Interior [2])**.** *Let $(X,\mathcal{U})$ be a topological space. A point p in X is said to be an* interior point *of S relatively to the topology $\mathcal{U}$ iff there exists $U \in \mathcal{U}$ such that $p \in U \subseteq S$. The set of all the interior points of a set $S \subseteq X$ is denoted by $\mathrm{Int}_{(X,\mathcal{U})}(S)$.*

Note that the interior of a set $S \subseteq X$ is an open set in X.

Definition 49 (Topological boundary [2])**.** *Let $(X,\mathcal{U})$ be a topological space. The* boundary *of a set $S \subseteq X$ is $\mathrm{Clo}(S) \setminus \mathrm{Int}_{(X,\mathcal{U})}(S)$.*

Definition 50 (Relative topology [49])**.** *Let $(X,\mathcal{U})$ be a topological space and let S be a subset of X. We call* relative topology *induced in S by $\mathcal{U}$ the set of all the sets which can be written $U \cap S$ where $U \in \mathcal{U}$. A set which is open in the relative topology of S is said to be a* relatively open set*.*

Definition 51 (Connectedness [49])**.** *Let $(X,\mathcal{U})$ be a topological space. A set $S \subset X$ is said to be* connected *iff there is no decomposition $S = T_1 \cup T_2$ such that $T_1 \cap T_2 = \emptyset$, both $T_1, T_2 \neq \emptyset$, and relatively open sets with respect to S.*

Proposition 27 (Union of non disjoint connected sets ([2], p. 14, Prop. 3.13))**.** *Let $(X,\mathcal{U})$ be a topological space. Let A, B be two connected subsets of X. If $A \cap B \neq \emptyset$, then $A \cup B$ is connected.*

Definition 52 (Components [2])**.** *Let p a point of a topological space $(X,\mathcal{U})$. The union of all connected sets containing p is connected, is the largest connected set in $(X,\mathcal{U})$ containing p, and is called the* component *of the point p in $(X,\mathcal{U})$. We denote it $\mathcal{CC}(X,p)$ where X represents abusively $(X,\mathcal{U})$.*

Proposition 28 (Continuous functions)**.** *A function f mapping a topological space $(X,\mathcal{U})$ to $(Y,\mathcal{V})$ is said to be* continuous *iff for any set $U \subseteq Y$ which is open in Y, its inverse image:*

$$f^{-1}(U) \equiv \{x \in X \,;\, f(x) \in U\}$$

is open in X.

Proposition 29 (Image of a connected set)**.** *The image by a continuous mapping of a connected topological space is a connected topological space.*

C.2 REGULAR OPEN/CLOSED SETS

Let $\mathcal{T}$ be a topological space. Then, $\text{Int}_\mathcal{T}$ denotes the interior operator and $\text{Clo}_\mathcal{T}$ the closure operator in this topological space.

Definition 53. *A set X subset of a topological space $\mathcal{T}$ is said to be a* regular open set *iff $X = \text{Int}_\mathcal{T}(\text{Clo}_\mathcal{T}(X))$.*

Definition 54. *A set X subset of a topological space $\mathcal{T}$ is said to be a* regular closed set *iff $X = \text{Clo}_\mathcal{T}(\text{Int}_\mathcal{T}(X))$.*

C.3 $T0$-SPACES AND ALEXANDROV SPACES

Definition 55 (Degenerate sets [2])**.** *Let $(X,\mathcal{U})$ be a topological space. A set $M \subseteq (X,\mathcal{U})$ is said to be* degenerate *if it consists of only one point.*

Definition 56 ($T0$ axiom and $T0$-spaces [5, 84, 2].)**.** *We say that a topological space $(X,\mathcal{U})$ verifies the $T0$* axiom of separation *iff it for any two different points in X, at least one has a neighborhood not containing the other, or equivalently iff two distinct degenerate subsets of X have distinct closures in $(X,\mathcal{U})$. A topological space which verifies the $T0$ axiom of separation is said to be a* $T0$-space*.*

Definition 57 (Discrete spaces [7])**.** *A topological space $(X,\mathcal{U})$ is said* discrete *iff the intersection of any family of open sets of X is open in X, or equivalently iff the union of any family of closed sets of X is closed in X.*

Definition 58 (Alexandrov spaces [49])**.** *A discrete To-space is said to be an* Alexandrov space*.*

Proposition 30 (Smallest open/closed sets [49])**.** *Let $(X,\mathcal{U})$ be an Alexandrov space. For any point $P \in X$, there exists a* smallest neighborhood *of P is X:*

$$OP = \bigcap_{U \in \mathcal{U} \text{ s.t. } P \in U} U.$$

Due to the symmetry of Alexandrov spaces, there exists also a smallest closed set *containing P:*

$$CP = \bigcap_{U \text{ closed in } X \text{ s.t. } P \in U} U.$$

Alexandrov spaces get some interesting properties [49]:

Theorem 9. *Let $(X,\mathcal{U})$ be an Alexandrov space, and P, Q be two points of X.*

1. *if* $P \neq Q$*, then:*
   - $P \in OQ \Rightarrow Q \notin OP$,
   - $P \in CQ \Rightarrow Q \notin CP$,
2. $P \in CQ \Leftrightarrow Q \in OP$,
3. $CP \subseteq CQ \Leftrightarrow OQ \subseteq OP$.

Definition 59 (Locally finite)**.** *A topological space* $(X, \mathcal{U})$ *is said to be* locally finite *if each point* $P \in X$ *has as finite neighborhood and a finite closed set containing* P*.*

Theorem 10 (Path-connectivity and connectivity in Alexandrov spaces [49])**.** *Let* $(X, \mathcal{U})$ *be an Alexandrov space. Then* $S \subseteq X$ *is connected iff it is path-connected.*

C.4 PARTIALLY ORDERED SETS

Definition 60 (Binary relation [15])**.** *Let* X *be an arbitrary set. A* binary relation R on X *is as subset of the Cartesian product* $X \times X$*:*

$$R \subseteq X \times X.$$

Equivalently, a binary relation R *on* X *is a mapping from* $X \times X$ *to* $\{0, 1\}$ *such that* $\forall x, y \in X$*:*

$$\{(x, y) \in R\} \Rightarrow \{R(x, y) = 1\}, \text{ and } \{(x, y) \notin R\} \Rightarrow \{R(x, y) = 0\}.$$

Sometimes will denote by xRy *or by* $y \in R(x)$ *the fact that* $(x, y) \in R$*.*

Definition 61 (Properties of binary relations [15])**.** *A binary relation is said:*

- reflexive *iff,* $\forall x \in X$, $(x, x) \in R$,
- irreflexive *iff,* $\forall x \in X$, $(x, x) \notin R$,
- symmetrical *iff,* $\forall x, y \in X$, $(x, y) \in R \Leftrightarrow (y, x) \in R$,
- asymmetrical *iff,* $\forall x, y \in X$, $(x, y) \in R$ *and* $(y, x) \in R \Rightarrow x = y$,
- transitive *iff,* $\forall x, y, z \in X$, $(x, y) \in R$ *and* $(y, z) \in R \Rightarrow (x, z) \in R$.

Definition 62 (Inverse of a binary relation [15])**.** *Let* X *be a set, and* R *a relation order on* X*. We say that the binary relation* R' *on* X *such that* $\forall x, y \in X$, $(x, y) \in R \Leftrightarrow (y, x) \in R'$*, is the* inverse *of* R*.*

Notations 4 ($R^{\square}$ [15])**.** *Let* X *be a set, and* R *a relation order on* X*. We will note* $R^{\square}$ *the relation order defined such that,* $\forall x, y \in X$*:*

$$\left\{(x, y) \in R^{\square}\right\} \Leftrightarrow \{(x, y) \in R \text{ and } x \neq y\}.$$

Definition 63 (Order relation [15])**.** *Let* $\mathcal{O}$ *be a set of arbitrary elements. An* order relation *on* $\mathcal{O}$ *is a binary relation on* X *such that* R *is reflexive, asymmetrical, and transitive.*

Definition 64 (Posets/orders [15])**.** *A set* X *of arbitrary elements supplied with an order relation* R *on* X *is denoted* (X, R) *or* $|X|$ *and is said to be a* partially ordered set (poset) *or simply an* order*. We will also say that the order relation* R *is* associated *to* X*, and that* X *is the* domain *of the poset* (X, R)*.*

Notations 5 (α, β and θ [15])**.** *Let* $|X|$ *be a partially ordered set. We will usually denote by* α_X *the order relation associated to its domain* X*, in such a way that* $\mathcal{O} = (X, \alpha_X)$*. Also, we will write* β_X *the inverse of* α_X*, and* $\theta_X = \alpha_X \cup \beta_X$*.*

Notations 6 (α, β and θ applied to sets)**.** *By extension, we will define for any X subset of a partially ordered set:*

$$\alpha(X) = \bigcup_{x \in X} \alpha(x),$$

$$\beta(X) = \bigcup_{x \in X} \beta(x),$$

$$\theta(X) = \bigcup_{x \in X} \theta(x).$$

Notations 7 ($\alpha_X(x)$, $\beta_X(x)$, $\theta_X(x)$ [15])**.** *Let $|X|$ be a partially ordered set, and let x be a point in its domain X. Then we denote:*

- $\alpha_X(x) = \{p \in X \ ; \ p \leq x\}$,
- $\beta_X(x) = \{p \in X \ ; \ x \leq p\}$,
- $\theta_X(x) = \alpha_X(x) \cup \beta_X(x)$.

$\alpha_X(p)$ is called the closure *of p in $|X|$ and is the minimal closed set in X containing x, $\beta_X(p)$ is called the* star *of p in $|X|$, and is the minimal open set in X containing X, and $\theta_X(x)$ is called the* neighborhood *of p in $|X|$.*

To forge the intuition let us cite an example [2] of partially ordered sets: the set consisting of the points, straight lines, and planes of an Euclidian space is partially ordered by letting a point (respectively a straight line) precedes any straight line (respectively plane) containing it. In this case, if $p \in \mathcal{O}$ is a point, $\alpha(p)$ is simply the set made of this point $\{p\}$. If p is a straight line, $\alpha(p)$ is this straight line plus all the points lying on this line. If p is a plane, $\alpha(p)$ is this plane, plus all the straight lines lying in this plane, plus all the points lying in this plane. Also, if p is a point, $\beta(p)$ is this point, plus all the straight lines containing this point, plus all the planes containing this point. If p is a straight line, $\beta(p)$ is this straight line, plus all the planes containing this straightline. Finally, if p is a plane, $\beta(p)$ is the set made of this plane.

Note that the set $\mathcal{O}$ of all the subsets of an arbitrary set M:

$$\mathcal{O} = \{A \ ; \ A \subseteq M\},$$

is also a partially ordered set. Furthermore, if $A_1, A_2 \in \mathcal{O}$, $A_1 > A_2$ means that A_2 is a proper subset of A_1, which can be written $A_2 \subset A_1$. The resulting order is called the *natural order* in the collection of set $\mathcal{O}$. It is also called the *order based on the inclusion*. We will see the importance of this order using *Khalimsky grids* in a further subsection.

Definition 65 (Isomorphic orders [15])**.** *Let $|X| = (X, \alpha_X)$ and $(|Y| = (Y, \alpha_Y)$ be two orders. Then, these two orders are said* isomorphic (in the order sense) *iff there exists an* isomorphism in the order sense *between $|X|$ and $|Y|$, that is, a bijection $f : X \to Y$ such that for any couple (x_1, x_2) of elements of X:*

$$\{x_1 \in \alpha_X(x_2)\} \Leftrightarrow \{f(x_1) \in \alpha_Y(f(x_2))\}.$$

Notations 8 (Empty order [42])**.** *Note that all the orders whose domain is empty are isomorph, and we denote them by $|\emptyset|$.*

Definition 66 (Suborders [15])**.** *Let $|X| = (X, \alpha_X)$ be an order, and let S be a subset of X. The* suborder *of $|X|$ relative to S is the order (S, α_S) with $\alpha_S = \alpha_X \cap (S \times S)$. If no ambiguity is possible, we will write $(S, \alpha_S) = |S|$.*

Proposition 31 ($\alpha_S(x)$, $\beta_S(x)$, $\theta_S(x)$ [15])**.** *Let $(X, \alpha_X) = |X|$ be an order, and S be a subset of X inducing a suborder $(S, \alpha_S) = |S|$. Then for any $x \in S$, $\alpha_S(x) \equiv \alpha_X(x) \cap S$, $\beta_S(x) \equiv \beta_X(x) \cap S$, and $\theta_S(x) \equiv \theta_X(x) \cap S$.*

Definition 67 (Rank [15]). *Let* $(X, \alpha_X) = |X|$ *be an order. The* rank $\rho_X(x)$ *of an element* x *in* $|X|$ *is* 0 *when* $\alpha_X^{\square}(x) = \emptyset$*; otherwise, it is equal to:*

$$\max_{y \in \alpha_X^{\square}(x)} (\rho_X(y)) + 1.$$

The rank *of an order* $|X|$ *is denoted by* $\rho(|X|)$ *and is equal to the maximal rank of its elements:*

$$\rho(|X|) = \max_{x \in X}(\rho_X(x)).$$

As underlined by Daragon [42], the notion of dimensions and of ranks are different, even if they often match: the dimension of an object is inherent to an object, when the notion of rank depends of the elements that lie into the neighborhood.

Definition 68 (Point/k-element [15]). *Let* $(X, \alpha_X) = |X|$ *be an order. An element of* X *such that* $\rho_X(x) = k$ *is called* point *or* k-element *of* X.

C.5 FROM POSETS TO $T0$-SPACES

There comes a much important theorem of Alexandrov [2] relating orders and Alexandrov spaces.

Theorem 11 (Theorem 6.52 [2] (p. 28)). *Let* $\mathcal{O}$ *be a partially ordered set, and let* A *be a subset of* $\mathcal{O}$*. We shall say that* A *is* closed *iff for any* $p, p' \in \mathcal{O}$*:*

$$\{p \in A \text{ and } p' < p\} \Rightarrow \{p' \in A\}.$$

This topology (based on the closed sets) converts $\mathcal{O}$ *into an Alexandrov space* $(X, \mathcal{U}) = f(\mathcal{O})$*. Conversely, every Alexandrov space* $(X, \mathcal{U})$ *can be turned into a partially ordered set* $\mathcal{O} = \phi((X, \mathcal{U}))$ *if, for any two distinct elements* $p, p' \in (X, \mathcal{U})$*,* $p' < p$ *is taken to mean that* $p' \in \alpha(p)$*. It follows that* $f(\phi((X, \mathcal{U}))) = (X, \mathcal{U})$ *and* $\phi(f(\mathcal{O})) = \mathcal{O}$.

As explained by this theorem [2], partially ordered sets can be identified with Alexandrov spaces in such a way that $\alpha_{\mathcal{O}}(p)$ is synonymous with the (topological) closure in the equivalent Alexandrov space $f(\mathcal{O})$, and $\beta_{\mathcal{O}}(p)$ is equal to the minimal (open) neighborhood of the point p in $f(\mathcal{O})$ (where $\beta = \alpha^{-1}$).

C.6 KHALIMSKY GRIDS

Definition 69 (Khalimsky grids [87]). *The* Khalimsky grid *of dimension* n *is denoted* $|\mathbb{H}^n| = (\mathbb{H}^n, \supseteq)$ *and is defined as the order such that:*

$$\begin{aligned}
\mathbb{H}_0^1 &= \{\{a\} \ ; \ a \in \mathbb{Z}\}, \\
\mathbb{H}_1^1 &= \{\{a, a+1\} \ ; \ a \in \mathbb{Z}\}, \\
\mathbb{H}^1 &= \mathbb{H}_0^1 \cup \mathbb{H}_1^1, \\
\mathbb{H}^n &= \{h_1 \times \cdots \times h_n \ ; \ \forall i \in [\![1, n]\!], h_i \in \mathbb{H}^1\}.
\end{aligned}$$

Definition 70 (Cubical complexes). *Let* $\mathcal{X}$ *be a subset of* $(\mathbb{H}^n, \alpha_{\mathbb{H}^n})$*. We say that* $\mathcal{X}$ *is a* cubical complex *iff it is* closed under inclusion*, that is, for any element* h *of* $\mathcal{X}$*, all the elements* h' *of* $\mathbb{H}^n$ *such that* $h' \subseteq h$ *are elements of* X*. In other words,* $X = \alpha_{\mathbb{H}^n}(X)$.

Figure 1 shows two usual representations depicting a same cubical complex. On the left, we perceive the elements of $\mathbb{H}^n$ as sets of points of $\mathbb{Z}^n$, and we clearly see when their interection is empty or not. On the right, we perceive elements of $\mathbb{H}^n$ as geometric objects (vertices, edges,

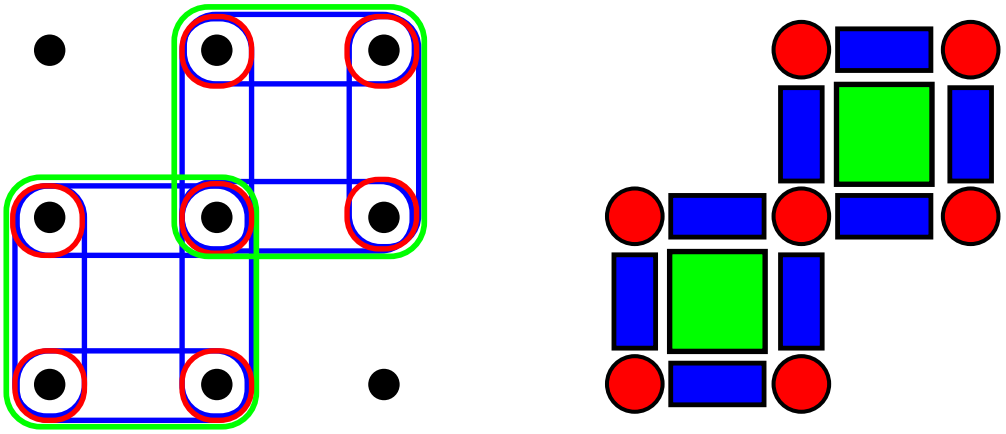

Figure 1.: Different representations of the same cubical complex

squares, cubes, and so on), this is the *splitted representation*, whose name is justified by the fact that even elements whose intersection is non empty are separated on the representation.

A consequence of Definition 69, showing that $\alpha = \supseteq$, is that for any $h \in \mathbb{H}^n$, we have the following equalities for the closure, the opening, and the neighborhood:

$$\alpha(h) = \{h' \in \mathbb{H}^n \ ; \ h' \subseteq h\},$$
$$\beta(h) = \{h' \in \mathbb{H}^n \ ; \ h \subseteq h'\},$$
$$\theta(h) = \{h' \in \mathbb{H}^n \ ; \ h' \subseteq h \text{ or } h \subseteq h'\}.$$

Obviously, any suborder $|X|$ of $|\mathbb{H}^n|$ verifies that its associated order relation α_X equals $\supseteq \cap X \times X$, which corresponds to the inclusion order restricted to X, and then for any $h \in X$:

$$\alpha_X(h) = \{h' \in X \ ; \ h' \subseteq h\},$$
$$\beta_X(h) = \{h' \in X \ ; \ h \subseteq h'\},$$
$$\theta_X(h) = \{h' \in X \ ; \ h' \subseteq h \text{ or } h \subseteq h'\}.$$

Definition 71 (Dimension and $\mathbb{H}^n_k$)**.** *Any element h of $\mathbb{H}^n$ which is the Cartesian product of k elements, with $k \in [\![0, n]\!]$, of $\mathbb{H}^1_1$ and of $(n-k)$ elements of $\mathbb{H}^1_0$ is said to be of* dimension k*, which is denoted by $\dim(h) = k$, and the set of all the elements of $\mathbb{H}^n$ which are of dimension k is denoted by $\mathbb{H}^n_k$.*

Property 1. *For any $k \in [\![0, n]\!]$, any element h in $\mathbb{H}^n_k$ is of rank $\rho(h, |\mathbb{H}^n|) = k$. In other words, in the Khalimsky grids, the dimension is equal to the rank in $|\mathbb{H}^n|$.*

Proof: Let us proceed by induction on the dimension of $h \in \mathbb{H}^n$.

Initialization ($\dim(h) = 0$): When $\dim(h) = 0$, there exists $a \in \mathbb{Z}^n$ such that $h = \otimes_{i \in [\![1,n]\!]} \{a_i\}$, and then $\alpha(h) = \otimes_{i \in [\![1,n]\!]} \{\{a_i\}\} = \{h\}$, then $\alpha^{\square}(h) = \emptyset$, and then the rank of h in $|\mathbb{H}^n|$ is equal to 0.

Induction ($\dim(h) \in [\![1, n]\!]$): We assume that for any $i \in [\![0, k-1]\!]$, when the dimension of h is lower than or equal to $(k-1)$, the dimension is equal to the rank in $|\mathbb{H}^n|$. Let us now assume that $\dim(h) = k$, we can rearrange the space coordinates such that h can be written:

$$h = \otimes_{i \in [\![1,k]\!]} \{a_i, a_i + 1\} \otimes \otimes_{i \in [\![k+1,n]\!]} \{a_i\},$$

and then by the closure operator we obtain that:

$$\alpha(h) = \otimes_{i \in [\![1,k]\!]} \{\{a_i\}, \{a_i, a_i + 1\}, \{a_i + 1\}\} \otimes \otimes_{i \in [\![k+1,n]\!]} \{\{a_i\}\}.$$

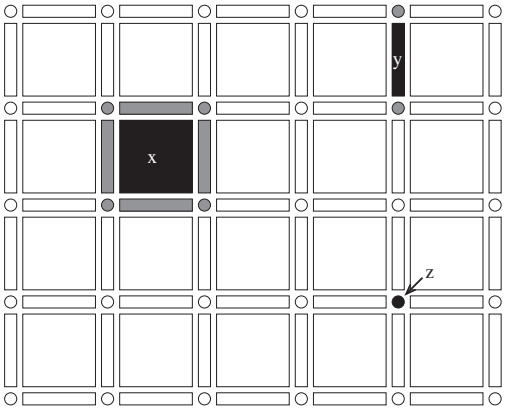

Figure 2.: The closures $\alpha(x)$, $\alpha(y)$, $\alpha(z)$ in $\mathbb{H}^2$ [42] (p. 34).

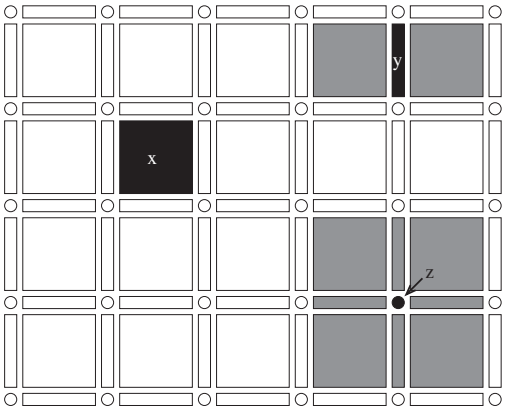

Figure 3.: The openings $\beta(x)$, $\beta(y)$, $\beta(z)$ in $\mathbb{H}^2$ [42] (p. 34).

In other words, the only element of $\alpha(h)$ of dimension k is h itself, all the other elements being of dimension in $[\![0, k-1]\!]$, and then:

$$\max\left\{\dim(h')\ ;\ h' \in \alpha^{\square}(h)\right\} = k-1.$$

When the dimension il lower than or equal to $(k-1)$, the dimension equals the rank in $|\mathbb{H}^n|$, and then we obtain:

$$\max\left\{\rho(h', |\mathbb{H}^n|)\ ;\ h' \in \alpha^{\square}(h)\right\} = k-1,$$

and then the rank of h is k.

Finally, we obtained that for any value of k, and then for any element of $\mathbb{H}^n$, the dimension equals the rank in $|\mathbb{H}^n|$. □

Proposition 32 (Khalimsky grids are Alexandrov spaces [15])**.** *For any $n \geq 1$, the Khalimsky grids $|\mathbb{H}^n = (\mathbb{H}^n, \alpha)|$ supplied with the order relation $\alpha = \supseteq$, as defined in Theorem 11, is an Alexandrov space.*

Figure 2, Figure 3, and Figure 4 show the different possible closures/openings/neighborhoods in the case of a "point", an "edge", and a "square" in $\mathbb{H}^2$. We will see next that these *Kovalevsky cells* will be called respectively 0-*faces*, 1-*faces*, and 2-*faces* and that these notions exist in any finite dimension.

Starting from a binary image u_{bin}, or equivalently from a set whose u_{bin} is the characteristical image depicted on Figure 5, we can supply this image with the $(4,8)$-topology, or the $(8,4)$-topology, which are very usual in digital topology: Figure 6 shows that connected com-

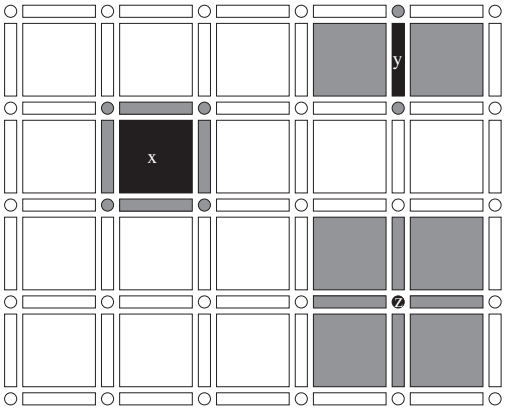

Figure 4.: The neighborhoods $\theta(x)$, $\theta(y)$, $\theta(z)$ in $\mathbb{H}^2$ [42] (p. 34).

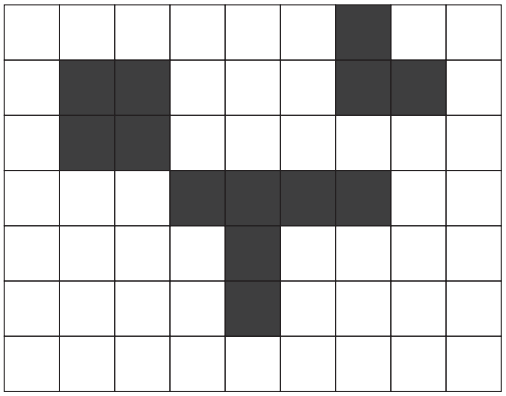

Figure 5.: A binary image u_{bin} in $\mathbb{Z}^2$ [42] (p. 31).

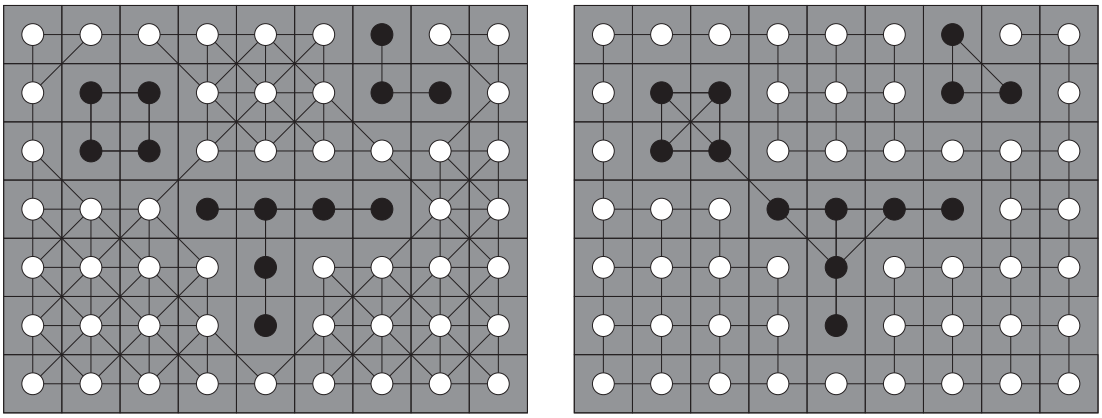

Figure 6.: u_{bin} [42] (p. 31) supplied with the $(4, 8)$-topology on the left and with the $(8, 4)$-topology on the right (the foreground is in black and the background in white).

ponents of the foreground that result from this choice are different depending on the chosen connectivities.

Now, let us immerse this same image in $\mathbb{H}^2$ in different manners. The first approach in the raster scan order corresponds to a $(1-1)$- mapping between the two spaces. However, this space is not invariant by translation. The second approach uses the *miss strategy* (which reflects the $(4, 8)$-topology, and that we will use next as *immersions*): the elements of $\mathbb{Z}^2$ are mapped to the squares of $\mathbb{H}^2$, and each point or edge in $\mathbb{H}^2$ whose all the neighboring squares are in the foreground are assigned as foreground too. The third approach uses the *hit strategy* (which reflects the $(8, 4)$-topology): the elements of $\mathbb{Z}^2$ are mapped to the squares of $\mathbb{H}^2$, and each

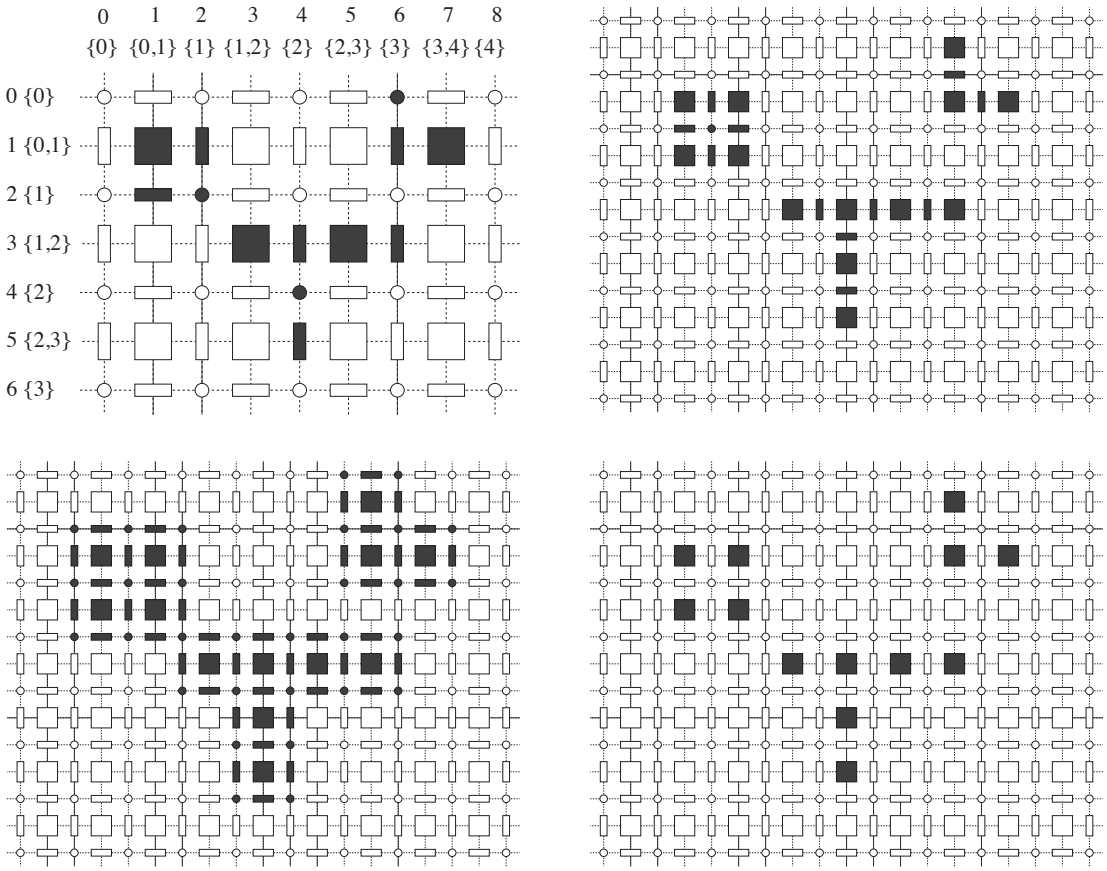

Figure 7.: Different immersions of u_{bin} into $\mathbb{H}^2$ [42] (p. 31)

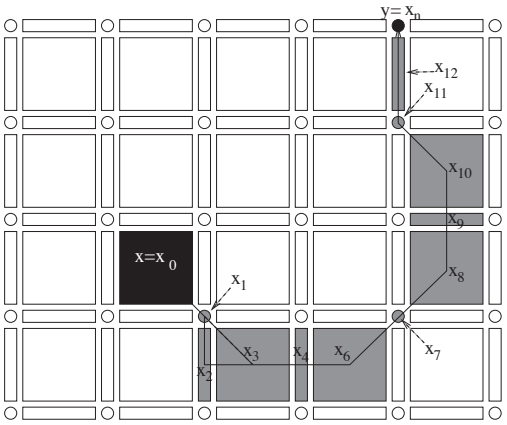

Figure 8.: A path in $\mathbb{H}^2$ [42] (p. 34)

point or edge in $\mathbb{H}^2$ which is a face of a square of the foreground is assigned as foreground too. The fourth approach corresponds to the *isomorphism* we will use in a next section (points become n-cubes).

Definition 72 (Paths [15])**.** *Let $|X|$ be an order. A* path *from $x \in X$ to $y \in X$ is a sequence $(p^0 = x, p^1, \ldots, p^{k-1}, p^k = y)$ of elements of X such that for any $i \in [\![0, k-1]\!]$, $x \in \theta_X^{\square}(y)$.*

Figure 8 depicts a path in $\mathbb{H}^2$.

Definition 73 (Connectivity of an order [15])**.** *An order, as every topological space, is* connected *iff it cannot be partitioned into two non-empty open sets.*

Effectively, this definition holds since Alexandrov spaces and partially ordered sets are equivalent by Theorem 11 [2].

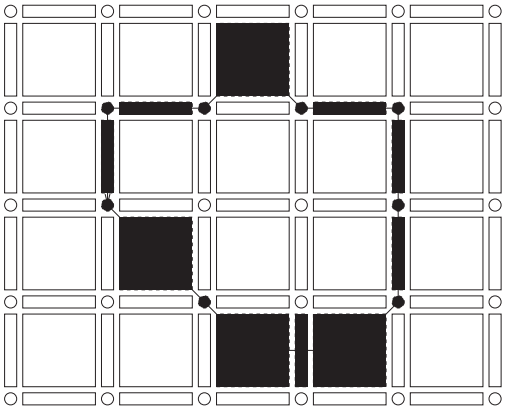

Figure 9.: A simple closed curve in $\mathbb{H}^2$ [42] (p. 34).

Definition 74 (Path-connectivity of an order [15]). *An order $|X|$ is said* connected by path *or* path-connected *iff for any couple (x, y) of elements of X, there exists a path from x to y into $|X|$.*

Theorem 12 (Connectivity vs path-connectivity [15]). *Let $|X|$ be a partially ordered set. Then $|X|$ is connected iff it is path-connected.*

Since the pathwise-connectivity between two points x, y belonging to an order constitutes a binary relation which is reflexive, symmetrical, and transitive, that is, an *equivalence relation* on X, we can define the equivalence classes of X in $\mathbb{H}^n$ as the *connected components* of X in $\mathbb{H}^n$.

Definition 75 (Connected components [15]). *Let $|X|$ be an order. A* connected component *C of $|X|$ is a subset of X such that for any couple (x, y) of elements of C, there exists a path from x to y lying entirely into C, and such that C is maximal for this property.*

Definition 76 (Simple closed curves [15]). *An order $|X| = (X, \alpha_X)$ is a simple closed curve if for any point $x \in X$, $\mathrm{Card}(\theta^{\square}_X(x)) = 2$ and such that the couple (y, z) of elements of $\theta^{\square}_X(x)$ verifies that $y \notin \theta^{\square}_X(z)$.*

As proved in [87], a simple closed curve (see Figure 9) separates $\mathbb{H}^2$ and then satisfies an analog of the Jordan curve theorem in 2D Khalimsky grids.

C.7 ORDER JOINS

Definition 77 (Order join [15]). *Let $|X|, |Y|$ be two orders. It is said that $|X|$ and $|Y|$ can be* joined *if $X \cap Y = \emptyset$. If $|X|$ and $|Y|$ can be joined, the* join *of $|X|$ and $|Y|$ is defined as the order:*

$$|X| * |Y| = (X \cup Y, \alpha_X \cup \alpha_Y \cup X \times Y).$$

Some properties [42] of the join are important to remark:

- the empty order $|\emptyset|$ is the neutral element of the join operator: $|X| * |\emptyset| = |\emptyset| * |X| = |X|$,
- the operator $*$ is not commutative,
- the operator $*$ does not create new elements, it adds some order relations between the elements of X and the elements of Y,
- the elements of Y keep their initial rank when the join operation is applied, when the elements of X have a rank which is incremented by the rank of Y plus one.

The construction of an order join can be made in this way: we put on the top each element of X, and at the bottom all the elements of Y. Then we connect the elements of X according to α_X, and then the elements of Y according to α_Y. Finally, we connect each element of X to each element of Y, and we have obtained the Hasse diagram of the order join.

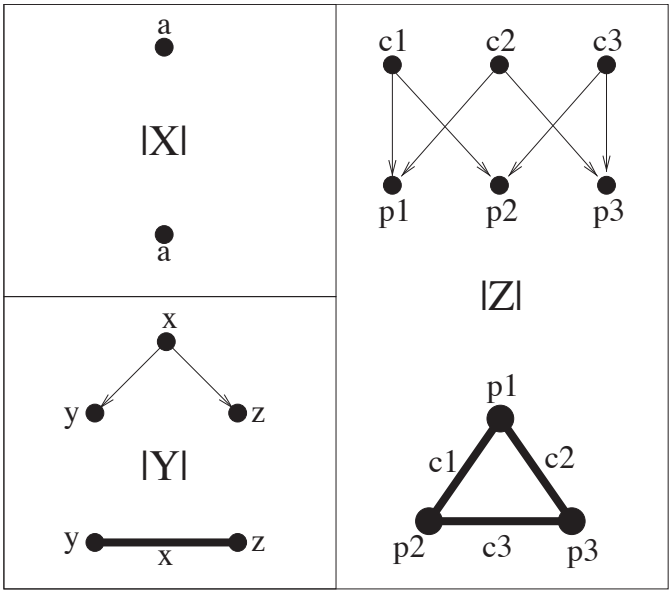

Figure 10.: Three examples of orders $|X|, |Y|, |Z|$ ([42], p. 37)

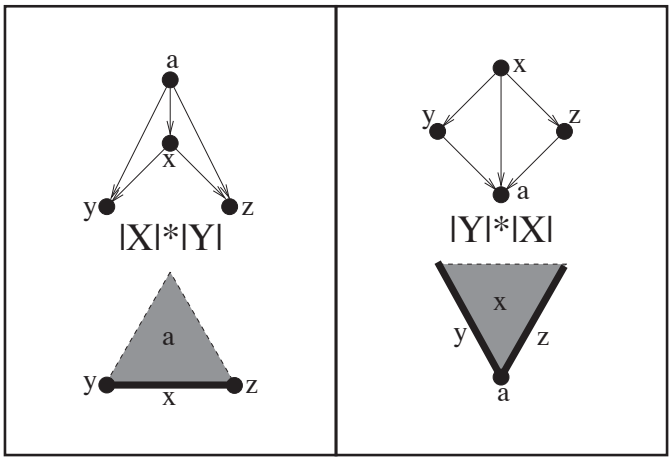

Figure 11.: The join operator $*$ is not commutative ([42], p. 37)

Property 2 (Order join and $\theta^{\square}_{X}(x)$ [42](Property 1))**.** *Let $|X|$ be an order. Then for any $x \in X$:*

$$|\theta^{\square}_{X}(x)| = |\beta^{\square}_{X}(x)| * |\alpha^{\square}_{X}(x)|.$$

We will see in this section that, as in [42], this equality is particularily crucial, since it allows to "decompose" the neighborhood of a point of $\mathbb{H}^n$ into two orders which own many very strong topological properties.

Property 3 ($\theta^{\square}_{X*Y}(x)$ [42](Property 2))**.** *Let $|X|$ and $|Y|$ be two orders that can be joined. Let x be an element of X and y be an element of Y. Then we obtain that $|\theta^{\square}_{X*Y}(x)| = |\theta^{\square}_{X}(x)| * |Y|$ and $|\theta^{\square}_{X*Y}(y)| = |X| * |\theta^{\square}_{Y}(y)|$.*

On Figure 10, three orders of increasing complexity are depicted. Their joins are depicted on Figure 11 and Figure 12. Note that the Hasse diagrams are on the top, and the geometrical representation at the bottom. Observe that the rank of these orders is straightforward to compute, looking at their Hasse diagrams.

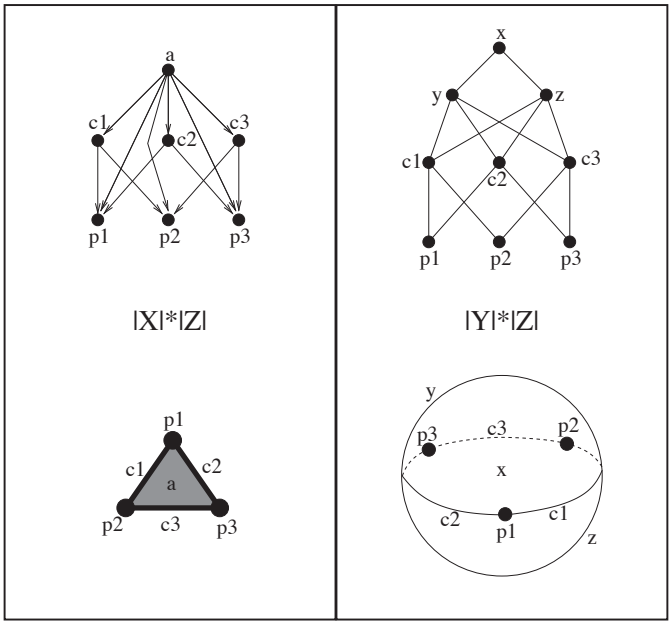

Figure 12.: Some order joins representing a *simplicial complex* on the left and a sphere on the right [42] (p. 37)

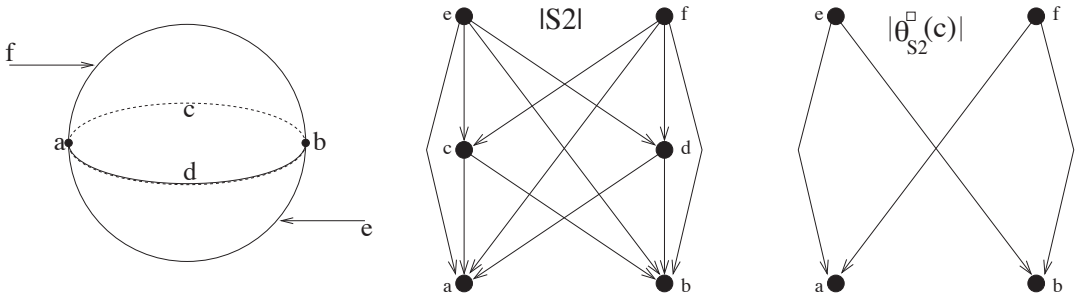

Figure 13.: A 2-surface: the sphere $\mathcal{S}_2$ [42] (p. 50)

C.8 n-SURFACES

Definition 78 (CF-orders [15])**.** *Let $|X| = (X, \alpha_X)$ be a partially ordered set. $|X|$ is said* countable *iff its domain X is countable. Also, $|X|$ is said* locally finite *iff for any element $x \in X$, the set $\theta_X(x) = \{y \in X\ ;\ (x, y) \in \theta_X\}$ is finite. A partially ordered set which is countable and locally finite is said to be a* CF-order*.*

Now let us recall the definition of *discrete surfaces* or *n-surfaces* of Evako, Kopperman and Mukhin [53] which will be essential to define well-composedness in the sense of Alexandrov.

Definition 79 (n-surface)**.** *Let $|X| = (X, \alpha_X)$ be a CF-order. The order $|X|$ is said to be:*

- *a (-1)-surface iff $X = \emptyset$,*
- *a 0-surface iff X is made of two elements $x, y \in X$ which are not neighbors the one of the other one: $x \notin \alpha_X(y)$ and $y \notin \alpha_X(x)$,*
- *a n-surface, $n \geq 1$, iff $|X|$ is connected and for any $x \in X$, the order $|\theta_X^{\square}(x)|$ is a $(n-1)$-surface.*

To forge the intuition on discrete surfaces, we propose to show an example extracted from [42]. On Figure 13, we can observe according to Daragon [42] the most simple 2-surface: the *sphere* $|\mathcal{S}_2|$. It is made of 6 elements: $\mathcal{S}_2 = \{a, b, c, d, e, f\}$, and any point $x \in \mathcal{S}_2$ verifies that its neighborhood $|\theta_{\mathcal{S}_2}^{\square}(x)|$ is a 1-surface. Effectively, the neighborhood of any point

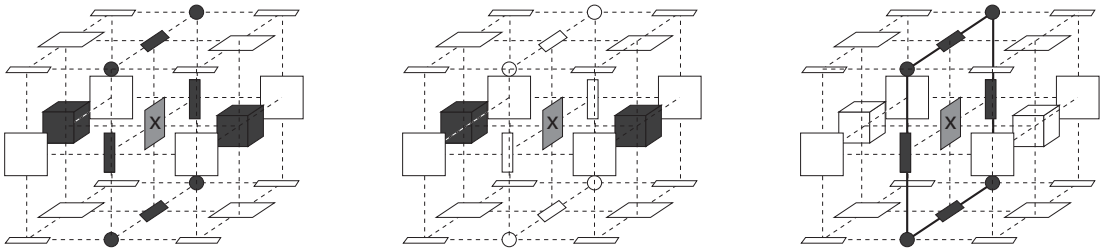

Figure 14.: Different kinds of *adherences* of a 2-element in $\mathbb{H}^3$ [42] (p. 54)

$y \in \theta^{\square}_{\mathcal{S}_2}(x)$, we have that $\left|\theta^{\square}_{\theta^{\square}_{\mathcal{S}_2}(x)}(y)\right|$ is made of two points which are not neighbors, that is, is a 0-surface.

Another example of 2-surface is simply $|\mathbb{H}^2|$: the neighborhood of any point of $\mathbb{H}^2$ is a simple close curve. Effectively, as proven by Evako *et al.* in [53]:

Theorem 13. *The order $|\mathbb{H}^n|$ is a (discrete) n-surface.*

Note that this theorem is fundamental and will have many implications later in our study of the relation between well-composedness in the sense of Alexandrov and digital well-composedness.

Also, Daragon [42] proved this following theorem on partially ordered sets:

Theorem 14. *Let $|X|$ and $|Y|$ be two orders that can be joined, and let $n \in \mathbb{N}$ be an integer. The order $|X|*|Y|$ is a $(n+1)$-surface iff there exists some $p \in [\![-1, n+1]\!]$ such that $|X|$ is a p-surface and $|Y|$ is a $(n-p)$-surface.*

The proof of this theorem is based on Property 3 due to Bertrand [15].

Definition 80 (Homogeneity [42])**.** *An order $|X|$ is said* homogeneous *iff for any element $x \in X$, $\theta_X(x)$ contains a n-element.*

Property 4 (Rank of a n-surface [53])**.** *Let $|X|$ be a n-surface. The rank of $|X|$ is equal to n.*

Property 5 (Homogeneity of n-surfaces [42])**.** *Let $|X|$ be a n-surface. Any element x of $|X|$ is θ-neighbor of a n-element of $|X|$.*

Property 6 (Decomposition of a n-surface [42] (Property 10))**.** *Let $|X| = (X, \alpha_X)$ be an order. Then $|X|$ is a n-surface iff for any $x \in X$, $|\alpha^{\square}_X(x)|$ is a $(k-1)$-surface and $|\beta^{\square}_X(x)|$ is a $(n-k-1)$-surface, with $k = \rho(x, |X|)$.*

Since this property will be fundamental next, let us show an example of the $\beta^{\square}$-adherence and of the $\alpha^{\square}$-adherence of a point $x \in \mathbb{H}^3$ of rank 2 in $|\mathbb{H}^3|$ (see Figure 14). Since x is a 2-element, its $\alpha^{\square}$-adherence is a 1-surface, and its $\beta^{\square}$-adherence is a 0-surface.

Definition 81 (Separation [42])**.** *Let $|X|$ be an order, and let Y be a strict subset of X. Then it is said that $|Y|$* separates *$|X|$ iff $|X \setminus Y|$ is not connected.*

If $|X|$ is a n-surface, and Y is a strict subset of X such that $|Y|$ is a k-surface, then necessarily $k = n-1$ (as in continuous topology using topological n-manifolds).

C.9 CLOSED ORDERS

Definition 82 (Closed orders [42])**.** *Let $|X| = (X, \alpha_X)$ be an order. $|X|$ is said to be* closed *iff for any $z \in X$, and for any $y \in \alpha^{\square}_X(x)$, for any value $i \in]\rho(y, |X|), \rho(x, |X|)[$:*

$$\exists z \in \alpha^{\square}_X(x) \cap \beta^{\square}_X(x) \text{ s.t. } \rho(z, |X|) = i.$$

In other words, this relation means that there exists in a closed order elements "between" x and y which are of any rank between the rank of x and the rank of y in the order. It recalls simplicial complexes which are *closed by inclusion* in the sense that for any k-simplex in a simplicial complex S, there exists at least one l-simplex in S which is a face of s for any value l in $[\![0, k]\!]$ (since a simplicial complex contains by definition all the faces of its elements).

Property 7 (n-surfaces are closed orders [42] (Property 20 p. 63))**.** *Let $|X|$ be an order. If $|X|$ is a n-surface, $|X|$ is a closed order.*

C.10 GEOMETRIC SIMPLICIAL COMPLEXES (IN $\mathbb{R}^n$)

Since *polyhedral complexes* are made of *convex polyhedral domains* which lies in $\mathbb{R}^n$, let us first recall some basics in linear algebra.

Definition 83 (r-planes and linear independency)**.** *An r-dimensional subspace, $0 \leq r \leq n$, of $\mathbb{R}^n$ is called a* r-plane*. The points $x^0, \ldots, x^r$ are said* linearly independent *iff they are not contained in any k-plane with $k < r$.*

Definition 84 (Affine combination and affinely independency)**.** *Let $u^0, \ldots, u^k$ be $(k+1)$ points in $\mathbb{R}^n$. A point $x = \sum_{i \in [\![0,k]\!]} \lambda_i u^i$ is said to be an* affine combination *of the u^i iff $\sum_{i \in [\![0,k]\!]} \lambda_i = 1$. Also, these $(k+1)$ points are said* affinely independent *iff any two affine combinations $x = \sum_{i \in [\![0,k]\!]} \lambda_i u^i$ and $y = \sum_{i \in [\![0,k]\!]} \mu_i u^i$ are equal iff $\forall i \in [\![0, k]\!], \lambda_i = \mu_i$.*

A consequence is that the $(k+1)$ points $u^0, \ldots, u^k$ are affinely independent iff the k vectors $(u^i - u^0)$, $\forall i \in [\![1, k]\!]$, are linearly independant. In $\mathbb{R}^n$, we can have at most n linearly dependent vectors and then $(n+1)$ affinely independent points.

Definition 85 (Convexity)**.** *The straight line defined by two points a, b is the set of all the points of the form $\lambda a + \mu b$, where $\lambda + \mu = 1$. The subset of this straight line defined by the conditions $\lambda \geq 0, \mu \geq 0$ is called the* closed segment *$[ab]$. Then, a set M is said to be* convex *if for any two points a and b in M, it contains also the whole segment $[ab]$.*

Definition 86 (Convex polyhedral domains [2] (p. 212))**.** *A bounded nonempty subset of $\mathbb{R}^n$ which is the intersection of a finite number of closed half-planes of $\mathbb{R}^n$ is called a (closed) convex polyhedral domain.*

Definition 87 (Dimension of convex polyhedral domains [2] (p. 210))**.** *The* dimension *of a convex polyhedral domain Q is the maximum number r such that Q contains $(r+1)$ linearly independent points.*

Definition 88 (Supporting planes [2] (p. 213))**.** *Let Q^n be a n-dimensional convex polyhedral domain in $\mathbb{R}^n$. The intersection of every $(n-1)$-plane $R^{n-1} \subset \mathbb{R}^n$ with Q^n is convex. A plane R^{n-1} is called* plane of support *of the polyhedral domain Q^n if $Q^n \cap R^{n-1} \neq \emptyset$ and $R^{n-1} \cap \mathrm{Int}(Q) = \emptyset$ (where $\mathrm{Int}(Q)$ denotes the topological interior of Q).*

Definition 89 (Faces of a convex polyhedral domain [2] (p. 213))**.** *The intersection of every supporting plane R^{n-1} with the topological boundary ∂Q^n of the convex polyhedral domain Q^n coincides with the set $R^{n-1} \cap Q^n$ and is therefore a closed convex polyhedral domain Q^r of dimension $r \leq n-1$; if $r = (n-1)$, Q^r is called a $(n-1)$-face of the polyhedral domain Q^n. Following the same reasoning, the $(n-2)$-faces of the $(n-1)$-faces of Q^n are called the $(n-2)$-*faces *of Q^n, and so on.*

Definition 90 ((Closed) polyhedral complexes)**.** *Let K be a finite set K of (closed) convex polyhedral domains situated in some $\mathbb{R}^n$. K is said to be a a* (closed) polyhedral complex *iff :*

1. *any intersection of two different elements h^1, h^2 of K is an element h^3 of K such that h^3 is a common face of h^1 and h^2,*

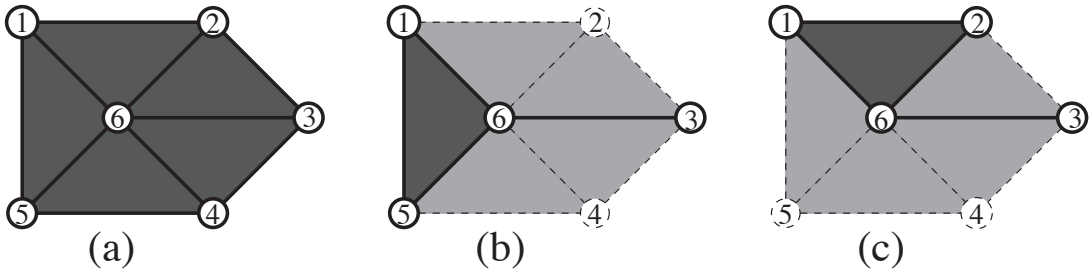

Figure 15.: Examples of simplicial complexes ([42], p. 40)

2. *every face of every convex polyhedral domain of K is also an element of K.*

Note that this family of complexes is also known as *convex linear cell complexes* in Hudson's book [79].

Even if these complexes are basically geometric structures, we will see later that they have also very nice topological properties as orders, when they are supplied with the binary relation $\supseteq$.

Definition 91 (Dimension of a polyhedral complex [2])**.** *The* dimension *of a polyhedral complex is the maximum dimension of its convex polyhedral domains.*

Definition 92 (Convex combinations and convex hull)**.** *Let $u^1, \ldots, u^n$ be n points in $\mathbb{R}^N$. The sum $\sum_{i\in[\![1,n]\!]} \lambda_i u^i$ such that each λ_i, $i \in [\![1, n]\!]$, is nonnegative, is said to be a* convex combination *of the u^i. The* convex hull *of these points is the set of convex combinations of u^i.*

Definition 93 (Geometric n-simplex, vertices of a geometric simplex [79])**.** *A* geometric n-simplex *in $\mathbb{R}^N$ is the convex hull of $(n+1)$ linearly independent points, called its* vertices*.*

Definition 94 (Simplicial complex [79])**.** *A* geometrical simplicial complex *is a polyhedral complex whose convex polyhedral domains are all geometric simplices.*

Definition 95 (Vertex set of a geometric simplicial complex)**.** *The* vertex set *of a geometric simplicial complex C is denoted by $\mathrm{Vert}(C)$ and is equal to:*

$$\{\sigma \in C \,;\, \dim(\sigma) = 0\}\,.$$

Definition 96 (Underlying polyhedron [79])**.** *If K is any geometric simplicial complex, we denote by $\mathrm{Poly}(K)$ the pointwise union in $\mathbb{R}^n$ of all the faces in K, and we call $\mathrm{Poly}(K)$ the* underlying polyhedron *of K.*

C.11 ABSTRACT SIMPLICIAL COMPLEXES

Now, we recall some results in combinatorial topology, mainly applied to *abstract simplices* and *abstract simplicial complexes*.

Definition 97 ((Abstract) simplex)**.** *Let Λ be a countable space of arbitrary elements. We will say that $s \subseteq \Lambda$ is a* abstract simplex *(in Λ) iff it is a non-empty finite subset of Λ. We will also say that an abstract simplex is an abstract n-simplex (in Λ) if it is made of $(n+1)$ elements of Λ. We will sometimes call it* abstract simplex of dimension n*.*

Definition 98 (Faces)**.** *Let Λ be a countable space of arbitrary elements. We will say that an abstract simplex $f \subseteq \Lambda$ is a* face *of the abstract simplex $s \in \Lambda$ iff $f \subseteq s$, and that it is a* proper/strict face *of s iff $f \subset s$.*

Definition 99 (Abstract simplicial complex)**.** *Let Λ be a countable space of arbitrary elements, and let C be a family of simplices if Λ. We will say that C is an* abstract simplicial complex *iff $\mathrm{Card}\,(C) < \infty$ and C its* closed by inclusion*, which means that for any face s belonging to C, any of its faces $f \subseteq s$ belongs also to C.*

Note that in this manner, an abstract simplicial complex is a finite set of finite subsets of Λ.

Definition 100 (Support). *Let Λ be a countable space of arbitrary elements, and let C be an abstract simplicial complex in Λ. We will say that the minimal set Λ_C such that any element $s \in C$ is a subset of Λ_C is the* support *of C.*

Definition 101 (Subcomplex). *Let Λ be a countable space of arbitrary elements, and let C be an abstract simplicial complex in Λ of support Λ_C. We will say that the subset K of C such that $\Lambda_K \subseteq \Lambda_C$ is a* subcomplex *of C iff it is an abstract simplicial complex.*

Definition 102 (Full subcomplex). *Let Λ be a countable space of arbitrary elements, let C be an abstract simplicial complex in Λ of support Λ_C, and let be K a subcomplex of C. Then K is said to be a* full *subcomplex of C iff any face $f \in C$ such that $f \subseteq \Lambda_C$ is an element of K.*

Figure 15 depicts on (a) an abstract simplicial complex C of support $\Lambda_C = [\![1, 6]\!]$. On (b), we can observe a subcomplex K of C of support $\Lambda_K = \{1, 3, 5, 6\}$. Each face of C which is included in Λ_K belongs to K, and in this manner K in full into C. On (c), we can see the subcomplex K' of C, whose support is $\Lambda_{K'} = \{1, 2, 3, 6\}$. The abstract simplex $\{2, 3, 6\}$ belongs to C, is a subset of $\Lambda_{K'}$, but does not belong to K'. In this manner, K' is not full into C.

Definition 103 (Vertex set of an abstract simplicial complex). *The* vertex set *of an abstract simplicial complex A is denoted by $\mathrm{Vert}(A)$ and is equal to:*

$$\bigcup_{s \in A} s.$$

C.12 ABSTRACT VS GEOMETRIC SIMPLICIAL COMPLEXES

Edelsbrunner defined a *geometric realization* of an abstract simplicial complex in the following manner:

Definition 104 (Geometric realization and abstraction [50]). *A* geometric realization *of an abstract simplicial complex A is a geometric simplicial complex K together with a bijection $\phi : \mathrm{Vert}(A) \to \mathrm{Vert}(K)$ such that $s \in A$ iff $\mathrm{ConvHull}(\phi(s)) \in K$. Conversely, A is called an* abstraction *of K.*

Roughly speaking, any abstract simplicial complex can be "transformed" into a geometric simplicial complex, by attributing coordinates to its vertices, such that they are equivalent, that is to say, two geometric simplices will intersect iff their corresponding abstract simplices intersect:

Theorem 15 (Geometric realization theorem [51]). *Every abstract simplicial complex of dimension $d \geq 0$ has a geometric realization in $\mathbb{R}^{2d+1}$.*

Proof: The proof we propose here is based on the argumentation of Edelsbrunner in [51].

Let us assume that an abstract simplicial complex A, made of finite sets of finite arbitrary elements in Λ, is of dimension $d \geq 0$. Now, let $\varphi : \mathrm{Vert}(A) \to \mathbb{R}^{2d+1}$ be an injection such that for any set $\{p^0, \ldots, p^{2d+1}\} \subseteq \Lambda_A$, the set $\{\varphi(p^0), \ldots, \varphi(p^{2d+1})\}$ is affinely independent. Let us define:

$$G = \{\mathrm{ConvHull}(\varphi(a)) \; ; \; a \in A\}.$$

We want to prove: that:

1. for any $a \subseteq \Lambda$ such that $a \in A$, $\mathrm{ConvHull}(\varphi(a)) \in G$,
2. $\varphi : \mathrm{Vert}(A) \to \mathrm{Vert}(G)$ is a bijection,
3. G is a geometric simplicial complex.

The first property is simply the consequence of the definition of G. For the second property, let us prove first that the image of $\mathrm{Vert}(A)$ is $\mathrm{Vert}(G)$. Starting from the definition of G, we obtain:

$$\begin{aligned}
\mathrm{Vert}(G) &= \{\mathrm{ConvHull}(\varphi(a)) \; ; \; a \in A, \dim(\mathrm{ConvHull}(\varphi(a)))) = 0\}, \\
&= \{\mathrm{ConvHull}(\varphi(p)) \; ; \; \{p\} \in A\}, \\
&= \{\{\varphi(p)\} \; ; \; \{p\} \in A\}, \\
&= \{\varphi(\{p\}) \; ; \; \{p\} \in A\}, \\
&= \{\varphi(a) \; ; \; a \in \mathrm{Vert}(A)\}, \\
&= \varphi(\mathrm{Vert}(A)).
\end{aligned}$$

This way, φ is injective and surjective from $\mathrm{Vert}(A)$ to $\mathrm{Vert}(G)$, and then bijective.

For the third property, that is, G is a geometric simplicial complex, we first have to show the property (a) defined such that for any geometric simplex $g \in G$, any face f of g belongs also to G. Secondly, we have to show the property (b) defined such that for any pair of geometric simplices g^1, g^2 of G such that $g^1 \cap g^2 \neq \emptyset$, $g^1 \cap g^2$ is also a geometric simplex of G; otherwise, $g^1 \cap g^2$ must be an empty set. Thirdly, we have to show the property (c) defined such that for any faces g^1, g^2 of G such that $g^1 \cap g^2 \neq \emptyset$, $g^1 \cap g^2$ is a common face of g^1 and g^2.

(a): For any geometric simplex g element of G, there exists $a_g \in A$ such that $g = \mathrm{ConvHull}(\varphi(a_g))$. This can be rewritten such that:

$$g = \mathrm{ConvHull}\{\varphi(a_g^1), \ldots, \varphi(a_g^k)\},$$

where a_g is decomposed into $\{a_g^1, \ldots, a_g^k\}$. Also, each face f of this geometric simplex g can be rewritten this way:

$$f = \mathrm{ConvHull}\{\varphi(a_g^{i_1}), \ldots, \varphi(a_g^{i_l})\},$$

with $\{i_1, \ldots, i_l\} \subseteq [\![1, k]\!]$. Since $a_f \equiv \{a_g^{i_1}, \ldots, a_g^{i_l}\} \subseteq a_g$, a_f belongs to A and then $f = \mathrm{ConvHull}\{\varphi(a_f)\}$ belongs to G.

(b): Let g^1, g^2 be two elements of G. Then, there exist $a^1, a^2 \in A$ which are not empty and which are such that:

$$\begin{cases} g^1 = \mathrm{ConvHull}(\varphi(a^1)), \\ g^2 = \mathrm{ConvHull}(\varphi(a^2)). \end{cases}$$

Then, two cases are possible:

1. If $g^1 \cap g^2 = \emptyset$, it means that:

$$\mathrm{ConvHull}(\varphi(a^1)) \cap \mathrm{ConvHull}(\varphi(a^2)) = \emptyset,$$

   and then $\varphi(a^1) \cap \varphi(a^2) = \emptyset$, and then $a^1 \cap a^2 = \emptyset$ by bijectivity of φ.

2. If $g^1 \cap g^2 \neq \emptyset$, then for any element $z \in g^1 \cap g^2 \subset \mathbb{R}^{2d+1}$, we can rewrite z as the following convex sums:

$$z = \sum_{p \in a^1} \lambda_p \varphi(p) = \sum_{p \in a^2} \mu_p \varphi(p),$$

   which implies that:

$$\sum_{p \in a^1 \cup a^2} \xi_p \varphi(p) = 0,$$

with:

$$\xi_p = \begin{cases} \lambda_p & \text{if } p \in a^1 \setminus a^2, \\ (-\mu_p) & \text{if } p \in a^2 \setminus a^1, \\ (\lambda_p - \mu_p) & \text{if } p \in a^1 \cap a^2. \end{cases}$$

Since $a^1 \cup a^2$ contains at most $(2d+2)$ elements, then $\{\varphi(p)\}_{p \in a^1 \cup a^2}$ is affinely independent, and then all the coefficients ξ_p are equal to zero, which means that:

$$\begin{cases} \lambda_p = 0 & \text{if } p \in a^1 \setminus a^2, \\ \mu_p = 0 & \text{if } p \in a^2 \setminus a^1, \\ \lambda_p = \mu_p & \text{if } p \in a^1 \cap a^2. \end{cases}$$

Then, if $a^1 \cap a^2 = \emptyset$, all the coefficients λ_p such that $p \in a^1$ are equal to 0, which would contradict that $\sum_{p \in a^1} \lambda_p = 1$. We are then in the case $a^1 \cap a^2 \neq \emptyset$.

We have then proven that $a^1 \cap a^2 = 0$ is equivalent to $g^1 \cap g^2 = 0$.

Furthermore, when $a^1 \cap a^2 \neq \emptyset$, we have $z = \sum_{p \in a^1 \cap a^2} \lambda_p \varphi(p)$, with $\sum_{p \in a^1 \cap a^2} \lambda_p = 1$, and $\forall p \in a^1 \cap a^2, \lambda_p \geq 0$. This means that $g^1 \cap g^2$ is a subset of $\mathrm{ConvHull}(\varphi(a^1 \cap a^2))$. Furthermore,

$$\mathrm{ConvHull}(\varphi(a^1 \cap a^2)) \subseteq \mathrm{ConvHull}(\varphi(a^1)) \cap \mathrm{ConvHull}(\varphi(a^2)),$$

since the convex hull is an increasing operator. This implies that:

$$g^1 \cap g^2 = \mathrm{ConvHull}(\varphi(a^1 \cap a^2)).$$

Since $a^1 \cap a^2 \subseteq a^1 \in A$, $a^1 \cap a^2 \in A$, then $\mathrm{ConvHull}(\varphi(a^1 \cap a^2)) \in G$, that is, $g^1 \cap g^2 \in G$.

(c): since $g^1 = \mathrm{ConvHull}(\varphi(a^1))$ is a simplex, its faces are the convex hulls of any subset of a^1. The same reasoning applies for $g^2 = \mathrm{ConvHull}(\varphi(a^2))$. Then $g^1 \cap g^2 = \mathrm{ConvHull}(\varphi(a^1 \cap a^2))$ is a common face to g^1 and g^2. □

Note that this bound of $2d+1$ is optimal in the sense that there exist examples of k-complexes which need $\mathbb{R}^{2k+1}$ to be realized. For example, the set of all faces of dimension lower than or equal to k (called the *k-skeleton*) of a $(2k+2)$-simplex needs to be realized in $\mathbb{R}^{2k+1}$. Also, the complete graph of five vertices usually denoted by K_5 identified by Kuratowski [95] as being one of the obstruction to graph planarity, is a 1-complex which can only be realized in $\mathbb{R}^3$. Some other examples like these ones are given in [59] and in [174].

Summarily, the definitions and the theorems recalled or introduced in the sequel hold for both abstract and geometric simplicial complexes in an equivalent manner.

C.13 SIMPLICIAL COMPLEXES AS ORDERS

Like we did with the Khalimsky grids, we can associate a *canonical order relation* $\alpha = \supseteq$ based on the inclusion to any simplicial complex C: $|C| = (C, \alpha)$. This way, simplicial complexes are partially ordered sets. For this reason, the reader is invited to refer to Section C.4 and to Section C.5 for some recalls in matter of partially ordered sets and Alexandrov spaces.

Now let us recall some properties about simplical complexes extracted from [42].

Property 8. *Let Λ be a countable space of arbitrary elements, and let C be a simplicial complex in Λ. Then the order $|C| = (C, \alpha)$ with $\alpha = \supseteq$ defined as in Theorem 11 where α is the* closure operator, *is an Alexandrov space.*

Property 9. *Let Λ be a countable space of arbitrary elements, and let C be a simplicial complex in Λ. Then for any $s \in C$, $\alpha_C(s)$ does not depend on the structure of the simplicial complex C and then can be written $\alpha(s)$.*

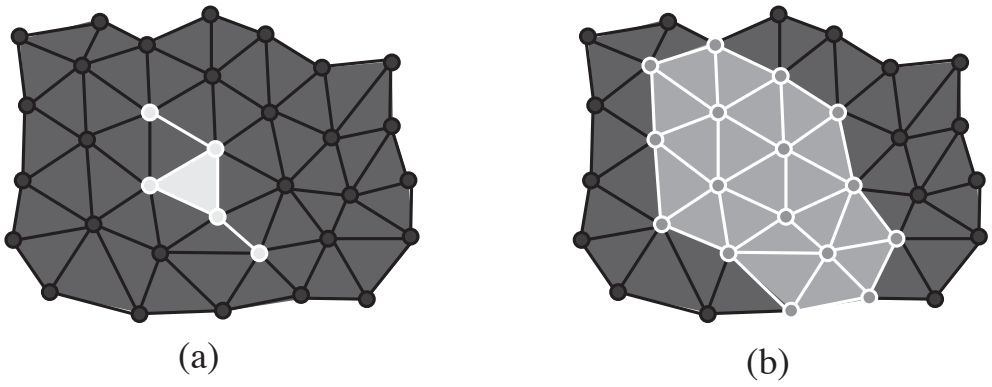

Figure 16.: From a subcomplex to its simplicial neighborhood ([42], p. 46)

Property 10. *Let Λ be a countable space of arbitrary elements, and let C be a simplicial complex in Λ. Then, for any $s \in C$, the rank of any k-simplex in $|C|$ is $\rho(s, |C|) = k$.*

In other words, the dimension of an abstract simplex equals its rank into the simplicial complex it belongs to.

Property 11. *Let Λ be a countable space of arbitrary elements, and let C be a simplicial complex in Λ. Then, for any $s \in C$, $\alpha(s)$ is a simplicial complex. Also, let S be a subset of C, the set $\alpha(S) = \bigcup_{s \in S} \alpha(s)$ is a simplicial complex.*

Since we have defined the closure α_C in a simplicial complex C, we have induced the definition of its inverse binary relation $\beta_C = \alpha_C^{-1}$, called the *star operator* (in C):

$$\forall s \in C, \beta_C(s) = \{t \in C \; ; \; s \subseteq t\}.$$

Note that, contrary to the closure operator α, we cannot simplify this notation, since $\beta_C(s)$ clearly depends on the structure of the simplicial complex C.

C.14 SIMPLICIAL NEIGHBORHOODS

Definition 105 (Simplicial neighborhood)**.** *Let Λ be a countable space of arbitrary elements, let C be a simplicial complex in Λ, and let be K a subcomplex of C. We denote by $N(K, C)$ the* simplicial neighborhood *of the subcomplex K into the simplicial complex C, and we define it such as:*

$$N(K, C) = \bigcup_{s \in K} \alpha(\beta_C(s)).$$

Property 12. *Let C be a simplicial complex and let K be a subcomplex of C. Then then simplicial neighborhoord $N(K, C)$ of K in C is a simplicial complex.*

Subfigure (a) of Figure 16 depicts in dark gray a simplicial complex C, and in light gray a simplicial subcomplex K of C. Subfigure (b) depicts in light gray the closure of the star of K in C, that is, $N(K, C)$.

C.15 CHAIN COMPLEXES

Now that we have defined simplices, simplicial complexes and subcomplexes, we can define *chain complexes*.

Definition 106 (Chain)**.** *Let $|X| = (X, \alpha_X)$ be a partially ordered set. Any subset c of X such that $|c| = (c, \alpha_c)$ is totally ordered is called a* chain *of $|X|$.*

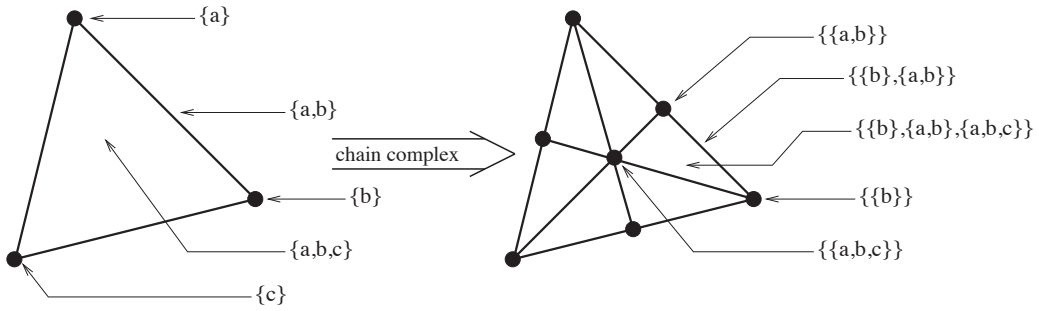

Figure 17.: From an order to its chain complex ([42], p. 46)

Definition 107 (Chain complex)**.** *Let $|X| = (X, \alpha_X)$ be a partially ordered set. Then the set of all the chains of $|X|$ is denoted by $\mathcal{C}^X$ and is called the* chain complex *of $|X|$.*

Property 13. *Let $|X| = (X, \alpha_X)$ be a partially ordered set. Then $\mathcal{C}^X$ is a simplicial complex, and its support is equal to X.*

Effectively, for any element $s \in \mathcal{C}^X$, each face of s belongs to $\mathcal{C}^X$ since it is also a total order. This way, $\mathcal{C}^X$ is closed by the inclusion order, and is a simplicial complex. Also, $\mathcal{C}^X$ is the set of the subsets of X which are totally ordered (in $|X|$), and in this manner its support is the set of the elements in X, that is, X itself.

Figure 17 shows on the right an order $|X|$ made of all the simplices in $\Lambda = \{a, b, c\}$ and on the right its chain complex $\mathcal{C}^X$. Since any set made of only one element is totally ordered, obviously $\{\{a\}\}$, $\{\{b\}\}$, $\{\{c\}\}$, $\{\{a, b\}\}$, $\{\{b, c\}\}$, $\{\{a, c\}\}$, and $\{\{a, b, c\}\}$ belong to $\mathcal{C}^X$. Also, $\{\{a\}, \{a, b\}\}$ is made of $\{a\}$ and $\{a, b\}$ which belong both to X and are ordered in $|X|$, and then $\{\{a\}, \{a, b\}\}$ belongs to $\mathcal{C}^X$. We can continue this way until we obtain the simplicial complex $\mathcal{C}^X$.

Now that we have defined chain complexes, we can cite a fundamental theorem of Daragon [42], based of prerequisites defined in Section C.8:

Theorem 16 (Theorem 17 (p. 58 of [42]))**.** *Let $|X|$ be an order. Then, $|\mathcal{C}^X|$ is a n-surface iff $|X|$ is a n-surface.*

Intuitively, this theorem means that if an order is a discrete surface, then its "triangulation", that is, its decomposition into triangles, is also a discrete surface, and, conversely, if a "triangulation" of an order is a n-surface, this order is a n-surface too.

C.16 FRONTIER ORDERS

Definition 108 (Frontier orders [42])**.** *Let C be a simplicial complex, and Λ_C its support. Let us decompose now Λ_C into the union of K the* foreground *and K' the* background*:*

$$\Lambda_C = K \sqcup K'.$$

Then C can be decomposed into 3 disjoint parts: C_K which is the set of the simplices contained into K, $C_{K'}$ which is the set of simplices contained into K', and $C_{K/K'}$ which is the set of simplexes not contained into K and not contained into K'. Then $|C_{K/K'}| = (C_{K/K'}, \supseteq)$ is called the frontier order *of K into Λ_C relatively to C.*

Note that a frontier order is not a simplicial complex: since any vertex belongs either to K or to K', it does not belong to $C_{K/K'}$.

Subfigure a) of Figure 18 depicts a simplicial complex C; Subfigure b) depicts a subset K of the support of C (c.f. the white points); Subfigure c) depicts the tripartition of C into K

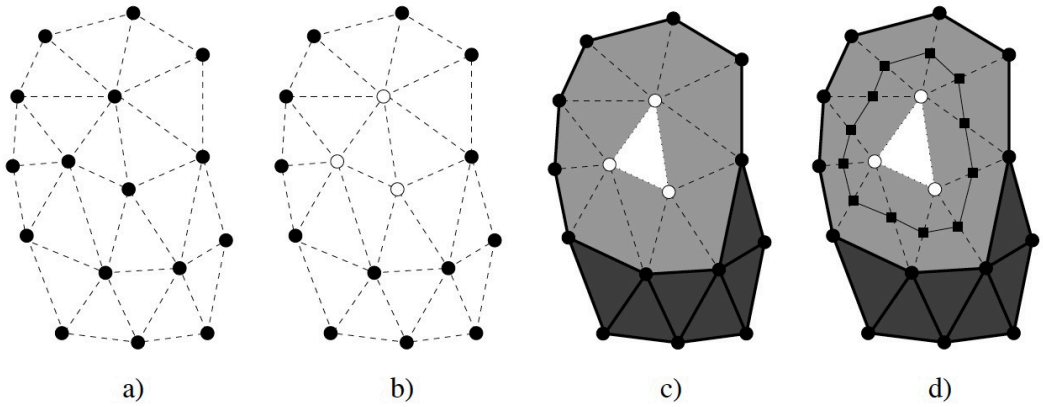

Figure 18.: From a simplicial complex to a frontier order ([42], p. 86)

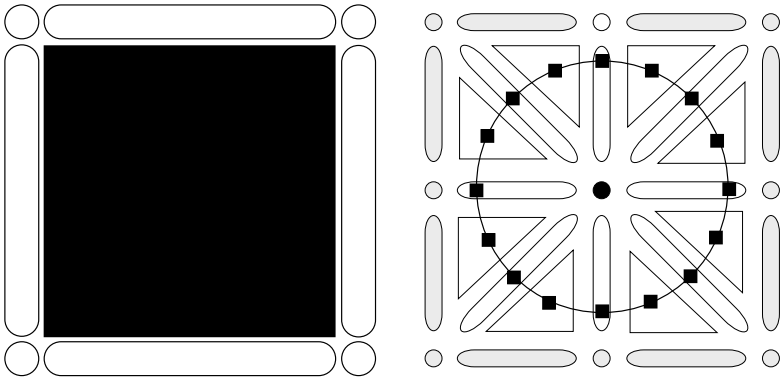

Figure 19.: A cubical complex and the frontier order of the central square into this order

in white, K' in dark gray, and the frontier order $C_{K/K'}$ in light gray; Subfigure $d)$ depicts the "immersion" of the frontier order represented with black squares and the edges that link them.

The definition of a frontier order exists also for any order [42].

Definition 109. *Let $|X|$ be an order, and let $|Y|$ and $|Y'|$ be two suborders of $|X|$ such that $Y \sqcup Y' = X$. The order $|\mathcal{C}^X_{Y/Y'}| = (\mathcal{C}^X_{Y/Y'}, \supseteq)$, where $\mathcal{C}^X_{Y/Y'}$ denotes the set of simplices of $\mathcal{C}^X$ such that they are not contained into Y and not contained into Y', is called the* frontier order *of $|Y|$ into $|X|$.*

Figure 19 depicts a cubical complex $|X|$ (on the left), where X is decomposed into $Y \sqcup Y'$. Y is depicted by the black square, and Y' corresponds to $X \setminus Y$ (the white faces of the complex). Then, by computing the chain complex of this order, we obtain the right figure, where the complex whose support is Y is made of the black vertex, the greatest complex whose support is Y' is made of the gray vertices and edges, and the remaining part of the chain complex is the frontier order $\mathcal{C}^X_{Y/Y'}$ whose *immersion* is represented with the black squares and the black edges linking them.

Theorem 17 (Frontier orders of a simplicial complex [42] (Theorem 37 p. 89))**.** *Let C be a simplicial complex which is a n-surface, $n \geq 2$, and let be Λ_C its support. Let K be a strict non-empty subset of Λ_C. Then the order $|C_{K/K'}|$ is an union of disjoint $(n-1)$-surfaces.*

Theorem 18 (Frontier orders of an order [42] (Theorem 38 p. 90))**.** *Let $|X|$ be an order which is a n-surface, and let $|Y|$ be a strict suborder of $|X|$. Then the order frontier $|\mathcal{C}^X_{Y/Y'}|$ is a disjoint union of $(n-1)$-surfaces.*

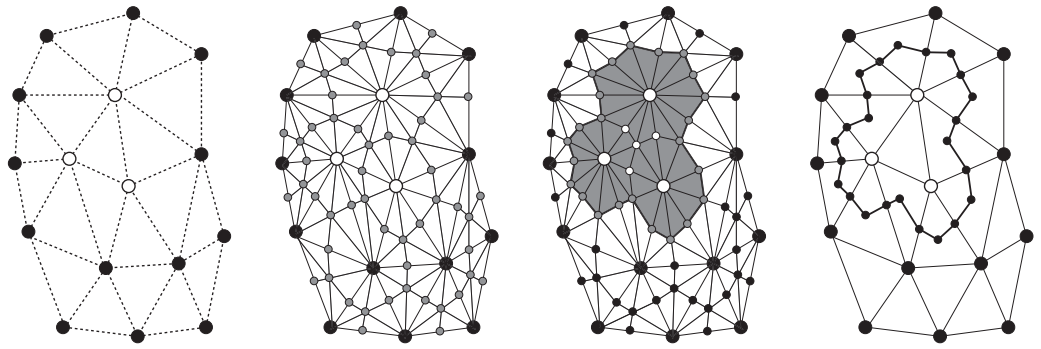

Figure 20.: From a full subcomplex to its derived neighborhood ([42], p. 98)

C.17 DERIVED NEIGHBORHOODS

As we are going to recall, a chain complex can be effectively seen as a triangulation.

Definition 110 (Derived subdivision)**.** *Let C be a simplicial complex. The first* derived subdivision *of C is denoted C^1 and is defined such that:*

$$C^1 = \{\{c_0, \ldots, c_n\} \subseteq C \ ; \ c_0 \subset \cdots \subset c_n\}.$$

The n^{th} derived subdivision *is defined such that:*

$$C^n = (C^{n-1})^1.$$

As we can see, the first derived of a simplicial complex C is simply its chain complex $\mathcal{C}^C$.

Definition 111 (Derived neighborhood)**.** *Let C be a simplicial complex of support Λ_C. Let also K be a full subcomplex of C such that its support Λ_Y satisfies $\Lambda_Y \subseteq \Lambda_X$. The* first derived neigborhood *of K in C is denoted by $N^1(K, C)$ and is equal to the simplicial neighborhood of K^1 into C^1:*

$$N^1(K, C) = \bigcup_{k^1 \in K^1} \alpha(\beta_{C^1}(k^1)).$$

Figure 20 shows the step-by-step process to compute a derived neighborhood of a subcomplex K which is full in a simplicial complex C. On (a), the entire figure corresponds to the simplicial complex C, and the triangle whose corners are white, with all its faces, corresponds to the full subcomplex K. Then, in (b), a derived subdivision is processed. It is equivalent to compute the chain complex of C. On (c), we can see in light gray the derived neighborhood of K which is equal to the union of the closures of the stars of K^1 into C^1. On (d), we can see the *border* of the derived neighborhood of K in C, its definition will come hereafter.

C.18 BORDER OF A DERIVED NEIGHBORHOOD

Let us now recall the definition of a border, since it is the link between a derived neighborhood and a frontier order.

Definition 112 (Border of a derived neighborhood (p. 98 [42]))**.** *Let C be a simplicial complex and K be a full subcomplex of C. The* border *of the derived neighborhood of K into C is denoted by $\Delta(K, C)$ and is equal to:*

$$\Delta(K, C) = \left\{h \in N^1(K, C) \ ; \ \beta_{C^1}(h) \not\subseteq N^1(K, C)\right\}.$$

Theorem 19 (Theorem 40 (p. 99 [42])). *Let X be a simplicial complex of support Λ_X, let Y be a full subcomplex of X of support K, and let K' be the complement of K into Λ_X. Then $\Delta(Y, X)$ is equal to the chain complex of the frontier order $X_{K/K'}$, that is:*

$$\Delta(Y, X) = [X_{K/K'}]^1.$$

In other words, the chain complex of the frontier order is equal to the border of the derived neighborhood.

Combined with Theorem 16, Theorem 17, and Theorem 19, Daragon obtains that:

Theorem 20 (Theorem 42 (p. 101 [42])). *Let X be a simplicial complex. If X is a n-surface, $n \geq 1$, and if Y is a subcomplex full in X, then $\Delta(Y, X)$ is a disjoint union of $(n-1)$-surfaces.*

C.19 PLAIN MAPS

Let us now recall some mathematical background coming from [10, 127].

Let $\mathcal{A} = (X, \mathcal{U})$ be an Alexandrov space.

Definition 113. *An application $F : X \to \mathcal{P}(\mathbb{R})$ (which is also written $F : X \rightsquigarrow \mathbb{R}$) is said to be a* set-valued map. *The* domain *of F is the set $\mathcal{D}(F) \subseteq X$ such that $\forall x \in X$, $F(x) \neq \emptyset \Leftrightarrow x \in \mathcal{D}(F)$.*

Definition 114. *A set-valued map $F : X \rightsquigarrow \mathbb{R}$ is said to be* upper semi-continuous (USC) *at $x \in \mathcal{D}(F)$, for any neighborhood $\mathcal{U}$ of $F(x)$, $\forall x' \in \beta(x)$, $F(x') \subseteq \mathcal{U}$. A set-valued map is said to be* upper semi-continuous (USC) *iff it is USC at each point $x \in \mathcal{D}(F)$.*

Definition 115. *A set-valued USC map $F : X \rightsquigarrow \mathbb{R}$ is said to be a* (closed) quasi-simple map *iff for any $x \in \mathcal{D}(F)$, $F(x)$ is a closed connected set and furthermore, for any $x \in \mathcal{D}(F)$ such that $\{x\} = \beta(x)$, $F(x)$ is degenerate.*

Definition 116. *A quasi-simple map $F : X \rightsquigarrow \mathbb{R}$ is said to be a* simple map *iff for any quasi-simple map $F_2 : X \rightsquigarrow \mathbb{Z}$ such that $F(x) = F_2(x)$ when $x \in \mathcal{D}$ is such that $\beta(x) = \{x\}$, then for any $x \in \mathcal{D}(F)$, $F(x) \subseteq F_2(x)$.*

Definition 117. *A set-valued map $F : X \rightsquigarrow \mathbb{R}$ is said to be a* plain map *iff it is a closed-valued interval-valued simple map.*

Now, let us assume that A and B are two topological spaces.

Definition 118. *Let $F : A \rightsquigarrow B$ be a set-valued map. We call the* inverse image *of M by F the set $F^-(M) = \{x \in A \ ; \ F(x) \cap M \neq \emptyset\}$. Also, we call* core *of M by F the set $F^+(M) = \{x \in A \ ; \ F(x) \subseteq M\}$.*

Then some properties [10] follow for USC maps:

Proposition 33. *A set-valued map $F : A \rightsquigarrow B$ is USC at x iff the core of any neighborhood of $F(x)$ is a neighborhood of x. Hence, a set-valued map $F : A \rightsquigarrow B$ is USC iff the core of any open subset is open.*

Proposition 34. *If $\mathcal{D}(F)$ is closed, then F is USC iff the inverse image of any closed set is closed.*

D

ABOUT THE EQUIVALENCE BETWEEN AWCNESS AND DWCNESS

Today, 4D signals (and beyond) are of primary importance, and then it is crucial to determine the relations between the different definitions in matter of well-composedness. In this section, we investigate the relation between digital well-composedness and well-composedness in the sense of Alexandrov. In fact, if these two definitions are equivalent, it means that well-composed in the sense of Alexandrov images can easily be obtained on cubical grids thanks to digitally well-composed interpolations, and conversely, that digitally well-composed images share the strong topological properties of images that are well-composed in the sense of Alexandrov when they are immersed into Khalimsky grids.

So, in the following sections, after having presented a counter-example showing that this proof is not straightforward, we will present a sketch of the proof.

Note that the complete proof can be found at the following address:
https://hal-upec-upem.archives-ouvertes.fr/hal-01375621

Note: since this proof has not been verified yet, it will be considered in this thesis as a conjecture.

D.1 PREAMBLE

Before beginning the study of the equivalence between these two kinds of well-composednesses, we propose to illustrate the difficulty of this proof with an example. Let $X \subset \mathbb{Z}^n$ be a digitally well-composed set, and let S be a block of $\mathbb{Z}^n$. Now let us denote by $l \in \mathbb{N}$ the number of points of $X \cap S$, and let us denote by $(X_i)_{i \in [\![0,l]\!]}$ the sequence such that $X_0 = \emptyset$, and such that $X_i = X_{i-1} \sqcup \{p_i\}$ for $i \in [\![1,l]\!]$ with $p_i \in X \cap S$. Intuitively, we could assume that there always exists a sequence such that $X_l = X \cap S$ and such that X_i is digitally well-composed for any $i \in [\![0,l]\!]$. However, Figure 1 contradicts this assumption. Effectively, removing/adding any point to this set made of yellow points linked by blue edges creates a critical configuration of dimension 2. Then, there exists no strictly increasing/decreasing sequence of digitally well-composed sets which converges to this set in this manner.

D.2 A SKETCH OF THE PROOF

Let us present the main steps of the proof that AWCness (see Section 3.1) and DWCness are equivalent on cubical grids.

FROM $\left(\frac{\mathbb{Z}}{2}\right)^n$ TO $\mathbb{H}^n$ We define the bijection $\mathcal{H} : (\mathbb{Z}/2) \to \mathbb{H}^1$ such that:

$$\forall z \in (\mathbb{Z}/2), \mathcal{H}(z) = \begin{cases} \{z + 1/2\} & \text{if} \quad z \in (\mathbb{Z}/2) \setminus \mathbb{Z}, \\ \{z, z+1\} & \text{if} \quad z \in \mathbb{Z}. \end{cases}$$

We can then deduce the bijection $\mathcal{H}_n : \left(\frac{\mathbb{Z}}{2}\right)^n \to \mathbb{H}^n$ defined such that:

$$\mathcal{H}_n(z) = \otimes_{i \in [\![1,n]\!]} \mathcal{H}(z_i),$$

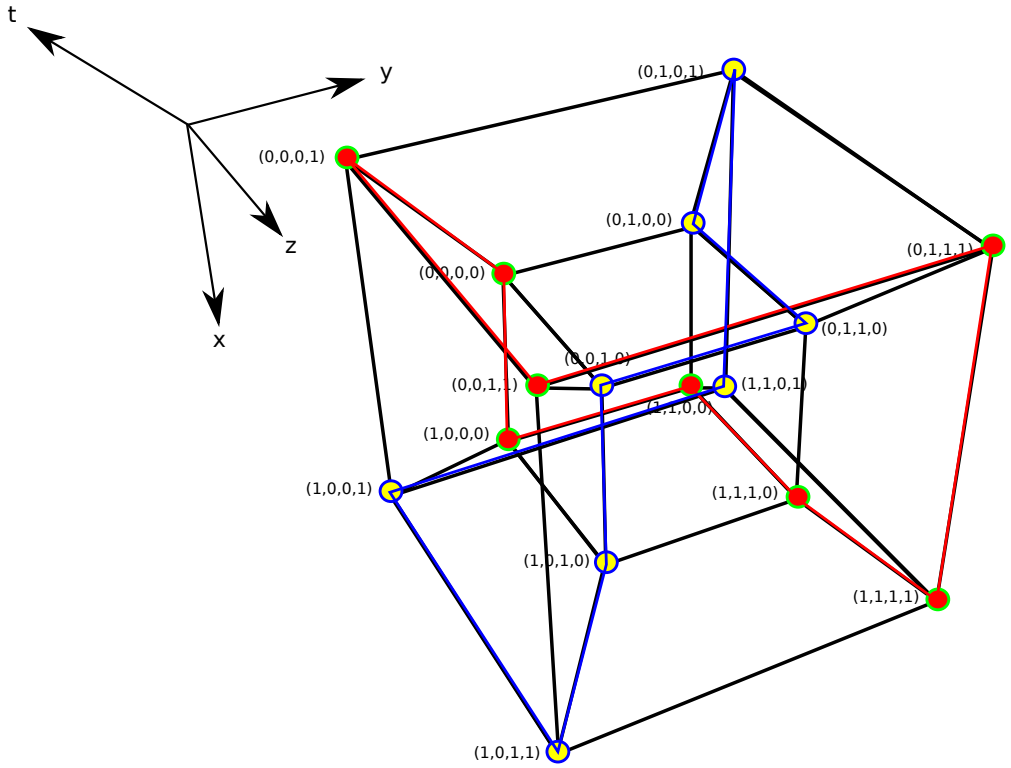

Figure 1.: A 4D digitally well-composed set (depicted in blue) and its complement (in red)

where z_i denote the i^{th} coordinate of $z \in \left(\frac{\mathbb{Z}}{2}\right)^n$.

We can compute the inverse bijection of $\mathcal{H}$, that we denote by $\mathcal{Z} : \mathbb{H}^1 \to (\mathbb{Z}/2)$, and defined such that:

$$\forall h \in \mathbb{H}^1, \mathcal{Z}(h) = \begin{cases} a & \text{if} \quad \exists a \in \mathbb{Z} \text{ s.t. } h = \{a, a+1\}, \\ a - 1/2 & \text{if} \quad \exists a \in \mathbb{Z} \text{ s.t. } h = \{a\}. \end{cases}$$

We can then deduce the bijection $\mathcal{Z}_n : \mathbb{H}^n \to \left(\frac{\mathbb{Z}}{2}\right)^n$ defined such that:

$$\mathcal{Z}_n(h) = \otimes_{i \in [\![1,n]\!]} \mathcal{Z}(h_i),$$

where h_i denote the i^{th} coordinate of $h \in \mathbb{H}^n$.

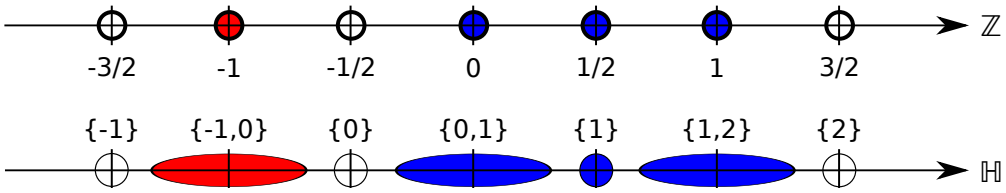

Figure 2.: Bijection between $\mathbb{H}^1$ and $(\mathbb{Z}/2)$

Figure 2 shows how $(\mathbb{Z}/2)$ is mapped to $\mathbb{H}^1$. Furthermore, it can be shown that supplying $\left(\frac{\mathbb{Z}}{2}\right)^n$ with a particular topology, $\mathcal{Z}_n$ (respectively $\mathcal{H}_n$) is in fact a *topological isomorphism*, that is a bicontinuous bijection, between $\mathbb{H}^n$ and $\left(\frac{\mathbb{Z}}{2}\right)^n$ (respectively between $\left(\frac{\mathbb{Z}}{2}\right)^n$ and $\mathbb{H}^n$). In other words, these two spaces have the same topological structure.

IMMERSION INTO KHALIMSKY GRIDS Starting from a given digital set $X \subset \mathbb{Z}^n$, we can immerse it into $\mathbb{H}^n$ in the following manner:

$$\mathcal{IMM}(X) \equiv \mathrm{Int}(\alpha(\mathcal{H}_n(X))),$$

where Int it the topological interior in $\mathbb{H}^n$:

$$\mathrm{Int}(X) = \{h \in X \; ; \; \beta(h) \subseteq X\}.$$

STATING THE PROBLEM The context is the following: we have a set X made of points in $\mathbb{Z}^n$, from which we compute its immersion $\mathcal{IMM}(X)$ in the Khalimsky grids. X is digitally well-composed iff it does not contain any critical configuration, and X (or its immersion $\mathcal{IMM}(X)$ by identification) is said well-composed in the sense of Alexandrov iff the topological boundary $\mathfrak{N}$ of $\mathcal{IMM}(X)$ defined such as:

$$\mathfrak{N} = \alpha(\mathcal{IMM}(X)) \cap \alpha(\mathbb{H}^n \setminus \mathcal{IMM}(X)),$$

is made of disjoint discrete $(n-1)$-surfaces.

We want to establish that these two concepts are equivalent.

REFORMULATING THE TOPOLOGICAL BOUNDARY The topological boundary $\partial\mathcal{IMM}(X)$ can be reformulated as a function of $\mathcal{X} = \mathcal{H}_n(X)$ and the complement $\mathcal{Y} = \mathbb{H}^n_n \setminus \mathcal{X}$ of $\mathcal{X}$ in $\mathbb{H}^n_n$. Effectively, we have the following proposition:

$$\mathfrak{N} = \alpha(\mathcal{X}) \cap \alpha(\mathcal{Y}).$$

Summarily, we can reformulate this way the boundary because these following properties are verified in $\mathbb{H}^n$:

- $\mathbb{H}^n$ is a n-surface and then is homogeneous,
- $\forall z \in \mathbb{H}^n$, $\alpha(\beta(z) \cap \mathbb{H}^n_n) = \alpha(\beta(z))$,
- $\forall z \in \mathbb{H}^n$, $\alpha(z)$ is a regular closed set,
- $\forall z \in \mathbb{H}^n$, $\beta(z)$ is a regular open set.

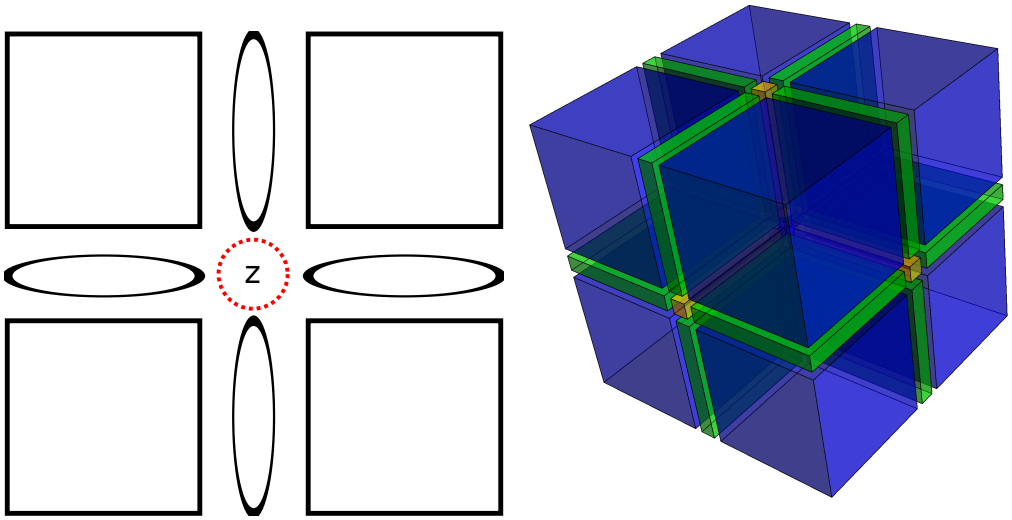

Figure 3.: The subspace $|\beta^{\square}(z)|$ we are working in to study AWCness (2D/3D cases)

REFORMULATING THE PROBLEM IN A LOCAL WAY We could then directly prove that the fact that $\mathcal{IMM}(X)$ is well-composed in the sense of Alexandrov implies that X is digitally

well-composed, and the converse, and we would be done. However, we observed that we can reformulate the condition "$\mathcal{IMM}(X)$ is well-composed in the sense of Alexandrov" with another condition, much simpler to handle and manipulate, since it is a local criteria, like digital well-composedness. Effectively, $\mathcal{IMM}(X)$ is well-composed in the sense of Alexandrov if and only if:

$$\left\{\forall z \in \mathfrak{N}, |\beta^{\square}_{\mathfrak{N}}(z)| \text{ is a } (n-2-\dim(z))-\text{surface}\right\}.$$

Since $|\beta^{\square}_{\mathfrak{N}}(z)|$ is equal to $|\mathfrak{N} \cap \beta^{\square}(z)|$, we understand effectively that we are studying a restriction of the boundary $\mathfrak{N}$ in a small subspace, that is, $|\beta^{\square}(z)|$, depicted on Figure 3, where we can observe that the point z in the middle of the subspace has been omitted, since it is not taken into account in the local criteria.

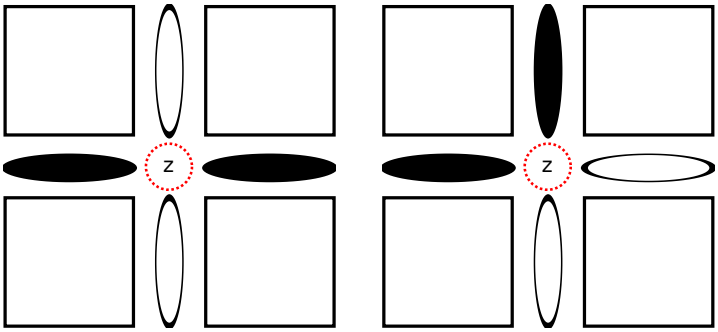

Figure 4.: Examples of 0-surfaces (in black)

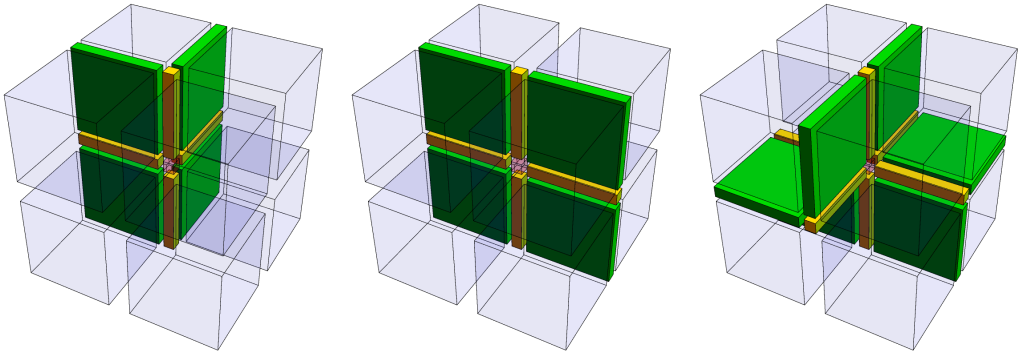

Figure 5.: Examples of 1-surfaces

The question is then: what does the fact that $|\beta^{\square}_{\mathfrak{N}}(z)|$ is an $(n-2-\dim(z))$-surface represent? When $\dim(z) = (n-2)$, that is, when $\beta(z)$ is a subspace of dimension 2 as on the left of Figure 3, it means that $|\beta^{\square}_{\mathfrak{N}}(z)|$ is a 0-surface, that is, the restriction $|\beta^{\square}_{\mathfrak{N}}(z)|$ of the boundary $\mathfrak{N}$ to the subspace $\beta^{\square}(z)$ is made of two elements which are not neighbors the one of the other one (see Figure 4). When $\dim(z) = (n-3)$, that is when $\beta(z)$ is a subspace of dimension 3 as on the right of Figure 3, it means that the restriction $|\beta^{\square}_{\mathfrak{N}}(z)|$ of the boundary $\mathfrak{N}$ to the 3D subspace $\beta^{\square}(z)$ is a 1-surface, that is, is a simple closed curve (see Figure 5).

Our aim is then to prove that X is digitally well-composed iff for any element z of the boundary $\mathfrak{N}$, we have that $|\beta^{\square}_{\mathfrak{N}}(z)|$ is a $(n-\dim(z)-2)$-surface.

STUDY OF THE CONVERSE SENSE Let us begin with the converse sense: we admit that for any element z of the boundary $\mathfrak{N}$, we have that $|\beta^{\square}_{\mathfrak{N}}(z)|$ is a $(n-\dim(z)-2)$-surface, and we want to prove that X is digitally well-composed. For that, we will prove the counterposition: we assume that X is not digitally well-composed, and then contains a critical configuration, and we show that it implies that there exists a "critical point" z^* such that $|\beta^{\square}_{\mathfrak{N}}(z^*)|$ is not a discrete surface.

So, let assume that X contains a primary critical configuration in a block S of dimension $k \geq 2$, that is, $X \cap S = \{p, p'\}$ such that p and p' are antagonist into S (the secondary case follows the same reasoning, by duality of well-composedness in the sense of Alexandrov and digital well-composedness). It is then clear that all the other points of the block S belong to the complement Y of X in $\mathbb{Z}^n$.

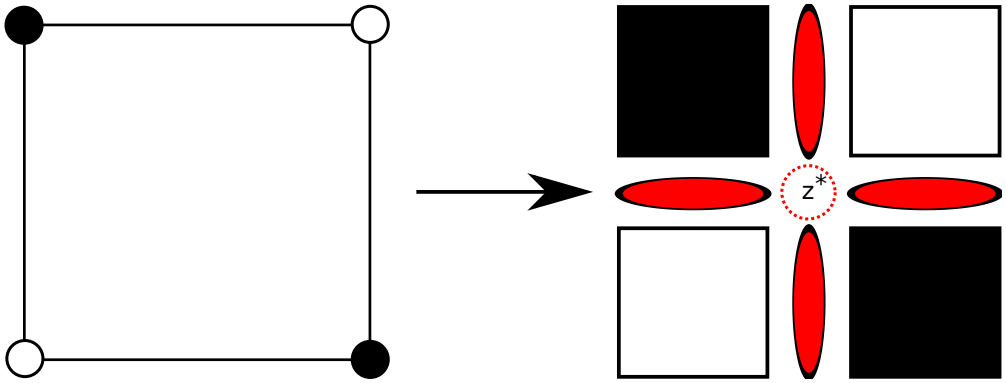

Figure 6.: From a 2D critical configuration in $\mathbb{Z}^2$ to a critical point z^* in $\mathbb{H}^2_0$

Let us begin with the 2D case, that is, when the block S is of dimension $k = 2$ in $\mathbb{Z}^n$. In this case, its isomorph in $\mathbb{H}^n$, which is made of n-cubes, can be represented using squares, as depicted on Figure 6. Then, the center of these four squares, that we will call z^*, has a dimension $(n-2)$. Let us show that this point is critical in the sense that $|\beta^{\square}_{\mathfrak{N}}(z)|$ is not a 0-surface. For that, as shown on Figure 6, we work into the space $\beta^{\square}(z^*)$, which contains our four colored squares, and we compute their respective closures (into the subspace $\beta^{\square}(z^*)$), their intersection will then be $\beta^{\square}_{\mathfrak{N}}(z^*)$. Effectively, $|\beta^{\square}_{\mathfrak{N}}(z^*)|$ is not a o-surface, because it is made of 4 points and a o-surface is made of two points, then z^* is "critical" and we have proven the reciprocal sense for $k = 2$.

Let us now proceed to the 3D case, that is, when the block S is of dimension $k = 3$ in $\mathbb{Z}^n$. In this case, its isomorph in $\mathbb{H}^n$ can be represented using cubes, as depicted on Figure 7. Then, the center z^* of these 8 cubes has a dimension $(n-3)$ and is critical in the sense that $|\beta^{\square}_{\mathfrak{N}}(z^*)|$ is an union of two disjoint 1-surfaces, and then it is not a 1-surface. So we proved the case $k = 3$ too.

In fact, for the general case $k \in [\![2, n]\!]$, it can be proven that, if we denote by $\mathfrak{p}$ (respectively $\mathfrak{p}'$) the isomorphism of the points p (respectively p') into $\mathbb{H}^n$, starting from the formulation $\mathfrak{N} = \alpha(\mathcal{X}) \cap \alpha(\mathcal{Y})$, we obtain:

$$\beta^{\square}_{\mathfrak{N}}(z^*) = \left(\alpha^{\square}(\mathfrak{p}) \cup \alpha^{\square}(\mathfrak{p}')\right) \cap \beta^{\square}(z^*),$$

which can be decomposed into two orders $|\alpha^{\square}(\mathfrak{p}) \cap \beta^{\square}(z^*)|$ and $|\alpha^{\square}(\mathfrak{p}') \cap \beta^{\square}(z^*)|$ which are disjoint $(n-2-\dim(z))$-surfaces, and then their union is not a $(n-2-\dim(z))$-surface.

STUDY OF THE DIRECT SENSE Since we have explained how we proceed in the counter-sense, let us show how we proceed in the direct sense.

We want to prove that if X is digitally well-composed, then $\mathcal{IMM}(X)$ is well-composed in the sense of Alexandrov, which can be proven by the fact that for any element z of the boundary $\mathfrak{N}$, we have that $|\beta^{\square}_{\mathfrak{N}}(z)|$ is a $(n-\dim(z)-2)$-surface. In fact, we will proceed by induction. We define the property $(\mathcal{P}_k)$ such that if this property is true for any value $k \in [\![1, n]\!]$, then X is well-composed in the sense of Alexandrov:

$$(\mathcal{P}_k) = \left\{\forall z \in \mathfrak{N} \cap \mathbb{H}^n_{n-k},\ |\beta^{\square}_{\mathfrak{N}}(z)| \text{ is a } (n-2-\dim(z)) - \text{surface}\right\}.$$

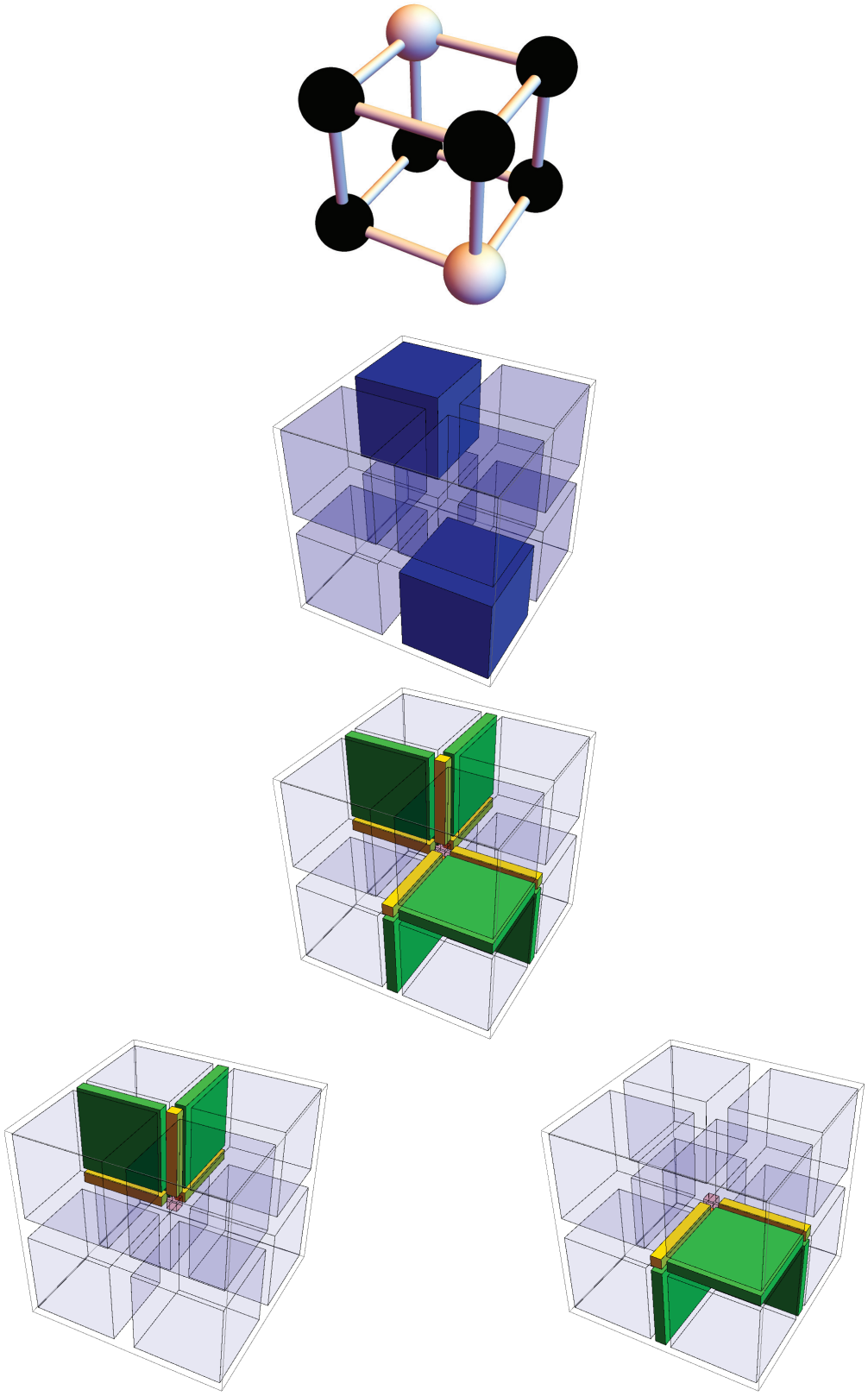

Figure 7.: From the 3D critical configuration to the critical point

Obviously, the case $k = 0$ is not necessary, since no point of the boundary $\mathfrak{N}$ is a n-cube.

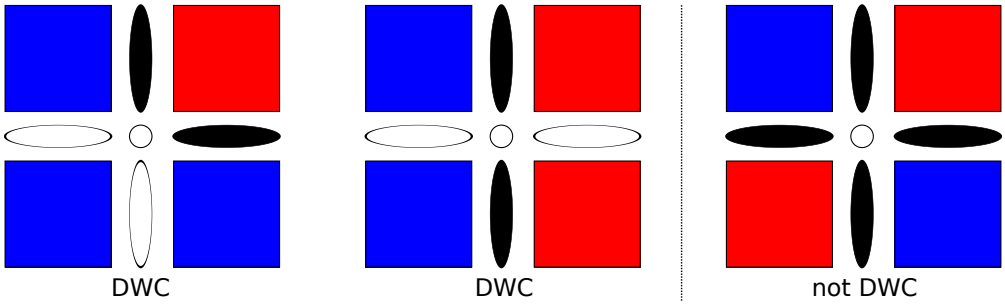

Figure 8.: Assuming that X is DWC, $|\beta^{\square}_{\mathfrak{N}}(z)|$ is a 0-surface when $\dim(z) = n - 2$

So let start with $k = 1$: in this case, z is a $(n-1)$-face, and then $\beta^{\square}(z)$ is empty, which means that $|\beta^{\square}_{\mathfrak{N}}(z)|$ is a (-1)-surface since it is the empty order. Let us continue with $k = 2$. In this case, z is a $(n-2)$-face, and then it is sufficient to proceed cases by case (modulo symmetry, rotation, and complementation), as shown bony Figure 8. The isomorphism of X restricted to $\beta^{\square}(z)$ is depicted using blue faces, and the isomorphism of $Y = \mathbb{Z}^n \setminus X$ restricted to $\beta^{\square}(z)$ is depicted using red faces. Since we have the relation $\mathfrak{N} = \alpha(\mathcal{X}) \cap \alpha(\mathcal{Y})$, we obtain in the two DWC cases (on the left and at the middle) that the intersection of the closure of the blue faces and the closure of the red faces is a 0-surface in $\beta^{\square}(z)$ (depicted in black), since its restriction to $\beta^{\square}(z)$ is made of two points which are not neighbors the one of the other one. The case $k = 2$ is then treated.

When $k \in [\![3, n]\!]$, we can proceed by induction on k since the initialization succeeded. So let us assume that $k \in [\![3, n]\!]$ is given and that the property $(\mathcal{P}_l)$ is true for any $l \in [\![1, k-1]\!]$, we want to prove it for k.

In this case, z is a $(n-k)$-face with $k \geq 3$, which means that $\dim(z) \leq (n-3)$, and then $(n - 2 - \dim(z)) \geq 1$. It is clear then that $|\beta^{\square}_{\mathfrak{N}}(z)|$ is a $(n - 2 - \dim(z))$-surface iff we have two conditions: (1) $|\beta^{\square}_{\mathfrak{N}}(z)|$ must be connected, and (2) for any point u of $\beta^{\square}_{\mathfrak{N}}(z)$, $|\theta^{\square}_{\beta^{\square}_{\mathfrak{N}}(z)}(u)|$ must be a $(n - 3 - \dim(z))$-surface.

Even if the second condition seems to be much more complicated than the first one, it is in fact the converse. Effectively, it it easy to prove by a simple calculus that $|\theta^{\square}_{\beta^{\square}_{\mathfrak{N}}(z)}(u)|$ is equal to:

$$|\beta^{\square}_{\mathfrak{N}}(u)| * \left|\alpha^{\square}(u) \cap \beta^{\square}(z)\right|,$$

which corresponds to an order join of $|\beta^{\square}_{\mathfrak{N}}(u)|$, which is a $(n - 2 - \dim(u))$-surface by the induction hypothesis, and of

$$\left|\alpha^{\square}(u) \cap \beta^{\square}(z)\right|,$$

which is a $(\dim(u) - \dim(z) - 2)$-surface (the proof is left to the reader). Since an order join of a k_1-surface and of a k_2-surface is a $(k_1 + k_2 + 1)$-surface by Theorem 14, $|\theta^{\square}_{\beta^{\square}_{\mathfrak{N}}(z)}(u)|$ is a $(n - 3 - \dim(z))$-surface. Then (2) is proven.

To prove (1), we assume that there exists $z \in \mathbb{H}^n_{n-k}$ such that $|\beta^{\square}_{\mathfrak{N}}(z)|$ is <u>not</u> connected. We will see that this hypothesis is essential, since many properties will follow on, until we reach a contradiction.

Assuming $|\beta^{\square}_{\mathfrak{N}}(z)|$ is not connected obviously means that it is made of several connected components, that we will denote by $\{F_i\}_{i \in \mathcal{I}}$. The first fundamental property is that each component F_i, $i \in \mathcal{I}$, is a $(n - 2 - \dim(z))$-surface because they are connected (by definition) and because we can prove that for any $u \in F_i$, we have $|\theta^{\square}_{F_i}(u)|$ which is equal to $|\theta^{\square}_{\beta^{\square}_{\mathfrak{N}}(z)}(u)|$, which is a $(n - 3 - \dim(z))$-surface.

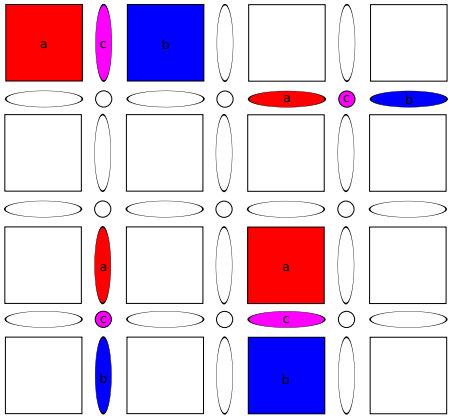

Figure 9.: Examples of opposites in $\mathbb{H}^2$

Starting from this first property, a second fundamental property follows on: for $i \in \mathcal{I}$, a same component F_i cannot contain *opposite* faces relatively to z. Roughly speaking, opposite faces are two faces which are symmetrical relatively to a third face (see Figure 9). Effectively, we can feel that if one first component contains two opposite face in $\beta^{\square}(z)$, it will separate any other component of $|\beta^{\square}_{\mathfrak{R}}(z)|$, which is impossible since each F_i is connected by hypothesis.

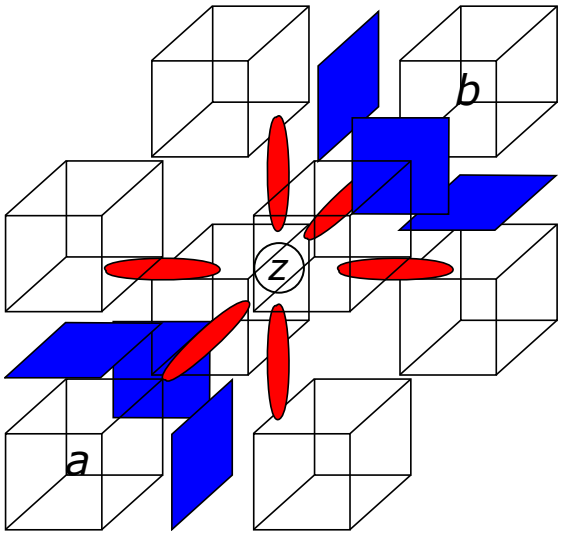

Figure 10.: Structure of $\beta^{\square}_{\mathfrak{R}}(z)$ when we have $(n - \dim(z)) = 3$ assuming that $|\beta^{\square}_{\mathfrak{R}}(z)|$ is not connected

Now that we know that each component F_i cannot contain two opposite faces, the third fundamental property can be proven: each of them contains exactly $(n - \dim(z))\ (\dim(z) + 1)$-faces of $\beta^{\square}(z)$. For example, in the 3D case, that is for $\dim(z) = (n - 3)$ as on Figure 10, where $(\dim(z) + 1)$-faces are depicted in red, each component contains exactly 3 $(\dim(z) + 1)$-faces. Since there are $2(n - \dim(z))$ of these faces in $\beta^{\square}(z)$, $|\beta^{\square}_{\mathfrak{R}}(z)|$ is made of 2 components F_1 and F_2.

Using these three fundamental properties, it can be proven that each of these two components F_1 and F_2 lies in the closure of *characteristical* n-faces $\mathfrak{a}, \mathfrak{b} \in \mathbb{H}^n_n$ that we define here as the supremum of the $(\dim(z) + 1)$-faces contained in each of them. More precisely, $|F_1| \subseteq \left|\alpha^{\square}(\mathfrak{a}) \cap \beta^{\square}(z)\right|$ and $|F_2| \subseteq \left|\alpha^{\square}(\mathfrak{b}) \cap \beta^{\square}(z)\right|$. Furthermore, since we can prove that two k-surfaces which are included the one in the other one are equal and since

$\left|\alpha^{\square}(\mathfrak{a}) \cap \beta^{\square}(z)\right|$ and $\left|\alpha^{\square}(\mathfrak{b}) \cap \beta^{\square}(z)\right|$ are two $(n - \dim(z) - 2)$-surfaces like the components F_1 and F_2, we obtain that:

$$\begin{cases} |F_1| &= \left|\alpha^{\square}(\mathfrak{a}) \cap \beta^{\square}(z)\right|, \\ |F_2| &= \left|\alpha^{\square}(\mathfrak{b}) \cap \beta^{\square}(z)\right|. \end{cases}$$

On Figure 10, representing the 3D case ($\dim(z) = n - 3$), the first component made of red 1-faces and of blue 2-faces on the left lies in the closure of the 3-face a (in the subspace $\beta^{\square}(z)$) and the second component made of red 1-faces and of blue 2-faces on the right lies in the closure of the 3-face b (in the subspace $\beta^{\square}(z)$).

The link between the configuration we obtained in $\mathbb{H}^n_n$ by assuming that $|\beta^{\square}_{\mathfrak{N}}(z)|$ is not connected and a critical conguration is then clear: since $\beta^{\square}_{\mathfrak{N}}(z) \subseteq \mathfrak{N}$, if a belongs to X, then the rest of the block minus b belongs to Y, and then b belongs to X to, and we obtain a critical configuration of primary type in X. The dual reasoning leads to a secondary critical configuration in X. In both cases, we obtain a contradiction. Then $|\beta^{\square}_{\mathfrak{N}}(z)|$ is connected. Finally, $\mathcal{IMM}(X)$ is well-composed in the sense of Alexandrov when X is digitally well-composed.

CONCLUSION FOR SETS Finally, we obtain the following conjecture:

Conjecture 8. *A set $X \subset \mathbb{Z}^n$ is DWC iff its immersion $\mathcal{IMM}(X)$ into the Khalimsky grids $|\mathbb{H}^n|$ is AWC, that is, is such that its topological boundary $\partial\mathcal{IMM}(X)$ is made of disjoint $(n-1)$-surfaces.*

CONCLUSION FOR PLAIN MAPS Starting from a function $u : \mathbb{Z}^n \to \mathbb{R}$, we can compute its *immersion* $U : \mathbb{H}^n \rightsquigarrow \mathbb{R}$ into the Khalimsky grids, defined such that:

$$\forall h \in \mathbb{H}^n, U(h) = \begin{cases} \{u(\mathcal{Z}_n(h))\} & \text{if } z \in \mathbb{H}^n_n, \\ \mathrm{Span}\,\{U(q)\ ;\ q \in \beta(z) \cap \mathbb{H}^n_n\} & \text{otherwise.} \end{cases}$$

Note that U is a *plain map* (see Section C.19).

On Khalimsky grids, for a given plain map $U : \mathbb{H}^n \rightsquigarrow \mathbb{R}$, the following threshold sets exist [127]:

$$\begin{aligned} [U \trianglerighteq \lambda] &= \{\, z \in \mathbb{H}^n \mid \exists\, v \in U(z),\, v \geq \lambda \,\}, \\ [U \triangleright \lambda] &= \{\, z \in \mathbb{H}^n \mid \forall\, v \in U(z),\, v > \lambda \,\}, \\ .[U \triangleleft \lambda] &= \{\, z \in \mathbb{H}^n \mid \forall\, v \in U(z),\, v < \lambda \,\}, \\ [U \trianglelefteq \lambda] &= \{\, z \in \mathbb{H}^n \mid \exists\, v \in U(z),\, v \leq \lambda \,\}. \end{aligned}$$

Definition 119. *Let $U : \mathbb{H}^n \rightsquigarrow \mathbb{R}$ be a given plain map. We say that this map is* well-composed in the sense of Alexandrov *or* AWC *iff, for any value of $\lambda \in \mathbb{R}$, the connected components of the topological boundary of each of its threshold sets $[U \trianglerighteq \lambda]$, $[U \triangleright \lambda]$, $[U \triangleleft \lambda]$, and $[U \trianglelefteq \lambda]$ are $(n-1)$-surfaces.*

We obtain finally the following conjecture for maps:

Conjecture 9. *A real-valued image $u : \mathbb{Z}^n \to \mathbb{R}$ is DWC iff its immersion $U : \mathbb{H}^n \rightsquigarrow \mathbb{R}$ into the Khalimsky grids is AWC.*

Obviously, we can use functions $u : \mathcal{D} \to \mathbb{R}$ defined on a bounded hyperrectangle $\mathcal{D}$ as domain, in this case we obtain with the same procedure an immersion $U : \alpha(\mathcal{H}_n(\mathcal{D})) \rightsquigarrow \mathbb{R}$ defined on the closed subset $\alpha(\mathcal{H}_n(\mathcal{D}))$. We will still have that u is DWC iff U is AWC.

E

WELL-COMPOSED INTERPOLATIONS ON POLYHEDRAL COMPLEXES

In this chapter, we assume that the domain of the initial function is made of the n-faces of either a discrete n-surface, or of what we call a *bordered n-surface* (see the definition below), defined in a polyhedral complex or rank $n \geq 0$. We also assume that this domain is *finite* in the sense that it is made of a finite number of faces, to ensure the convergence of the front propagation we will use on the image defined on this domain. The first interpolation that we propose is based on the derived neighborhoods and the second is based on the chain complex of the *hierarchical subdivision* (introduced in this thesis). In both cases, we obtain AWC interpolations in the sense that the topological boundaries of the (closure of) threshold sets are disjoint union of $(n-1)$-surfaces. Also, by computing the *underlying polyhedra* of the n-faces of the *dual cells* on which are defined the interpolations, we will see that our interpolations are also *CWC*: the boundaries of underlying polyhedra of their threshold sets are $(n-1)$-manifolds.

E.1 INTRODUCING NEW MATHEMATICAL BACKGROUND

In this section, we extend the usual definition of *border* and *interior* to *homogeneous* orders, that we will use to define AWCness for subsets of polyhedral complexes. Then, we follow with the introduction of a combinatorial version of the *dual cells* of Hudson (coming from PL topology), and with our definition of *cell complexes*. We continue with the natural extension of *AWCness* to cell complexes and functions defined on cell complexes, and we finish with the definition of CWCness applied to cell complexes and function defined on them.

E.1.1 *Border and interior*

Let us recall the definition of *homogeneity* of an order.

Definition 120 (Homogeneity [42])**.** *Let $|X| = (X, \alpha_X)$ be a CF-order of finite rank $n \geq 0$. We say that $|X|$ is* homogeneous *iff for any element $f \in X$, the set $\beta(f) \cap X_n$ is non-empty.*

Since orders are in equivalent to Alexandrov spaces, that is, supplied with a topology, we can define the *border* (drew from the *face boundary* of Latecki), and then the *interior*, of an order in this manner:

Definition 121 (Border and Interior of an order)**.** *Let $|X| = (X, \alpha_X)$ be an homogeneous CF-order of finite rank $n \geq 0$. We denote by* $\mathrm{Char}(X)$ *the* characteristical faces *of $|X|$ defined such that:*

$$\mathrm{Char}(X) = \{f \in X_{n-1} \; ; \; \mathrm{Card}\,(\beta(f) \cap X_n) = 1\}\,,$$

we can then define the border*, denoted by ΔX, of $|X|$ such that it is the closure of the characteristical faces of X:*

$$\Delta X = \bigcup_{f \in \mathrm{Char}(X)} \alpha_X(f).$$

Then we call the interior of $|X|$ *the set $|X \setminus \Delta X|$ and we denote it* $\mathrm{Int}(X)$.

Note that we differentiate in this thesis the the topological boundary ∂X, where X is a subset of an Alexandrov space A, from the border ΔX, which does not need a greater space

like A to be well-defined. Since we are going to work with Alexandrov spaces which can be finite, we will use borders and not topological boundaries.

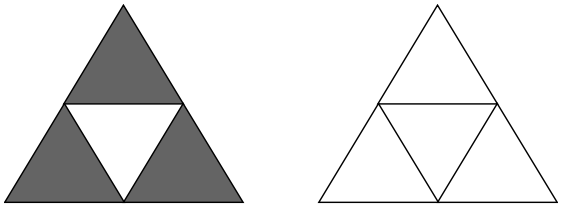

Figure 1.: A polyhedral complex on the left and its border on the right

Figure 1 depicts the border of a polyhedral complex being an homogeneous order.

From now on, we will only work with homogeneous orders.

E.1.2 *Bordered n-surfaces*

Real signals are always definite on a bounded domain, which justifies the introduction of a definition of (finite) *bordered n-surfaces*, which represent low constrained domains with nice topological properties.

Definition 122 (Bordered n-surfaces)**.** *Let $|X| = (X, \alpha_X)$ be a CF-order, whose cardinal is finite, of rank $n \geq 1$, such that it is connected and such that its border ΔX is non-empty. Then, if, for any $z \in \mathrm{Int}(X)$, $|\theta^{\square}_X(x)|$ is a $(n-1)$-surface, and if ΔX is a disjoint union of $(n-1)$-surfaces, then $|X|$ is said to be a* bordered n-surface*.*

Figure 2 shows some examples of topological structures that are not bordered n-surfaces except the last one which is a bordered 2-surface. The interior is depicted in red in the Hasse diagrams, and the border is depicted in blue. The first example is a CF-order of rank 2, but its boundary is not a 0-surface since the two faces in it are neighbors. The second example is a CF-order of rank 1, and then is not a bordered n-surface. The same reasoning holds for the third example. For the fourth example, which is of rank 2, we can see that the border is connected, but is not a 1-surface, and then this structure is not a bordered 2-surface. Finally, the fifth example verifies all the constraints, and then is a bordered 2-surface.

Also, Figure 3 shows a Möbius ruban which has been triangulated: it is a bordered 2-surface since its boundary is a 1-surface, and since for any point x at the interior of the ruban, the neighborhood $|\theta^{\square}(x)|$ is a 1-surface.

Finally, note that these examples are made of simplices, but any complex supplied with an order relation can be a bordered n-surface, as shown of Figure 4. On the left, we have a cubical complex of rank 2, whose border is not a 1-surface: there exists one "critical point" in the boundary such that it admits four neighbors, and then the border is not a 1-surface, which implies that this structure is not a bordered 2-manifold. At the contrary, on the right, we have a connected CF-order of rank 2, with a non-empty border which is made of two disjoint $(n-1)$-surfaces, and such that for any interior point, the $\theta^{\square}$-neighborhood is a 1-surface. Then, this is a bordered 2-surface.

In fact, we will see in the sequel that these orders seem to be the lowest constrained orders needed to obtain AWC interpolations using our method.

Conjecture 10. *The chain complex of a bordered n-surface is also a bordered n-surface.*

E.1.3 *AWCness on polyhedral complexes*

Now, let us recall the definition of well-composedness in the sense of Alexandrov according to L. Najman [127] for any polyhedral complex supplied with the canonical order $\supseteq$.

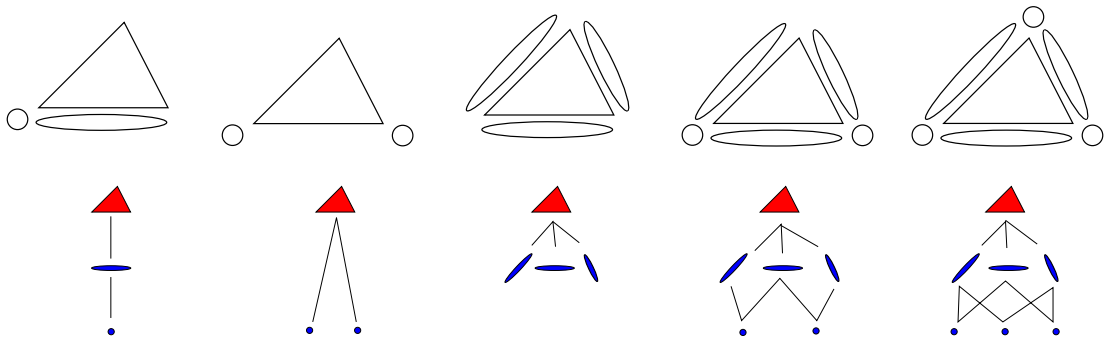

Figure 2.: Among these orders, the only bordered 2-surface is the one on the right

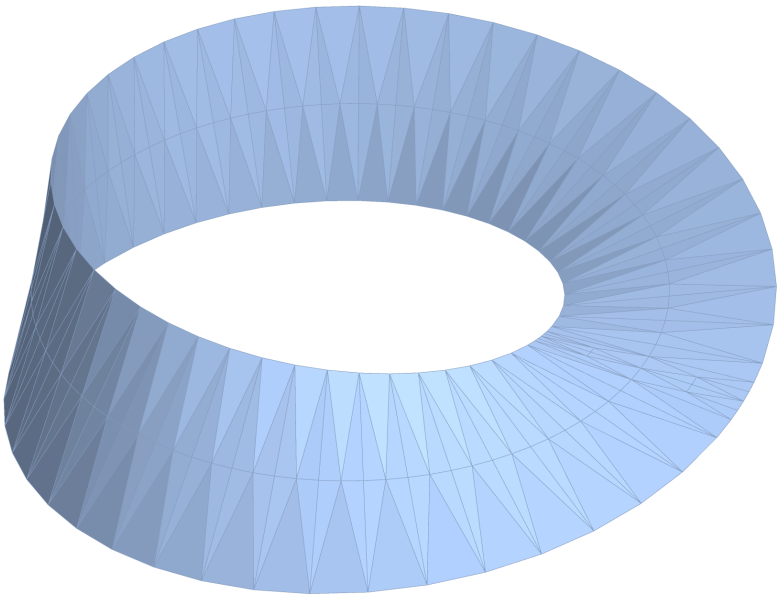

Figure 3.: A triangulated Möbius ruban is a bordered 2-manifold

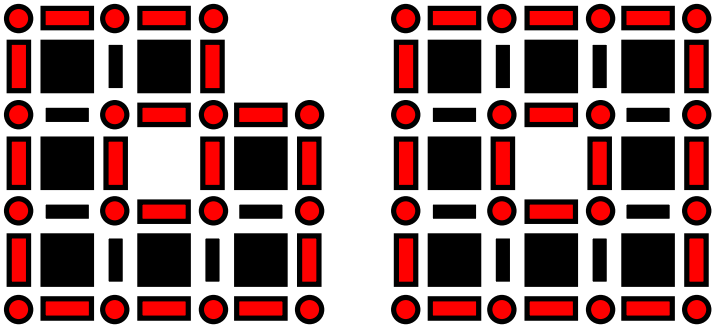

Figure 4.: On the left a topological structure that is not a bordered 2-surface, and on the right a bordered 2-surface. Interiors are depicted in black and borders in red.

We recall that a polyhedral complex is said *locally finite* iff for any element of this complex, the neighborhood of this point in this complex has a finite cardinality.

Definition 123 (AWC polyhedral complexes [127])**.** *Let* $|\mathfrak{P}\mathfrak{C}^n| = (\mathfrak{P}\mathfrak{C}^n, \alpha)$ *be a (locally finite) polyhedral complex of rank* $n \geq 0$ *supplied with the canonical order* $\alpha = \supseteq$*, and let* $\Delta\mathfrak{P}\mathfrak{C}^n$ *be its border. We say that* $|\mathfrak{P}\mathfrak{C}^n|$ *is* well-composed in the sense of Alexandrov *iff its border is a disjoint*

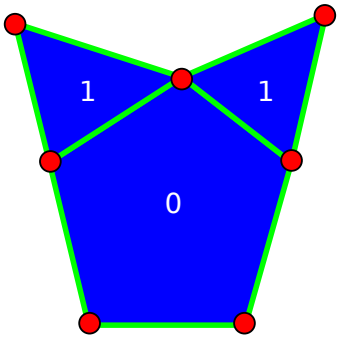

Figure 5.: $[u \leq 0]$ and $[u \leq 1]$ are AWC, but $[u \geq 1]$ is not AWC

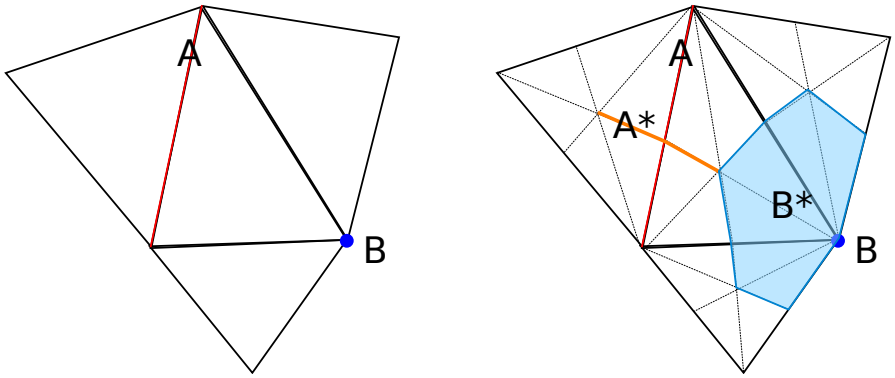

Figure 6.: Dual cells

union of (bordered or not) $(n-1)$-surfaces. Also, we say that a subset $S \subseteq \mathfrak{PC}^n$ is well-composed in the sense of Alexandrov *if $|\alpha(S)|$ is an AWC simplicial complex.*

By extension, we can define well-composedness in the sense of Alexandrov for functions using threshold sets:

Definition 124 (Threshold sets on orders)**.** *Let $|\mathfrak{PC}^n| = (\mathfrak{PC}^n, \alpha)$ be a polyhedral complex of rank $n \geq 0$, and let $\mathcal{D}$ be a subset of $\mathfrak{PC}^n_n$: u is then defined only on the n-faces of the polyhedral complex. Then, we define the* threshold sets *of $u : \mathcal{D} \to \mathbb{R}$ such that:*

$$
\begin{aligned}
[u \geq \lambda] &= \{x \in \mathcal{D} \; ; \; u(x) \geq \lambda\}, \\
[u > \lambda] &= \{x \in \mathcal{D} \; ; \; u(x) > \lambda\}, \\
[u \leq \lambda] &= \{x \in \mathcal{D} \; ; \; u(x) \leq \lambda\}, \\
[u < \lambda] &= \{x \in \mathcal{D} \; ; \; u(x) < \lambda\}.
\end{aligned}
$$

Definition 125 (AWC functions on polyhedral complexes)**.** *Let $|\mathfrak{PC}^n| = (\mathfrak{PC}^n, \alpha)$ be a polyhedral complex of rank $n \geq 0$ supplied with the canonical order $\alpha = \supseteq$, and let $\mathcal{D}$ be a finite subset of $\mathfrak{PC}^n_n$. Now let $u : \mathcal{D} \to \mathbb{R}$ be a real-valued function defined on $\mathcal{D}$. We say that u is* well-composed in the sense of Alexandrov *on $\mathcal{D}$ iff the border (of the closure in $|\mathfrak{PC}^n|$) of any threshold set of u is a disjoint union of (bordered or not) $(n-1)$-surfaces.*

Let us denote that, without particular constraints on the domain of u, we need to check the AWCness of both upper and lower threshold sets to know if a function u is well-composed in the sense of Alexandrov, as shown on Figure 5.

E.1.4 *Dual cells*

As we will see in the sequel, the following definition, using derivate neighborhoods, will be needed:

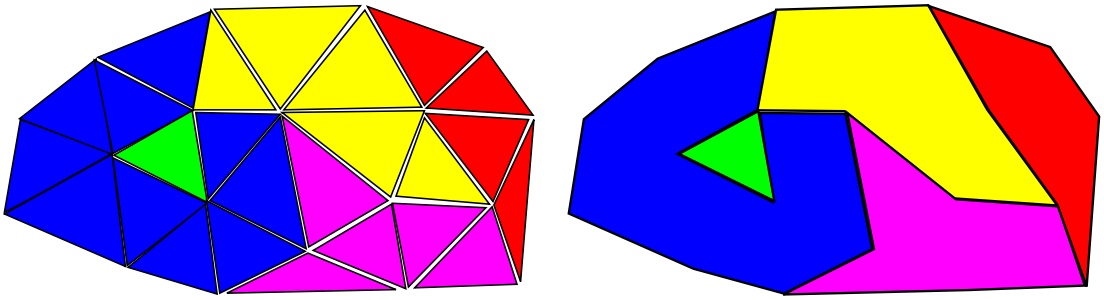

Figure 7.: From a partition of a simplicial complex to its corresponding cell complex (one color by 2-cell)

Definition 126 (Dual cells). *Let K be a simplicial complex, and K^1 its first derived neighborhood. For any element $A \in K$. Then, we define A^*, the* dual cell *of A, to be the following subcomplex:*

$$A^* = \bigcap_{\{v\} \subseteq A} \alpha(\beta_{K^1}(\{\{v\}\})).$$

Note that this definition is the combinatorial version of *dual cells* of Hudson [79]. The difference between these two definitions is that in PL topology a point in $\mathbb{R}^n$ is this same point after a subdivision (like a *barycentric subdivision*) when in combinatorial topology, a vertex $\{x\}$ becomes a vertex containing this vertex $\{\{x\}\}$ after having computed a subdivision like the chain complex, which explains this term in Definition 126.

Figure 6 shows on the left a simplicial complex C, where A is a 1-simplex and where B is a 0-simplex. Both are elements of C. On the right, we subdivided the complex C by computing its first derived C^1, that is, its chain complex, in dotted lines. A^* is then the intersection of the closures of the stars of each 0-simplex contained in A, and is the subcomplex depicted in orange. B^*, the dual cell of B, is computed in the same manner, and is the subcomplex depicted in light blue.

E.1.5 *Cell complexes and AWCness*

Definition 127 (k-adjacency). *Let $|C^n| = (C^n, \alpha)$ be any simplicial complex of rank $n \geq 0$ supplied with the canonical order $\alpha = \supseteq$. Two different faces are said* k-adjacent, *$k \in [\![0, n]\!]$, iff they share a face of rank equal to k but not more.*

Definition 128 (Strong connectedness). *Let $|C^n| = (C^n, \alpha)$ be any simplicial complex of rank $n \geq 0$ supplied with the canonical order $\alpha = \supseteq$. A set S of n-faces of C^n is said* strongly connected *iff for any couple (h^1, h^2) of elements of S, there exists a finite sequence $(q^0 = h^1, \ldots, q^r = h^2)$ of $(r+1)$ elements of S such that for any $i \in [\![0, r-1]\!]$, q^i and q^{i+1} are $(n-1)$-adjacent.*

Since we want to be able to group together simplices of dimension n and their faces into cells, we propose the following definitions.

Definition 129 (Cells and cell complexes). *Let $|C^n| = (C^n, \alpha)$ be any simplicial complex of rank $n \geq 0$ supplied with the canonical order $\alpha = \supseteq$. Now let be any partition $\{P^i\}_{i \in \mathcal{I}}$ of the set C^n_n of n-faces of C^n:*

$$\bigsqcup_{i \in \mathcal{I}} P^i = C^n_n,$$

*such that for any $i \in \mathcal{I}$, P^i is strongly connected. We say that each simplicial subcomplex $\alpha(P^i)$ of C^n is a n-*cell *of C with respect to the partition $\{P^i\}_{i \in \mathcal{I}}$. Then, any closure $\alpha(f)$ of any $(n-1)$-face f of the border of a n-cell is a subcomplex of dimension $(n-1)$ that we call $(n-1)$-*cell *with respect to $\{P^i\}_{i \in \mathcal{I}}$, and so on. The set $\mathfrak{CC}^n$ of all these k-cells, $k \in [\![0, n]\!]$, is said to be a* cell complex *corresponding to the partition $\{P^i\}_{i \in \mathcal{I}}$. Note that we will denote the k-*cells *of the cell complex $\mathfrak{CC}^n$ by $\mathfrak{CC}^n_k$.*

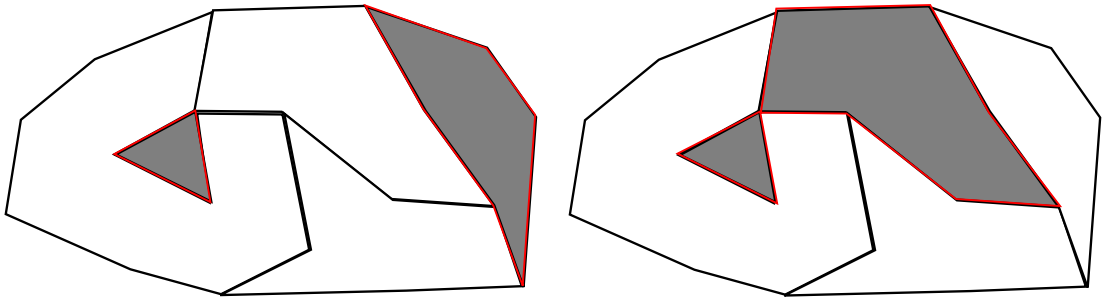

Figure 8.: Families of n-cells: AWC on the left and not AWC on the right

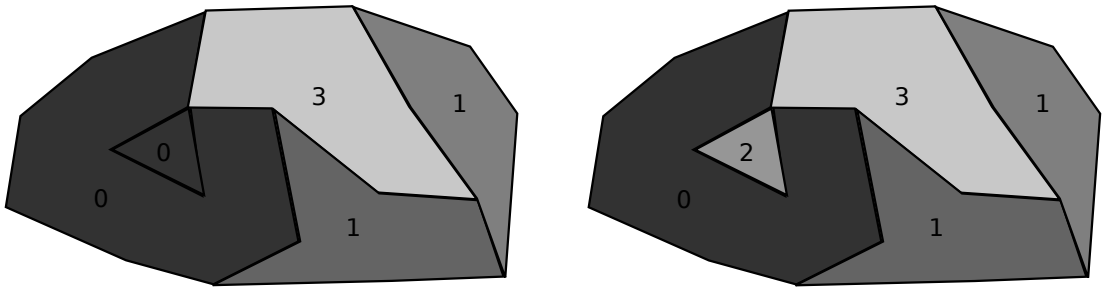

Figure 9.: Functions on cell complexes: AWC on the left and not AWC on the right

Figure 7 depicts a partition of the set of 2-cells of a simplicial complex and its corresponding cell complex.

Definition 130 (AWC family of n-cells)**.** *Let $|C^n| = (C^n, \alpha)$ be any simplicial complex of rank n supplied with the canonical order $\alpha = \supseteq$ and let $\mathfrak{CC}^n$ be a cell complex corresponding to any partition of C^n_n. Now let $X = \{S^i\}_{i\in\mathcal{I}}$ be a family of n-cells of $\mathfrak{CC}^n$. Then we say that X is* well-composed in the sense of Alexandrov into C^n *iff the border Δ of the simplicial subcomplex $\bigcup_{i\in\mathcal{I}} S^i$ subset of C^n is a disjoint union of (bordered or not) $(n-1)$-surfaces.*

Figure 8 shows an AWC family of 2-cells on the left since its boundary is made of a disjoint union of 1-surfaces, and on the right a family of n-cells which is not AWC, since its boundary owns a "pinch".

E.1.6 *AWC functions on cell complexes*

Definition 131 (Threshold sets on a cell complex)**.** *Let $|C^n| = (C^n, \alpha)$ be any simplicial complex of rank n supplied with the canonical order $\alpha = \supseteq$ and let $\mathfrak{CC}^n$ be an cell complex corresponding to any partition of C^n_n. Now let $u : \mathcal{D} = \mathfrak{CC}^n_n \to \mathbb{R}$ be a real-valued function mapping a real value to any n-cell of C. Then, we define for any $\lambda \in \mathbb{R}$ the* threshold sets *of u on $\mathcal{D}$ such that:*

$$
\begin{aligned}
[u \geq \lambda] &= \{x \in \mathcal{D} \,;\, u(x) \geq \lambda\},\\
[u > \lambda] &= \{x \in \mathcal{D} \,;\, u(x) > \lambda\},\\
[u \leq \lambda] &= \{x \in \mathcal{D} \,;\, u(x) \leq \lambda\},\\
[u < \lambda] &= \{x \in \mathcal{D} \,;\, u(x) < \lambda\}.
\end{aligned}
$$

In other words, a threshold set is made of families of n-cells, and since we have defined well-composedness for this kind of sets, we can define well-composedness for functions defined on the n-cells of a cell complex.

Definition 132 (AWC functions on cell complexes)**.** *Let $|C^n| = (C^n, \alpha)$ be any simplicial complex of rank n supplied with the canonical order $\alpha = \supseteq$ and let $\mathfrak{CC}^n$ be an cell complex corresponding to any partition of C^n_n. Now let $u : \mathfrak{CC}^n_n \to \mathbb{R}$ be a real-valued function. Then we say that u is* well-composed in the sense of Alexandrov *in C^n iff all the closures of the threshold sets of u on $\mathfrak{CC}^n_n$ are well-composed in the sense of Alexandrov in C^n.*

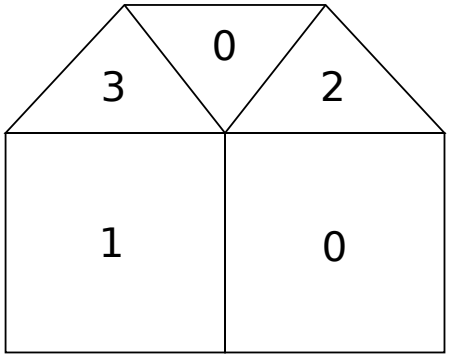

Figure 10.: An image defined u on the n-dimensional convex polyhedral domains of a polyhedral complex

Figure 9 shows an AWC function defined on a cell complex on the left: any non-empty threshold set is a family of n-cells such that its boundary is made of disjoint 1-surfaces, when on the right, we can observe that the boundary of the threshold set $[u \geq 2]$ of the function u defined on this same cell complex is not made of simple closed curves.

E.1.7 *Cell complexes and CWCness*

Let us recall that the definition of an underlying polyhedron of a geometric simplex is given in Definition 96. Also, in the sequel, we will only consider geometric simplices or geometric simplicial complexes.

Definition 133 (Underlying polyhedron of a cell complex)**.** *Let C^n be any simplicial complex or subcomplex of rank $n \geq 0$. Then its* underlying polyhedron *is denoted by $\mathrm{Poly}(C^n)$ and is equal to:*

$$\mathrm{Poly}(C^n) = \bigcup_{s \in C^n} \mathrm{Poly}(s).$$

Definition 134 (CWC family of n-cells)**.** *Let $|C^n| = (C^n, \alpha)$ be any simplicial complex of rank n supplied with the canonical order $\alpha = \supseteq$ and let $\mathfrak{CC}^n$ be a cell complex corresponding to any partition of C_n^n. Now let $X = \{S^i\}_{i \in \mathcal{I}}$ be a family of n-cells of $\mathfrak{CC}^n$. Then we say that X is* continuous well-composed *iff the topological boundary in $\mathbb{R}^n$ of the underlying polyhedron of the simplicial subcomplex $\bigcup_{i \in \mathcal{I}} S^i$ a $(n-1)$-manifold.*

Definition 135 (CWC functions on cell complexes)**.** *Let $|C^n| = (C^n, \alpha)$ be any simplicial complex of rank n supplied with the canonical order $\alpha = \supseteq$ and let $\mathfrak{CC}^n$ be a cell complex corresponding to any partition $\{S^i\}_{i \in \mathcal{I}}$ of C_n^n. Now let $u : \mathfrak{CC}_n^n \to \mathbb{R}$ be a real-valued function. We say that u is* continuous well-composed *iff each non-empty thresholds sets is CWC.*

E.2 DIRECT USE OF THESE TOOLS FAIL TO PRODUCE A SELF-DUAL AWC FUNCTION

Let us now explain how we could have used the existing mathematical tools in matter of combinatorial topology and in piecewise linear topology to extract the boundaries of an function defined on a polyhedral complex such that their boundaries would have been discrete surfaces. We are going to see that these solutions are not satisfying.

Among the different tools we are going to speak about: chain complexes, simplicial neighborhoods, derived neighborhoods, and frontier orders.

Let now assume that a function $u : \mathfrak{PC}_n^n \to \mathbb{R}$ is defined on the n-dimensional convex polyhedral domains of a polyhedral complex which is either a n-surface, or a bordered n-surface (which seems more usual). Figure 10 depicts such an image, which is obviously not well-composed in the sense of Alexandrov: the boundary of the threshold set $[u \leq 1]$ is not a simple closed curve.

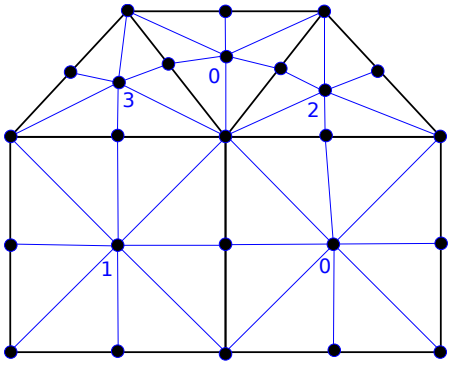

Figure 11.: Chain complex of the initial image

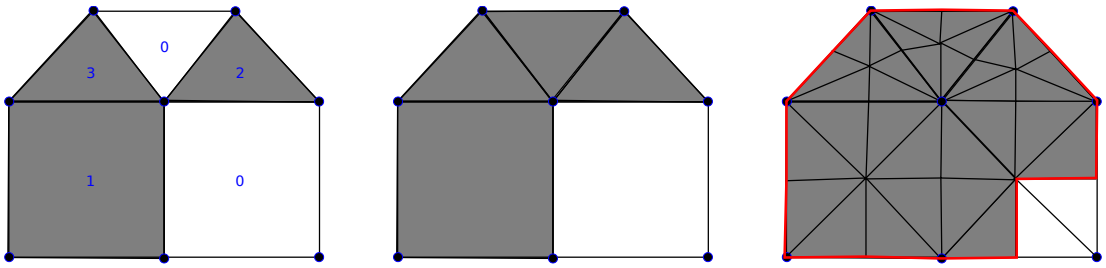

Figure 12.: Using derived neighborhoods directly on the initial domain does not lead to a satisfactory result

If we compute the chain complex of the domain of this image u, we obtain Figure 11. We can observe that each face becomes a vertex in the chain complex, and then we preserve the geometry of the whole domain, but we loose the one of the convex polyhedral domains which are valued. A solution to give back the geometry to these cells could be that we use the simplicial neighborhoods on the valued vertices, but in this manner we come back to the initial configuration, and the pinches in the images are preserved.

Another available mathematical tool is the simplicial neighborhood, but as we have just seen before, it is the inverse operation of the chain complex, and then it will not permit us to increase the resolution of the cells in such a way that we delete the pinches, and furthermore we need a simplicial structure to use them.

Another possibility is then to use the derived neighborhoods. This structure needs to be applied on a simplicial complex, but the given domain of u is a polyhedral complex. Let us then try to apply the same principle as the one of the derived neighborhood but on the polyhedral complex: we start from the set of n-faces corresponding to some threshold set, let us say $[u \geq 2]$, and then we deduce the corresponding polyhedral subcomplex K as depicted on the left of Figure 12 in gray. Furthermore, we need this subcomplex to be full (see Theorem 20), which leads to the definition of a new subcomplex, K', as depicted in at the center of Figure 12 in gray. Then we can compute the border of its derived neighborhood on the polyhedral complex that we could define as the simplicial neighborhood of the chain complex of K' in the chain complex of the initial polyhedral complex (we have then extended the definition of the derived neighborhood to polyhedral complexes). At the end, we can observe that we effectively obtain a border made of one $(n-1)$-surface, and then we can imagine that in more complex cases, this border will also be made of disjoint union of $(n-1)$-surfaces. However, we have completely destroyed the structure of the initial subcomplex K by making it full, so this solution does not correspond to our needs.

Let us now try another approach with derived neighborhoods, but on simplicial complexes to avoid pathological situations as the one seen just before. Let us then use the chain complex on the polyhedral domain of the image u, and let us transpose the values of the image u onto the new image defined on $\mathcal{C}^u$, which gives a new image u'. We obtain Figure 13, where

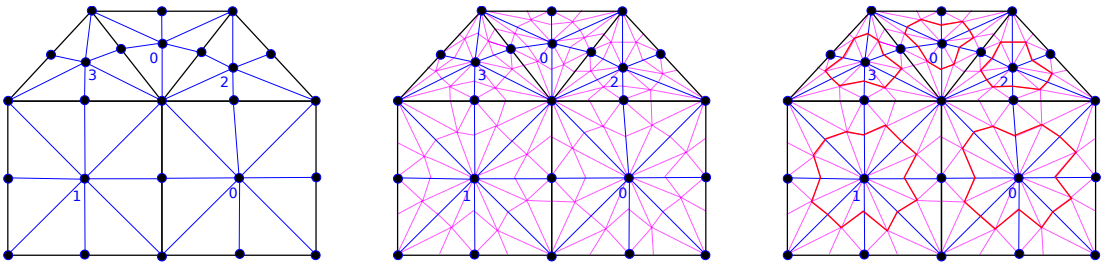

Figure 13.: Using derived neighborhoods on the chain complex of the domain of u does not lead to a satisfactory result neither.

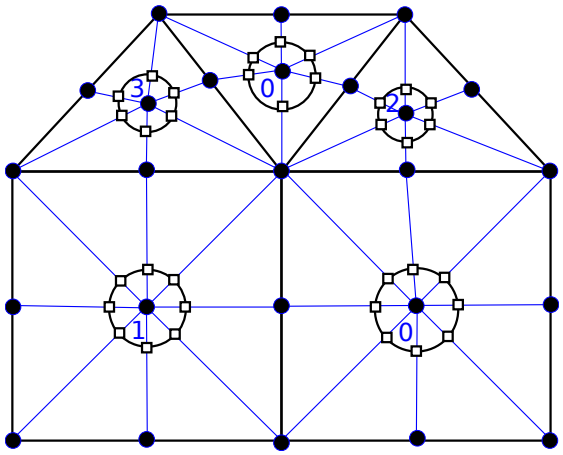

Figure 14.: Using frontier orders on the chain complex of the closure of the domain of the image disconnects the pixels

we can see that the derived neighborhood of any threshold set has a border made of disjoint $(n-1)$-surfaces. However, we can observe that the border of the derived neighborhood of the threshold set $[u' \geq 0]$ does not cover the whole domain of u, which is problematic. Furthermore, we have lost the connectivity between the initial cells, which means that the contours we will obtain by thresholding u will not be representative. Then this solution is not good neither.

The last "simple" solution seems then to be the frontier orders. Let us first try them on a simplicial complex, since they can be used either on a simplicial complex or on any partially ordered set. In this case, we have to use it on the chain complex of the (closure of the) domain of u. Like before, even if the borders are disjoint union of $(n-1)$-surfaces, we have disconnected the initial pixels as shown on Figure 14. Then we have to try the second solution, which leads finally to the same solution, since using frontier orders on an order which is not a simplicial complex is the same thing as applying it on its chain complex.

Note that if the (closed) domain of u had been a simplicial complex C, we could have used directly the frontier orders as depicted on Figure 15: we compute the threshold set $[u \geq 1]$ and we deduce its support K. Then K' is the complement of K into the support of C, and we obtain the frontier order depicted by the red line and the squares. The result is a frontier order which overlaps the simplices corresponding to $[u < 1]$, and then this solution is not self-dual: it overemphasizes the ones over the zeros. This solution does not correspond neither to our needs.

E.3 AN n-D AWC INTERPOLATION

Now let us present our solution, which finally seems very natural: starting from the observation that derived neighborhoods "disconnect the pixels", we can simply proceed to an (in-

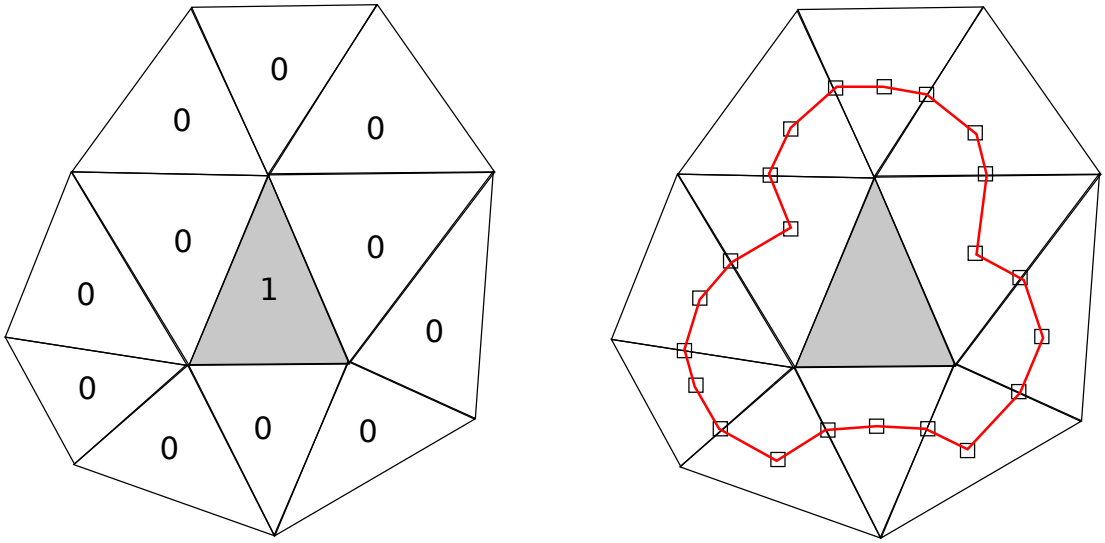

Figure 15.: Using directly frontier orders on a simplicial complex is not self-dual

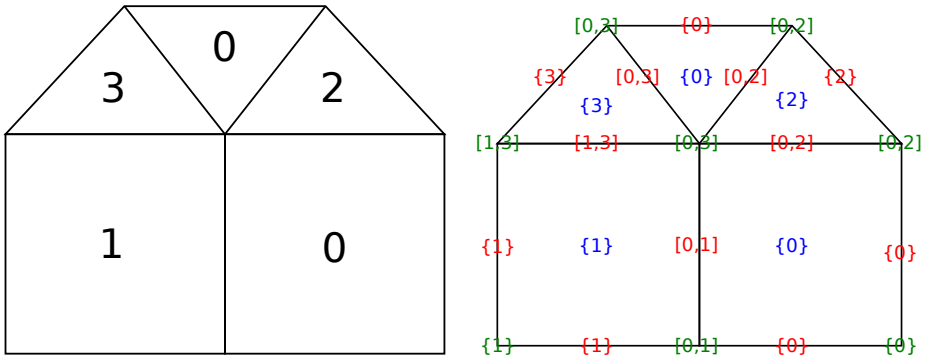

Figure 16.: From u defined on the n-cells of a polyhedral complex to U defined on all the faces of the complex

between) interpolation on the whole (finite) polyhedral complex, such that the connection between the pixels is preserved.

As for our digitally well-composed self-dual interpolation, we value all the faces of our polyhedral complex using a new function, U defined such that, $\forall z \in \mathfrak{PC}^n$:

$$U(z) = \begin{cases} \{u(z)\} & \text{if } z \in \mathfrak{PC}^n_n, \\ \text{Span}\{u(z') \ ; \ z' \in \beta(z) \cap \mathfrak{PC}^n_n\} & \text{otherwise.} \end{cases}$$

Then we transpose as depicted on Figure 17 the image U defined on all the cells of the cell complex to its derived subdivision (depicted in blue) by the operation (using the chain complex as described above):

$$\forall \{z\} \in \mathcal{C}^{\mathfrak{PC}^n}, U'(\{z\}) = U(z).$$

Then, to be able to compute a self-dual interpolation, we add a border to the subdivided domain initialized at the median value of the border of the initial image, which leads to Figure 18.

We can finally apply the propagation algorithm explained before (see Algorithm 3), which leads to the image $u^\flat_+$ depicted on Figure 19, and $u^\flat : (\mathcal{C}^{\mathfrak{PC}^n})_0 \to \mathbb{R}$ as depicted on Figure 20 after we have removed the temporary border.

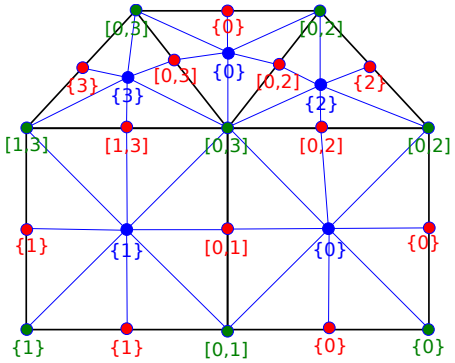

Figure 17.: U' defined on all the 0-faces of the subdivided complex

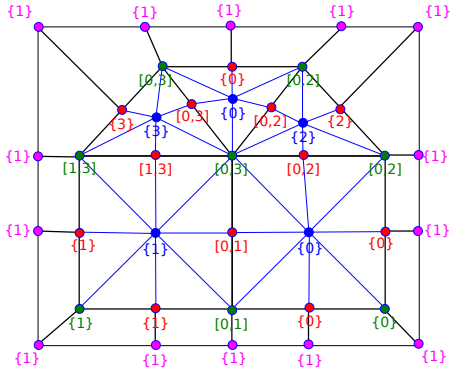

Figure 18.: The same image U' with an additional border

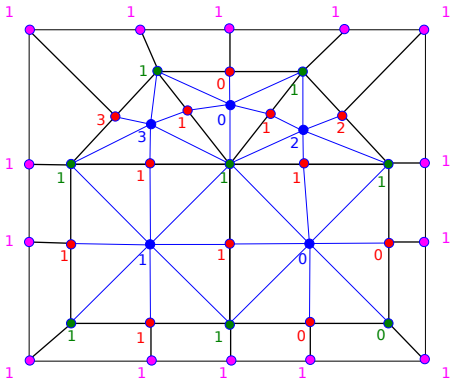

Figure 19.: $u^{\flat}_{+}$ (with the temporary border)

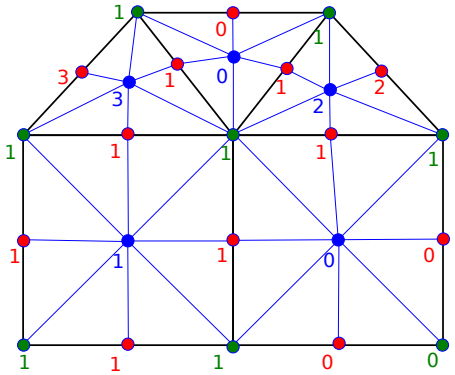

Figure 20.: $u^{\flat}$ (without the temporary border)

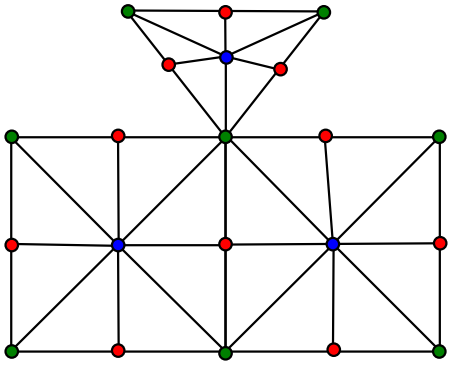

Figure 21.: $\mathcal{F}([u^\flat \leq 1], \mathcal{C}^{\mathfrak{P}\mathfrak{C}^n})$

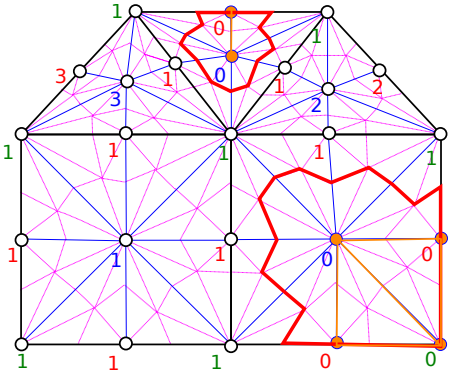

Figure 22.: $\Delta N^1(\mathcal{F}([u^\flat \leq 0], \mathcal{C}^{\mathfrak{P}\mathfrak{C}^n}), \mathcal{C}^{\mathfrak{P}\mathfrak{C}^n})$

Note that the front propagation will assurely end since we are working with domains of finite cardinals.

Note that this front-propagation algorithm does not need a structure of cubical grid to be able to proceed: it works on any graph $G = (V, E)$ where V are the vertices, that is, the domain of the propagation, and where E denotes the "directions" of the propagation, that is, the (direct) connectivity between cells.

Since we do not have yet drawn the contours of the future cells, we can define the following subcomplex of $\mathcal{C}^{\mathfrak{P}\mathfrak{C}^n}$ for any $\lambda \in \mathbb{R}$:

$$\mathcal{F}([u^\flat \leq \lambda], \mathcal{C}^{\mathfrak{P}\mathfrak{C}^n}) = \left\{ f \in \mathcal{C}^{\mathfrak{P}\mathfrak{C}^n} \; ; \; f \subseteq [u^\flat \leq \lambda] \right\}.$$

An example of this kind of subcomplex is depicted on Figure 21 where we drew $\mathcal{F}([u^\flat \leq 1], \mathcal{C}^{\mathfrak{P}\mathfrak{C}^n})$.

Some remarks about this subcomplex:

- it is full into $\mathcal{C}^{\mathfrak{P}\mathfrak{C}^n}$ by construction,
- when $\mathfrak{P}\mathfrak{C}^n$ is a bordered n-surface, $\mathcal{C}^{\mathfrak{P}\mathfrak{C}^n}$ is also a bordered n-surface (if Conjecture 10 is true), and then by Theorem 20, the border of the derived neighborhood of the full subcomplex $\mathcal{F}([u^\flat \leq 1], \mathcal{C}^{\mathfrak{P}\mathfrak{C}^n})$ is a disjoint union of $(n-1)$-surfaces.

The second property is depicted on Figures 22, 23, and 24 where $\mathcal{F}([u^\flat \leq \lambda], \mathcal{C}^{\mathfrak{P}\mathfrak{C}^n})$ is drawn in orange and the corresponding border is in red. As we can observe, these boundaries are simple closed curves, that is, 1-surfaces in the derived subdividision of the chain complex of the initial cell complex.

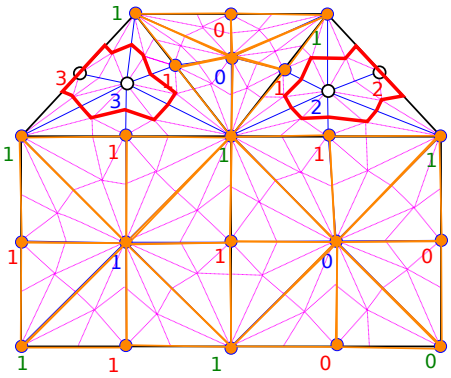

Figure 23.: $\Delta N^1(\mathcal{F}([u^\flat \leq 1], \mathcal{C}^{\mathfrak{P}\mathfrak{C}^n}), \mathcal{C}^{\mathfrak{P}\mathfrak{C}^n})$

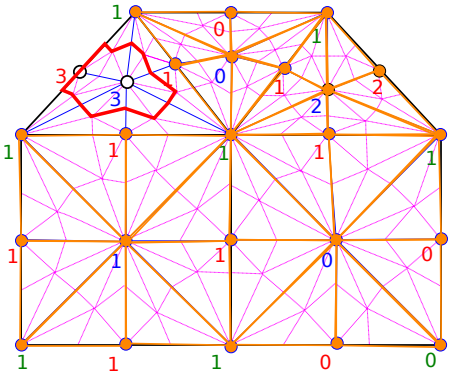

Figure 24.: $\Delta N^1(\mathcal{F}([u^\flat \leq 2], \mathcal{C}^{\mathfrak{P}\mathfrak{C}^n}), \mathcal{C}^{\mathfrak{P}\mathfrak{C}^n})$

Now let us use the formula of dual cells of Hudson [79]. Then, starting from any element A of $\mathcal{C}^{\mathfrak{P}\mathfrak{C}^n}$, we can compute its dual cell A^* as follows:

$$A^* = \bigcap_{\{x\} \subseteq A} \alpha(\beta_{[\mathcal{C}^{\mathfrak{P}\mathfrak{C}^n}]^1}(\{\{x\}\})),$$

where $[\mathcal{C}^{\mathfrak{P}\mathfrak{C}^n}]^1$ denotes the first derived neighborhood of $\mathcal{C}^{\mathfrak{P}\mathfrak{C}^n}$. A 0-face which is valued in $\mathcal{C}^{\mathfrak{P}\mathfrak{C}^n}$ becomes a simplicial complex of rank n by duality, and we are able to group these simplices into a simplicial n-cell to form a valued cell complex which is well-composed in the sense of Alexandrov (since any union of any cells in this cell complex is AWC by construction).

Effectively, since the union of the n-faces of the dual cells of the o-faces of $\mathcal{C}^{\mathfrak{P}\mathfrak{C}^n}$ covers $[\mathcal{C}^{\mathfrak{P}\mathfrak{C}^n}]^1$, we can partition the set of n-faces of this last set such that: $([\mathcal{C}^{\mathfrak{P}\mathfrak{C}^n}]^1)_n = \sqcup_{A \in \mathcal{C}^{\mathfrak{P}\mathfrak{C}^n}} P(A)$ with $P(A) = (A^*)_n$. Using this partition, we can defined a cell complex $\mathfrak{C}\mathfrak{C}^n_n$ corresponding to $\{P(A)\}_{A \in \mathcal{C}^{\mathfrak{P}\mathfrak{C}^n}}$. This way, we obtain finally $u_{\mathrm{AWC}} : \mathfrak{C}\mathfrak{C}^n_n \to \mathbb{R}$ defined such that $\forall z \in \mathfrak{C}\mathfrak{C}^n_n, u_{\mathrm{AWC}}(z) = u^\flat(C)$ where $C \in (\mathcal{C}^{\mathfrak{P}\mathfrak{C}^n})_0$ is such that $z \in C^*$.

Note that since the function u_{AWC} is only defined on n-cells, the threshold sets of u_{AWC} are sets of n-cells, and then we compute the borders based on the closures of the threshold sets: $\Delta\alpha([u_{\mathrm{AWC}} \geq \lambda])$, $\Delta\alpha([u_{\mathrm{AWC}} < \lambda])$, $\Delta\alpha([u_{\mathrm{AWC}} \leq \lambda])$ and $\Delta\alpha([u_{\mathrm{AWC}} > \lambda])$.

We obtain finally the equalities:

$$\forall \lambda \in \mathbb{R}, \Delta\alpha([u_{\mathrm{AWC}} \geq \lambda]) = \Delta N^1(\mathcal{F}([u^\flat \geq \lambda], \mathcal{C}^{\mathfrak{P}\mathfrak{C}^n}), \mathcal{C}^{\mathfrak{P}\mathfrak{C}^n}),$$

$$\forall \lambda \in \mathbb{R}, \Delta\alpha([u_{\mathrm{AWC}} \leq \lambda]) = \Delta N^1(\mathcal{F}([u^\flat \leq \lambda], \mathcal{C}^{\mathfrak{P}\mathfrak{C}^n}), \mathcal{C}^{\mathfrak{P}\mathfrak{C}^n}),$$

$$\forall \lambda \in \mathbb{R}, \Delta\alpha([u_{\mathrm{AWC}} > \lambda]) = \Delta N^1(\mathcal{F}([u^\flat > \lambda], \mathcal{C}^{\mathfrak{P}\mathfrak{C}^n}), \mathcal{C}^{\mathfrak{P}\mathfrak{C}^n}),$$

$$\forall \lambda \in \mathbb{R}, \Delta\alpha([u_{\mathrm{AWC}} < \lambda]) = \Delta N^1(\mathcal{F}([u^\flat < \lambda], \mathcal{C}^{\mathfrak{P}\mathfrak{C}^n}), \mathcal{C}^{\mathfrak{P}\mathfrak{C}^n}),$$

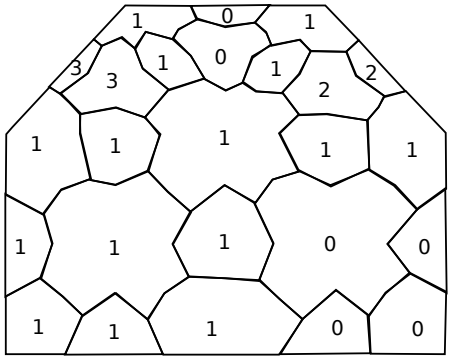

Figure 25.: The new valued cell complex representing an AWC function

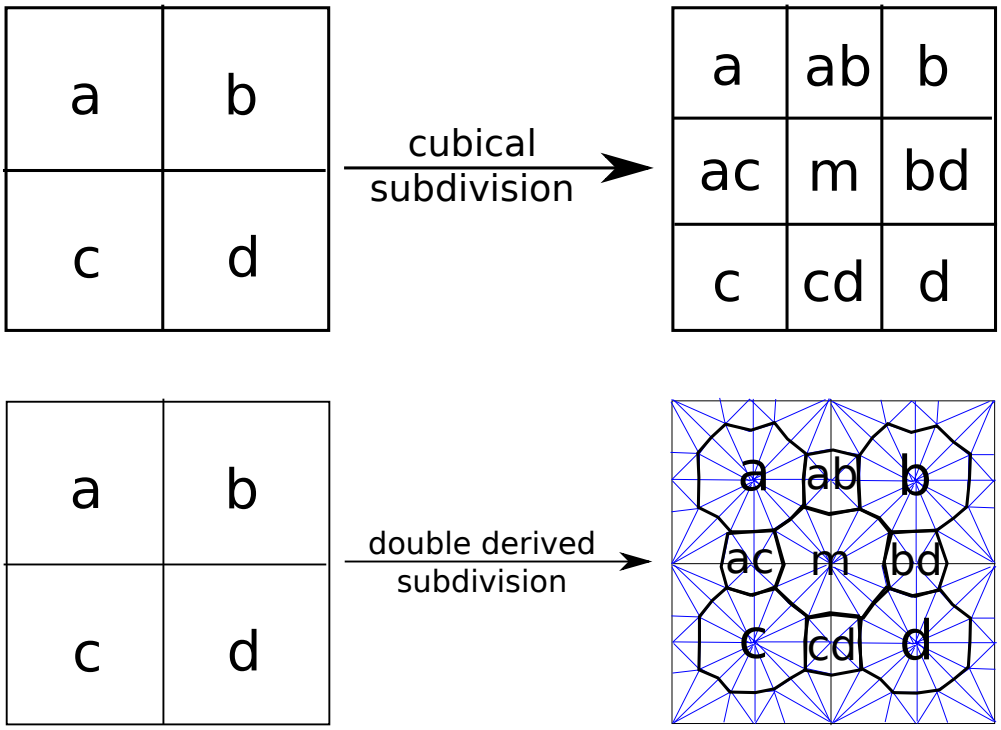

Figure 26.: Cubical subdivision vs double derived subdivision

and for this reason, we propose the following conjecture:

Conjecture 11 (A first AWC/CWC interpolation)**.** *Let n be a finite integer such that $n \geq 2$, and let u be a real-valued image defined on the n-dimensional convex polyhedral domains of a polyhedral complex, which is a n-surface (with or without border). Then, any image u_{AWC} valued on the cell complex computed like it is described in this section is well-composed in the sense of Alexandrov and continuous well-composed. This method is self-dual.*

Note that the geometry of the cells is not preserved.

E.4 ANOTHER n-D AWC INTERPOLATION

We observed that due to the derived neighborhood, the geometry of the cells are not preserved (see Figure 26), even if we start from a cubical cell complex. Then, we propose an alternative: we still use a sequence of two subdivisions, but the first one is replaced by an *hierarchical subdivision* (introduced hereafter), which attenuates the deformation of the original cells.

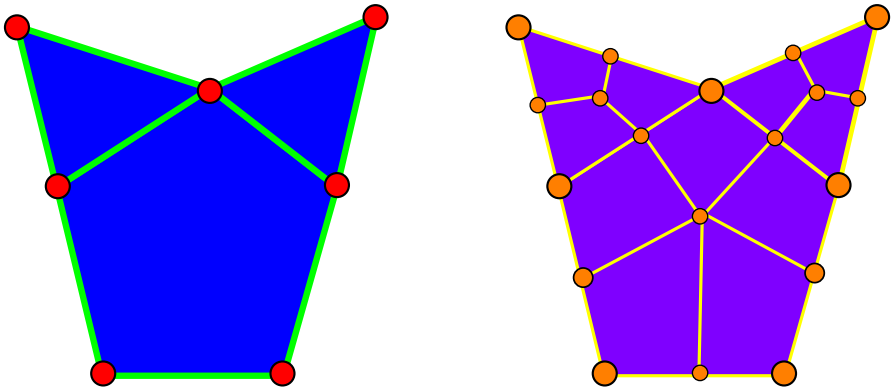

Figure 27.: From a cell complex to its hierarchical subdivision

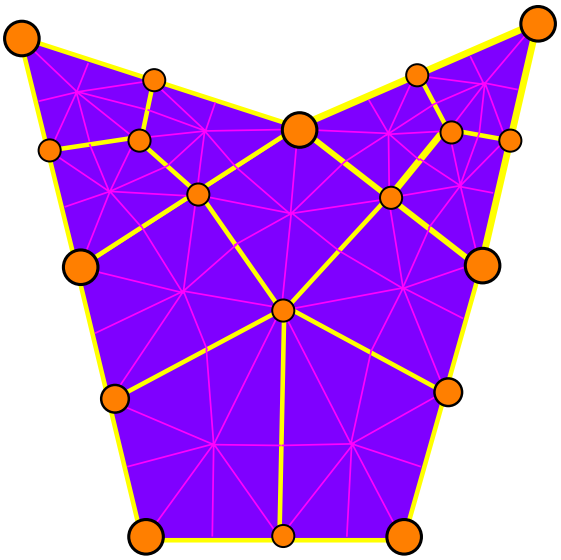

Figure 28.: From the hierarchical subdivision of a polyhedral complex to its chain complex

E.4.1 *Introducing the hierarchical subdivision*

We define an hierarchical subdivision as following:

Definition 136 (Hierarchical subdivision)**.** *Let $|\mathcal{O}| = (\mathcal{O}, \alpha)$ be a partially ordered set. Then we define the* hierarchical subdivision *of the order $\mathcal{O}$ as:*

$$\mathcal{SH}(\mathcal{O}) = \{\alpha(a) \cap \beta(b) \ ; \ \exists a, b \in \mathcal{O}, \alpha(a) \cap \beta(b) \neq \emptyset\},$$

supplied with the canonical relation order $\supseteq$. Obviously, $|\mathcal{SH}(\mathcal{O})|$ is an order.

E.4.2 *An AWC interpolation based on hierarchical subdivision*

Applied to a polyhedral complex $|\mathfrak{PC}^n|$, which is closed by inclusion, the hierarchical subdivision provides a new structure that is depicted on Figure 27. On the left, we draw the initial cell complex, where 2-faces are depicted in blue, 1-faces are depicted in green, and 0-faces are depicted in red. On the right, since any face $h \in \mathfrak{PC}^n$ leads to a 0-face $\alpha(h) \cap \beta(h) = \{h\}$ into $\mathcal{SH}(\mathfrak{PC}^n)$, we represent them using the orange points. Note that the 0-faces in $\mathcal{SH}(\mathfrak{PC}^n)$ which come from 0-faces in $\mathcal{O}$ are depicted using bigger disks. Then, for any couple $(a, b) \in \mathcal{O}$ such that $a \succ b$, it is clear that $\alpha(a) \cap \beta(b) = \{a, b\}$, and since $\rho(\{a, b\}) = 1$, we depict it using an edge (in yellow) linking $\{a\}$ and $\{b\}$. Finally, for the couples (a, b) of elements

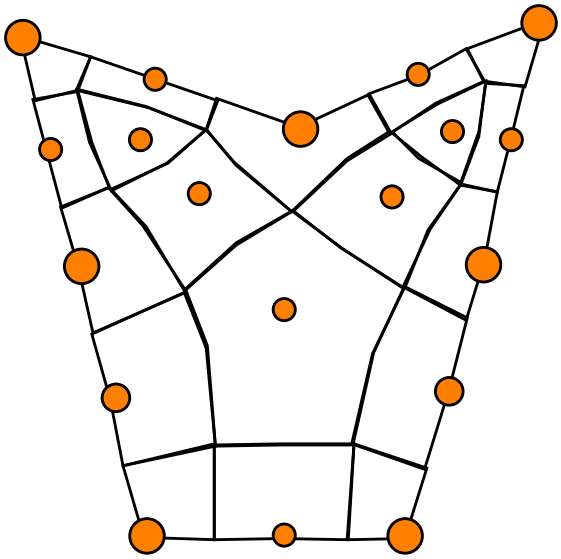

Figure 29.: The cell complex resulting of the chain complex of the hierarchical subdivision: the geometry of the initial cells is preserved.

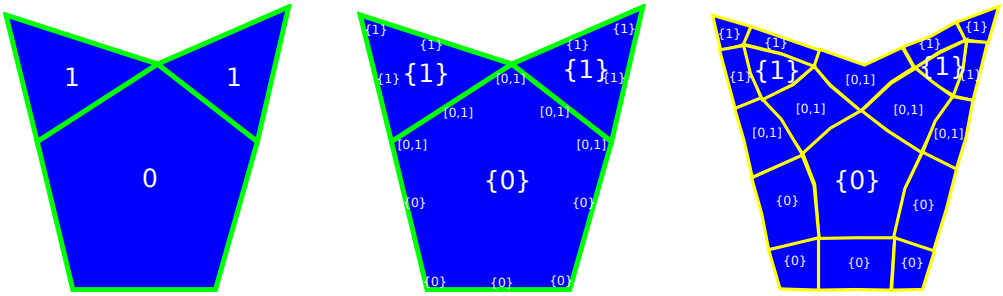

Figure 30.: From u to U

of $\mathcal{O}$ such that there exists a third element $c \in \mathcal{O}$ such that $a \succ c \succ b$, then $\alpha(a) \cap \beta(b)$ is of rank 2 in $|\mathcal{SH}(\mathcal{O})|$, and then is depicted by a purple polygon.

When we have computed the hierarchical subdivision, we have the "centers" of the new cells, but we still need to draw the cells around these centers. To this aim, we compute the chain complex of $|\mathcal{SH}(\mathcal{O})|$, which results in a triangulation of $\mathcal{SH}(\mathcal{O})$. On Figure 28, this chain complex is depicted in pink.

Now that we have drawn the triangulation of the hierarchical subdivision, we are able to compute the dual cells of the orange vertices. For any element $A \in \mathcal{SH}(\mathcal{O})$, its dual cell A^* is the subcomplex resulting from the intersection of the star in the chain complex of the vertices of A in the hierarchical subdivision:

$$A^* = \bigcap_{\{x\} \subseteq A} \alpha(\beta_{\mathcal{C}^{\mathcal{SH}(\mathcal{O})}}(\{\{x\}\})).$$

By grouping all these subcomplexes in one set, we obtain a cell complex where the geometry of the cells has been preserved.

Figure 30 shows that, as for the AWC interpolation we presented before, we value each face of the face of the cell complex by the span of the values of the image on the star neighborhood of the face, which makes U. Then, we transpose the computed values on the sudivided domain, and we obtain U'.

Then we are able to proceed to the front propagation, after having added the border valued at the median of the border of the initial image (see Figure 31).

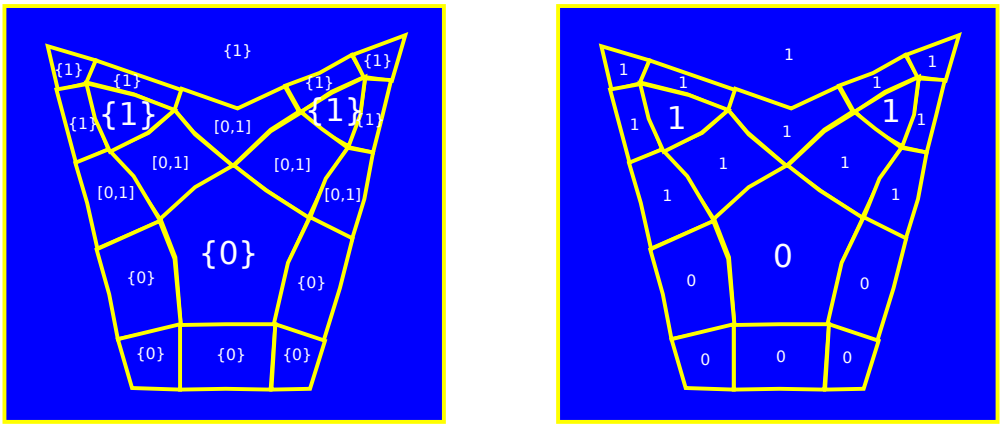

Figure 31.: The propagation computation

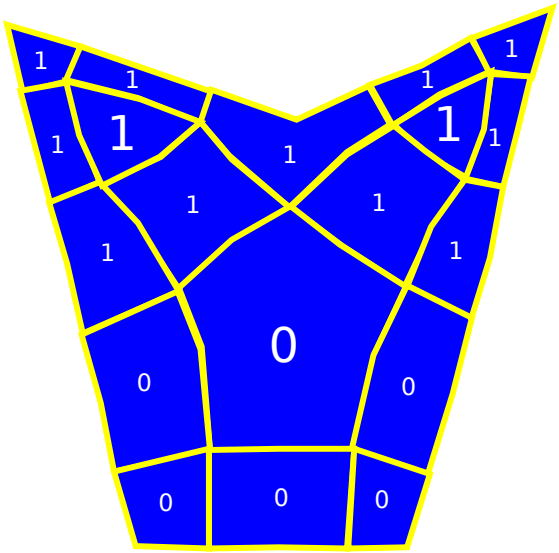

Figure 32.: A self-dual interpolation of u

According to us, the resulting image u_{AWC} on the cell complex is well-composed in the sense of Alexandrov, continuous well-composed, and self-dual, since we use the median of the border of the initial image to intialize the outer border before the propagation (as shown on Figure 32 where the median is equal to 1).

Conjecture 12 (A second AWC/CWC interpolation)**.** *Let n be a finite integer such that $n \geq 2$, and let u be a real-valued image defined on the n-dimensional convex polyhedral domains of a polyhedral domain, which is a n-surface (with or without border). Then, any image u_{AWC} valued on the cell complex computed like it is described in this section is well-composed in the sense of Alexandrov and continuous well-composed. This method is self-dual. Furthermore, the geometry of the cells in the initial domain is preserved.*

E.4.3 *Mathematical properties of the hierarchical subdivision*

In this section, we denote some remarkable properties of our hierarchical subdivision.

Property 14. *Let $|\mathcal{O}| = (\mathcal{O}, \alpha)$ be a partially ordered set which is connected. Then, its hierarchical subdivision is also connected.*

Proof: Let $|\mathcal{O}|$ be a connected poset, and let $|\mathcal{SH}(\mathcal{O})|$ be its hierarchical subdivision. Now, let x, y be two elements of $|\mathcal{SH}(\mathcal{O})|$ and let show that they are connected: x belongs

to $\mathcal{SH}(\mathcal{O})$ and this way there exist a_x, b_x in $\mathcal{O}$ such that $x = \alpha(a_x) \cap \beta(b_x) \neq \emptyset$. For the same reason, there exist a_y, b_y in $\mathcal{O}$ such that $y = \alpha(a_y) \cap \beta(b_y) \neq \emptyset$. Obviously, $\alpha(a_x) \cap \beta(b_x)$ is connected to $\{b_x\}$ into $|\mathcal{SH}(\mathcal{O})|$, and $\alpha(a_y) \cap \beta(b_y)$ is connected to $\{b_y\}$ into $|\mathcal{SH}(\mathcal{O})|$. It is clear that b_x and b_y are connected by hypothesis. Then there exists a path $\pi = (q^0 = b_x, \ldots, q^r = b_y)$ such that for any $i \in [\![0, r-1]\!]$, $q^{i+1} \in \theta^{\square}_{\mathcal{O}}(q^i)$ joining x and y into $\mathcal{O}$. From this path, we can deduce the following sequence $\pi' =$

$$(\{q^0\} = \{b_x\}, \alpha(q^0 \vee q^1) \cap \beta(q^0 \wedge q^1), \{q^1\}, \ldots, \{q^r\} = \{b_y\}),$$

which is clearly a path in $|\mathcal{SH}(\mathcal{O})|$. The existence of this path implies that x and y are connected into $|\mathcal{SH}(\mathcal{O})|$. The proof is done. □

Conjecture 13. *Let $|\mathcal{O}|$ be a non-empty, closed order of finite rank, and let $\mathcal{SH}(\mathcal{O})$ be its hierarchical subdivision. Then $\rho(|\mathcal{SH}(\mathcal{O})|) = \rho(\mathcal{O})$.*

Conjecture 14. *Let $|\mathcal{O}|$ be a non-empty, closed order of finite rank, and let $\mathcal{SH}(\mathcal{O})$ be its hierarchical subdivision. Then, if $|\mathcal{O}|$ is a n-surface, $|\mathcal{SH}(\mathcal{O})|$ is a n-surface too.*

Note that this property is easy to verify for the cases $n = 0$ and $n = 1$ by observing the Hasse diagrams of these n-surfaces and their respective hierarchical subdivisions.

Apllied to a convex linear cell complex, we obtain:

Conjecture 15. *Let $|\mathfrak{PC}^n|$ be a convex linear cell complex of dimension n supplied with the order relation $\supseteq$, and let $|\mathcal{SH}(\mathfrak{PC}^n)|$ be its hierarchical subdivision. Then, if $|\mathfrak{PC}^n|$ is a n-surface (respectively a bordered n-surface), $|\mathcal{SH}(\mathfrak{PC}^n)|$ is a n-surface (respectively a bordered n-surface).*

We also observed that the borders of each cells in the new cell complex were 1-surfaces in the 2D case, and we think it can be generalized in n-D. Effectively, starting from a convex linear cell complex such that it is a n-surface, its hierarchical subdivision is also a n-surface. Then, when we compute the dual cell of a vertex $\{x\}$ of the hierarchical subidivision, we obtain its dual cell A^* such that:

$$A^* = \alpha(\beta_{\mathcal{C}^{\mathcal{SH}(\mathfrak{PC}^n)}}(\{\{x\}\})),$$

which is equal to the simplicial neighborhood of $\{\{x\}\}$ into $\mathcal{C}^{\mathcal{SH}(\mathfrak{PC}^n)}$ which we assume to be a n-surface and a simplicial complex. For this reason, we think that computing the border of this cell has the same properties as the border of a derived neighborhood, and then is a $(n-1)$-surface.

Conjecture 16. *Let $|\mathfrak{PC}^n|$ be a convex linear cell complex of dimension n supplied with the order relation $\supseteq$, and let $|\mathcal{SH}(\mathfrak{PC}^n)|$ be its hierarchical subdivision. Then, if $|\mathfrak{PC}^n|$ is a n-surface (with or without border), then the border of the dual cells of the vertices of the hierarchical subdivision are $(n-1)$-surfaces (in the chain complex of the hierarchical subdivision).*

Figure 33 shows in the raster scan order a convex cell that is a tetrahedron, its hierarchical subdivision, the chain complex of the hierarchical subdivision, and (a part of) the dual cell. The final cell preverves the geometry of the original cell, and its boundary is a $(n-1)$-surface.

E.5 A SELF-DUAL CONTINUOUS REPRESENTATION ON POLYHEDRAL COMPLEXES

As seen in Section 5.2, we can easily obtain a self-dual plain map (see Section C.19) representing a given image u defined on the n-faces of a cubical complex. This is also true on polyhedral complexes, as depicted on Figure 34.

Conjecture 17. *Let $u : \mathfrak{PC}^n_n \to \mathbb{R}$ be a real-valued image defined on the n-faces of a polyhedral complex. Using the numerical scheme described in Figure 34, the image $U_{\mathrm{AWC}} : \mathfrak{CC}^n \to \mathbb{R}$ defined on a cell complex and resulting from a span-based immersion of one of our two self-dual interpolations $u_{\mathrm{AWC}} : \mathfrak{CC}^n_n \to \mathbb{R}$ is an AWC plain map.*

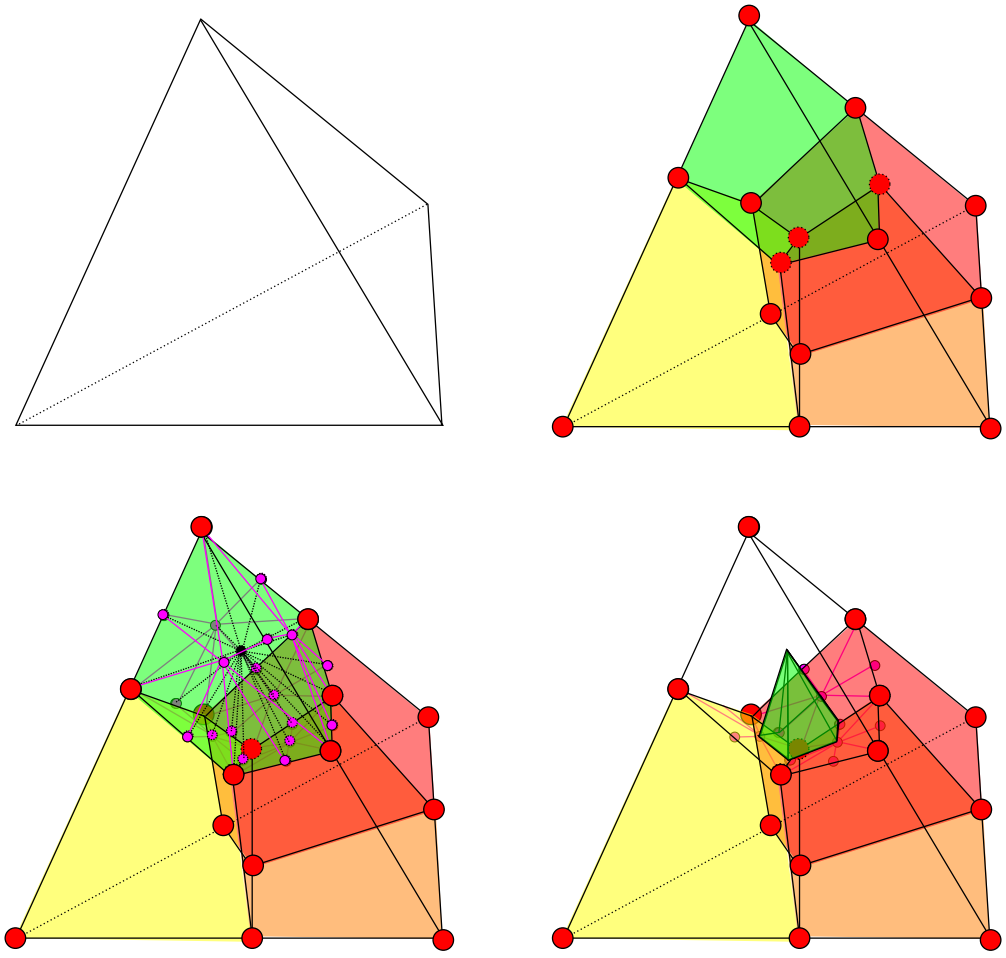

Figure 33.: The dual cell resulting from the chain complex of the hierarchical subdivision

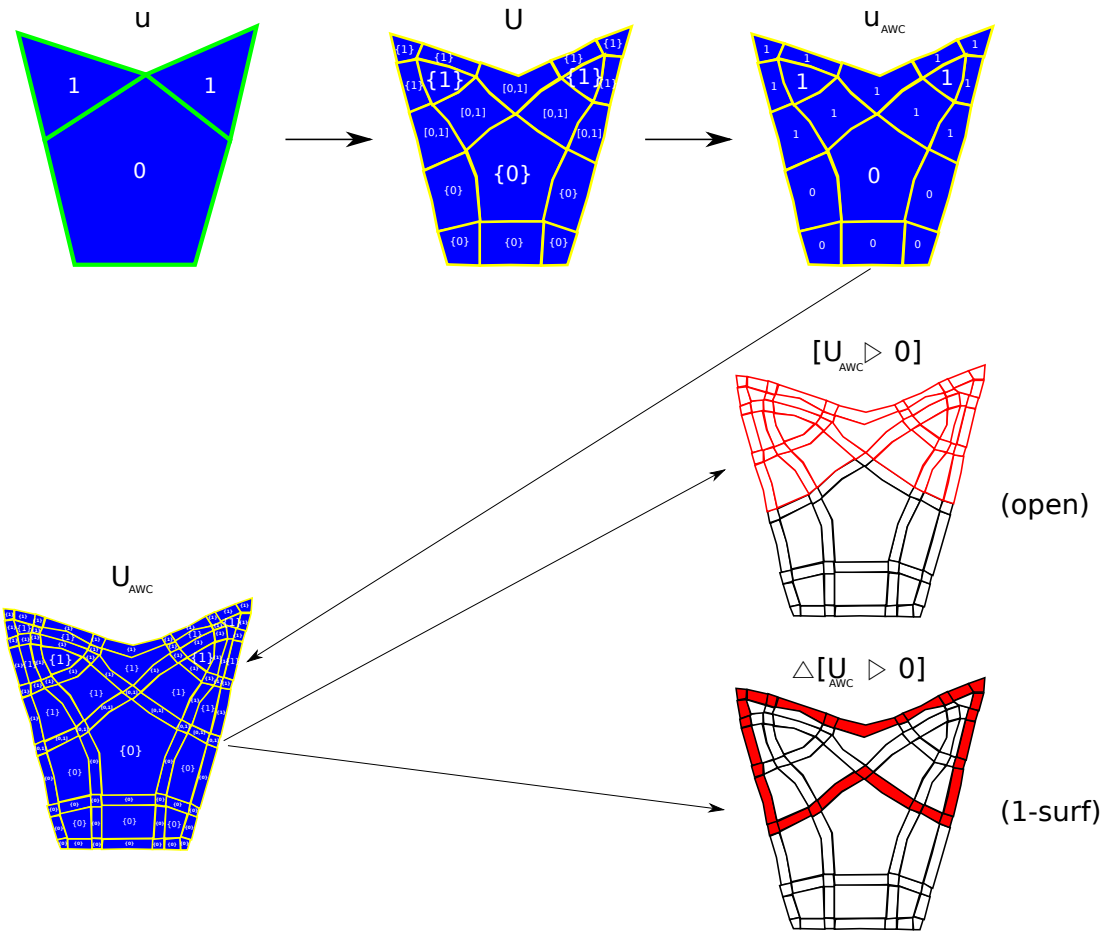

Figure 34.: Our self-dual representation on cell complexes

LIST OF PUBLICATIONS

TECHNICAL REPORTS

[1] Nicolas Boutry, Laurent Najman, and Thierry Géraud. *About the equivalence between AWCness and DWCness*. Research Report. LIGM - Laboratoire d'Informatique Gaspard-Monge ; LRDE - Laboratoire de Recherche et de Développement de l'EPITA, Oct. 2016. URL: https://hal-upec-upem.archives-ouvertes.fr/hal-01375621.

COMMUNICATIONS

[1] Nicolas Boutry, Thierry Géraud, and Laurent Najman. *Une généralisation du bien-composé à la dimension n*. Journée du Groupe de Travail de Géometrie Discrète (GT GéoDis, Reims Image 2014). In French. Nov. 2014.

POSTERS

[1] Nicolas Boutry, Thierry Géraud, and Laurent Najman. "How to make n-D images well-composed without interpolation". In: *IEEE International Conference on Image Processing*. IEEE. 2015, pp. 2149–2153.

CONFERENCE PAPERS

[1] Nicolas Boutry, Thierry Géraud, and Laurent Najman. "How to make n-D functions digitally well-composed in a self-dual way". In: *International Symposium on Mathematical Morphology and Its Applications to Signal and Image Processing*. Springer. 2015, pp. 561–572.

[2] Nicolas Boutry, Thierry Géraud, and Laurent Najman. "On making n-D images well-composed by a self-dual local interpolation". In: *International Conference on Discrete Geometry for Computer Imagery*. Springer. 2014, pp. 320–331.

[3] Thierry Géraud, Yongchao Xu, Edwin Carlinet, and Nicolas Boutry. "Introducing the Dahu pseudo-distance (submitted)". In: *International Symposium on Mathematical Morphology and Its Applications to Signal and Image Processing*. 2017.

JOURNAL PAPERS

[1] Nicolas Boutry, Thierry Géraud, and Laurent Najman. "Digitally well-composed sets and functions on the n-D cubical grid (in preparation)". In: *Journal of Mathematical Imaging and Vision*. 2017.

BIBLIOGRAPHY

[1] Wisam Al Faqheri and Syamsiah Mashohor. "A real-time Malaysian automatic license plate recognition (M-ALPR) using hybrid fuzzy". In: *IJCSNS International Journal of Computer Science and Network Security* 9.2 (2009), pp. 333–340.

[2] Pavel S Aleksandrov. *Combinatorial topology*. Vol. 1. Courier Corporation, 1956.

[3] James W Alexander. "A proof and extension of the Jordan-Brouwer separation theorem". In: *Transactions of the American Mathematical Society* 23.4 (1922), pp. 333–349.

[4] James W Alexander. "The combinatorial theory of complexes". In: *Annals of Mathematics* (1930), pp. 292–320.

[5] Paul Alexandroff and Heinz Hopf. *Topologie I: Erster Band. Grundbegriffe der Mengentheoretischen, Topologie ,Topologie der Komplexe· Topologische Invarianzsätze und Anschliessende Begriffsbildungen· Verschlingungen im n-Dimensionalen Euklidischen Raum Stetige Abbildungen von Polyedern*. Springer-Verlag, 2013.

[6] Oleg Alexandrov and Fadil Santosa. "A topology-preserving level set method for shape optimization". In: *Journal of Computational Physics* 204.1 (2005), pp. 121–130.

[7] Pavel Sergueïevitch Alexandrov. "Diskrete Räume". In: *Matematicheskij Sbornik* 2.44 (1937), pp. 501–519.

[8] Carlo Arcelli. "Pattern thinning by contour tracing". In: *Computer Graphics and Image Processing* 17.2 (1981), pp. 130–144.

[9] Ehud Artzy, Gideon Frieder, and Gabor T Herman. "The theory, design, implementation and evaluation of a three-dimensional surface detection algorithm". In: *Computer Graphics and Image Processing* 15.1 (1981), pp. 1–24.

[10] Jean-Pierre Aubin and Hélène Frankowska. *Set-valued analysis*. Springer Science & Business Media, 2009.

[11] Coloma Ballester, Vicent Caselles, and Pascal Monasse. "The tree of shapes of an image". In: *ESAIM: Control, Optimisation and Calculus of Variations* 9 (2003), pp. 1–18.

[12] Pierre-Louis Bazin, Lotta Maria Ellingsen, and Dzung L Pham. "Digital homeomorphisms in deformable registration". In: *International Conference on Information Processing in Medical Imaging*. Springer. 2007, pp. 211–222.

[13] Gordon O Berg, William H Julian, Ray Mines, and Fred Richman. "The constructive Jordan curve theorem". In: *Rocky Mountain Journal of Mathematics* 5.2 (June 1975), pp. 225–236.

[14] Gilles Bertrand. "A Boolean characterization of three-dimensional simple points". In: *Pattern Recognition Letters* 17.2 (1996), pp. 115–124.

[15] Gilles Bertrand. "New notions for discrete topology". In: *Discrete Geometry for Computer Imagery*. Springer. 1999, pp. 218–228.

[16] Gilles Bertrand. "Simple points, topological numbers and geodesic neighborhoods in cubic grids". In: *Pattern Recognition Letters* 15.10 (1994), pp. 1003–1011.

[17] Gilles Bertrand, Jean-Christophe Everat, and Michel Couprie. "Image segmentation through operators based on topology". In: *Journal of Electronic Imaging* 6.4 (1997), pp. 395–405.

[18] Gilles Bertrand, Jean-Christophe Everat, and Michel Couprie. "Topological approach to image segmentation". In: *SPIE's 1996 International Symposium on Optical Science, Engineering, and Instrumentation*. International Society for Optics and Photonics. 1996, pp. 65–76.

[19] Gilles Bertrand and Grégoire Malandain. "A new characterization of three-dimensional simple points". In: *Pattern Recognition Letters* 15.2 (1994), pp. 169–175.

[20] Serge Beucher and Christian Lantuéjoul. "Use of watersheds in contour detection". In: *International Workshop on Image Processing: Real-time Edge and Motion Detection/Estimation* (1979).

[21] Serge Beucher and Fernand Meyer. "The morphological approach to segmentation: The watershed transformation". In: *Optical Engineering, New York, Marcel Dekker Incorporated* 34 (1992), pp. 433–433.

[22] Hanspeter Bieri and Walter Nef. "Algorithms for the Euler characteristic and related additive functionals of digital objects". In: *Computer vision, graphics, and image processing* 28.2 (1984), pp. 166–175.

[23] Errett Bishop and Douglas S Bridges. *Constructive analysis*. Vol. 279. Springer Science & Business Media, 2012.

[24] Ethan D Bloch. *A first course in geometric topology and differential geometry*. Springer Science & Business Media, 1997.

[25] Isabelle Bloch, Henk Heijmans, and Christian Ronse. "Mathematical morphology". In: *Handbook of Spatial Logics*. Springer, 2007, pp. 857–944.

[26] Nicolas Boutry, Thierry Géraud, and Laurent Najman. "How to make n-D functions digitally well-composed in a self-dual way". In: *International Symposium on Mathematical Morphology and Its Applications to Signal and Image Processing*. Springer. 2015, pp. 561–572.

[27] Nicolas Boutry, Thierry Géraud, and Laurent Najman. "How to make n-D images well-composed without interpolation". In: *IEEE International Conference on Image Processing*. IEEE. 2015, pp. 2149–2153.

[28] Nicolas Boutry, Thierry Géraud, and Laurent Najman. "On making n-D images well-composed by a self-dual local interpolation". In: *Discrete Geometry for Computer Imagery*. Springer. 2014, pp. 320–331.

[29] Jean-Pierre Braquelaire and Luc Brun. "Image segmentation with topological maps and inter-pixel representation". In: *Journal of Visual Communication and Image Representation* 9.1 (1998), pp. 62–79.

[30] Michal Busta, Lukas Neumann, and Jiri Matas. "FASText: Efficient unconstrained scene text detector". In: *IEEE International Conference on Computer Vision*. IEEE. 2015, pp. 1206–1214.

[31] Vicent Caselles and Pascal Monasse. "Geometric description of images as topographic maps, ser". In: *Lecture Notes in Mathematics. Springer-Verlag* 1984 (2009).

[32] Vicent Caselles and Pascal Monasse. "Grain filters". In: *Journal of Mathematical Imaging and Vision* 17.3 (2002), pp. 249–270.

[33] Thomas Christopher Cecil. "Numerical methods for partial differential equations involving discontinuities". PhD thesis. University of California Los Angeles, 2003.

[34] Li Chen. "Algorithms for Computing Topological Invariants in 2D and 3D Digital Spaces". In: *arXiv preprint arXiv:1309.4109* (2013).

[35] Li Chen. "Genus computing for 3D digital objects: Algorithm and implementation". In: *arXiv preprint arXiv:0912.4936* (2009).

[36] Adam Coates, Blake Carpenter, Carl Case, Sanjeev Satheesh, Bipin Suresh, Tao Wang, David J Wu, and Andrew Y Ng. "Text detection and character recognition in scene images with unsupervised feature learning". In: *International Conference on Document Analysis and Recognition*. IEEE. 2011, pp. 440–445.

[37] Yann Cointepas. "Modélisation homotopique et segmentation tridimensionnelles du cortex cérébral à partir d'IRM pour la résolution des problèmes directs et inverses en EEG et en MEG". PhD thesis. 1999.

[38] Yann Cointepas, Isabelle Bloch, and Line Garnero. "A cellular model for multi-objects multi-dimensional homotopic deformations". In: *Pattern Recognition* 34.9 (2001), pp. 1785–1798.

[39] Jean Cousty and Gilles Bertrand. "Uniqueness of the Perfect Fusion Grid on $\mathbb{Z}^d$". In: *Journal of Mathematical Imaging and Vision* 34.3 (2009), pp. 291–306.

[40] Jean Cousty, Michel Couprie, Laurent Najman, and Gilles Bertrand. "Grayscale watersheds on perfect fusion graphs". In: *International Workshop on Combinatorial Image Analysis*. Springer. 2006, pp. 60–73.

[41] Sébastien Crozet and Thierry Géraud. "A first parallel algorithm to compute the morphological tree of shapes of n-D images". In: *IEEE International Conference on Image Processing*. IEEE. 2014, pp. 2933–2937.

[42] Xavier Daragon. "Surfaces discrètes et frontières d'objets dans les ordres". PhD thesis. Université de Marne-la-Vallée, 2005.

[43] Xavier Daragon, Michel Couprie, and Gilles Bertrand. "Discrete surfaces and frontier orders". In: *Journal of Mathematical Imaging and Vision* 23.3 (2005), pp. 379–399.

[44] Xavier Daragon, Michel Couprie, and Gilles Bertrand. "Marching chains algorithm for Alexandroff-Khalimsky spaces". In: *International Symposium on Optical Science and Technology*. International Society for Optics and Photonics. 2002, pp. 51–62.

[45] Marc Pierrot Deseilligny, Georges Stamon, and Ching Y Suen. "Veinerization: A new shape description for flexible skeletonization". In: *IEEE Transactions on Pattern Analysis and Machine Intelligence* 20.5 (1998), pp. 505–521.

[46] Tamal K Dey and Sumanta Guha. "Computing homology groups of simplicial complexes in $\mathbb{R}^3$". In: *Journal of the ACM* 45.2 (1998), pp. 266–287.

[47] Richard O Duda and John H Munson. *Graphical-data-processing research study and experimental investigation*. Tech. rep. DTIC Document, 1967.

[48] Charles R Dyer. "Computing the Euler number of an image from its quadtree". In: *Computer graphics and image processing* 13.3 (1980), pp. 270–276.

[49] Ulrich Eckhardt and Longin Jan Latecki. *Digital topology*. Institut für Angewandte Mathematik, 1994.

[50] Herbert Edelsbrunner. *Geometry and topology for mesh generation*. Cambridge University Press, 2001.

[51] Herbert Edelsbrunner and John Harer. *Computational topology: An introduction*. American Mathematical Society, 2010.

[52] Boris Epshtein, Eyal Ofek, and Yonatan Wexler. "Detecting text in natural scenes with stroke width transform". In: *IEEE Conference on Computer Vision and Pattern Recognition*. IEEE. 2010, pp. 2963–2970.

[53] Alexander V Evako, Ralph Kopperman, and Yurii V Mukhin. "Dimensional properties of graphs and digital spaces". In: *Journal of Mathematical Imaging and Vision* 6.2–3 (1996), pp. 109–119.

[54] Jonathan Fabrizio, Myriam Robert-Seidowsky, Séverine Dubuisson, Stefania Calarasanu, and Raphaël Boissel. "TextCatcher: A method to detect curved and challenging text in natural scenes". In: *International Journal on Document Analysis and Recognition* 19.2 (2016), pp. 99–117.

[55] Sylvain Faisan, Nicolas Passat, Vincent Noblet, Renée Chabrier, and Christophe Meyer. "Topology preserving warping of 3D binary images according to continuous one-to-one mappings". In: *IEEE Transactions on Image Processing* 20.8 (2011), pp. 2135–2145.

[56] Evgraf Stepanovitch Fedorov. "Course of Crystallography". In: *Published by RK Rikker, Saint-Petersburg (in Russian)* (1901).

[57] Christophe Fiorio. "A topologically consistent representation for image analysis: The frontiers topological graph". In: *Discrete Geometry for Computer Imagery*. Springer. 1996, pp. 151–162.

[58] Christophe Fiorio. "Approche interpixel en analyse d'images, une topologie et des algorithmes de segmentation". PhD thesis. Technische Universität Wien, 1995.

[59] Antonio Flores. "Über n-dimensionale Komplexe, die im $\mathbb{R}^{2k+1}$ absolut selbstverschlungen sind". In: *Ergebnisse eines Mathematischen Kolloquiums*. Vol. 34. 1933, pp. 4–6.

[60] Thierry Géraud, Edwin Carlinet, and Sébastien Crozet. "Self-duality and digital topology: Links between the morphological tree of shapes and well-composed gray-level images". In: *International Symposium on Mathematical Morphology and Its Applications to Signal and Image Processing*. Springer. 2015, pp. 573–584.

[61] Thierry Géraud, Edwin Carlinet, Sébastien Crozet, and Laurent Najman. "A quasi-linear algorithm to compute the tree of shapes of n-D images". In: *International Symposium on Mathematical Morphology and Its Applications to Signal and Image Processing*. Springer. 2013, pp. 98–110.

[62] Thierry Géraud, Jean-François Mangin, Isabelle Bloch, and Henri Maître. "Segmenting internal structures in 3D MR images of the brain by Markovian relaxation on a watershed based adjacency graph". In: *IEEE International Conference on Image Processing*. Vol. 3. IEEE. 1995, pp. 548–551.

[63] Rocío González-Díaz, María José Jiménez, and Belén Medrano. "3D well-composed polyhedral complexes". In: *Discrete Applied Mathematics* 183 (2015), pp. 59–77.

[64] Rocío González-Díaz, María José Jiménez, and Belén Medrano. "Cohomology ring of 3D cubical complexes." In: *IWCIA Special Track on Applications*. 2009, pp. 139–150.

[65] Rocío González-Díaz, María José Jiménez, and Belén Medrano. "Cubical cohomology ring of 3D photographs". In: *International Journal of Imaging Systems and Technology* 21.1 (2011), pp. 76–85.

[66] Rocío González-Díaz, María José Jiménez, and Belén Medrano. "Encoding specific 3D polyhedral complexes using 3D binary images". In: *Discrete Geometry for Computer Imagery*. Springer. 2016, pp. 268–281.

[67] Rocío González-Díaz, María José Jiménez, and Belén Medrano. "Well-composed cell complexes". In: *Discrete Geometry for Computer Imagery*. Springer. 2011, pp. 153–162.

[68] Rocío González-Díaz, Javier Lamar, and Ronald Umble. "Cup products on polyhedral approximations of 3D digital images". In: *International Workshop on Combinatorial Image Analysis*. Springer. 2011, pp. 107–119.

[69] Rocío González-Díaz and Pedro Real. "On the cohomology of 3D digital images". In: *Discrete Applied Mathematics* 147.2 (2005), pp. 245–263.

[70] Rocío González-Díaz and Pedro Real. "Towards digital cohomology". In: *Discrete Geometry for Computer Imagery*. Springer. 2003, pp. 92–101.

[71] Stephen B Gray. "Local properties of binary images in two dimensions". In: *IEEE Transactions on Computers* 100.5 (1971), pp. 551–561.

[72] Marvin J Greenberg. *Lectures on algebraic topology*. Vol. 9. WA Benjamin New York, 1967.

[73] Ari Gross and Longin Jan Latecki. "Digitizations preserving topological and differential geometric properties". In: *Computer Vision and Image Understanding* 62.3 (1995), pp. 370–381.

[74] Xiao Han, Chenyang Xu, and Jerry L Prince. "A topology preserving deformable model using level sets". In: *IEEE Conference on Computer Vision and Pattern Recognition*. Vol. 2. IEEE. 2001, pp. 765–770.

[75] Xiao Han, Chenyang Xu, and Jerry L Prince. "A topology preserving level set method for geometric deformable models". In: *IEEE Transactions on Pattern Analysis and Machine Intelligence* 25.6 (2003), pp. 755–768.

[76] Henk Heijmans. "Morphological image operators". In: *Advances in Electronics and Electron Physics Supplement* 1 (1994).

[77] Henk Heijmans. "Theoretical aspects of gray-level morphology". In: *IEEE Transactions on Pattern Analysis and Machine Intelligence* 13.6 (1991), pp. 568–582.

[78] Gabor T Herman. "Discrete multidimensional Jordan surfaces". In: *Graphical Models and Image Processing* 54.6 (1992), pp. 507–515.

[79] John FP Hudson. "Piecewise linear topology". In: *New York* (1969).

[80] Lê Duy Huynh, Yongchao Xu, and Thierry Géraud. "A Morphological Hierarchical Representation with Application to Text Segmentation in Natural Images". In: *(to appear)* (2016).

[81] Ludvik Janos and Azriel Rosenfeld. "Digital connectedness: An algebraic approach". In: *Pattern Recognition Letters* 1.3 (1983), pp. 135–139.

[82] C. Jordan. *Cours d'Analyse de l'Ecole Polytechnique*. Vol. 3. Gauthier-Villars, Paris, 1887, pp. 587–594.

[83] Tao Ju, Frank Losasso, Scott Schaefer, and Joe Warren. "Dual contouring of Hermite data". In: *ACM Transactions on Graphics*. Vol. 21. 3. ACM. 2002, pp. 339–346.

[84] John L Kelley. *General Topology. The University Series in Higher Mathematics*. 1955.

[85] Efim Khalimsky. *Applications of connected ordered topological spaces in topology*. 1970.

[86] Efim Khalimsky. *Ordered Topological Spaces*. 1977.

[87] Efim Khalimsky, Ralph Kopperman, and Paul R Meyer. "Computer graphics and connected topologies on finite ordered sets". In: *Topology and its Applications* 36.1 (1990), pp. 1–17.

[88] Robert M Kirby, Valerio Pascucci, Cláudio T Silva, Thomas J Peters, Julien Tierny, Carlos Scheidegger, L Gustavo Nonato, and Tiago Etiene. "Topology verification for isosurface extraction". In: *IEEE Transactions on Visualization and Computer Graphics* 6 (2012), pp. 952–965.

[89] T Yung Kong and Azriel Rosenfeld. "Digital topology: Introduction and survey". In: *Computer Vision, Graphics, and Image Processing* 48.3 (1989), pp. 357–393.

[90] T Yung Kong and Azriel Rosenfeld. "If we use 4-or 8-connectedness for both the objects and the background, the Euler characteristics is not locally computable". In: *Pattern Recognition Letters* 11.4 (1990), pp. 231–232.

[91] Ralph Kopperman. "The Khalimsky line as a foundation for digital topology". In: *Shape in Picture*. Springer, 1994, pp. 3–20.

[92] Ralph Kopperman, Paul R Meyer, and Richard G Wilson. "A Jordan surface theorem for three-dimensional digital spaces". In: *Discrete & Computational Geometry* 6.2 (1991), pp. 155–161.

[93] Ullrich Köthe. *Generische Programmierung für die Bildverarbeitung*. BoD–Books on Demand, 2000.

[94] Vladimir A Kovalevsky. "Finite topology as applied to image analysis". In: *Computer Vision, Graphics, and Image Processing* 46.2 (1989), pp. 141–161.

[95] Casimir Kuratowski. "Sur le problème des courbes gauches en topologie". In: *Fundamenta Mathematicae* 15.1 (1930), pp. 271–283.

[96] Jacques-Olivier Lachaud and Annick Montanvert. "Continuous analogs of digital boundaries: A topological approach to iso-surfaces". In: *Graphical Models and Image Processing* 62.3 (2000), pp. 129–164.

[97] Longin Jan Latecki. "3D well-composed pictures". In: *Graphical Models and Image Processing* 59.3 (1997), pp. 164–172.

[98] Longin Jan Latecki. *Discrete representation of spatial objects in computer vision*. Vol. 11. Springer Science & Business Media, 1998.

[99] Longin Jan Latecki. "Multicolor well-composed pictures". In: *Photonics for Industrial Applications*. International Society for Optics and Photonics. 1995, pp. 63–70.

[100] Longin Jan Latecki. "Well-composed sets". In: *Advances in Electronics and Electron Physics* 112 (2000), pp. 95–163.

[101] Longin Jan Latecki, Christopher Conrad, and Ari Gross. "Preserving topology by a digitization process". In: *Journal of Mathematical Imaging and Vision* 8.2 (1998), pp. 131–159.

[102] Longin Jan Latecki, Ulrich Eckhardt, and Azriel Rosenfeld. "Well-composed sets". In: *Computer Vision and Image Understanding* 61.1 (1995), pp. 70–83.

[103] Carole Le Guyader and Luminita A Vese. "Self-repelling snakes for topology-preserving segmentation models". In: *IEEE Transactions on Image Processing* 17.5 (2008), pp. 767–779.

[104] Chung-Nim Lee, Timothy Poston, and Azriel Rosenfeld. "Winding and Euler numbers for 2D and 3D digital images". In: *Graphical Models and Image Processing* 53.6 (1991), pp. 522–537.

[105] Chung-Nim Lee and Azriel Rosenfeld. "Computing the Euler number of a 3D image". In: *Center for Automation Research Technical Report CAR-TR-205* (1986).

[106] John Lee. *Introduction to topological manifolds*. Vol. 940. Springer Science & Business Media, 2010.

[107] Jung-Jin Lee, Pyoung-Hean Lee, Seong-Whan Lee, Alan L Yuille, and Christof Koch. "AdaBoost for Text Detection in Natural Scene." In: *ICDAR*. 2011, pp. 429–434.

[108] Juan Luis Diaz-de Leon and Juan Humberto Sossa-Azuela. "On the computation of the Euler number of a binary object". In: *Pattern Recognition* 29.3 (1996), pp. 471–476.

[109] Roland Levillain, Thierry Géraud, and Laurent Najman. "Why and how to design a generic and efficient image processing framework: The case of the Milena library". In: *IEEE International Conference on Image Processing*. IEEE. 2010, pp. 1941–1944.

[110] Roland Levillain, Thierry Géraud, and Laurent Najman. "Writing reusable digital topology algorithms in a generic image processing framework". In: *Applications of Discrete Geometry and Mathematical Morphology*. Springer, 2012, pp. 140–153.

[111] William Bernard Raymond Lickorish. "Simplicial moves on complexes and manifolds". In: *Geometry and Topology Monographs* 2 (1999), pp. 299–320.

[112] Elon L Lima. "The Jordan-Brouwer separation theorem for smooth hypersurfaces". In: *The American Mathematical Monthly* 95.1 (1988), pp. 39–42.

[113] William E Lorensen and Harvey E Cline. "Marching cubes: A high resolution 3D surface construction algorithm". In: *Special Interest Group on Computer GRAPHics and Interactive Techniques*. Vol. 21. 4. ACM. 1987, pp. 163–169.

[114] Wolfram HHJ Lunscher and Michael P Beddoes. "Fast binary-image boundary extraction". In: *Computer Vision, Graphics, and Image Processing* 38.3 (1987), pp. 229–257.

[115] Jean-François Mangin, Olivier Coulon, and Vincent Frouin. "Robust brain segmentation using histogram scale-space analysis and mathematical morphology". In: *International Conference on Medical Image Computing and Computer-Assisted Intervention*. Springer. 1998, pp. 1230–1241.

[116] Jocelyn Marchadier, Didier Arquès, and Sylvain Michelin. "Thinning grayscale well-composed images". In: *Pattern Recognition Letters* 25.5 (2004), pp. 581–590.

[117] David Martin, Charless Fowlkes, Doron Tal, and Jitendra Malik. "A Database of Human Segmented Natural Images and its Application to Evaluating Segmentation Algorithms and Measuring Ecological Statistics". In: *International Conference on Computer Vision*. Vol. 2. 2001, pp. 416–423.

[118] Loïc Mazo. "Déformations homotopiques dans les images digitales n-aires". PhD thesis. Université de Strasbourg, 2011.

[119] Loïc Mazo, Nicolas Passat, Michel Couprie, and Christian Ronse. "Digital imaging: A unified topological framework". In: *Journal of Mathematical Imaging and Vision* 44.1 (2012), pp. 19–37.

[120] Enric Meinhardt-Llopis. "Morphological and statistical techniques for the analysis of 3D images". PhD thesis. Universitat Pompeu Fabra, Spain, 2011.

[121] Fernand Meyer. "Skeletons and perceptual graphs". In: *Signal Processing* 16.4 (1989), pp. 335–363.

[122] Fernand Meyer and Petros Maragos. "Morphological scale-space representation with levelings". In: *International Conference on Scale-Space Theories in Computer Vision*. Springer. 1999, pp. 187–198.

[123] Pascal Monasse and Frederic Guichard. "Fast computation of a contrast-invariant image representation". In: *IEEE Transactions on Image Processing* 9.5 (2000), pp. 860–872.

[124] John P Mylopoulos and Theodosios Pavlidis. "On the topological properties of quantized spaces, I. The notion of dimension". In: *Journal of the ACM* 18.2 (1971), pp. 239–246.

[125] John P Mylopoulos and Theodosios Pavlidis. "On the topological properties of quantized spaces, II. Connectivity and order of connectivity". In: *Journal of the ACM* 18.2 (1971), pp. 247–254.

[126] Laurent Najman and Michel Couprie. "Watershed algorithms and contrast preservation". In: *Discrete Geometry for Computer Imagery*. Springer. 2003, pp. 62–71.

[127] Laurent Najman and Thierry Géraud. "Discrete set-valued continuity and interpolation". In: *Mathematical Morphology and Its Applications to Signal and Image Processing*. Springer, 2013, pp. 37–48.

[128] Laurent Najman and Michel Schmitt. "Watershed of a continuous function". In: *Signal Processing* 38.1 (1994), pp. 99–112.

[129] Laurent Najman and Hugues Talbot. *Mathematical Morphology*. John Wiley & Sons, 2013.

[130] Mikio Nakahara. *Geometry, topology and physics*. CRC Press, 2003.

[131] Maxwell Herman Alexander Newman. *Elements of the topology of plane sets of points*. Cambridge, 1939.

[132] Phuc Ngo, Yukiko Kenmochi, Nicolas Passat, and Hugues Talbot. "Combinatorial structure of rigid transformations in 2D digital images". In: *Computer Vision and Image Understanding* 117.4 (2013), pp. 393–408.

[133] Phuc Ngo, Yukiko Kenmochi, Nicolas Passat, and Hugues Talbot. "Sufficient conditions for topological invariance of 2D images under rigid transformations". In: *Discrete Geometry for Computer Imagery*. Springer. 2013, pp. 155–168.

[134] Phuc Ngo, Nicolas Passat, Yukiko Kenmochi, and Hugues Talbot. "Topology-preserving rigid transformation of 2D digital images". In: *IEEE Transactions on Image Processing* 23.2 (2014), pp. 885–897.

[135] Phuc Ngo, Nicolas Passat, Yukiko Kenmochi, and Hugues Talbot. "Well-composed images and rigid transformations". In: *IEEE International Conference on Image Processing*. 2013, pp. 3035–3039.

[136] Seymour Papert and Marvin Minsky. "Perceptrons: An Introduction to Computational Geometry". In: *The MIT Press* (1969).

[137] Theodosios Pavlidis. *Algorithms for Graphics and Image Processing*. Springer Science & Business Media, 2012.

[138] Dzung L Pham, Pierre-Louis Bazin, and Jerry L Prince. "Digital topology in brain imaging". In: *Signal Processing Magazine* 27.4 (2010), pp. 51–59.

[139] Jos BTM Roerdink and Arnold Meijster. "The watershed transform: Definitions, algorithms and parallelization strategies". In: *Fundamenta Informaticae* 41.1–2 (2000), pp. 187–228.

[140] Christian Ronse. "Flat morphological operators on arbitrary power lattices". In: *Geometry, Morphology, and Computational Imaging*. Springer, 2003, pp. 1–21.

[141] Azriel Rosenfeld. "Adjacency in digital pictures". In: *Information and Control* 26.1 (1974), pp. 24–33.

[142] Azriel Rosenfeld. "Arcs and curves in digital pictures". In: *Journal of the ACM* 20.1 (1973), pp. 81–87.

[143] Azriel Rosenfeld. "Connectivity in digital pictures". In: *Journal of the ACM* 17.1 (1970), pp. 146–160.

[144] Azriel Rosenfeld. "Digital topology". In: *American Mathematical Monthly* (1979), pp. 621–630.

[145] Azriel Rosenfeld. "Fuzzy digital topology". In: *Information and Control* 40.1 (1979), pp. 76–87.

[146] Azriel Rosenfeld. "On connectivity properties of grayscale pictures". In: *Pattern Recognition* 16.1 (1983), pp. 47–50.

[147] Azriel Rosenfeld. *Picture Languages-Formal Model of Picture Recognition*. Academic Press, New York, 1979.

[148] Azriel Rosenfeld, T Yung Kong, and Akira Nakamura. "Topology-preserving deformations of two-valued digital pictures". In: *Graphical Models and Image Processing* 60.1 (1998), pp. 24–34.

[149] Azriel Rosenfeld, T Yung Kong, and Angela Y Wu. "Digital surfaces". In: *Graphical Models and Image Processing* 53.4 (1991), pp. 305–312.

[150] Azriel Rosenfeld and John L Pfaltz. "Sequential operations in digital picture processing". In: *Journal of the ACM* 13.4 (1966), pp. 471–494.

[151] Punam K Saha, Robin Strand, and Gunilla Borgefors. "Digital topology and geometry in medical imaging: A survey". In: *IEEE Transactions on Medical Imaging* 34.9 (2015), pp. 1940–1964.

[152] Philippe Salembier and Jean Serra. "Flat zones filtering, connected operators, and filters by reconstruction". In: *IEEE Transactions on Image Processing* 4.8 (1995), pp. 1153–1160.

[153] Florent Ségonne. "Active contours under topology control – Genus preserving level sets". In: *International Journal of Computer Vision* 79.2 (2008), pp. 107–117.

[154] Jean Serra. *Image Analysis and Mathematical Morphology, Vol. 1*. Academic Press, 1982.

[155] Jean Serra and B Ravi Kiran. "Digitization of Partitions and Tessellations". In: *Discrete Geometry for Computer Imagery*. Springer. 2016, pp. 323–334.

[156] Raj Shekhar, Elias Fayyad, Roni Yagel, and J Fredrick Cornhill. "Octree-based decimation of marching cubes surfaces". In: *Visualization'96*. IEEE. 1996, pp. 335–342.

[157] Marcelo Siqueira, Longin Jan Latecki, and Jean Gallier. "Making 3D binary digital images well-composed". In: *Electronic Imaging 2005*. International Society for Optics and Photonics. 2005, pp. 150–163.

[158] Marcelo Siqueira, Longin Jan Latecki, Nicholas Tustison, Jean Gallier, and James Gee. "Topological repairing of 3D digital images". In: *Journal of Mathematical Imaging and Vision* 30.3 (2008), pp. 249–274.

[159] Lauro Snidaro and Gian Luca Foresti. "Real-time thresholding with Euler numbers". In: *Pattern Recognition Letters* 24.9 (2003), pp. 1533–1544.

[160] Pierre Soille. *Morphological Image Analysis: Principles and Applications*. Springer Science & Business Media, 2013.

[161] Pierre Soille and Martino Pesaresi. "Advances in mathematical morphology applied to geoscience and remote sensing". In: *IEEE Transactions on Geoscience and Remote Sensing* 40.9 (2002), pp. 2042–2055.

[162] Juan Humberto Sossa-Azuela, R Santiago-Montero, M Pérez-Cisneros, and E Rubio-Espino. "Computing the Euler number of a binary image based on a vertex codification". In: *Journal of Applied Research and Technology* 11.3 (2013), pp. 360–370.

[163] Peer Stelldinger. *Image Digitization and its Influence on Shape Properties in Finite Dimensions*. Vol. 312. IOS Press, 2008.

[164] Peer Stelldinger and Ullrich Köthe. "Towards a general sampling theory for shape preservation". In: *Image and Vision Computing* 23.2 (2005), pp. 237–248.

[165] Peer Stelldinger and Longin Jan Latecki. "3D object digitization: Majority interpolation and marching cubes". In: *IEEE International Conference on Pattern Recognition*. Vol. 2. IEEE. 2006, pp. 1173–1176.

[166] Peer Stelldinger, Longin Jan Latecki, and Marcelo Siqueira. "Topological equivalence between a 3D object and the reconstruction of its digital image". In: *IEEE Transactions on Pattern Analysis and Machine Intelligence* 29.1 (2007), pp. 126–140.

[167] Peer Stelldinger and Robin Strand. "Topology preserving digitization with FCC and BCC grids". In: *International Workshop on Combinatorial Image Analysis*. Springer. 2006, pp. 226–240.

[168] Lawrence Neff Stout. "Two discrete forms of the Jordan curve theorem". In: *The American Mathematical Monthly* 95.4 (1988), pp. 332–336.

[169] Ganesh Sundaramoorthi and Anthony Yezzi. "Global regularizing flows with topology preservation for active contours and polygons". In: *IEEE Transactions on Image Processing* 16.3 (2007), pp. 803–812.

[170] Mohamed Tajine and Christian Ronse. "Topological properties of Hausdorff discretizations". In: *Mathematical Morphology and its Applications to Image and Signal Processing*. Springer, 2002, pp. 41–50.

[171] Junichiro Toriwaki and Hiroyuki Yoshida. *Fundamentals of three-dimensional digital image processing*. Springer Science & Business Media, 2009.

[172] Nicholas J Tustison, Brian B Avants, Marcelo Siqueira, and James C Gee. "Topological well-composedness and glamorous glue: A digital gluing algorithm for topologically constrained front propagation". In: *IEEE Transactions onImage Processing* 20.6 (2011), pp. 1756–1761.

[173] Helge Tverberg. "A proof of the Jordan curve theorem". In: *Bulletin of the London Mathematical Society* 12.1 (1980), pp. 34–38.

[174] Egbert R Van Kampen. "Komplexe in Euklidischen Räumen". In: *Abhandlungen aus dem Mathematischen Seminar der Universität Hamburg*. Vol. 9. 1. Springer. 1933, pp. 72–78.

[175] Lucas J Van Vliet, Ian T Young, and Guus L Beckers. "An edge detection model based on non-linear Laplace filtering". In: *International workshop on Pattern Recognition and Artificial Intelligence, towards an Integration*. 1988.

[176] K Voss. "Images, objects, and surfaces in $\mathbb{Z}^n$". In: *International Journal of Pattern Recognition and Artificial Intelligence* 5.05 (1991), pp. 797–808.

[177] Tao Wang, David J Wu, Adam Coates, and Andrew Y Ng. "End-to-end text recognition with convolutional neural networks". In: *International Conference on Pattern Recognition*. IEEE. 2012, pp. 3304–3308.

[178] Yang Wang and Prabir Bhattacharya. “Digital connectivity and extended well-composed sets for gray images”. In: *Computer Vision and Image Understanding* 68.3 (1997), pp. 330–345.

[179] Paul R Wilson. “Euler formulas and geometric modeling”. In: *IEEE Computer Graphics and Applications* 8.5 (1985), pp. 24–36.

[180] Yongchao Xu, Thierry Géraud, and Laurent Najman. “Context-based energy estimator: Application to object segmentation on the tree of shapes”. In: *IEEE International Conference on Image Processing*. IEEE. 2012, pp. 1577–1580.

[181] Yongchao Xu, Thierry Géraud, and Laurent Najman. “Morphological filtering in shape spaces: Applications using tree-based image representations”. In: *International Conference on Pattern Recognition*. IEEE. 2012, pp. 485–488.

[182] Yongchao Xu, Thierry Géraud, and Laurent Najman. “Two applications of shape-based morphology: Blood vessels segmentation and a generalization of constrained connectivity”. In: *International Symposium on Mathematical Morphology and Its Applications to Signal and Image Processing*. Springer. 2013, pp. 390–401.

[183] Hyun S Yang and Sanjay Sengupta. “Intelligent shape recognition for complex industrial tasks”. In: *IEEE Control Systems Magazine* 8.3 (1988), pp. 23–30.

[184] Qixiang Ye and David Doermann. “Text detection and recognition in imagery: A survey”. In: *IEEE Transactions on Pattern Analysis and Machine Intelligence* 37.7 (2015), pp. 1480–1500.

[185] Shigeki Yokoi, Jun-Ichiro Toriwaki, and Teruo Fukumura. “An analysis of topological properties of digitized binary pictures using local features”. In: *Computer Graphics and Image Processing* 4.1 (1975), pp. 63–73.

[186] Yingying Zhu, Cong Yao, and Xiang Bai. “Scene text detection and recognition: Recent advances and future trends”. In: *Frontiers of Computer Science* 10.1 (2016), pp. 19–36.

Abstract Digitization of the real world using real sensors has many drawbacks; in particular, we loose "well-composedness" in the sense that two digitized objects can be connected or not depending on the connectivity we choose in the digital image, leading then to ambiguities. Furthermore, digitized images are arrays of numerical values, and then do not own any topology by nature, contrary to our usual modeling of the real world in mathematics and in physics. Loosing all these properties makes difficult the development of algorithms which are "topologically correct" in image processing: e.g., the computation of the tree of shapes needs the representation of a given image to be continuous and well-composed; in the contrary case, we can obtain abnormalities in the final result. Some well-composed continuous representations already exist, but they are not in the same time n-dimensional and self-dual. n-dimensionality is crucial since usual signals are more and more 3-dimensional (like 2D videos) or 4-dimensional (like 4D Computerized Tomography-scans), and self-duality is necessary when a same image can contain different objects with different contrasts. We developed then a new way to make images well-composed by interpolation in a self-dual way and in n-D; followed with a span-based immersion, this interpolation becomes a self-dual continuous well-composed representation of the initial n-D signal. This representation benefits from many strong topological properties: it verifies the intermediate value theorem, the boundaries of any threshold set of the representation are disjoint union of discrete surfaces, and so on.

Résumé Le processus de discrétisation faisant inévitablement appel à des capteurs, et ceux-ci étant limités de par leur nature, de nombreux effets secondaires apparaissent alors lors de ce processus; en particulier, nous perdons la propriété d'être "bien-composé" dans le sens où deux objects discrétisés peuvent être connectés ou non en fonction de la connexité utilisée dans l'image discrète, ce qui peut amener à des ambiguïtés. De plus, les images discrétisées sont des tableaux de valeurs numériques, et donc ne possèdent pas de topologie par nature, contrairement à notre modélisation usuelle du monde en mathématiques et en physique. Perdre toutes ces propriétés rend difficile l'élaboration d'algorithmes topologiquement corrects en traitement d'images : par exemple, le calcul de l'arbre des formes nécessite que la représentation d'une image donnée soit continue et bien-composée ; dans le cas contraire, nous risquons d'obtenir des anomalies dans le résultat final. Quelques représentations continues et bien-composées existent déjà, mais elles ne sont pas simultanément n-dimensionnelles et auto-duales. La n-dimensionalité est cruciale sachant que les signaux usuels sont de plus en plus tridimensionnels (comme les vidéos 2D) ou 4-dimensionnels (comme les CT-scans). L'auto-dualité est nécessaire lorsqu'une même image contient des objets à contrastes divers. Nous avons donc développé une nouvelle façon de rendre les images bien-composées par interpolation de façon auto-duale et en n-D; suivie d'une immersion par l'opérateur span, cette interpolation devient une représentation auto-duale continue et bien-composée du signal initial n-D. Cette représentation bénéficie de plusieurs propriétés topologiques fortes : elle vérifie le théorème de la valeur intermédiaire, les contours de chaque coupe de la représentation sont déterminés par une union disjointe de surfaces discrètes, et ainsi de suite.